frontiers
RESEARCH TOPICS

AUDITORY NEUROANATOMY: A SOUND FOUNDATION FOR SOUND PROCESSING

Topic Editors
Miguel A. Merchán, Enrique Saldaña and Douglas L. Oliver

frontiers in NEUROANATOMY

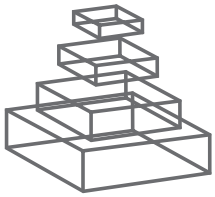

frontiers

Cover image provided by Ibbl sarl, Lausanne CH

ISSN 1664-8714
ISBN 978-2-88919-101-7
DOI 10.3389/978-2-88919-101-7

ABOUT FRONTIERS

Frontiers is more than just an open-access publisher of scholarly articles: it is a pioneering approach to the world of academia, radically improving the way scholarly research is managed. The grand vision of Frontiers is a world where all people have an equal opportunity to seek, share and generate knowledge. Frontiers provides immediate and permanent online open access to all its publications, but this alone is not enough to realize our grand goals.

FRONTIERS JOURNAL SERIES

The Frontiers Journal Series is a multi-tier and interdisciplinary set of open-access, online journals, promising a paradigm shift from the current review, selection and dissemination processes in academic publishing.
All Frontiers journals are driven by researchers for researchers; therefore, they constitute a service to the scholarly community. At the same time, the Frontiers Journal Series operates on a revolutionary invention, the tiered publishing system, initially addressing specific communities of scholars, and gradually climbing up to broader public understanding, thus serving the interests of the lay society, too.

DEDICATION TO QUALITY

Each Frontiers article is a landmark of the highest quality, thanks to genuinely collaborative interactions between authors and review editors, who include some of the world's best academicians. Research must be certified by peers before entering a stream of knowledge that may eventually reach the public - and shape society; therefore, Frontiers only applies the most rigorous and unbiased reviews.
Frontiers revolutionizes research publishing by freely delivering the most outstanding research, evaluated with no bias from both the academic and social point of view.
By applying the most advanced information technologies, Frontiers is catapulting scholarly publishing into a new generation.

WHAT ARE FRONTIERS RESEARCH TOPICS?

Frontiers Research Topics are very popular trademarks of the Frontiers Journals Series: they are collections of at least ten articles, all centered on a particular subject. With their unique mix of varied contributions from Original Research to Review Articles, Frontiers Research Topics unify the most influential researchers, the latest key findings and historical advances in a hot research area!
Find out more on how to host your own Frontiers Research Topic or contribute to one as an author by contacting the Frontiers Editorial Office: researchtopics@frontiersin.org

AUDITORY NEUROANATOMY: A SOUND FOUNDATION FOR SOUND PROCESSING

Topic Editors:
Miguel A. Merchán, Universidad de Salamanca, Spain
Enrique Saldaña, Universidad de Salamanca, Spain
Douglas L. Oliver, University of Connecticut Health Center, USA

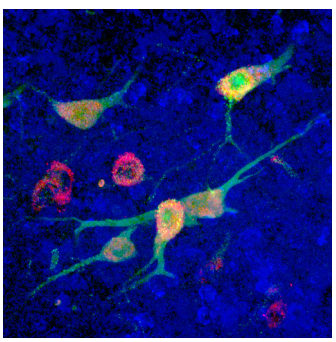

The image is owned by Tetsufumi Ito, Douglas L. Oliver, and the University of Connecticut Health Center.

In the last two decades, the ever increasing pace of auditory research has generated an undreamed of knowledge about the molecular and cellular bases of hearing, the physiopathology of hearing loss, the activity of the brain evoked by sounds, and the possibilities of imaginative strategies to restore hearing.

The aim of this Research Topic is to contribute to the development of auditory neuroscience by placing in an up-to-date morphological context some of the latest developments in the field.

This Research Topic for *Frontiers in Neuroanatomy* will consist of peer-reviewed articles dealing with the development, evolution, function and plasticity of the auditory system through a broad range of anatomical approaches. Articles combining neuroanatomy with other disciplines, such as molecular biology, genetics, physiology, pharmacology, behavior, neuroimaging, clinical medicine or bioinformatics, will be considered for publication insofar as they contribute to the understanding of the structure of the auditory regions of the central nervous system.

The authors of the papers published in this Research Topic will be invited to present and discuss their results during a symposium organized by the Instituto de Neurociencias of Castilla y León (INCyL), to be held in Salamanca, Spain, in 2010.

Table of Contents

frontiers in
NEUROANATOMY

EDITORIAL
published: 06 December 2012
doi: 10.3389/fnana.2012.00048

Auditory neuroanatomy: a sound foundation for sound processing

Miguel A. Merchán[1]*, Enrique Saldaña[1]* and Douglas L. Oliver[2]*

[1] *Laboratory 6, Neuroscience Institute of Castilla y León, Universidad de Salamanca, Salamanca, Spain*
[2] *Department of Neuroscience, University of Connecticut Health Center, Farmington, CT, USA*
**Correspondence: merchan@usal.es; saldana@usal.es; doliver@neuron.uchc.edu*

Edited by:
Javier DeFelipe, Cajal Institute, Spain

Auditory neuroanatomy has a long and distinguished history. Santiago Ramón y Cajal and Hans Held were pioneers who began the process of identifying the cellular components of the central auditory system. The stature of these early neurohistologists keeps growing today as the field of auditory neuroanatomy moves from the gross identification of brain structure to the analysis of neuronal morphology and function.

Auditory neuroanatomy, the topic of this special issue and E-Book, focuses on the study of the morphology of the neurons and nuclei in central auditory system and is now at the interface between cell biology, electrophysiology, and molecular biology. Because hearing is a complex phenomenon, researchers select the animal models that are best suited to investigate particular issues. Thus, the chapters of this E-Book include studies done with mice (normal and transgenic), rats, guinea pigs, cats (normal and congenitally deaf), ferrets, pallid bats, and primates. Moreover, given the morphological complexity of the nervous system, the authors of this volume have applied an arsenal of classical and state-of-the-art techniques that, alone or in daring combinations, cover the methodological spectrum found in modern neuroscience. Here, electron microscopy, histochemistry, immunocytochemistry, confocal microscopy, anterograde, and retrograde tract-tracing, surgical lesions, genetic engineering, molecular biology, *in situ* hybridization, auditory brainstem recordings, extracellular single-unit recordings, or magnetic resonance imaging are used to provide meaningful answers to pertinent questions about the morphological substrate of normal and abnormal hearing.

The E-Book begins with a detailed longitudinal study of the insulin-like growth factor-I (IGF-I) gene on hearing in wild type $Igf1^{+/+}$ and null $Igf1^{-/-}$ mice (Riquelme et al., 2010). Using a skilled combination of auditory brainstem recordings, *in vivo* magnetic resonance imaging, histological and immunocytochemical stains, quantitative PCR, and biochemical assays, the authors demonstrate that $Igf1^{-/-}$ mice present a profound deafness at all ages studied. In contrast, $Igf1^{+/+}$ mice suffer significant age-related cochlear alterations and hearing loss parallel to a decrease in circulating levels of IGF-1.

David K. Ryugo and his coworkers (Baker et al., 2010) investigate postnatal development of the endbulbs of Held (the giant synapses between the fibers of the cochlear nerve and spherical bushy cells of the ventral cochlear nucleus) in the congenitally deaf white cat. The endbulbs are present at birth, but they have an abnormal synaptic ultrastructure despite the seemingly intact cochlear structure. Because these alterations in kittens can be reversed by electric stimulation applied though cochlear implants, Ryugo's findings underscore the importance of early intervention in congenitally deaf children.

Ito and Oliver (2010) use the gene expression of vesicular glutamate transporters to identify glutamatergic neurons that send inputs to the inferior colliculus. Identification of a glutamatergic synapse is often much easier than identifying the neuronal source of the presynaptic terminal, especially when it is in a distant location. Here, the glutamatergic neurons that use the VGLUT2 transporter are identified, and these are the likely sources of the dense VGLUT2 axosomatic terminals on the large GABAergic tectothalamic neurons in the colliculus.

The article from Enrique Saldaña's laboratory (Viñuela et al., 2011) analyzes the relationships between two enigmatic nuclei: the superior paraolivary nucleus (SPON) and the tectal longitudinal column (TLC). Experiments with the bidirectional tracer biotinylated dextran amine (BDA) reveal that the rat SPON sends hitherto unknown projections to the entire ipsilateral TLC and the rostral and caudal portions of the contralateral TLC. They also show that SPON projects to the deep layers of the superior colliculus and to the periaqueductal gray matter, and that the SPON and the ipsilateral TLC are reciprocally connected.

Miguel A. Merchán's group (Clarkson et al., 2010) employs immunocytochemistry to analyze how the unilateral ablation of the cerebral auditory cortex modifies the sound-induced expression of c-Fos in the inferior colliculus of the rat. Using stereology, morphometry, and densitometry, they determined the number of labeled neurons, and the size and the intensity of the immunostaining of their nuclei at various times after injury (1, 15, 90, and 180 days). The number of immunoreactive neurons decreases for 15 days after lesions, but then there is a progressive partial recovery that suggests a successful long-range repair or adaptation in the IC.

Motts and Schofield (2010) use fluorescent retrograde tracers to show that the medial geniculate body of the guinea pig receives direct projections from neurons in the pedunculopontine tegmental nucleus (PPT) and the laterodorsal tegmental nucleus (LDT). These two nuclei are associated with arousal and control of the sleep/wake cycle. By combining retrograde tracers and immunocytochemistry for choline acetyltransferase (ChAT), they further demonstrate that approximately 50% of these neurons are cholinergic.

The study headed by Andrew J. King (Bajo et al., 2010) uses neuroanatomical tracers to investigate the projections from

the auditory neocortex to the superior colliculus in the ferret. These projections arise from layer V pyramidal neurons located preferentially in the anterior ventral field (anterior ectosylvian gyrus) and in the posterior suprasylvian field (posterior ectosylvian gyrus), are predominantly ipsilateral, and end more densely in the caudal half of the superior colliculus, particularly in the posteromedial quadrant.

Razak and Fuzessery (2010) review the organization and development of auditory thalamocortical pathways in the pallid bat. Two parallel pathways extend from the inferior colliculus to the cortex and process information about echolocation calls and passive listening. These pathways become adult-like after only 2 months of postnatal development and it is suggested that they depend on experience-dependent plasticity to segregate.

Finally, the paper from Ricardo Insausti's laboratory (Munoz-Lopez et al., 2010) reviews the evidence supporting the two prevailing hypothesis for the organization of the circuits that underlie the memory for the recognition of sounds in primates. The "direct stream" circuit is made of projections from the auditory association areas of the superior temporal gyrus to the medial temporal cortex, while the "indirect stream" circuit predicts one or more synapses in intermediate, polymodal cortical areas before the information reaches the medial temporal cortex.

REFERENCES

Bajo, V. M., Nodal, F. R., Bizley, J. K., and King, A. J. (2010). The non-lemniscal auditory cortex in ferrets: convergence of corticotectal inputs in the superior colliculus. *Front. Neuroanat.* 4:18. doi: 10.3389/fnana.2010.00018

Baker, C. A., Montey, K. L., Pongstaporn, T., and Ryugo, D. K. (2010). Postnatal development of the endbulb of Held in congenitally deaf cats. *Front. Neuroanat.* 4:19. doi: 10.3389/fnana.2010.00019

Clarkson, C., Juíz, J. M., and Merchán, M. A. (2010). Transient down-regulation of sound-induced c-Fos protein expression in the inferior colliculus after ablation of the auditory cortex. *Front. Neuroanat.* 4:141. doi: 10.3389/fnana.2010.00141

Ito, T., and Oliver, D. L. (2010). Origins of glutamatergic terminals in the inferior colliculus identified by retrograde transport and expression of VGLUT1 and VGLUT2 genes. *Front. Neuroanat.* 4:135. doi: 10.3389/fnana.2010.00135

Motts, S. D., and Schofield, B. R. (2010). Cholinergic and non-cholinergic projections from the pedunculopontine and laterodorsal tegmental nuclei to the medial geniculate body in guinea pigs. *Front. Neuroanat.* 4:137. doi: 10.3389/fnana.2010.00137

Munoz-Lopez, M. M., Mohedano-Moriano, A., and Insausti, R. (2010). Anatomical pathways for auditory memory in primates. *Front. Neuroanat.* 4:129. doi: 10.3389/fnana.2010.00129

Razak, K. A., and Fuzessery, Z. M. (2010). Development of parallel auditory thalamocortical pathways for two different behaviors. *Front. Neuroanat.* 4:134. doi: 10.3389/fnana.2010.00134

Riquelme, R., Cediel, R., Contreras, J., Rodriguez-de la Rosa, L., Murillo-Cuesta, S., Hernandez-Sanchez, C., et al. (2010). A comparative study of age-related hearing loss in wild type and insulin-like growth factor I deficient mice. *Front. Neuroanat.* 4:27. doi: 10.3389/fnana.2010.00027

Viñuela, A., Aparicio, M.-A., Berrebi, A. S., and Saldaña, E. (2011). Connections of the superior paraolivary nucleus of the rat: II. Reciprocal connections with the tectal longitudinal column. *Front. Neuroanat.* 5:1. doi: 10.3389/fnana.2011.00001

Received: 20 November 2012; accepted: 21 November 2012; published online: 06 December 2012.

*Citation: Merchán MA, Saldaña E and Oliver DL (2012) Auditory neuroanatomy: a sound foundation for sound processing. Front. Neuroanat. **6**:48. doi: 10.3389/fnana.2012.00048*

frontiers in
NEUROANATOMY

ORIGINAL RESEARCH ARTICLE
published: 23 June 2010
doi: 10.3389/fnana.2010.00027

A comparative study of age-related hearing loss in wild type and insulin-like growth factor I deficient mice

Raquel Riquelme[1†], Rafael Cediel[1,2,3†], Julio Contreras[1,2,4†], Lourdes Rodriguez-de la Rosa[1,2], Silvia Murillo-Cuesta[1,2], Catalina Hernandez-Sanchez[5,6], Jose M. Zubeldia[2,7], Sebastian Cerdan[1] and Isabel Varela-Nieto[1,2]*

[1] *Instituto de Investigaciones Biomedicas "Alberto Sols", CSIC-UAM, Madrid, Spain*
[2] *Centro de Investigación Biomédica en Red de Enfermedades Raras, Madrid, Spain*
[3] *Departamento de Medicina y Cirugia, Facultad de Veterinaria, Universidad Complutense de Madrid, Madrid, Spain*
[4] *Departamento de Anatomia, Facultad de Veterinaria, Universidad Complutense de Madrid, Madrid, Spain*
[5] *Centro de Investigaciones Biologicas, CSIC, Madrid, Spain*
[6] *Centro de Investigacion Biomedica en Red de Diabetes y Enfermedades Metabolicas, Madrid, Spain*
[7] *Servicio de Alergia, Hospital General Universitario Gregorio Marañon, Madrid, Spain*

Edited by:
Miguel A. Merchán, Universidad de Salamanca, Spain

Reviewed by:
Matthew C. Holley, The University of Sheffield, UK
Julie A. Chowen, Hospital Infantil Universitario Niño Jesús, Spain

***Correspondence:**
Isabel Varela-Nieto, Instituto de Investigaciones Biomédicas "Alberto Sols", CSIC-UAM, Arturo Duperier 4, 28029 Madrid, Spain.
e-mail: ivarela@iib.uam.es

†*Raquel Riquelme, Rafael Cediel and Julio Contreras have contributed equally to this work.*

Insulin-like growth factor-I (IGF-I) belongs to the family of insulin-related peptides that fulfils a key role during the late development of the nervous system. Human *IGF1* mutations cause profound deafness, poor growth and mental retardation. Accordingly, *Igf1*$^{-/-}$ null mice are dwarfs that have low survival rates, cochlear alterations and severe sensorineural deafness. Presbycusis (age-related hearing loss) is a common disorder associated with aging that causes social and cognitive problems. Aging is also associated with a decrease in circulating IGF-I levels and this reduction has been related to cognitive and brain alterations, although there is no information as yet regarding the relationship between presbycusis and IGF-I biodisponibility. Here we present a longitudinal study of wild type *Igf1*$^{+/+}$ and null *Igf1*$^{-/-}$ mice from 2 to 12 months of age comparing the temporal progression of several parameters: hearing, brain morphology, cochlear cytoarchitecture, insulin-related factors and IGF gene expression and IGF-I serum levels. Complementary invasive and non-invasive techniques were used, including auditory brainstem-evoked response (ABR) recordings and *in vivo* MRI brain imaging. *Igf1*$^{-/-}$ null mice presented profound deafness at all the ages studied, without any obvious worsening of hearing parameters with aging. *Igf1*$^{+/+}$ wild type mice suffered significant age-related hearing loss, their auditory thresholds and peak I latencies augmenting as they aged, in parallel with a decrease in the circulating levels of IGF-I. Accordingly, there was an age-related spiral ganglion degeneration in wild type mice that was not evident in the Igf1 null mice. However, the *Igf1*$^{-/-}$ null mice in turn developed a prematurely aged stria vascularis reminiscent of the diabetic strial phenotype. Our data indicate that IGF-I is required for the correct development and maintenance of hearing, supporting the idea that IGF-I-based therapies could contribute to prevent or ameliorate age-related hearing loss.

Keywords: aging, auditory brainstem responses, deafness, *Igf1*$^{-/-}$ null mouse, insulin-like factors, *in vivo* brain imaging, presbycusis, sensorineural deafness

INTRODUCTION

Neural development and the activity of the nervous system are regulated by a complex network of local and systemic factors. Insulin-like growth factors are fundamental modulators of nervous system structure, proliferation, growth, differentiation and metabolic demands during fetal and postnatal development (LeRoith, 2008). In mammals, the insulin gene family is comprised of three factors, insulin and the insulin-like growth factors I and II, which are recognized by three receptors (Varela-Nieto et al., 2007). These factors and receptors are expressed in neural cells during development in specific spatiotemporal patterns. Insulin-like growth factor-I (IGF-I) expression peaks in the nervous system during late embryonic and neonatal periods. While its expression is reduced in the adult but it is maintained in areas of high plasticity such as the olfactory bulb and the hippocampus (Aleman and Torres-Aleman, 2009; Aberg, 2010). In the adult brain, IGF-I is essential to maintain normal brain physiology and to promote neurogenesis (Sun and Bartke, 2007; Llorens-Martin et al., 2009). Partial or total IGF-I deficit is associated with severe alterations to the nervous system and disease. In humans, different mutations in the *IGF1* gene produce the functional loss of this protein, a genetic condition associated with the presence of severe intrauterine and postnatal growth impairment, microcephaly, mental retardation and sensorineural deafness, among other problems (Woods et al., 1997; Bonapace et al., 2003; Walenkamp et al., 2005; Walenkamp and Wit, 2007; Netchine et al., 2009). Indeed, sensorineural hearing loss is associated with poor growth rates in infancy and adolescence (Welch and Dawes, 2007), adult short stature (Barrenas et al., 2005) and Turner's syndrome (Barrenas et al., 2000).

Accordingly, mice lacking the *Igf1* gene suffer severe growth defects that are coupled to diminished survival and delayed nerve myelination, among other alterations (D'Ercole et al., 2002; Zeger et al., 2007). We have shown that cochlear gene expression is affected in the *Igf1*$^{-/-}$ null mouse, this organ displaying morphological

alterations (Camarero et al., 2001, 2002; Sanchez-Calderon et al., 2010) associated with bilateral hearing loss at the age of 1 month in these mice (Cediel et al., 2006).

In humans, IGF-I levels are highest during puberty and they decline with age (Leifke et al., 2000; Gomez, 2007). Aging is associated with a reduction in certain cognitive functions, such as hearing loss, and the onset of diseases like atherosclerosis and Alzheimer's disease (Dik et al., 2003; Watanabe et al., 2005). Similarly, changes in circulating IGF-I levels are also correlated with cognitive performance in older humans, as well as with the onset of age-related neurodegenerative diseases. For example, serum IGF-I levels are diminished in Alzheimer's disease and in other degenerative brain disorders, whereas there is an up-regulation after brain injury, suggesting that IGF-I is involved in neuroprotection (Torres-Aleman, 2008). Since recombinant human IGF-I therapy has been approved in humans to treat poor linear growth, several groups have contemplated the use of rhIGF-I in animal models of brain insults to explore its utility as a protective or neural repair agent (Bright et al., 2009; Torres-Aleman, 2010).

The genetic component of hearing loss is very diverse and involves hundreds of different genes (Dror and Avraham, 2009). Age-related hearing loss (ARHL – presbycusis) is the most common cause of adult auditory deficiency. It is usually a sensorineural hearing disorder in which hair cells and auditory nerve cells in the inner ear are damaged or lost. The genetic and molecular bases of susceptibility to ARHL are largely unknown and only a few genes that influence late onset or progressive hearing loss have been discovered (van Wijk et al., 2003; Zhu et al., 2003; Van Eyken et al., 2007; Dror and Avraham, 2009). However, many of these genes are likely to be linked to the aging and neurodegeneration related to susceptibility to oxidative stress, excitotoxicity and cell death (Holley, 2002).

IGF-I signaling regulates lifespan, apoptosis, sensitivity to oxidative stress and the programmed response to DNA damage across species (Christensen et al., 2006; Niedernhofer et al., 2006; Sanchez-Calderon et al., 2007; Narasimhan et al., 2009). Despite the importance of IGF-I in both aging and deafness, the influence of an IGF-I deficit in age-related hearing loss has not yet been studied. Here, we have carried out a longitudinal study of auditory function, cochlear and brain morphology, and IGF-I levels in wild type and *Igf1*$^{-/-}$ null mice to study the relationship between IGF-I deficit and hearing performance during aging. Our findings support the idea that IGF-I levels may predict premature age-related hearing loss.

MATERIALS AND METHODS

MOUSE HANDLING AND GENOTYPING

Heterozygous mice with a targeted disruption of the *Igf1* gene were bred and maintained on a hybrid MF1 and 129/sv mouse genetic background to increase nullizygous *Igf1* mutant survival (Liu et al., 1993). Null mouse mortality before adulthood is high, although between 20 and 30% survived. Both wild type and null mice were studied at the time points indicated to follow their progression from young adults (1 month) to aged mice (1 year). Mouse genotypes were identified using the REDExtract-N-Amp™Tissue PCR Kit (XNAT, Sigma) according to the manufacturer's instructions. The PCR was conducted with the following thermal cycle program: 1 cycle of 94°C for 10 min; 30 cycles of 94°C for 1 min, 59°C for 1 min, 72°C for 1 min; and a final elongation step at 72°C for 10 min. The wild type *Igf1* allele was detected using the 5′-GTCTAACACCAGCCCATTCTGATT-3′ and 5′-GACTCGATTTCACCCACTCGATCG-3′ primers, which produced a 250-bp amplicon. The neomycin cassette was detected using primers 5′-GCTTGGGTGGAGAGGCTATCC-3′ and 5′-CCAGCTCTTCAGCAATATCACGGG-3′, producing a 658-bp band. All primers were used simultaneously with no evidence of interference. All animal handling procedures were carried out in accordance with the European Council Directive (86/609/ECC) and with the approval of the Bioethics Committee of the CSIC.

AUDITORY BRAINSTEM RECORDING (ABR)

Mice were anesthetized by i.p. administration of ketamine (Ketolar © 50, Parke Davis Labs, 100 mg/kg) and xylazine (Rompum © 2%, Bayer Labs, 4 mg/kg), and they were maintained at 37°C throughout the testing period to avoid hypothermia. Both female and male mice were used; no sex-associated parameters were identified in this study. ABR was carried out in a sound-attenuating chamber in an electrically shielded room. Stimulus presentation, ABR amplification and data acquisition were performed with TDT System 3™ equipment and SigGeRPTM™ software (Tucker Davis Technologies, Alachua FL 32615), as described previously (Cediel et al., 2006). Briefly, an ES-1 electrostatic speaker was placed 10 cm from the animal's head and its hearing of different sound stimuli was tested. Tone-burst stimuli (4, 8, 16 and 32 kHz), with a 1-ms rise/fall time and a 5-ms plateau, or click stimuli (1–16 kHz) were applied. Stimuli were presented at decreasing intensities in steps from 90 dB SPL to 10 dB SPL until no waveform was obtained. The stimulus intensity was then increased in 5 dB SPL steps and two more responses were recorded in order to determine the auditory threshold. Auditory profiles were recorded using stainless steel needle electrodes (Spes Medica S.r.l., 20090 Milan, Italy) placed as follows: vertex-positive, mastoid area-negative and hip-ground. Responses were collected and amplified by a factor of 1×10^6, and the system was calibrated as recommended by the manufacturer with an ACO Pacific™ ¼ inch microphone connected to a specific TDT calibration module. We analyzed the following parameters obtained from waves registered during the ABR tests: auditory thresholds, latencies of peaks I–V and interpeak latencies.

MAGNETIC RESONANCE IMAGING (MRI) AND VOLUME ESTIMATES

MRI of the brains from wild type *Igf1*$^{+/+}$ and *Igf1*$^{-/-}$ null mice was performed with a 7-T Bruker PharmaScan™ 7T. T1 or T2 weighted images were acquired using the spin-echo sequence with values of TR = 300 ms/TE = 10 ms or TR = 2500 ms/TE = 60 ms, respectively. One day prior to the MRI experiments, animals were subcutaneously injected with a 30-mM solution of $MnCl_2$ at a dose of 0.4 mmol/kg body weight. Manganese is a positive MRI contrast agent that is taken up in brain regions with higher neuronal activity (McDaniel et al., 2001; Watanabe et al., 2004; Uchino et al., 2007). T1- and T2-weighted images were obtained every 1.1 mm and volume estimates were obtained according to the principle of Cavalieri (Gundersen and Jensen, 1987; Camarero et al., 2001). The Cavalieri principle of systematic sampling in combination with point counting is considered a reliable and efficient method to

estimate volumes in MRI (Jelsing et al., 2005). The points hitting the surface area of the cerebellum, brainstem, olfactory bulb and total brain were counted for each MRI section.

COCHLEAR MORPHOLOGY

Mice were anesthetized by i.p. injection of 0.12 mg/g ketamine hydrochloride and perfused transcardially with 4% paraformaldehyde in 0.1 M phosphate-buffered saline (PBS) [pH 7.4]. The animal's brain was removed and weighed after separating the medulla at the beginning of the spinal cord. Temporal bones were isolated, post-fixed for 1 day, decalcified in 0.3 M EDTA [pH 6.5] for 10 days and finally embedded in paraffin or gelatin. Paraffin sections (10 μm) or cryosections (20 μm) of temporal bones from *Igf1*$^{+/+}$ and *Igf1*$^{-/-}$ mice were processed for Nissl staining, hematoxylin/eosin or other techniques to study their cytoarchitecture. Serial sections were collected to detect the Na^+K^+-ATPase β2 isoform (rabbit anti-NaK-ATPase, Upstate Biotechnology, dilution 1:200) and Kir4.1 (rabbit anti-KCNJ10, Chemicon International, dilution 1:200), and phalloidin histochemistry was also performed (Alexa-488 conjugated phalloidin, Molecular Probes, Invitrogen, Carlsbad, CA, USA, dilution 1:100: Murillo-Cuesta et al., 2009, 2010a, 2010b; Sanchez-Calderon et al., 2010). For immunohistochemistry, paraffin sections were processed by the avidin-biotin-peroxidase (ABC) method using 3,3-DAB as chromogen.

RNA ISOLATION AND QUANTITATIVE RT-PCR

Total RNA was isolated using the Trizol reagent (Invitrogen) from the brainstem (BS), olfactory bulb (OB), cerebellum (CBL) and the remainder of the telencephalon-diencephalon (TD) of at least three to five postnatal day P90 mice per genotype. The purity of the RNA was assessed with an Agilent Bioanalyzer 2100 (Agilent Technologies). The reverse transcriptase reaction (RT) was typically performed on 5 μg RNA with the Superscript III Kit and random primers (Invitrogen). Quantitative PCR (RT-PCRq) was performed with the ABI Prism 7900HT Sequence Detection System (Applied Biosystems, Weiterstadt, Germany) using the TaqMan Universal PCR Master Mix, No AmpErase UNG (Applied Biosystems) and probes from the Universal Probe Library (UPL: Roche Applied Science). The primer sequences used and the respective UPL probes were: *Igf1* Universal ProbeLibrary probe: #67 (left primer CCGAGGGGCTTTTACTTCA and right primer CACAATGCCTGTCTGAGGTG); *Igf2* Universal ProbeLibrary probe: #40, (left primer CGCTTCAGTTTGTCTGTTCG and right primer GCAGCACTCTTCCACGATG; *Igf1r* Universal ProbeLibrary probe: #55 (left primer CCTGAAGAACCTTCGTCTCATC and right primer TGGTTGTCTAGGACATAGAAGGAGT); and 18 rRNA Universal ProbeLibrary probe: #70 (left primer TGCGAGTACTCAACACCAACA and right primer: TTCCTCAACACCACATGAGC). Assays were carried out according to the manufacturer's instructions and using the expression levels of eukaryotic 18S rRNA as a reference. The data are presented in arbitrary units.

DETERMINATION OF SERUM IGF-I LEVELS BY ELISA

The concentration of circulating IGF-I was measured in serum samples taken at the times indicated using a standard OCTEIA Rat/Mouse IGF-I kit (sensitivity 63 ng/ml and variability 4–8%) (IDS Ltd., Boldon, UK) according to the manufacturer's recommendations. Briefly, mouse serum samples were incubated with a reagent to inactivate binding proteins, and then diluted for the assay. These diluted samples were then incubated for 2 h at room temperature with a biotinylated polyclonal rabbit anti-rat IGF-I antiserum, in polystyrene microtiter wells coated with purified monoclonal anti-Rat IGF-I antibodies. The wells were washed and horseradish peroxidase-labeled avidin was added. After further washing, tetramethyl-benzidine was added to develop the color reaction and the absorbance of the developed reaction was read at dual wavelength (A450–A650 nm). ELISA data are expressed in ng/ml. Statistical comparisons of IGF-I sera levels between the different age groups were performed with a Mann-Whitney rank sum test using GraphPad InStat 3.06 (Software Inc., San Diego, CA, USA). The results were considered to be statistically significant when $P < 0.05$.

STATISTICAL ANALYSIS

Unless indicated otherwise, statistical analysis was performed with one-way ANOVA followed by Bonferroni adjustment as *post hoc* method, using SPSS™ 12 software. The results were considered significant at $P < 0.05$ and the data are presented as mean ± s.e.m. Where indicated the Pearson product moment correlation coefficient (r) was used as a measure of the linear dependence between two variables, r values are between +1 and −1 and 0 indicates no correlation. Specific records are represented with Origin™ 7.0 software.

RESULTS

TEMPORAL PATTERN OF AGE-RELATED HEARING LOSS IN *IGF1*$^{-/-}$ NULL AND *IGF1*$^{+/+}$ WILD TYPE MICE

Hearing was tested in mice using ABR evoked by transient click and tone-burst stimuli in 1, 3, 6, 9 and 12-month-old *Igf1*$^{-/-}$ null and *Igf1*$^{+/+}$ wild type littermates. The ABR curves obtained for the mice of either genotype showed the characteristic five peaks during the 10-ms post-stimulus period at all the ages studied (**Figure 1**). The ABR thresholds in response to click stimuli were 40 and 35 dB SPL in 1- and 3-month-old wild type mice, respectively, and they increased steadily to a mean value of 75 dB SPL in 1-year-old mice (**Figures 1 and 2A**). A different pattern of aging was reflected by the auditory click-ABR thresholds in the *Igf1*$^{-/-}$ null mice. Young, 1- to 3-month-old *Igf1*$^{-/-}$ mice were profoundly deaf and had a mean auditory threshold of 70 dB SPL, which remained constant as they aged since 1-year-old mice had a threshold of 75 dB SPL (**Figure 2A**). Hence, while the *Igf1*$^{+/+}$ mice had significantly lower auditory thresholds than the *Igf1*$^{-/-}$ mice at younger ages (1–6 months), as the mice aged their ABR thresholds converged to reach a similar value at 1 year of age (**Figure 2A**).

Pure tone audiograms were obtained in the same mice at the frequencies of 4, 8, 16 and 32 kHz using tone-burst ABR stimuli. At all ages tested, the general shape of the audiogram was similar in both mouse genotypes, and while the ABR peaks I to IV were clearly identified, peak V could only be distinguished in some recordings. The lowest threshold was obtained at 16 kHz, the best frequency for hearing in both the *Igf1*$^{+/+}$ and *Igf1*$^{-/-}$ mice at the ages studied (**Figure 2B**). At all four frequencies tested, an age-related increase in the thresholds was evident in *Igf1*$^{+/+}$ mice, whilst the audiograms

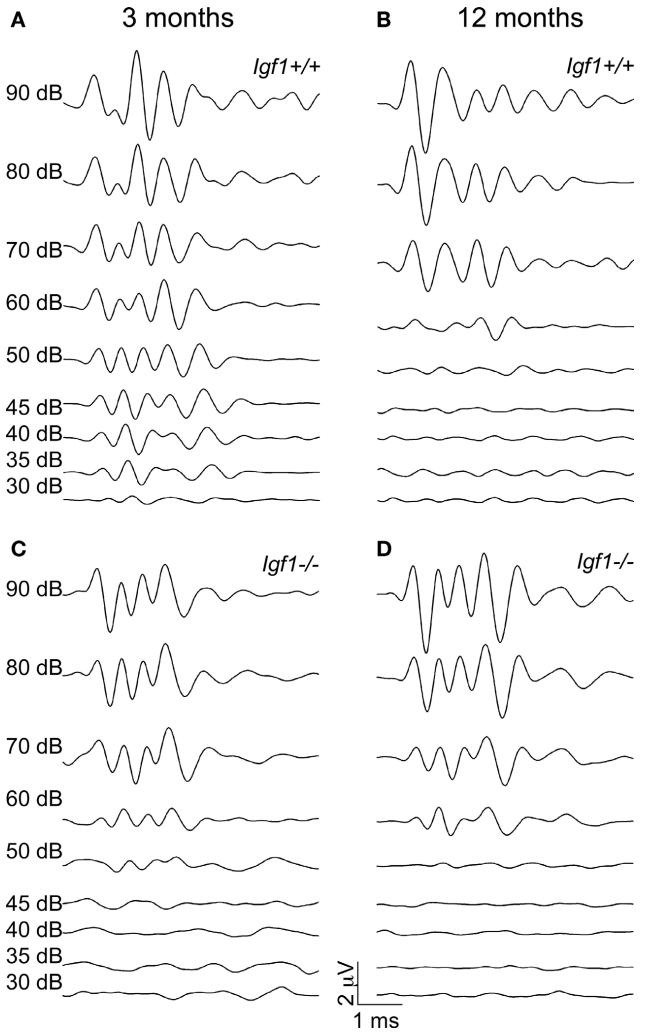

FIGURE 1 | ABR wave recordings from representative 3- and 12-month-old *Igf1*$^{+/+}$ wild type and *Igf1*$^{-/-}$ null mice. The waves represent the ABR in response to intensities of click stimuli decreasing from 90 dB SPL to 30 dB SPL of a representative mouse for each condition. **(A,B)** ABR waves from 3- **(A)** and 12- **(B)** month-old *Igf1*$^{+/+}$ mice. **(C,D)** ABR waves from 3- **(C)** and 12- **(D)** month-old *Igf1*$^{-/-}$ mice. In **(A)** and **(C)** the intensity of the stimulus for each response is indicated, and the range of intensities is the same in **(B)** and **(D)**.

from *Igf1*$^{-/-}$ null mice corresponded to profoundly deaf animals from the youngest age tested. Like the click stimuli, the tone-burst hearing thresholds were similar in 12-month-old *Igf1*$^{+/+}$ and *Igf1*$^{-/-}$ mice, both genotypes showing ABR thresholds corresponding to profound deafness, although a small number of *Igf1*$^{-/-}$ and wild type mice had hearing thresholds above the electrostatic speaker driver limit (90 dB SPL). The ABR data were further analyzed to calculate the percentage of mice in each of the five age groups tested with thresholds above the normal hearing threshold value of 50 dB SPL (**Figure 2C**). There was a progressive increase with age of the proportion of *Igf1*$^{+/+}$ mice with moderate to profound deafness, and while at 6 months of age 50% of the mice tested had auditory thresholds over 50 dB SPL, that figure reached 100% by 9 months of age. By contrast, the entire population of *Igf1*$^{-/-}$ mice presented hearing deficiencies at all the ages studied (**Figure 2C**).

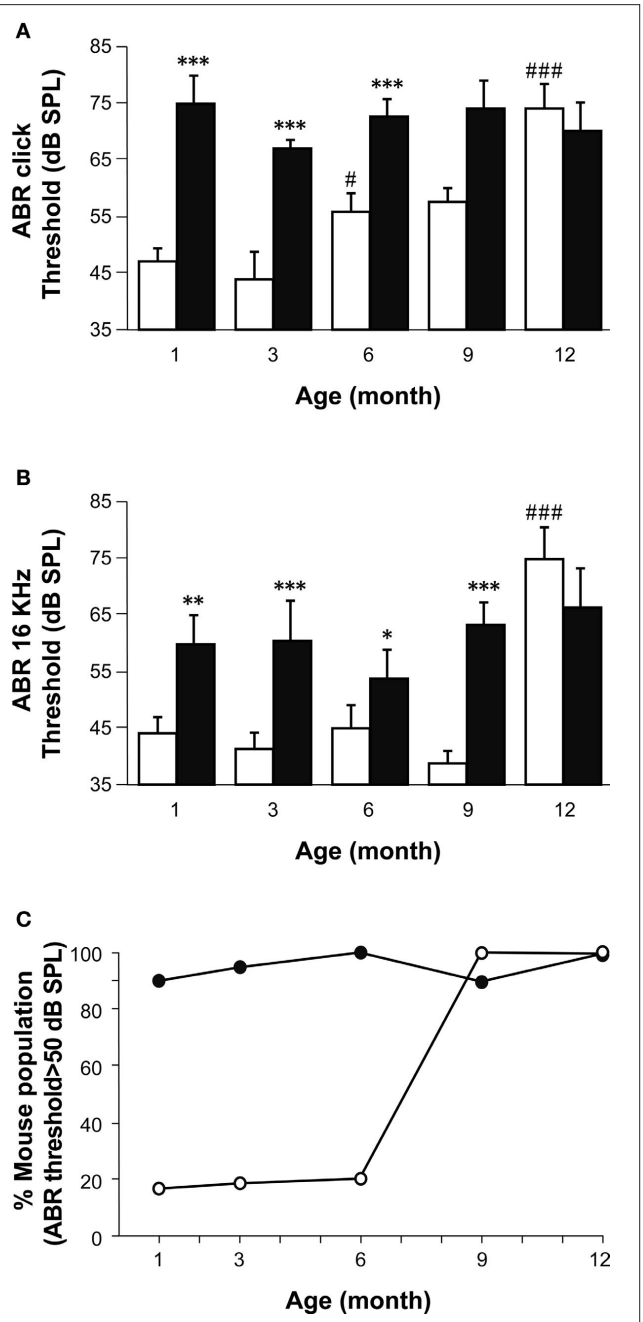

FIGURE 2 | A comparison of age-related hearing loss in *Igf1*$^{+/+}$ and *Igf1*$^{-/-}$ mice. (A) ABR thresholds in response to click stimulus in *Igf1*$^{+/+}$ (open bars) and *Igf1*$^{-/-}$ mice (closed bars) at different ages (1, 3, 6, 9 and 12 months). Wild type mice show an age-related increase in ABR thresholds, whereas the null mutant mice were deaf from the youngest age studied. **(B)** ABR responses to a 16 kHz stimuli were obtained at the same ages and showed a similar trait. **(C)** Percentage of individuals for each genotype showing ABR thresholds above normal hearing (≥50 dB SPL) at each of the ages studied. Wild type and null mice are represented as open and closed circles, respectively. Statistical analysis was performed with ANOVA and *post hoc* Bonferroni and Dunnet tests. Data are presented as the mean ± s.e.m; *indicates comparison between genotypes ***$P < 0.001$, **$P < 0.01$ and *$P < 0.05$; $^{\#}$indicates comparison between consecutive ages $^{\#\#\#}P < 0.001$. The number (*n*) of mice studied were 15, 13, 9, 8 and 7 wild type mice of 1, 3, 6, 9 and 12 month old, respectively; and 10, 11, 10, 6 and 5 null mice of the same ages.

The absolute ABR peak latencies increased with age in both *Igf1*$^{+/+}$ and *Igf1*$^{-/-}$ null mice (**Figure 3**). For the sake of simplicity and to reflect the ABR response in the peripheral auditory and central nervous system, data were only plotted for peaks I and IV (**Figures 3A,B**), the latencies of which can be considered as a readout of auditory nerve and auditory BS functions, respectively (Ponton et al., 1996). At all ages tested, the peak latencies were delayed in *Igf1*$^{-/-}$ mice when compared with wild type mice (**Figures 3A,B**). The Peak I latency differences between wild type and *Igf1*$^{-/-}$ mice became progressively shorter as the mice aged, differences that were significant ($P < 0.05$) at 3 and 6 months of age (**Figure 3**). The mean latency of peak IV followed a similar trend. Interestingly, mice of both genotypes showed a steeper increase in the peak I and IV latencies between 3 and 6 months of age. The age-related increase

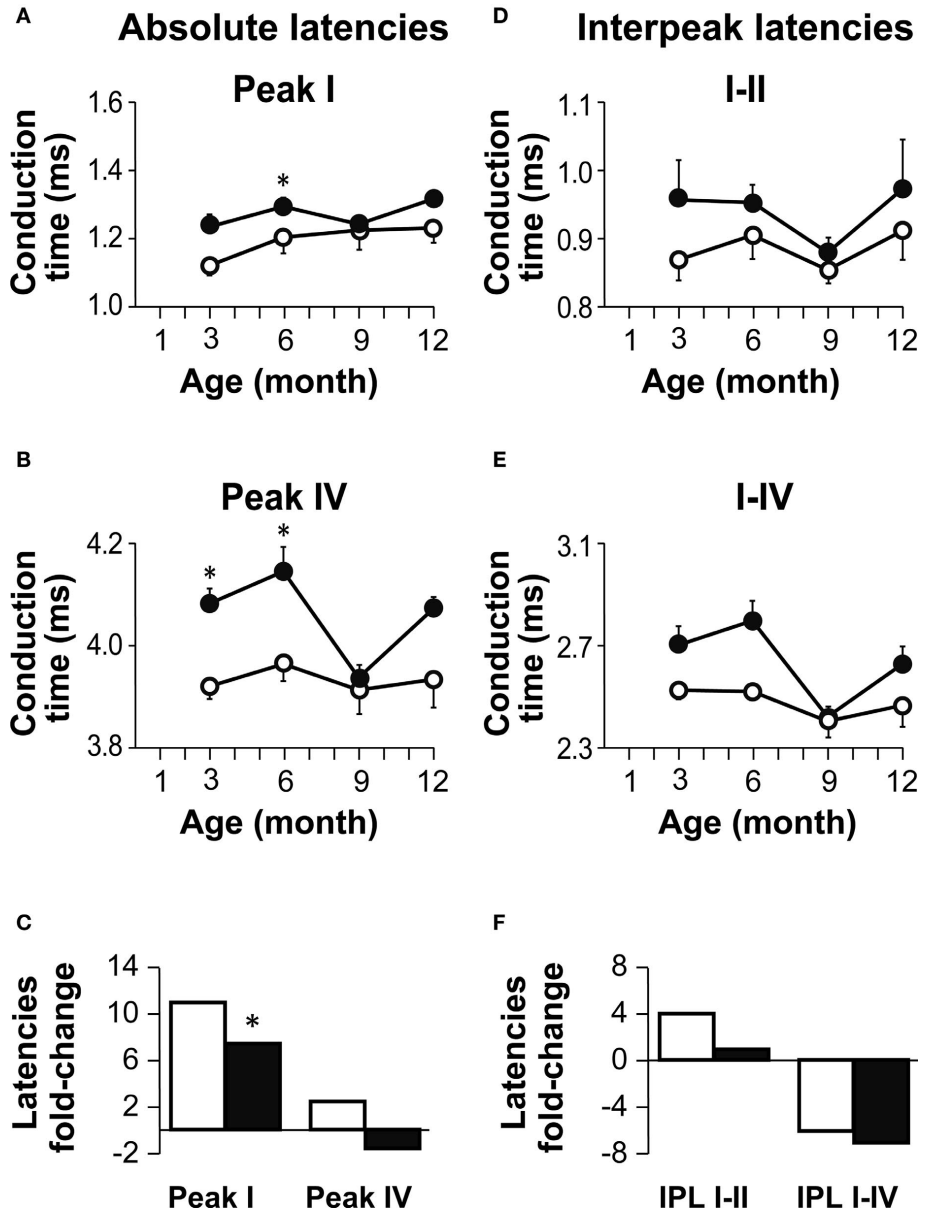

FIGURE 3 | Age-related changes in absolute and interpeak latencies in both genotypes. (A,B) Absolute Peak I **(A)** and peak IV **(B)** latencies obtained at 80 dB SPL. Absolute latencies are plotted for *Igf1*$^{+/+}$ (open circles) and *Igf1*$^{-/-}$ mice (closed circles) aged from 3 to 12 month old. **(C)** Percentage delay in latency with aging. Open and closed bars indicate wild type and null mice, respectively. The bars represent the percentage latency increase from 3 to 12 months of age for peaks I (bars to the left) and IV (bars to the right). The asterisk indicates that the 11% difference in peak I latency between 3- and 12-month-old wild type mice is significant ($P < 0.05$). Data are presented as the mean ± s.e.m. **(D,E)** Interpeak latencies (IPL) I–II **(D)** and I–IV **(E)** obtained at 80 dB SPL for *Igf1*$^{+/+}$ (open circles) and *Igf1*$^{-/-}$ mice (closed circles) aged from 3 to 12 months old. **(F)** Percentage IPL increases with aging. As in **(C)**, for wild type (open bars) and null mice (closed bars), the IPL I–II is shown by the bars on the left and IPL I–IV in the bars on the right. The number (*n*) of mice studied was: 7, 9, 4 and 5 wild type and 6, 6, 6 and 3 null mice of 3, 6, 9 and 12 month old, respectively.

in latency did not affect peaks I and IV in the same way, nor were the changes similar in *Igf1*$^{+/+}$ and *Igf1*$^{-/-}$ mice. Wild type *Igf1*$^{+/+}$ mice experienced a larger age-related change in latency between 3 to 12 months of age, that was 11% for peak I ($P < 0.05$). By contrast, the peak I latency did not increase significantly in *Igf1*$^{-/-}$ mice over the same period. Peak IV presented smaller age-related changes in both genotypes (**Figure 3C**).

The interpeak latencies (IPL) reflected the transmission of auditory information along the auditory pathway. The interval between peaks I and II is assumed to represent the conduction time in the auditory nerve axons and therefore, this value provides information about the peripheral auditory system. On the other hand, the value between peaks I and IV reflect axonal transmission along the BS, offering information on the central auditory system. These IPL were longer in *Igf1*$^{-/-}$ mice than in *Igf1*$^{+/+}$ mice at all the ages tested (**Figures 3D,E**), although in neither genotype were significant changes in the IPL evident at any age (**Figure 3F**).

To further compare the temporal profile of hearing, the relationship between age and auditory thresholds was assessed for both mouse genotypes using product moment Pearson correlation coefficients. A clear correlation was observed between both these parameters in the *Igf1*$^{+/+}$ animals (**Figure 4A**) but not in the *Igf1*$^{-/-}$ mice (**Figure 4B**). The correlation was less clear between aging and the increase in peak I latency as indicated by the product moment Pearson correlation coefficient, which was not statistically significant in *Igf1*$^{+/+}$ wild type and *Igf1*$^{-/-}$ null mice (**Figures 4C,D**) Since both the absolute latency for peak I and the auditory thresholds increased with age, the peak latency increase could be caused by the increase in the auditory threshold and not by aging. Product moment Pearson correlation coefficients were obtained between data pairs of auditory thresholds and absolute peak I latencies values for both genotypes at all the ages studied (**Figures 4E,F**). Accordingly, a significant correlation between auditory thresholds and cochlear nerve time conductions were observed in *Igf1*$^{+/+}$ (**Figure 4E**) but not in *Igf1*$^{-/-}$ mice (**Figure 4F**).

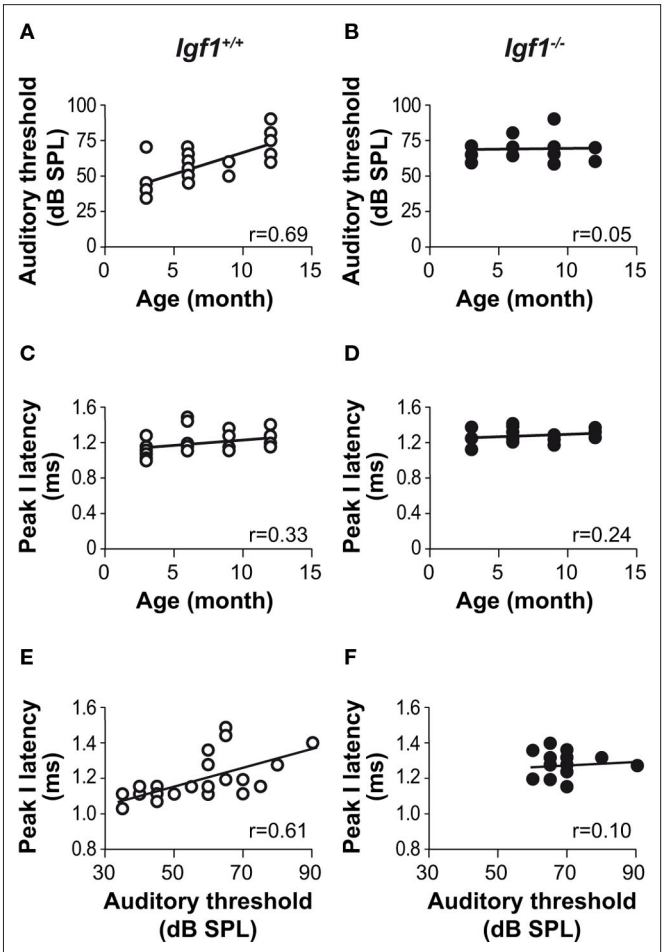

FIGURE 4 | Correlations between auditory thresholds and peak response latencies with aging and genotype. Product moment Pearson correlation coefficients were calculated for the pairs of parameters indicated. A clear correlation was evident between ABR thresholds and age in the *Igf1*$^{+/+}$ mice [open circles; **(A)** $P < 0.05$; $n = 24$; $r = 0.69$] but not in the *Igf1*$^{-/-}$ mice [closed circles; **(B)** ns; $n = 19$; $r = 0.05$]. The absolute peak I latency was weakly correlated with age in both *Igf1*$^{+/+}$ [**(C)** $P < 0.1$; $n = 24$; $r = 0.33$] and *Igf1*$^{-/-}$ [**(D)** $P < 0.25$; $n = 19$; $r = 0.24$] mice. The Pearson product moment correlation coefficient between peak I absolute latencies and auditory thresholds at different ages in *Igf1*$^{+/+}$ mice was statistically significant ($P < 0.05$) [**(E)** $P < 0.05$; $n = 24$; $r = 0.61$]. The same correlation in *Igf1*$^{-/-}$ mice was not statistically significant. [**(F)** ns; $n = 19$; $r = 0.09$].

AGE-RELATED REDUCTION IN THE DENSITY OF SPIRAL GANGLION NEURONS IN *IGF1*$^{+/+}$ WILD TYPE MICE AND DEGENERATION OF THE STRIA VASCULARIS IN THE *IGF1*$^{-/-}$ NULL MICE

Important cochlear alterations were evident in 1-month-old *Igf1*$^{-/-}$ mice that included reduced cochlear volume, neuronal loss, hypomyelinization, an immature tectorial membrane and a general delay in cell differentiation with increased presence of embryonic cell markers (Camarero et al., 2001, 2002; Sanchez-Calderon et al., 2010). Here, the morphology of the cochlea in 3-, 7- and 12-month-old *Igf1*$^{+/+}$ and *Igf1*$^{-/-}$ mice was analyzed. Generally, the cochlear cytoarchitecture was similar in both genotypes at the ages studied, although the differences reported in cochlear size were maintained between both mouse genotypes. Damage to the cochleae was evident in individual mice, although in general most mice had intact inner and outer hair cells, and the general cochlear structure was preserved until 1 year of age, the oldest mice studied (**Figures 5A,B**; **Figure S1** in Supplementary Material). By contrast, there were fewer spiral ganglion neurons in 1-year old than in the younger *Igf1*$^{+/+}$ mice (**Figures 5C,E,G**), resulting in a similar density of neurons in 1-year-old mice from both genotypes (**Figures 5C–H**). Hence, *Igf1*$^{+/+}$ mice suffer a loss of spiral ganglion neurons that progressed with aging, an alteration that might represent the anatomical basis for the elevation in the age-related hearing threshold and the delay in the absolute peak I latency. The morphology of the cochlea from *Igf1*$^{-/-}$ null mice did not change with age and the altered postnatal traits already reported persisted, in agreement with the functional ABR results. Indeed, there was a progressive degeneration of the stria vascularis in *Igf1*$^{-/-}$ mice from 3 months of age, but not in control wild type mice, which was shorter, thicker and with aberrant vascularization including dilated intra-strial capillaries when compared with that in the control *Igf1*$^{+/+}$ mice (**Figures 6A–H**). Kir4.1 (**Figures 6I–K**) and Na-K-ATPase levels (compare **Figures 6A,E** with **Figures 6B,F**) in 3- and 12-month-old *Igf1*$^{-/-}$ null mice reflected the important alterations in the stria vascularis.

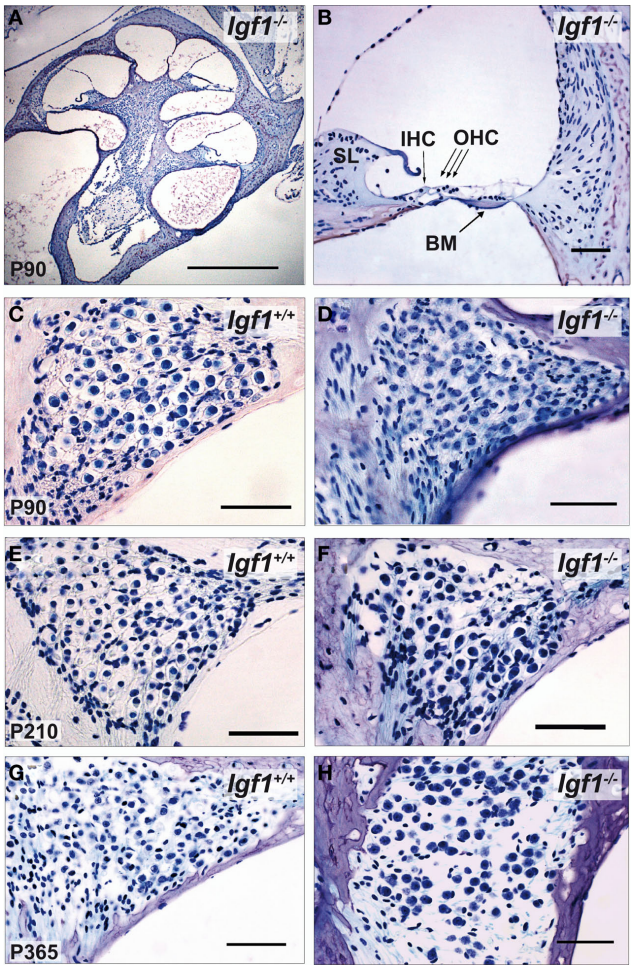

FIGURE 5 | Comparative study of cochlear morphology with aging in *Igf1*$^{+/+}$ wild type and *Igf1*$^{-/-}$ null mice. (A,B) Cochlear cross-section and close up of the cochlear basal turn in a representative 3-month-old null mice. The disposition of the cells in the organ of Corti is apparently normal. IHC: inner hair cell; OHC: outer hair cells; BM: basilar membrane. **(C–H)** Comparison in both genotypes of the spiral ganglion morphology and of the neuronal density in mice at the ages studied. The neuronal density decreased in the aged spiral ganglion, such that at the older ages studied the cochlear ganglia was morphologically similar in both genotypes. Some specimens displayed heavy hair cell loss at this age, which was correlated with the increase in hearing thresholds (data not shown). Scale bar 50 μm [0.5 mm in **(A)**].

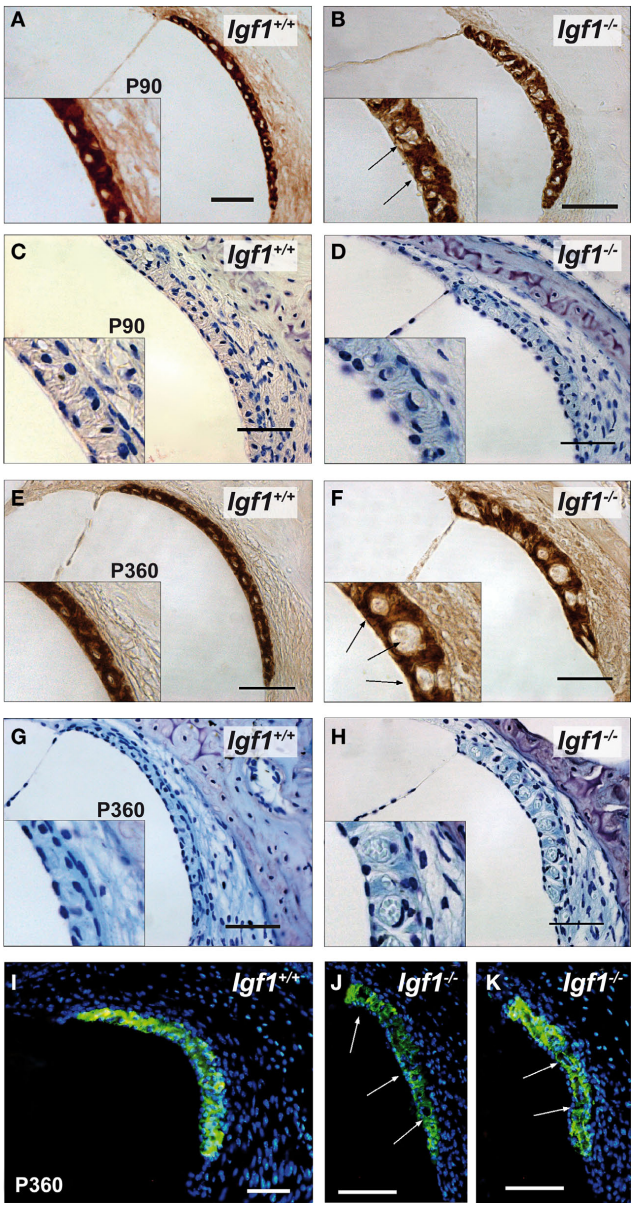

FIGURE 6 | Comparative study of the stria vascularis with the aging of *Igf1*$^{+/+}$ wild type and *Igf1*$^{-/-}$ null mice. Na-K-ATPase **(A,B,E,F)** and cresyl violet staining **(C,D,G,H)** expression in the stria vascularis of 3- **(A–D)** and 12-month-old mice **(E–H)** showing the morphological differences associated with the aging of each genotype. The stria vascularis in the *Igf1*$^{-/-}$ mice had an abnormal morphology, it was shorter and thicker, and with evident dilation of the vascular spaces (arrows). Kir4.1 (KCNJ10) expression **(I–K)** in the stria vascularis of aged null mice was altered and there was a relative loss of expression in the stria and sacular dilations. Four to six mice per condition were analyzed. Scale bar 50 μm.

AGE-RELATED CHANGES IN BODY WEIGHT, CIRCULATING IGF-I LEVELS AND BRAIN WEIGHT

The body weight of *Igf1*$^{+/+}$ and *Igf1*$^{-/-}$ null mice was measured at 1, 3, 6 and 12 months of age and both genotypes experienced an age-related increase in body weight. As expected, at all the ages studied the *Igf1*$^{-/-}$ mice were lighter than the *Igf1*$^{+/+}$ mice (**Figure 7A**). The greatest increase in body weight occurred at younger ages, between 1 and 3 months of age in both genotypes, whereas from 3 to 9 months of age their body weight reached a plateau and showed only minor increases. Indeed, there was a tendency to lose weight between 9 and 12 months in the wild type mice. Moreover, a significant correlation was identified between body weight and age.

Sera from wild type and null mice were collected at several times between 1 and 10 months of age to analyze the circulating IGF-I levels using a specific ELISA assay. An age-related decline in IGF-I was observed in *Igf1*$^{+/+}$ mice (**Figure 7B**), from the initial IGF-I levels in 1-month-old mice (1004 ± 220 ng/ml) to those in 10-month-old mice (517 ± 151 ng/ml, $P < 0.05$). These progressive age-related

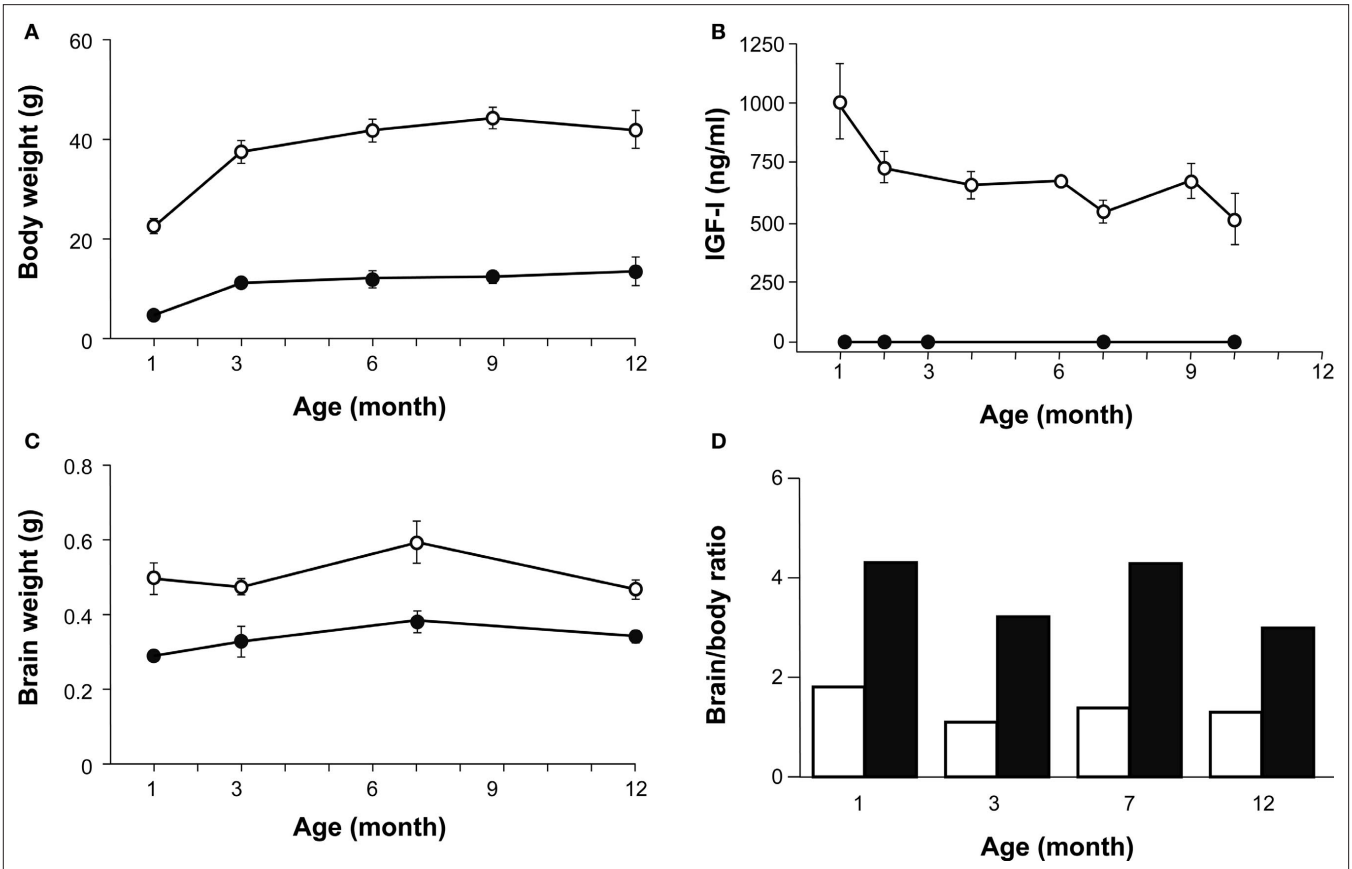

FIGURE 7 | A comparison of age-related changes in IGF-I levels, and body and brain weight in both genotypes. (A) Body weight of *Igf1*$^{+/+}$ (open circles) and *Igf1*$^{-/-}$ null (closed circles) mice was measured at 1, 3, 6 and 12 months of age. Statistical analysis in **(A)** and **(C)** was performed with ANOVA and *post hoc* Bonferroni and Dunnet tests. Data are presented as the mean ± s.e.m. Both genotypes presented a significant difference at all the ages studied ($P < 0.001$) and an age-related increase in body weight. **(B)** The serum IGF-I levels were followed during aging in *Igf1*$^{+/+}$ and *Igf1*$^{-/-}$ mice in parallel. An age-related decline in serum IGF-I was observed in wild type mice (open circles) whereas no IGF-I could be detected at any time in the null mice (closed circles). Data are given in ng/ml as median ± s.e.m. At least six to eight mice were studied per group. **(C)** Brain weight measurements did not change significantly as the mice aged, although there was a significant difference between the two genotypes at the ages studied ($P < 0.05$). **(D)** The brain/body weight ratio was calculated for each age group of *Igf1*$^{+/+}$ wild type (black bars) and *Igf1*$^{-/-}$ null mice (white bars). This ratio did not vary with age in any genotype. The number (*n*) of mice studied in **(A)**, **(C)** and **(D)** were 19, 7, 9, 8 and 5 wild type and 8, 6, 7, 6 and 5 null mice of 1, 3, 6, 9 and 12 month old, respectively.

decline in serum IGF-I levels mirrored the changes in body weight. By contrast, no detectable levels of IGF-I were measured at any time in the *Igf1*$^{-/-}$ null mice. IGF-I levels decline data were compared with those of increasing ABR thresholds (**Figure 2A**) in the different groups of wild type mice studied between 1 and 10 months. This comparison strongly suggest that there is a correlation between both parameters (Pearson $r = -0.33$; $n = 35$; $P < 0.05$).

Unlike body weight, brain weight measurements did not noticeably change as the animals aged, neither in *Igf1*$^{+/+}$ nor *Igf1*$^{-/-}$ null mice (**Figure 7C**). The brain/body weight ratio was calculated for each age group of wild type and null mice and the ratio was higher for *Igf1*$^{-/-}$ null mice than for wild type mice (**Figure 7D**). At each age tested, the *Igf1*$^{+/+}$ mouse brain represented less than 2% of the total body weight, whilst the *Igf1*$^{-/-}$ null mouse brain represented roughly 4% of their total body weight. Aging did not seem to affect these ratios, although the results indicated that there was an age-related tendency towards a small reduction in the brain to body weight ratio.

AGE-RELATED AND GENOTYPE-DEPENDENT BRAIN MORPHOLOGY

In vivo serial MRI of the brain has provided valuable insights into the changes associated with a range of neurodegenerative and aging conditions (Liu et al., 2003; Paul et al., 2009). MRI is a non-invasive procedure that allowed both mouse populations to be studied in parallel with the hearing tests to further study the brain areas participating in auditory processing (**Figures 8A–C**). Stereological procedures were used to calculate areas and volumes from the MRI images, and to analyze their progress over time (**Figure 8B** and **Table 1**). The gross brain morphology was similar between wild type and null mice, taking into account the difference in size, and except for the OB (**Figure S2** in Supplementary Material), all the main brain regions that could be observed in the wild type mice were also observed in the null mice (**Figure 8C**). Brain images were obtained from 3-, 6-, 9- and 12-month-old wild type and null mice, and the volumes of the whole brain and selected brain parts were obtained. Since it was not possible to identify the auditory BS, the whole BS was considered as an individual part, and this region

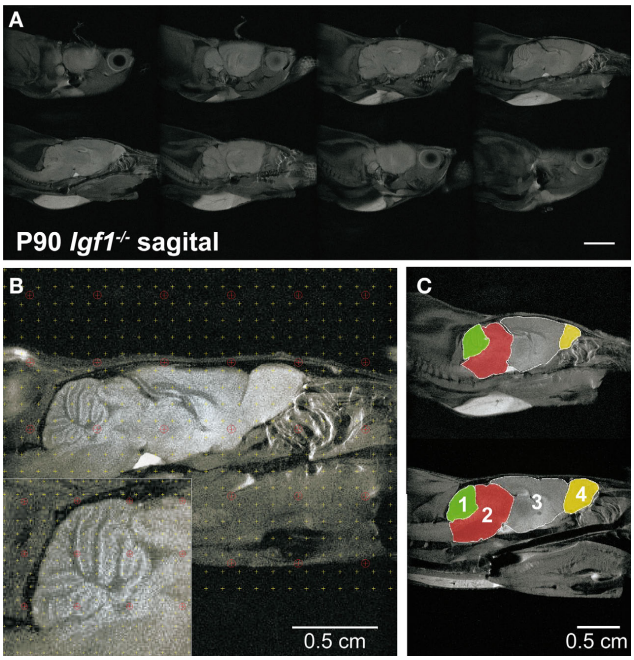

FIGURE 8 | *In vivo* brain images of $Igf1^{+/+}$ wild type and $Igf1^{-/-}$ null mice. (A) Complete series of brain slices in the sagittal plane of a representative 3-month-old $Igf1^{-/-}$ null mouse. **(B)** Sagittal MRI T2 weighted image of a representative 3-month-old wild type mouse showing the stereological grid that was randomly overlaid on each slide to estimate the volume. The inset shows the specific grid used to estimate the volume of specific brain areas, such as the cerebellum. **(C)** Comparison of the selected brain areas of $Igf1^{-/-}$ and $Igf1^{+/+}$ mice: cerebellum (1), brainstem (2), diencephalon-telencephalon (3) and olfactory bulb (4). Note the reduced olfactory bulb in the deficient mice (yellow).

was considered as a representative region for auditory information processing. The CBL and the OB were included for comparison (**Figure 8C**). The relative BS volumes were similar in $Igf1^{+/+}$ and $Igf1^{-/-}$ null mice, and these volumes did not changed with aging in either genotype (**Table 1**). No other morphological alterations were observed by MRI at the BS level. A different orientation of the cochlea with respect to the brain was observed when comparing wild type and null mice (**Figures S2A,B** in Supplementary Material). At all the ages studied, the OB was the brain structure that showed the most important differences between wild type and null mice, as well as an aberrant laminar structure in the $Igf1^{-/-}$ null mouse (**Figures S2C,D** in Supplementary Material; **Table 1**). Finally, there was a clear alteration of the ventricular system in the null mouse brain (**Figures S2E,F** in Supplementary Material). No evident age-related changes in brain morphology were observed in either genotype (**Table 1**).

The data presented above suggest that different brain areas may have distinct expression of IGF-I or that they may possess distinct compensatory mechanisms. Indeed, the *Igf1* gene is widely expressed in the mouse brain, albeit with regional variations in the levels of expression. Here, we quantified the *Igf1* mRNA levels in four regions of the adult P90 mouse brain by quantitative RT-PCR. The highest levels of *Igf1* expression were in the OB (**Figure S3** in Supplementary Material) where there were 5-fold more *Igf1* transcripts than in the BS, and 10-fold more than in the TD (excluding the OB) and CBL. Null mouse brain did not express *Igf1* as expected (data not shown). Since brain size is less strongly affected by *Igf1* deletion than the size of the rest of the body, we examined the possible compensatory effect of up-regulating *Igf1r* and/or *Igf2* expression in the brain. *Igf1r* and *Igf2* mRNA expression were analyzed by RT-qPCR in the four brain regions and they were not significantly different in $Igf1^{-/-}$ null mice than in the wild type mice (**Figures 9A,B**).

DISCUSSION

IGF-I is a member of the family of insulin-related peptides that fulfils a prominent role in the development of the central nervous system and in adult neurogenesis. Circulating levels of IGF-I decrease with age, this reduction being related to age-associated cognitive and brain alterations. Congenital mutations in the gene coding for IGF-I cause sensorineural deafness in mice and men, although it is not known whether hearing loss in the elderly population is related to the age-dependent reduction in IGF-I levels.

It is shown here that $Igf1^{+/+}$ wild type MF1/129/sv mice suffer age-related progressive elevation in hearing thresholds, which by the age of 1 year old reaches that presented at birth by the $Igf1^{-/-}$ null MF1/129/sv mouse. From 1 to 12 months of age, the click-ABR thresholds of $Igf1^{+/+}$ mice experienced a progressive elevation of 30 dB SPL, which was paralleled by the progressive decrease in circulating IGF-I levels. The $Igf1^{-/-}$ null mouse has elevated auditory thresholds, and morphological alterations in the auditory receptor and spiral ganglion could account for this functional disorder (Camarero et al., 2001; Cediel et al., 2006; Sanchez-Calderon et al., 2010).

Age-related hearing loss is characterized by a progressive deterioration of hearing sensitivity with increasing age, and it has been studied in mice of different strains (Zheng et al., 1999; Ouagazzal et al., 2006; Niu et al., 2007). The mice used in the present study are on a hybrid genetic background of MF1 and 129/sv mouse strains, and they present mild hearing loss when compared to mice on other genetic backgrounds. By contrast, the 1-month-old $Igf1^{-/-}$ null mouse is already deaf and does not present significant threshold variations as it ages.

In both $Igf1^{+/+}$ and $Igf1^{-/-}$ null mice the absolute latencies for waves I through IV show age-related increments, although the increment was larger in the $Igf1^{+/+}$ than in the $Igf1^{-/-}$ null mice, especially the peak I latency. These data confirm that the increase in peak I latency is a trait associated with hearing loss in the mouse, as reported in other mammals such as man (Rosenhall et al., 1986; Cooper et al., 1990; Martini et al., 1990; Ingham et al., 1998; Torre and Fowler, 2000; Burkard and Sims, 2002). However, the effect of aging on IPL is not yet clear. Many authors have reported that the interpeak I–V latency is prolonged in the elderly (Rosenhall et al., 1986; Cooper et al., 1990; Fraenkel et al., 2003), whilst others argue that aging is not associated with a delay in the central conduction time (Martini et al., 1990; Burkard and Sims, 2002). Neither the $Igf1^{-/-}$ nor the wild type mouse show significant variations in IPL, since IPL I–II shows a small increase and IPL I–IV a small compensatory decrease, neither of which are significant. These data suggest that aging has no effect on the central conduction time, in contrast with the acute impact of aging on auditory receptor

Table 1 | Body and brain of *Igf1*$^{-/-}$ and *Igf1*$^{+/+}$ mice with age.

	One month		Three months		Seven months		One year	
	WT	**KO**	**WT**	**KO**	**WT**	**KO**	**WT**	**KO**
(A)								
Body weight (g)	27.1 ± 3.2	6.7 ± 1.2	42.8 ± 5.8	10.4 ± 1.8	42.4 ± 5.5	8.8 ± 4.6	34.6 ± 4.5	10.8 ± 3.1
Change (%)	–75%		–76%		–79%		–69%	
Brain weight (g)	0.49 ± 0.04	0.29 ± 0.01	0.47 ± 0.02	0.33 ± 0.04	0.59 ± 0.06	0.38 ± 0.03	0.47 ± 0.03	0.33 ± 3.2
Change (%)	–41%		–30%		–35%		–30%	
Brain/body ratio	1.8	4.3	1.1	3.1	1.4	4.3	1.3	3
Change (%)	239%		287%		309%		223%	

	Three months		Seven months		One year	
	WT	**KO**	**WT**	**KO**	**WT**	**KO**
(B)						
Total brain	522 ± 32	322 ± 13	503 ± 37	316 ± 35	469 ± 24	324 ± 29
	100%	100%	100%	100%	100%	100%
Cerebellum	63.5 ± 2.9	41.4 ± 2.3	62.3 ± 8.6	42.7 ± 2.2	59.2 ± 4.2	44.2 ± 3.8
Relative volume	12%	13%	12%	13%	12%	13%
Brainstem	91.6 ± 5.6	58.8 ± 2.3	91.1 ± 6.6	59.2 ± 5	86.7 ± 3.5	52.3 ± 4.4
Relative volume	17%	18%	18%	19%	18%	16%
Olfactory bulb	29.5 ± 2.5	10.7 ± 0.9	27.2 ± 2.6	12.6 ± 1.42	27 ± 2.3	13.4 ± 1.7
Relative volume	5%	3%	5%	4%	6%	4%

(A) *Body and brain weights of Igf1*$^{-/-}$ *(KO) and Igf1*$^{+/+}$ *(WT) mice with aging. Brains were weighed after cutting off the medulla at the beginning of spinal cord. The values are represented as the mean ± s.e.m. of at least four to six animals from each condition. An statistically significant difference between both genotypes (P < 0.001) was found at all the ages studied. Change (%) indicates the % difference of each parameter between both genotypes, 100% corresponds to the wild type value.*

(B) *Volume of total brain and of different brain areas in Igf1*$^{-/-}$ *(KO) and Igf1*$^{+/+}$ *(WT) mice were estimated from MRI images taken in vivo at different ages. The volume estimates were obtained by stereological analysis according to the Cavalieri principle (Gundersen and Jensen, 1987). Volumes are expressed in mm*^{3} *as the mean ± s.e.m. of at least five animals for each genotype and age.*

Relative volume indicates the % of the total brain volume that each brain area represents, being 100% the brain volume of each genotype at each age studied. When genotypes were compared, a reduction in the olfactory bulb of the Igf1$^{-/-}$ *deficient mice but not in the other structures was observed.*

function that is associated with a loss in spiral ganglion cell density. Age-related modification of ABR parameters has been associated with increased auditory thresholds, whereas a tendency toward increased ABR latencies has only been reported when threshold increases were considerable (Hunter and Willott, 1987). Our data support these concepts and indeed, the correlation analysis shows that the increase in ABR latency with age is strongly related to the elevated thresholds.

The auditory alterations detected by physiological procedures have morphological substrates. We previously showed that the cochlea of 1-month-old *Igf1*$^{-/-}$ mice have morphological alterations that correlate with their elevated auditory thresholds (Camarero et al., 2001, 2002; Cediel et al., 2006). When compared to the wild type, *Igf1*$^{-/-}$ null mice have smaller cochlea and cochlear ganglion, with a significant decrease in the number and average size of cochlear ganglion neurons (Camarero et al., 2001, 2002). With aging, the altered cochlear morphology in *Igf1*$^{-/-}$ mice persists yet neuronal loss does not progress, indicating that the early phenotype of neuronal loss was not premature neurodegeneration but rather a failure in the late developmental program. A transcriptome study of the null mouse cochlea confirmed that the differentiation of neural cells and structures is delayed at birth (Sanchez-Calderon et al., 2010). However, the *Igf1*$^{+/+}$ cochlear ganglion suffers age-related neuronal loss, reaching levels that are similar to that of the neonatal *Igf1*$^{-/-}$ mice. These data suggest that a subpopulation of auditory neurons depend on IGF-I for their final differentiation and/or for their survival, although most adult cochlear neurons can survive in the absence of this factor. Accordingly, cochlear neurons of *Igf1*$^{+/+}$ mice die as they age with a time-course that follows the decay in circulating IGF-I levels.

Cochlear degeneration has been associated with a down-regulation of IGF-I levels and aging in other models of ARHL (Riva et al., 2007). No hair cell loss was evident in either genotype at the ages studied but interestingly, a lack of IGF-I caused long-term degeneration in the stria vascularis, the metabolic center of the cochlea. This phenomenon is reminiscent of the diabetic cochlear phenotype also seen in the insulin receptor substrate 2 null mice (unpublished observation). Degeneration of the stria vascularis is one of the most prominent aspects in the pathophysiology of presbycusis in several species (Schulte and Schmiedt, 1992; Spicer and Schulte, 2002; Spiess et al., 2002). The variations in absolute latency with age show that the increase in latency is age-related in both genotypes and thus, the impact of IGF-I deficiency in the central auditory pathways was further explored in a longitudinal *in vivo* brain MRI study. Several important alterations were observed and since the gross morphology of the null mouse brain was maintained, brain size was less affected by the loss of IGF-I than body weight, and no differences were associated

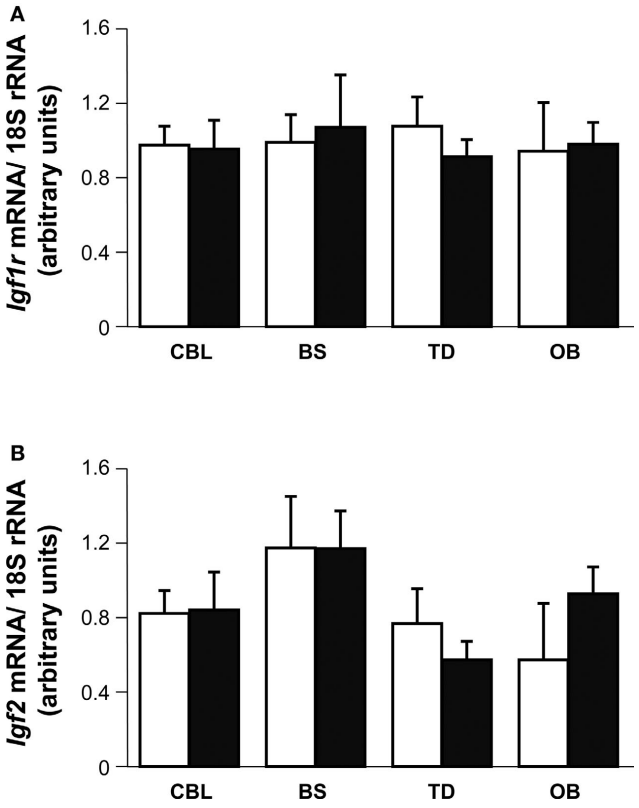

FIGURE 9 | Brain distribution and expression of *Igf2* and *Igf1r*. *Igf1r* **(A)** and *Igf2* **(B)** mRNA levels were measured by quantitative RT-PCR of RNA from the indicated mouse brain regions and normalized to the levels of the 18S ribosomal RNA 3–5 mice per genotype were used. The results represent the mean ± s.d. Brainstem (BS), olfactory bulb (OB), cerebellum (CBL) and the remainder of the telencephalon-diencephalon (TD). Open and closed bars indicate $Igf1^{+/+}$ and $Igf1^{-/-}$ mice, respectively.

with aging. In man, several aging related changes in MRI brain volume have been seen, although we failed to detect such changes in the mice studied here (Liu et al., 2003; Paul et al., 2009).

Age-related ABR and morphological alterations to the cochlea were clear in the $Igf1^{+/+}$ but not in the $Igf1^{-/-}$ mice, suggesting that the decreasing levels of IGF-I during aging of wild type mice play a role in the rising thresholds and thus, in promoting the delay in latency (Leifke et al., 2000; Gomez, 2007). The $Igf1^{-/-}$ null mouse shows hearing loss at young ages (ABR threshold 70 dB SPL), which persisted throughout the 1-year period studied here and that did not deteriorate with age as in the $Igf1^{+/+}$ mice. It might be speculated that the lack of IGF-I itself has a protective role since low IGF1R activity has been associated with caloric restriction, delayed aging and extended lifespan in several species, including mice and humans (Weindruch and Sohal, 1997; Shimokawa et al., 2003; Bartke, 2005; Berryman et al., 2008; Salminen and Kaarniranta, 2010). In mice, caloric restriction prevents late onset presbycusis that would otherwise occur in aging animals, and it also protects cochlear elements from degenerating such as spiral ganglion cells (Someya et al., 2007). Alternatively, the presence of compensatory mechanisms in chronic IGF-I deficiency could explain the persistence of the hearing phenotype in the $Igf1^{-/-}$ null mouse as it ages. No changes in the expression of related factors (e.g., insulin and IGF-II), or of the high affinity receptor IGF1R are evident, in the brain or cochlea of the null mouse when compared with the wild type mouse (see also Sanchez-Calderon et al., 2010), nor in other contexts (Moerth et al., 2007). Other compensatory factors, such as neurotrophins, may act during late development, leading to FoxM1 activation and cell cycle preservation (Sanchez-Calderon et al., 2007, 2010), which could explain the preservation of brain and cochlear size with respect to body size in the $Igf1^{-/-}$ null mouse.

In summary, the $Igf1^{-/-}$ null mouse is a model of chronic IGF-I deficit that leads to cochlear neuronal loss and profound deafness from the onset of hearing. With aging, chronic IGF-I deficit caused premature degeneration of the stria vascularis that was not observed in wild type mice. These data suggest that IGF-I is a candidate factor to control cochlear metabolic demands and hence, adult hearing. Conversely, wild type mice show age-related hearing loss that was associated with progressive loss of neurons and that paralleled the reduction in serum IGF-I levels. These data suggest that IGF-I is an otic protector whose levels may predict ARHL.

ACKNOWLEDGMENTS

This work was partially supported by grants to IVN from DIGNA Biotech, the Ministerio de Ciencia e Innovacion (SAF2008-00470) and from the Fundacion Mutua Madrileña to IVN and JMZ. Silvia Murillo-Cuesta and Lourdes Rodriguez-de la Rosa hold contracts from CIBERER.

SUPPLEMENTARY MATERIAL

The Supplementary Material for this article can be found online at http://www.frontiersin.org/neuroscience/neuroanatomy/paper/10.3389/fnana.2010.00027/

REFERENCES

Aberg, D. (2010). Role of the growth hormone/insulin-like growth factor 1 axis in neurogenesis. *Endocr. Dev.* 17, 63–76.

Aleman, A., and Torres-Aleman, I. (2009). Circulating insulin-like growth factor I and cognitive function: neuromodulation throughout the lifespan. *Prog. Neurobiol.* 89, 256–265.

Barrenas, M., Landin-Wilhelmsen, K., and Hanson, C. (2000). Ear and hearing in relation to genotype and growth in Turner syndrome. *Hear. Res.* 144, 21–28.

Barrenas, M. L., Bratthall, A., and Dahlgren, J. (2005). The association between short stature and sensorineural hearing loss. *Hear. Res.* 205, 123–130.

Bartke, A. (2005). Minireview: role of the growth hormone/insulin-like growth factor system in mammalian aging. *Endocrinology* 146, 3718–3723.

Berryman, D. E., Christiansen, J. S., Johannsson, G., Thorner, M. O., and Kopchick, J. J. (2008). Role of the GH/IGF-1 axis in lifespan and healthspan: lessons from animal models. *Growth Horm. IGF Res.* 18, 455–471.

Bonapace, G., Concolino, D., Formicola, S., and Strisciuglio, P. (2003). A novel mutation in a patient with insulin-like growth factor 1 (IGF1) deficiency. *J. Med. Genet.* 40, 913–917.

Bright, G. M., Mendoza, J. R., and Rosenfeld, R. G. (2009). Recombinant human insulin-like growth factor-1 treatment: ready for primetime. *Endocrinol. Metab. Clin. North Am.* 38, 625–638.

Burkard, R. F., and Sims, D. (2002). A comparison of the effects of broadband masking noise on the auditory brainstem response in young and older adults. *Am. J. Audiol.* 11, 13–22.

Camarero, G., Avendano, C., Fernandez-Moreno, C., Villar, A., Contreras, J., de Pablo, F., Pichel, J. G., and Varela-Nieto, I. (2001). Delayed inner ear maturation and neuronal loss in postnatal Igf-1-deficient mice. *J. Neurosci.* 21, 7630–7641.

Camarero, G., Villar, M. A., Contreras, J., Fernandez-Moreno, C., Pichel, J.

G., Avendano, C., and Varela-Nieto, I. (2002). Cochlear abnormalities in insulin-like growth factor-1 mouse mutants. *Hear. Res.* 170, 2–11.

Cediel, R., Riquelme, R., Contreras, J., Diaz, A., and Varela-Nieto, I. (2006). Sensorineural hearing loss in insulin-like growth factor I-null mice: a new model of human deafness. *Eur. J. Neurosci.* 23, 587–590.

Cooper, W. A., Jr., Coleman, J. R., and Newton, E. H. (1990). Auditory brainstem responses to tonal stimuli in young and aging rats. *Hear. Res.* 43, 171–179.

Christensen, K., Johnson, T. E., and Vaupel, J. W. (2006). The quest for genetic determinants of human longevity: challenges and insights. *Nat. Rev. Genet.* 7, 436–448.

D'Ercole, A. J., Ye, P., and O'Kusky, J. R. (2002). Mutant mouse models of insulin-like growth factor actions in the central nervous system. *Neuropeptides* 36, 209–220.

Dik, M. G., Pluijm, S. M., Jonker, C., Deeg, D. J., Lomecky, M. Z., and Lips, P. (2003). Insulin-like growth factor I (IGF-I) and cognitive decline in older persons. *Neurobiol. Aging* 24, 573–581.

Dror, A. A., and Avraham, K. B. (2009). Hearing loss: mechanisms revealed by genetics and cell biology. *Annu. Rev. Genet.* 43, 411–437.

Fraenkel, R., Freeman, S., and Sohmer, H. (2003). Susceptibility of young adult and old rats to noise-induced hearing loss. *Audiol. Neurootol.* 8, 129–139.

Gomez, J. M. (2007). Serum leptin, insulin-like growth factor-I components and sex-hormone binding globulin. Relationship with sex, age and body composition in healthy population. *Protein Pept. Lett.* 14, 708–711.

Gundersen, H. J., and Jensen, E. B. (1987). The efficiency of systematic sampling in stereology and its prediction. *J. Microsc.* 147, 229–263.

Holley, M. C. (2002). Application of new biological approaches to stimulate sensory repair and protection. *Br. Med. Bull.* 63, 157–169.

Hunter, K. P., and Willott, J. F. (1987). Aging and the auditory brainstem response in mice with severe or minimal presbycusis. *Hear. Res.* 30, 207–218.

Ingham, N. J., Thornton, S. K., Comis, S. D., and Withington, D. J. (1998). The auditory brainstem response of aged guinea pigs. *Acta Otolaryngol.* 118, 673–680.

Jelsing, J., Rostrup, E., Markenroth, K., Paulson, O. B., Gundersen, H. J., Hemmingsen, R., and Pakkenberg, B. (2005). Assessment of in vivo MR imaging compared to physical sections in vitro – a quantitative study of brain volumes using stereology. *Neuroimage* 26, 57–65.

Leifke, E., Gorenoi, V., Wichers, C., Von Zur Muhlen, A., Von Buren, E., and Brabant, G. (2000). Age-related changes of serum sex hormones, insulin-like growth factor-1 and sex-hormone binding globulin levels in men: cross-sectional data from a healthy male cohort. *Clin. Endocrinol. (Oxf)* 53, 689–695.

LeRoith, D. (2008). Insulin-like growth factors and the brain. *Endocrinology* 149, 5951.

Liu, J. P., Baker, J., Perkins, A. S., Robertson, E. J., and Efstratiadis, A. (1993). Mice carrying null mutations of the genes encoding insulin-like growth factor I (Igf-1) and type 1 IGF receptor (Igf1r). *Cell* 75, 59–72.

Liu, R. S., Lemieux, L., Bell, G. S., Sisodiya, S. M., Shorvon, S. D., Sander, J. W., and Duncan, J. S. (2003). A longitudinal study of brain morphometrics using quantitative magnetic resonance imaging and difference image analysis. *Neuroimage* 20, 22–33.

Llorens-Martin, M., Torres-Aleman, I., and Trejo, J. L. (2009). Mechanisms mediating brain plasticity: IGF1 and adult hippocampal neurogenesis. *Neuroscientist* 15, 134–148.

Martini, A., Comacchio, F., and Magnavita, V. (1990). Auditory evoked responses (ABR, MLR, SVR) and brain mapping in the elderly. *Acta Otolaryngol. Suppl.* 476, 97–103; discussion 104.

McDaniel, B., Sheng, H., Warner, D. S., Hedlund, L. W., and Benveniste, H. (2001). Tracking brain volume changes in C57BL/6J and ApoE-deficient mice in a model of neurodegeneration: a 5-week longitudinal micro-MRI study. *Neuroimage* 14, 1244–1255.

Moerth, C., Schneider, M. R., Renner-Mueller, I., Blutke, A., Elmlinger, M. W., Erben, R. G., Camacho-Hubner, C., Hoeflich, A., and Wolf, E. (2007). Postnatally elevated levels of insulin-like growth factor (IGF)-II fail to rescue the dwarfism of IGF-I-deficient mice except kidney weight. *Endocrinology* 148, 441–451.

Murillo-Cuesta, S., Contreras, J., Cediel, R., and Varela-Nieto, I. (2010a). Comparison of different aminoglycoside antibiotic treatments to refine ototoxicity studies in adult mice. *Lab. Anim.* 44,124–131.

Murillo-Cuesta, S., Contreras, J., Zurita, E., Cediel, R., Cantero, M., Varela-Nieto, I., and Montoliu, L. (2010b). Melanin precursors prevent premature age-related and noise-induced hearing loss in albino mice. *Pigment Cell Melanoma Res.* 23, 72–83.

Murillo-Cuesta, S., Garcia-Alcantara, F., Vacas, E., Sistiaga, J. A., Camarero, G., Varela-Nieto, I., and Rivera, T. (2009). Direct drug application to the round window: a comparative study of ototoxicity in rats. *Otolaryngol. Head Neck Surg.* 141, 584–590.

Narasimhan, S. D., Yen, K., and Tissenbaum, H. A. (2009). Converging pathways in lifespan regulation. *Curr. Biol.* 19, R657–R666.

Netchine, I., Azzi, S., Houang, M., Seurin, D., Perin, L., Ricort, J. M., Daubas, C., Legay, C., Mester, J., Herich, R., Godeau, F., and Le Bouc, Y. (2009). Partial primary deficiency of insulin-like growth factor (IGF)-I activity associated with IGF1 mutation demonstrates its critical role in growth and brain development. *J. Clin. Endocrinol. Metab.* 94, 3913–3921.

Niedernhofer, L. J., Garinis, G. A., Raams, A., Lalai, A. S., Robinson, A. R., Appeldoorn, E., Odijk, H., Oostendorp, R., Ahmad, A., van Leeuwen, W., Theil, A. F., Vermeulen, W., van der Horst, G. T., Meinecke, P., Kleijer, W. J., Vijg, J., Jaspers, N. G., and Hoeijmakers, J. H. (2006). A new progeroid syndrome reveals that genotoxic stress suppresses the somatotroph axis. *Nature* 444, 1038–1043.

Niu, X., Trifunovic, A., Larsson, N. G., and Canlon, B. (2007). Somatic mtDNA mutations cause progressive hearing loss in the mouse. *Exp. Cell Res.* 313, 3924–3934.

Ouagazzal, A. M., Reiss, D., and Romand, R. (2006). Effects of age-related hearing loss on startle reflex and prepulse inhibition in mice on pure and mixed C57BL and 129 genetic background. *Behav. Brain Res.* 172, 307–315.

Paul, R., Grieve, S. M., Chaudary, B., Gordon, N., Lawrence, J., Cooper, N., Clark, C. R., Kukla, M., Mulligan, R., and Gordon, E. (2009). Relative contributions of the cerebellar vermis and prefrontal lobe volumes on cognitive function across the adult lifespan. *Neurobiol. Aging* 30, 457–465.

Ponton, C. W., Moore, J. K., and Eggermont, J. J. (1996). Auditory brain stem response generation by parallel pathways: differential maturation of axonal conduction time and synaptic transmission. *Ear Hear.* 17, 402–410.

Riva, C., Donadieu, E., Magnan, J., and Lavieille, J. P. (2007). Age-related hearing loss in CD/1 mice is associated to ROS formation and HIF target proteins up-regulation in the cochlea. *Exp. Gerontol.* 42, 327–336.

Rosenhall, U., Pedersen, K., and Dotevall, M. (1986). Effects of presbycusis and other types of hearing loss on auditory brainstem responses. *Scand. Audiol.* 15, 179–185.

Salminen, A., and Kaarniranta, K. (2010). Insulin/IGF-1 paradox of aging: regulation via AKT/IKK/NF-kappaB signaling. *Cell. Signal.* 22, 573–577.

Sanchez-Calderon, H., Milo, M., Leon, Y., and Varela-Nieto, I. (2007). A network of growth and transcription factors controls neuronal differentiation and survival in the developing ear. *Int. J. Dev. Biol.* 51, 557–570.

Sanchez-Calderon, H., Rodriguez-de la Rosa, L., Milo, M., Pichel, J. G., Holley, M., and Varela-Nieto, I. (2010). RNA microarray analysis in prenatal mouse cochlea reveals novel IGF-I target genes: implication of MEF2 and FOXM1 transcription factors. *PLoS ONE* 5, e8699. doi: 10.1371/journal.pone.0008699.

Schulte, B. A., and Schmiedt, R. A. (1992). Lateral wall Na,K-ATPase and endocochlear potentials decline with age in quiet-reared gerbils. *Hear. Res.* 61, 35–46.

Shimokawa, I., Higami, Y., Tsuchiya, T., Otani, H., Komatsu, T., Chiba, T., and Yamaza, H. (2003). Life span extension by reduction of the growth hormone-insulin-like growth factor-1 axis: relation to caloric restriction. *FASEB J.* 17, 1108–1109.

Someya, S., Yamasoba, T., Weindruch, R., Prolla, T. A., and Tanokura, M. (2007). Caloric restriction suppresses apoptotic cell death in the mammalian cochlea and leads to prevention of presbycusis. *Neurobiol. Aging* 28, 1613–1622.

Spicer, S. S., and Schulte, B. A. (2002). Spiral ligament pathology in quiet-aged gerbils. *Hear. Res.* 172, 172–185.

Spiess, A. C., Lang, H., Schulte, B. A., Spicer, S. S., and Schmiedt, R. A. (2002). Effects of gap junction uncoupling in the gerbil cochlea. *Laryngoscope* 112, 1635–1641.

Sun, L. Y., and Bartke, A. (2007). Adult neurogenesis in the hippocampus of long-lived mice during aging. *J. Gerontol. A Biol. Sci. Med. Sci.* 62, 117–125.

Torre, P., 3rd, and Fowler, C. G. (2000). Age-related changes in auditory function of rhesus monkeys (*Macaca mulatta*). *Hear. Res.* 142, 131–140.

Torres-Aleman, I. (2008). Mouse models of Alzheimer's dementia: current concepts and new trends. *Endocrinology* 149, 5952–5957.

Torres-Aleman, I. (2010). Toward a comprehensive neurobiology of IGF-I. *Dev. Neurobiol.* 70, 384–396.

Uchino, A., Noguchi, T., Nomiyama, K., Takase, Y., Nakazono, T., Nojiri, J., and Kudo, S. (2007). Manganese accumulation in the brain: MR imaging. *Neuroradiology* 49, 715–720.

Van Eyken, E., Van Camp, G., and Van Laer, L. (2007). The complexity of age-related hearing impairment: contributing environmental and genetic factors. *Audiol. Neurootol.* 12, 345–358.

van Wijk, E., Krieger, E., Kemperman, M. H., De Leenheer, E. M., Huygen, P. L., Cremers, C. W., Cremers, F. P., and Kremer, H. (2003). A mutation in the gamma actin 1 (ACTG1) gene causes autosomal dominant hearing loss (DFNA20/26). *J. Med. Genet.* 40, 879–884.

Varela-Nieto, I., Hartl, M., Gorospe, I., and Leon, Y. (2007). Anti-apoptotic actions of insulin-like growth factors: lessons from development and implications in neoplastic cell transformation. *Curr. Pharm. Des.* 13, 687–703.

Walenkamp, M. J., Karperien, M., Pereira, A. M., Hilhorst-Hofstee, Y., van Doorn, J., Chen, J. W., Mohan, S., Denley, A., Forbes, B., van Duyvenvoorde, H. A., van Thiel, S. W., Sluimers, C. A., Bax, J. J., de Laat, J. A., Breuning, M. B., Romijn, J. A., and Wit, J. M. (2005). Homozygous and heterozygous expression of a novel insulin-like growth factor-I mutation. *J. Clin. Endocrinol. Metab.* 90, 2855–2864.

Walenkamp, M. J., and Wit, J. M. (2007). Genetic disorders in the GH IGF-I axis in mouse and man. *Eur. J. Endocrinol.* 157(Suppl. 1), S15–S26.

Watanabe, T., Miyazaki, A., Katagiri, T., Yamamoto, H., Idei, T., and Iguchi, T. (2005). Relationship between serum insulin-like growth factor-1 levels and Alzheimer's disease and vascular dementia. *J. Am. Geriatr. Soc.* 53, 1748–1753.

Watanabe, T., Radulovic, J., Spiess, J., Natt, O., Boretius, S., Frahm, J., and Michaelis, T. (2004). In vivo 3D MRI staining of the mouse hippocampal system using intracerebral injection of MnCl2. *Neuroimage* 22, 860–867.

Weindruch, R., and Sohal, R. S. (1997). Seminars in medicine of the Beth Israel Deaconess Medical Center. Caloric intake and aging. *N. Engl. J. Med.* 337, 986–994.

Welch, D., and Dawes, P. J. (2007). Childhood hearing is associated with growth rates in infancy and adolescence. *Pediatr. Res.* 62, 495–498.

Woods, K. A., Camacho-Hubner, C., Barter, D., Clark, A. J., and Savage, M. O. (1997). Insulin-like growth factor I gene deletion causing intrauterine growth retardation and severe short stature. *Acta Paediatr. Suppl.* 423, 39–45.

Zeger, M., Popken, G., Zhang, J., Xuan, S., Lu, Q. R., Schwab, M. H., Nave, K. A., Rowitch, D., D'Ercole, A. J., and Ye, P. (2007). Insulin-like growth factor type 1 receptor signaling in the cells of oligodendrocyte lineage is required for normal in vivo oligodendrocyte development and myelination. *Glia* 55, 400–411.

Zheng, Q. Y., Johnson, K. R., and Erway, L. C. (1999). Assessment of hearing in 80 inbred strains of mice by ABR threshold analyses. *Hear. Res.* 130, 94–107.

Zhu, M., Yang, T., Wei, S., DeWan, A. T., Morell, R. J., Elfenbein, J. L., Fisher, R. A., Leal, S. M., Smith, R. J., and Friderici, K. H. (2003). Mutations in the gamma-actin gene (ACTG1) are associated with dominant progressive deafness (DFNA20/26). *Am. J. Hum. Genet.* 73, 1082–1091.

Conflict of Interest Statement: The authors declare that the research was conducted in the absence of any commercial or financial relationships that could be construed as a potential conflict of interest.

Received: 31 March 2010; paper pending published: 20 April 2010; accepted: 01 June 2010; published online: 23 June 2010.
*Citation: Riquelme R, Cediel R, Contreras J, Rodriguez-de la Rosa L, Murillo-Cuesta S, Hernandez-Sanchez C, Zubeldia JM, Cerdan S and Varela-Nieto I (2010) A comparative study of age-related hearing loss in wild type and insulin-like growth factor I deficient mice. Front. Neuroanat. **4**:27. doi: 10.3389/fnana.2010.00027*

frontiers in
NEUROANATOMY

ORIGINAL RESEARCH ARTICLE
published: 21 May 2010
doi: 10.3389/fnana.2010.00019

Postnatal development of the endbulb of Held in congenitally deaf cats

Christa A. Baker[1,2], Karen L. Montey[1,3], Tan Pongstaporn[1] and David K. Ryugo[1,4,5]*

[1] *Department of Otolaryngology, Johns Hopkins University, Baltimore, MD, USA*
[2] *Program in Neuroscience, Division of Biology and Biomedical Sciences, Washington University, St. Louis, MO, USA*
[3] *Department of Biology, University of Maryland, College Park, MD, USA*
[4] *Department of Neuroscience, Johns Hopkins University, Baltimore, MD, USA*
[5] *Garvan Institute of Medical Research, Darlinghurst, NSW, Australia*

Edited by:
Enrique Saldaña, Universidad de Salamanca, Spain

Reviewed by:
Enrico Mugnaini, Northwestern University, USA
Nell B. Cant, Duke University, USA

****Correspondence:***
David K. Ryugo, Department of Otolaryngology, Johns Hopkins University, 720 Rutland Ave., 510 Traylor Bldg., Baltimore, MD 21205, USA.
e-mail: dryugo@jhu.edu

The endbulbs of Held are formed by the ascending branches of myelinated auditory nerve fibers and represent one of the largest synaptic endings in the brain. Normally, these endings are highly branched and each can form up to 1000 dome-shaped synapses. The deaf white cat is a model of congenital deafness involving a type of cochleosaccular degeneration that mimics the Scheibe deformity in humans. Endbulbs of mature deaf white cats exhibit reduced branching, hypertrophy of postsynaptic densities (PSDs), and changes in synaptic vesicle density. Because cats are essentially deaf at birth, we sought to determine if the progression of brain abnormalities was linked in time to the failure of normal hearing development. The rationale was that the lack of sound-evoked activity would trigger pathologic change in deaf kittens. The cochleae of deaf cats did not exhibit abnormal morphology at birth. After the first postnatal week, however, the presence of a collapsed scala media signaled the difference between deaf and hearing cats. By working backwards in age, endbulbs of deaf cats expressed flattened and elongated PSDs and increased synaptic vesicle density as compared to normal endbulbs. These differences are present at birth in some white kittens, presaging deafness despite their normal cochlear histology. We speculate that hearing pathology is signaled by a perinatal loss of spontaneous bursting activity in auditory nerve fibers or perhaps by some factor released by hair cell synapses before obliteration of the organ of Corti.

Keywords: auditory nerve, cochlear nucleus, hearing synapse, ultrastructure

INTRODUCTION

The endbulb of Held is a large auditory nerve ending which makes synaptic contact with spherical bushy cells (SBCs) in the anteroventral cochlear nucleus (AVCN). It represents one of the largest endings in the brain and has been implicated in the precise transmission of timing information from auditory stimuli (Pfeiffer, 1966a,b; Molnar and Pfeiffer, 1968; Ryugo and Fekete, 1982; Carr and Konishi, 1990; Smith et al., 1993; Koppl, 1994; Koppl and Carr, 1997). Detailed study of endbulb development in cats revealed that the most significant changes in structural features occur over the first twenty postnatal days (Ryugo and Fekete, 1982; Ryugo et al., 2006). During this time, the spoon-shaped endbulb elaborates into a highly branched arborization, intermembraneous cisternae form, postsynaptic densities (PSDs) elongate, and the concentration of synaptic vesicles increases. These morphological changes in the endbulb are correlated in time to changes in physiological properties of the parent auditory nerve fiber. Following this rapid postnatal development, endbulb structure and auditory nerve fiber response properties sustain a slow maturation until 90-days postnatal (Ryugo and Fekete, 1982).

Congenital deafness is associated with morphological changes in endbulb structure including reduced branching, hypertrophy of PSDs, and variations in synaptic vesicle density (Ryugo et al., 1997, 1998, 2005; Limb and Ryugo, 2000; Lee et al., 2003). The deaf white cat is a model of congenital deafness involving a type of cochleosaccular degeneration which mimics the Scheibe deformity in humans (Scheibe, 1892, 1895; Bosher and Hallpike, 1965, 1967; Deol, 1970; Suga and Hattler, 1970; Mair, 1973; Brighton et al., 1991). Unlike humans, however, cats are altricial animals whose ear canals are closed at birth. By postnatal day 30, the ear canal opens and kittens are considered fully hearing. The time course of canal opening is the same for deaf white kittens and normal hearing kittens (Ryugo et al., 2003).

Because cats are deaf at birth, we sought to determine whether the emergence of abnormalities at the endbulb of Held synapse in deaf white cats coincided in time with the development of hearing in normal cats. The rationale was that the lack of sound-evoked activity would trigger pathologic change in deaf kittens. To this end, we examined the ultrastructure of endbulbs in an age-graded series of deaf kittens and compared the results with those previously reported for normal hearing kittens (Ryugo et al., 2006).

MATERIALS AND METHODS

SUBJECTS

Forty-nine cats contributed new data that were used for this report (**Table 1**). Structural data were collected from an age-graded series of congenitally deaf cats of either sex that ranged in postnatal age (PN) from newborn (PN-0) to adult. The auditory nerve endings in the cochlear nucleus of two kittens were analyzed at each of the

Table 1 | Subjects.

Subject age	White cats				Pigmented cats			
	Number of subjects	Cochleae analyzed		Brains analyzed	Number of subjects	Cochleae analyzed		Brains analyzed
		LM	EM			LM	EM	
0 days	23	20	3	7	2* + 3	2* + 2	1	2* + 1
5 days	2	2		2	2*	2*		2*
10 days	2	2		2	2*	2*		2*
20 days	2	2		2	2*	2*		2*
30 days	2	2		2	2*	2*		2*
60 days	2	2		2	2*	2*		2*
90 days	2	2		2	2*	2*		2*
120 days	2	2		2	2*	2*		2*
150 days	2	2		2	2*	2*		2*
180 days	2	2		2	2*	2*		2*
Adult	5	5		5	5*	5*		5*

Pigmented kitten data are from Ryugo et al. (2006); they are included in* **Figures 5, 6, 7, 12, and 13 *for comparison purposes.*

following postnatal ages: 5, 10, 20, 30, 60, 90, 120, 150, and 180 days. In addition, five adult cats 240 days of age or older were used due to unexpected variability of the features measured for analysis. A total of 26 newborn kittens contributed brain and cochlear tissue. Twenty white PN-0 kittens and four pigmented PN-0 kittens were used to examine inner ear morphology using light microscopy. Three more white newborns and one pigmented newborn were prepared for electron microscopic examination of inner hair cell synapses onto spiral ganglia. All animals with the exception of three pigmented kittens and three pigmented adults were from our colony of white cats with a family history of congenital deafness.

For kittens 5 days of age or older, criteria for inclusion in this study consisted of: (1) bilateral profound deafness as determined by auditory brainstem responses (ABRs) and/or cochlear histology that documented the absence of an organ of Corti, and (2) good ultrastructural appearance of brain tissue when viewed with an electron microscope. Criteria for the inclusion of newborn kittens were healthy appearance at birth and adequately fixed tissue for examination with light and electron microscopy. Standard ABRs were recorded from animals 30-days postnatal and older. An animal was determined to be deaf after registering no response to clicks or noise bursts that were presented up to 100 dB SPL. All procedures were in accordance with NIH guidelines and were approved by the Animal Care and Use Committee of the Johns Hopkins University.

HISTOLOGICAL PREPARATION

Animals were deeply anesthetized with sodium pentobarbital (75 mg/kg, IP) and when unresponsive to corneal stimulation were perfused transcardially with 0.12 M PBS with 0.1% $NaNO_2$ followed by 2% paraformaldehyde/2% glutaraldehyde. Brains were allowed to post-fix overnight at 4°C in the same fixative. The brainstem was then embedded in bovine serum albumin gel hardened with glutaraldehyde. Coronal sections through the cochlear nuclei were cut using a Vibratome at a thickness of 50 μm for light microscopic analysis and 75 μm for electron microscopic analysis. Sections destined for light microscopy were mounted on glass slides, stained with cresyl violet, cleared with xylenes, and coverslipped with Permount. Sections for electron microscopy were en bloc stained with 1% OsO_4, incubated in uranyl acetate overnight, dehydrated, and embedded in PolyBed 812 resin between sheets of Aclar. After polymerization, relevant portions of the AVCN were cut out and embedded in BEEM capsules. Ultrathin sections were collected on Formvar-coated slotted grids and examined in a Hitachi H-7600 electron microscope.

Immediately after transcardial perfusion, the cochleae of each animal were perfused with the same fixative and dissected out of the temporal bone. Cochleae meant for electron microscopic analysis were also flushed with 1% OsO_4. After decalcification with 0.1 M ethylenediaminetetraacetic acid (EDTA), cochleae were dehydrated in increasing concentrations of alcohols, embedded in Araldite, and cut on a rotary microtome at 20 μm. Sections through the mid-modiolar plane were mounted on glass slides, stained with toluidine blue, cleared with xylenes, and coverslipped with Permount for viewing in a light microscope. Mid-modiolar sections through cochleae intended for electron microscopy were mounted in Epon and processed by the same method as described for brainstem sections.

DATA ANALYSIS

The histologic appearance of the cochlea was used to identify deaf kittens less than 30-days old. Deafness in our colony of white cats manifests as one of three pathologies: (1) a collapsed Reissner's membrane and obliteration of the scala media, (2) excessive epithelial growth on Reissner's membrane and within the scala media and scala tympani resulting in a spongiform appearance, or (3) a combination of spongiform growth in the apex of the cochlea and collapsed Reissner's membrane in the base (Ryugo et al., 2003). Light microscopic examination of the cochleae from 20 PN-0 white kittens revealed only one kitten with pathologic histology indicative

of deafness. This newborn kitten had spongiform growth in both cochleae. The rest of the newborn kittens exhibited normal cochlear histology in agreement with previous observations on newborn white cats (Mair, 1973). For synapse analysis, we selected six PN-0 white kittens from a breeding pair that only produced deaf offspring. These seven newborn kittens, one with and six without obvious cochlear pathology, represented newborn kittens for this study.

Electron micrographs of endbulbs of Held were subject to morphometric analyses described previously (Ryugo et al., 2006). Briefly, measurements of endbulb and mitochondrial area, PSD and apposition lengths, and number of PSDs, puncta adherentia, cisternae, SBC inclusions, large dense-core vesicles, and synaptic vesicles were collected using *Adobe Photoshop v7* and NIH *ImageJ v1.37*. For synaptic vesicle density measurements, the area of the endbulb within 0.5 μm of each PSD was defined and measured. The number of synaptic vesicles located within this region was then divided by the area of the region to yield synaptic vesicle density. Quantitative values are presented in the text as mean ± standard deviation, whereas in the figures they are given as mean ± standard error of the mean.

A minimum of eight endings was randomly selected from each animal, resulting in a total of 244 endbulb profiles. These data were compared to those of normal hearing cats (Ryugo et al., 2006), with the exception of synaptic vesicle density and large dense-core vesicle counts. Given the variability in shape of synaptic vesicles in electron micrographs even within the same ending, one observer recounted synaptic vesicles from normal animals. This step was necessary in order to allow direct comparison between synaptic vesicle density measurements from normal hearing and deaf cats. The recount changed the absolute values previously reported but the results remained qualitatively similar and the values were not statistically different. Since the other morphological features of endbulbs are readily identifiable, no additional re-analysis of normal data was performed. The quantification of large dense-core vesicles provided in this study was not previously reported for normal hearing animals. For the micrographs analyzed and presented here, only brightness and contrast were adjusted in *Photoshop*.

RESULTS

AGES 0–10 DAYS

Cochleae

At birth, light microscopic cochlear histology is similar in all pigmented (n = 4) and all but one white kitten (n = 20) studied. The cochleae of both cohorts (with the one mentioned exception) exhibit an intact Reissner's membrane, healthy stria vascularis, and a full complement of inner and outer hair cells (**Figure 1**, top). The first noticeable sign of degeneration is present at 5 days in white kittens, with Reissner's membrane beginning to collapse onto the tectorial membrane (**Figure 1**, middle). Inner and outer hair cells are still visible. By 10 days, however, Reissner's membrane has completely collapsed and obliterated the scala media. The organ of Corti deteriorates and hair cells are no longer distinguishable in white kittens (**Figure 1**, bottom). Sometimes unidentifiable cells occupy the site where the organ of Corti would normally reside, but they do not have apical tufts of stereocilia that would identify them as hair cells and it is not clear if they are residual supporting cells.

Mair (1973) reported the first sign of cochlear degeneration in deaf white kittens to be a wrinkling of Reissner's membrane. We found this feature unreliable as a harbinger of deafness because pigmented and white kittens exhibited considerable variations in Reissner's membrane, from being perfectly straight to undulating to bowed-out as in the case of hydrops (**Figure 1**). Some of the irregularity could be due to non-uniform fixation conditions. Examination of cochleae from newborn white kittens revealed only one with obvious pathologic morphology when viewed under a light microscope. This PN-0 kitten had spongiform growth in both cochleae (see Ryugo et al., 2003). Three other newborn kittens from genetically dominant deaf parents provided cochleae with adequate preservation where normal synapses could be observed between the inner hair cell and afferent ending in an electron microscope.

Endbulbs

The newborn kitten with spongiform cochlear pathology was a clear case for deafness at birth. Epithelial cells that lined the cochlear duct and the basilar membrane were hypertrophied and there was no evidence for inner or outer hair cells. Endbulbs from this cat exhibited PSDs that were on average longer (0.291 ± 0.148 μm, n = 50 PSDs) than those of newborn pigmented kittens (0.208 ± 0.151 μm, n = 242 PSDs). The other six PN-0 white kittens also displayed abnormally long PSDs (mean = 0.365 ± 0.271 μm, n = 144 PSDs). Collectively, these newborn white kittens had on average significantly larger PSDs ($p < 0.005$, Kruskal–Wallis Test) when compared to those of pigmented kittens destined to develop normal hearing. Therefore, we selected one of these newborn white kittens with large PSDs, in addition to the kitten with spongiform cochleae, for morphometric endbulb analysis.

The endbulb profile in newborn deaf animals is large in area and is considerably interdigitated with the SBC, as indicated by a highly irregular membrane and the presence of SBC "inclusions" within the endbulb (**Figures 2 and 3**). These inclusions are known to arise from the cell body as short filopodia or somatic spines as determined by reconstruction through serial sections. To quantify the extent of the interdigitation, the length of the straight-line segment of the endbulb-SBC apposition was divided by the length of the "wavy" apposition (see figure 1 of Ryugo et al., 2006). This ratio is called the apposition form factor. An apposition form factor of 1 indicates a perfectly straight apposition, whereas progressively smaller ratios denote increasingly more convoluted membrane appositions.

During the first ten postnatal days, the endbulb membrane abutting the SBC becomes more regular (apposition form factor approaches 1) and SBC inclusions disappear (**Figures 4 and 5**) in profiles from both cohorts. Endbulb profile area shrinks substantially as does the associated apposition length (**Figure 5**). This change is consistent with the developmental process whereby large components of the endbulb transform into progressively smaller swellings and finer fibers by sequential branching (Ryugo and Fekete, 1982; Limb and Ryugo, 2000). The number of puncta adherentia remains steady at about three per profile over this period (**Figure 6A**) in both pigmented and white kittens.

PSDs of deaf kittens steadily increase in length from 0.309 ± 0.212 μm at birth to 0.376 ± 0.176 μm at PN-10 (**Figure 6C**). The number of PSDs on endings of deaf subjects, however, is

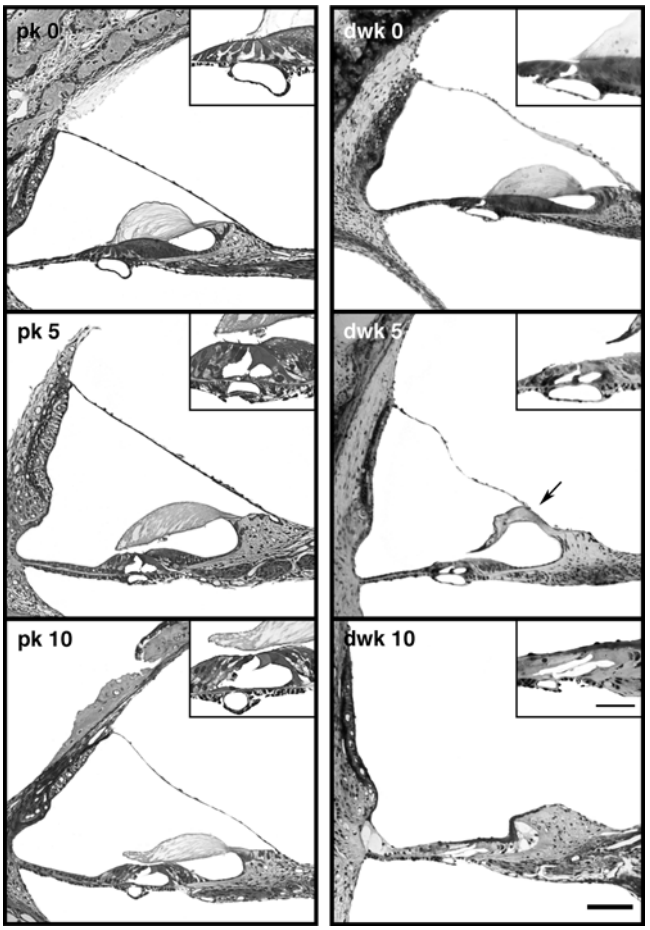

FIGURE 1 | Light micrographs of mid-modiolar cochlear sections from pigmented kittens (pk, left column) and deaf white kittens (dwk, right column). At day 0 (top row), the cochleae of white and pigmented kittens are similar in appearance. Reissner's membrane and inner and outer hair cells (inset) are intact. At postnatal day 5 (middle row), the first sign of cochlear degeneration is seen in white kittens as Reissner's membrane begins its collapse onto the tectorial membrane (arrow). By postnatal day 10 (bottom row), Reissner's membrane has fallen completely, obliterating the scala media and destroying the organ of Corti. Hair cells are no longer distinguishable in the damaged organ of Corti (inset). Scale bar equals 100 μm and 50 μm in the inset.

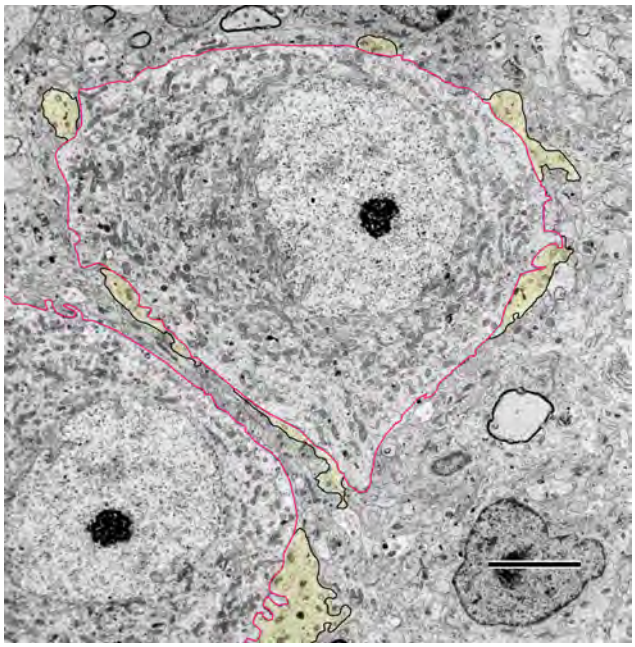

FIGURE 2 | Low magnification electron micrograph through the anteroventral cochlear nucleus (AVCN) of a newborn deaf white kitten. The cell body of spherical bushy cells (SBCs, outlined in red) is contacted by endbulbs of Held (yellow with black outlines). The segments of membrane contact between the two cells are irregular and "wavy" in appearance. Some lightly myelinated axons are visible in the AVCN at this age. Scale bar equals 5 μm.

reduced from four PSDs per profile at PN-0 to three at PN-10 (**Figure 6B**). The number of large dense-core vesicles decreases from 1 to 2 per profile in newborn deaf kittens to an average of less than 1 at PN-10 (**Figure 7E**). Synaptic vesicle density seemed to be the most variable parameter both within and across animals. This value fluctuates between 50 and 100 vesicles/μm^2 in endings from deaf cats (**Figure 7C**). If synaptic vesicle number is influenced by the amount of activity in the fiber (e.g., Murthy et al., 2001), then events immediately preceding fixation could be relevant and might account for some of these differences.

Although average mitochondria size remains relatively constant at 0.077 ± 0.052 μm^2 (**Figure 7A**), the proportion of profile area occupied by mitochondria increases (9.1 ± 6.5% to 11.7 ± 5.7%, **Figure 7B**) during the first few days of life. This increase in mitochondrial volume fraction appears linked to the profile reduction as the endbulb branches.

At these early ages, deafness is associated with a decrease in endbulb profile area (**Figure 5A**) and apposition length (**Figure 5B**) as compared to normal hearing animals. The interdigitation of membrane between endbulbs and SBCs in deaf animals is reduced as indicated by an apposition form factor approaching one (**Figure 5C**) and the presence of about half the number of inclusions (**Figure 5D**). While endings from deaf kittens exhibit fewer than half the number of PSDs as compared to normal endbulbs (**Figure 6B**), the PSDs they do have are considerably longer (**Figure 6C**). It is striking that even at the earliest ages, synaptic vesicles are more highly concentrated near PSDs of deaf kittens compared to those of hearing kittens (**Figure 7C**).

AGES 20 DAYS AND OLDER

Endbulbs of deaf kittens experience the most profound morphological changes between postnatal days 0 and 20. After 30 days, structural features stabilize (**Figures 8,9 and 10**). Profile area, apposition length, and apposition complexity plateau and SBC inclusions disappear (**Figure 5**). An average of two PSDs (**Figure 6B**) and one punctum adherens (**Figure 6A**) remain on each endbulb profile. The number of large dense-core vesicles decreases, with an average of fewer than 50% of endings containing a dense-core vesicle (**Figure 7E**). PSD length (**Figure 6C**), mitochondrial volume fraction (**Figure 7B**), and synaptic vesicle density (**Figure 7C**) continue to increase into adulthood.

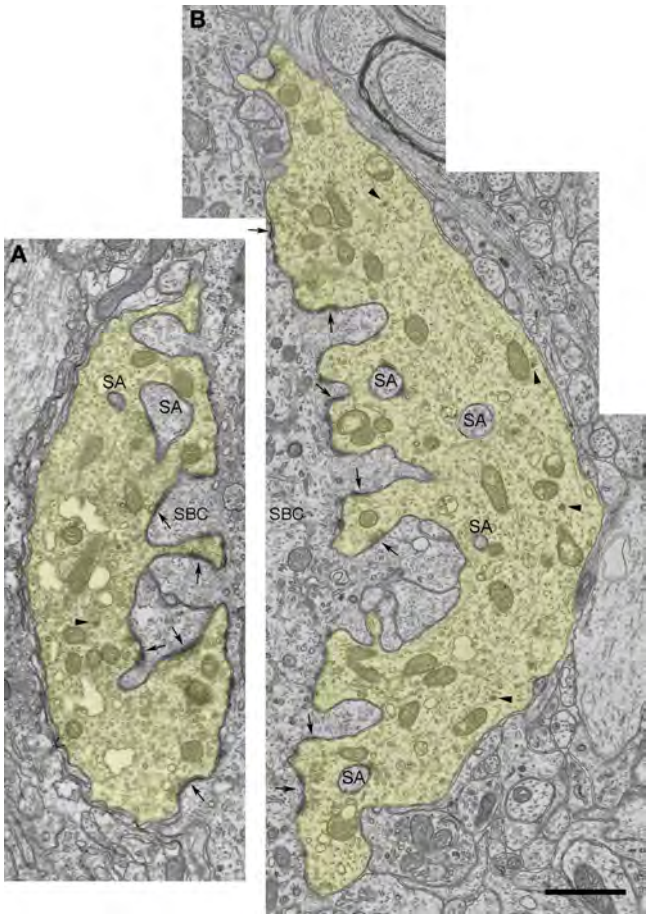

FIGURE 3 | Electron micrographs of endbulbs from a newborn (A) and 5-day old (B) deaf white kitten. (A) The endbulb (yellow) exhibits highly irregular surface contact with the spherical bushy cell (SBC) and contains somatic appendages (SA). Symmetric membrane thickenings mark puncta adherentia; asymmetric membrane thickenings and accumulations of synaptic vesicles mark PSDs (arrows). This newborn white kitten exhibited normal cochlear morphology but was produced by a breeding tom and queen that only give rise to deaf offspring; it had about half the normal number of PSDs in comparison to pigmented kittens, and its PSDs were about 50% longer than those of newborn pigmented animals. Large dense-core vesicles can be found away from active zones (arrowheads). **(B)** Electron micrograph of 5-day-old endbulb. This kitten exhibited cochlear pathology and its endbulb morphology was similar to that of a newborn white kitten. Scale bar equals 1 μm.

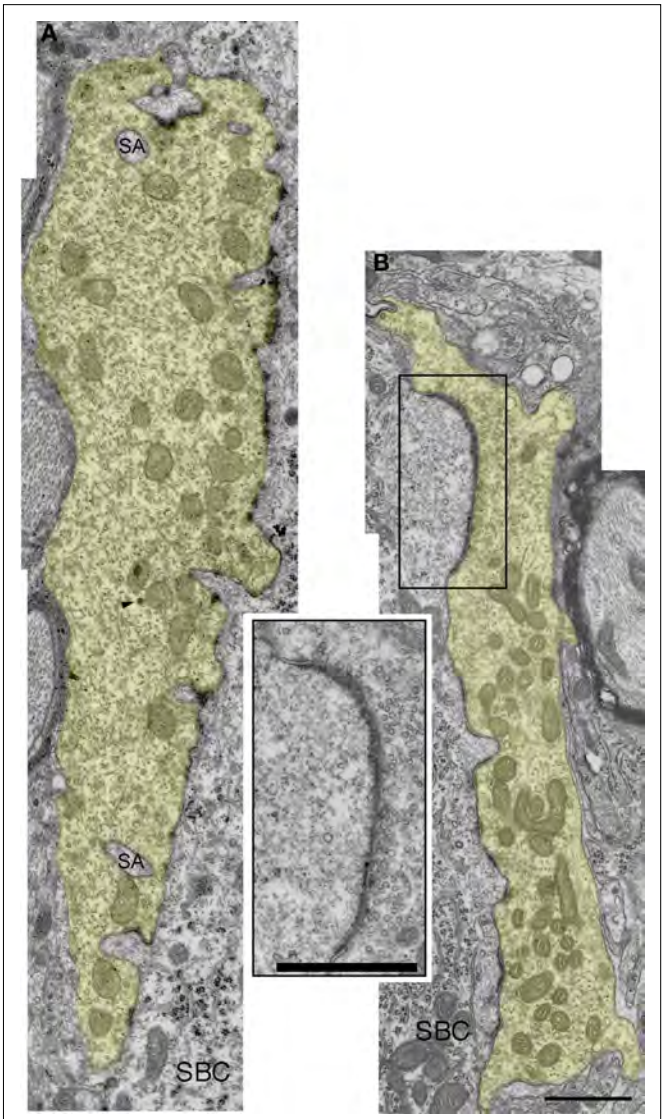

FIGURE 4 | Electron micrographs of endbulbs from a 10-day (A) and 20-day (B) deaf white kitten. (A) The surface between the endbulb (yellow) and SBC membranes has flattened out compared to 0- and 5-day endbulbs and somatic appendages (SA) have decreased. The number of large dense-core vesicles (arrowhead) has also diminished. **(B)** Endbulb-SBC surface contact continues to flatten and SBC inclusions have essentially vanished in the 20-day endbulb. PSDs appear as asymmetric membrane thickenings with associated synaptic vesicles. Extremely long, flat PSDs are common in young deaf animals (inset). Scale bars equal 1 μm.

Endbulbs of congenitally deaf cats are smaller than normal (Ryugo et al., 1997) so it follows that their profile area would also be smaller (**Figure 5A**). Although newborn normal animals exhibit more than twice the number of PSDs per profile than deaf, by 30 days the numbers in both cohorts are "pruned" to adult levels, and mature deaf animals exhibit the same number of PSDs as their normal hearing counterparts (**Figure 6B**). PSD length is greater in deaf animals compared to that of normals throughout development (**Figure 6C**), but the proportion of the endbulb apposition with SBCs occupied by PSDs was not affected by deafness (**Figure 6D**).

The PSDs of both normal and deaf cats double in length from birth to adulthood, although the PSDs of deaf animals are consistently larger than those of normals from birth (**Figures 8, 9, 10, and 11**).

Moreover, these PSDs are flattened compared to the dome-shaped structure of PSDs from normal hearing, pigmented cats (**Figure 12**). In general, more synaptic vesicles are associated with PSDs of deaf compared to hearing cats across all ages (**Figures 7C, 11, and 12**).

In endings from both normal hearing and deaf cats, the incidence of large dense-core vesicles decreases from about one per profile at birth to become much more rare in older animals (**Figure 7E**).

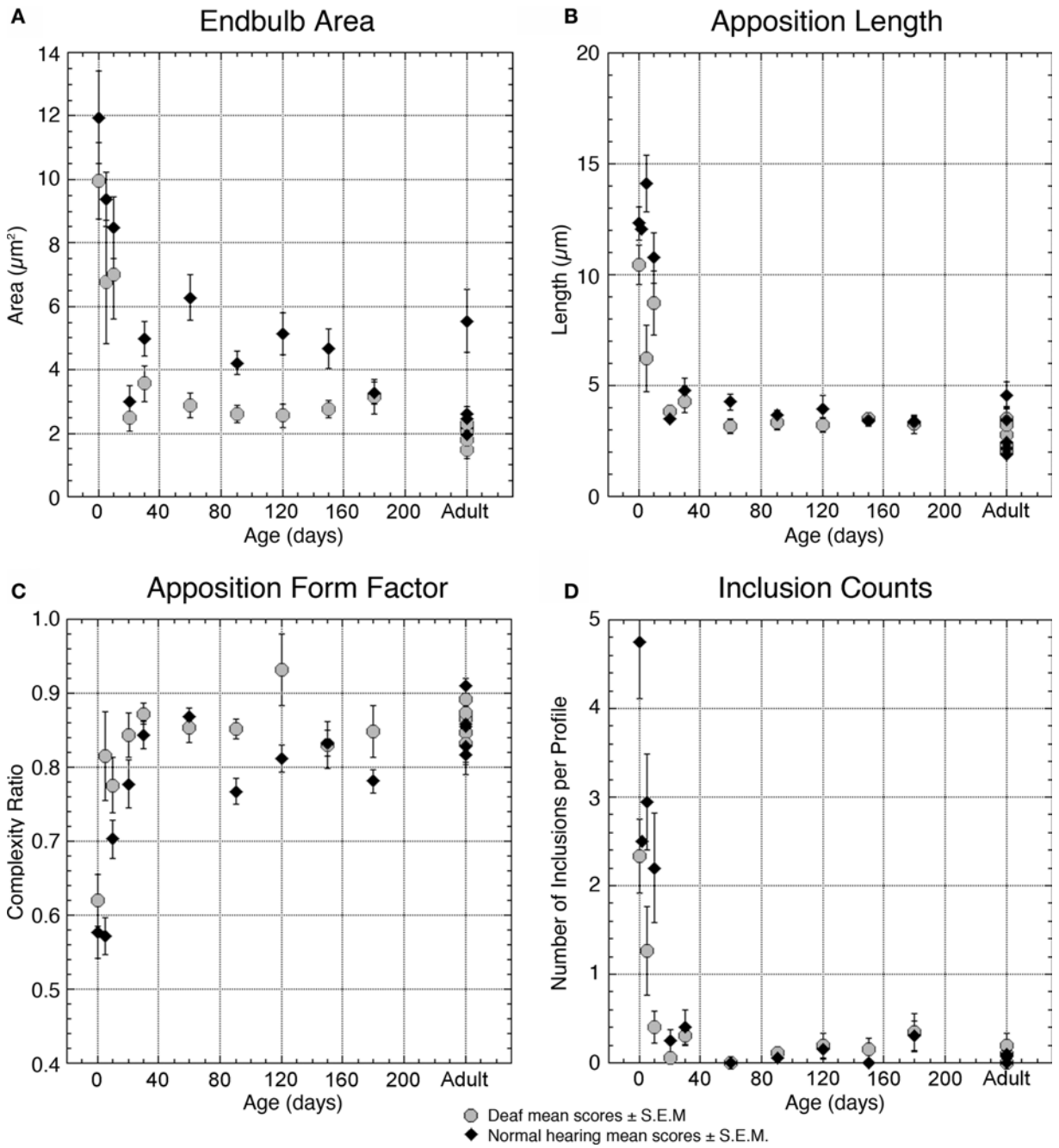

FIGURE 5 | Plots illustrating and comparing the profile features of endbulbs from deaf (gray circles) and normal hearing (black triangles) cats with respect to age. (A) Average area of the endbulb profile is relatively large in both groups at birth and decreases as the endbulb reorganizes into smaller components between 10- and 20-days postnatal. Endbulbs from deaf cats are generally smaller than endbulbs from hearing cats. **(B)** Apposition length is a measure of membrane contact between the endbulb and the SBC; this contact is shorter in endbulbs of deaf cats for the first 3 months but stabilizes in older animals. **(C)** The ratio of straight-line length from one edge to the opposite edge of the apposition compared to the contour length of the apposition provides a measure of contact complexity. This ratio approaches one as the membrane between the endbulb and SBC flattens. Endbulb appositions of deaf cats are in general less curvy than those of normal cats before 30 days of age. **(D)** Somatic inclusions are common in young animals but disappear by 20–30 days. Deaf animals have fewer than half the number of inclusions present in normal animals at early ages. Each point represents an average of multiple measures collected from two animals at all time points except adult, where each point represents the average for one animal. Data values from normal hearing cats are replotted from Ryugo et al. (2006).

While deaf animals seemed to exhibit greater variability during development, no drastic differences in large dense-core vesicle numbers are seen in deaf compared to normal cats.

Intermembraneous cisternae were first seen at 10-days postnatal in endings from pigmented kittens. Cisternae are created by the appearance of an extracellular space between the pre- and

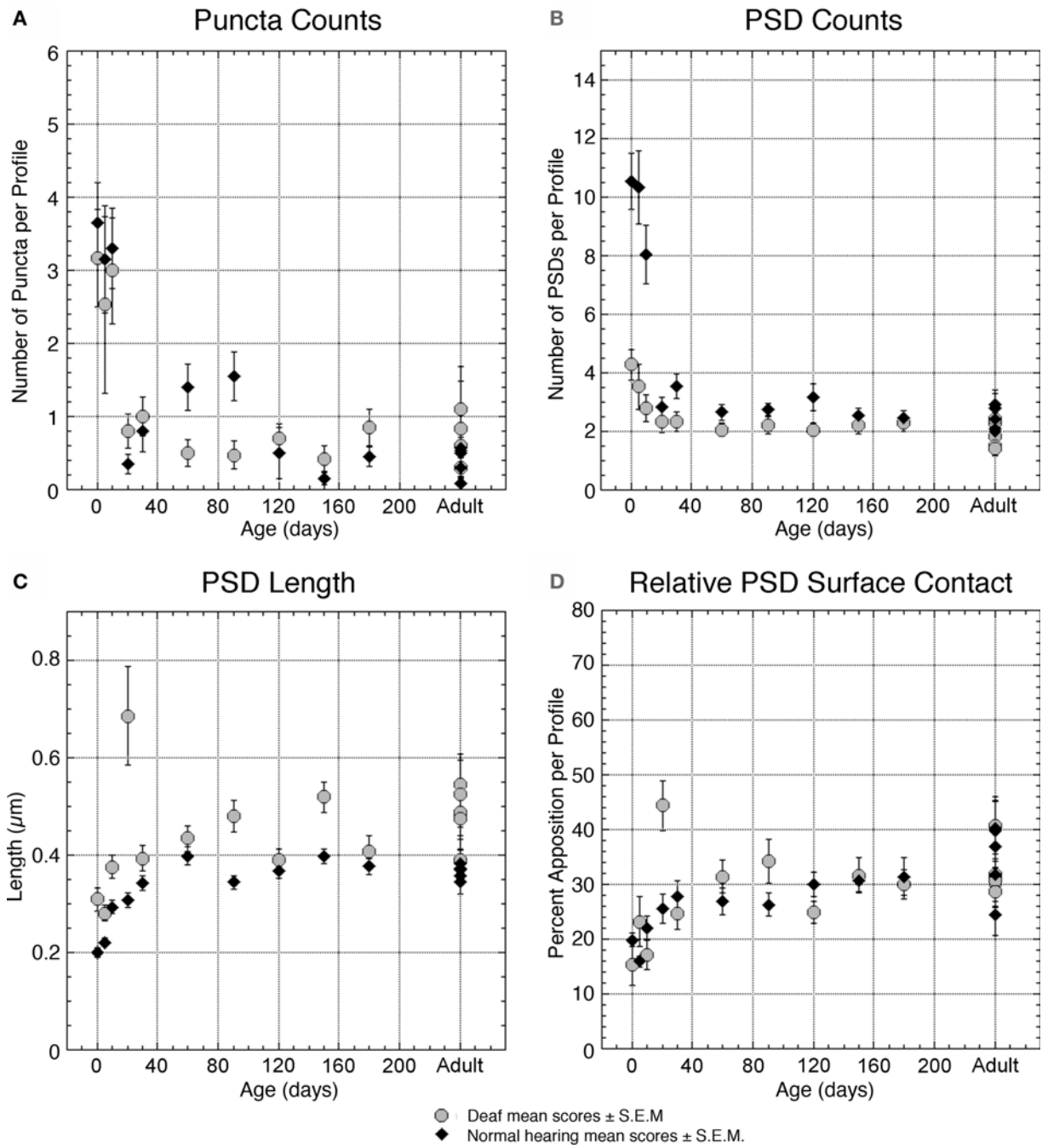

FIGURE 6 | Plots quantifying membrane features of deaf (gray circles) and normal hearing (black triangles) endbulbs with respect to age. The number of puncta adherentia **(A)** and PSDs **(B)** diminishes over time in both groups. Deaf animals start with remarkably fewer PSDs than normal and thus the degree of change in PSD density is reduced in deaf endbulbs. The effect of deafness on puncta adherentia is less prominent. **(C)** The PSDs of deaf and normal hearing cats almost double in length from birth to adulthood, with deaf PSDs consistently larger than those of normal animals. **(D)** The relative amount of PSD contact between the endbulb and SBC exhibits no pronounced changes as a result of deafness. Each point represents an average of multiple measures collected from two animals at all time points except adult, where each point represents the average for one animal. Data values from normal hearing cats are replotted from Ryugo et al. (2006).

postsynaptic membranes (**Figure 13**). Frequently, astrocytic processes are seen within the cisternae.

By adulthood, normal hearing animals average one to two cisternae per endbulb profile. Deaf animals, however, do not exhibit cisternae to any notable extent (**Figure 7D**).

Deafness was found to have no measurable effect on mitochondrial size (**Figure 7A**) or volume fraction (**Figure 7B**). The correlation between age and mitochondria size is not significant ($r = 0.025, p = 0.4$), whereas that for mitochondria volume fraction is significant ($r = 0.49, p < 0.05$).

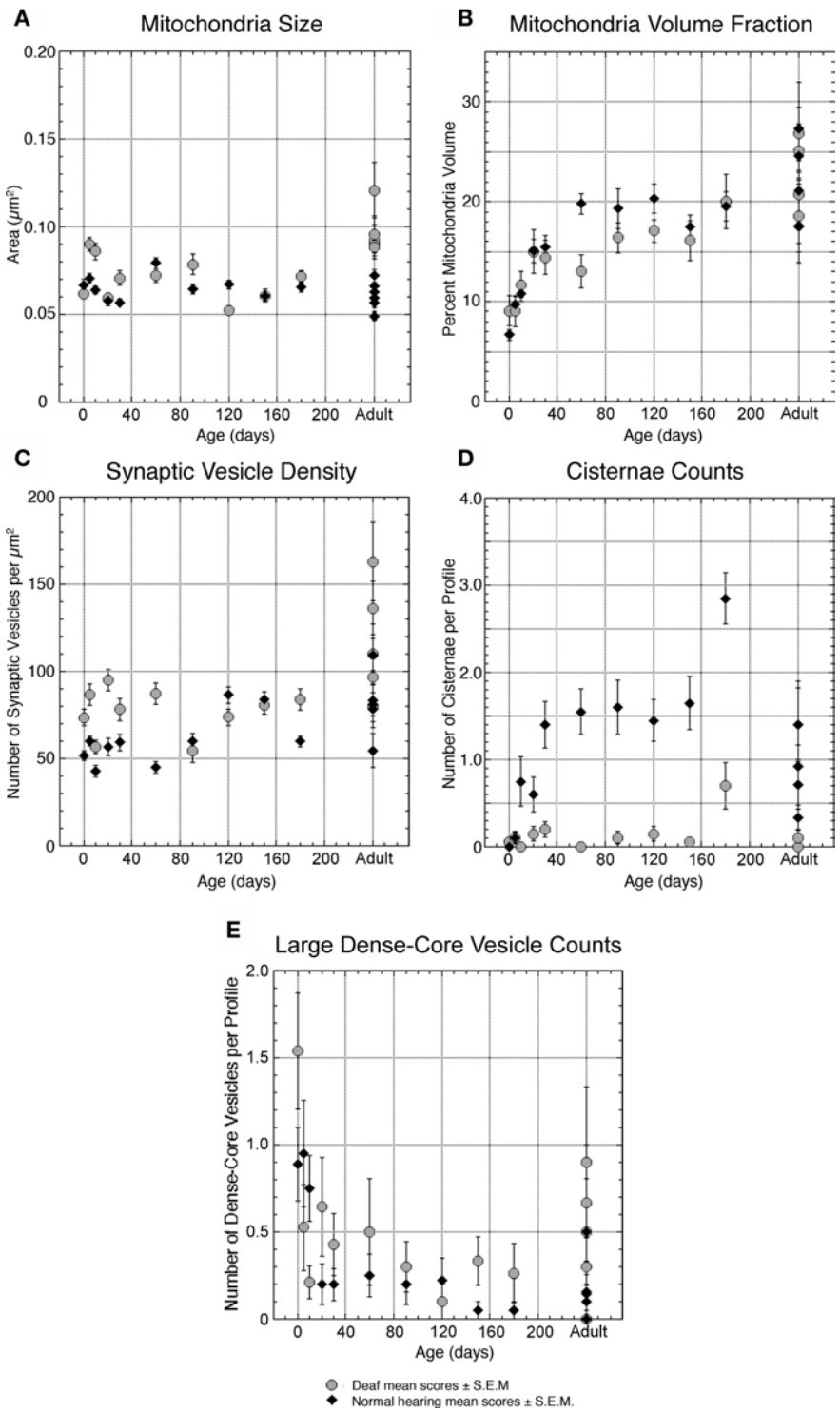

FIGURE 7 | Plots quantifying organelle features of deaf (gray circles) and normal hearing (black triangles) endbulbs with respect to age. (A) The average size (cross-sectional area) of mitochondria does not change with age and is largely unaffected by deafness. **(B)** The percentage of endbulb profile occupied by mitochondria, however, shows a steady increase with age, most likely due to the progressive reduction of endbulb component size. Deafness has no profound impact on mitochondrial volume fraction. **(C)** The density of synaptic vesicles surrounding the PSD increases with age in both groups. In general, PSDs of endbulbs from deaf cats are associated with higher numbers of synaptic vesicles. **(D)** In normal animals, intermembraneous cisternae develop at about 10 days and reach an average of one to two per profile by 30-days postnatal. Interestingly, deaf animals never develop cisternae. **(E)** The number of large dense-core vesicles decreases during development in both cohorts with endbulbs of deaf animals exhibiting slightly more dense-core vesicles. Each point represents an average of multiple measures collected from two animals at all time points except adult, where each point represents the average for one animal. The data points in **(E)** for deaf 60- and 120-day-old animals represent values for only one animal each. Normal data values in **(A**,**B** and **D)** are replotted from Ryugo et al. (2006).

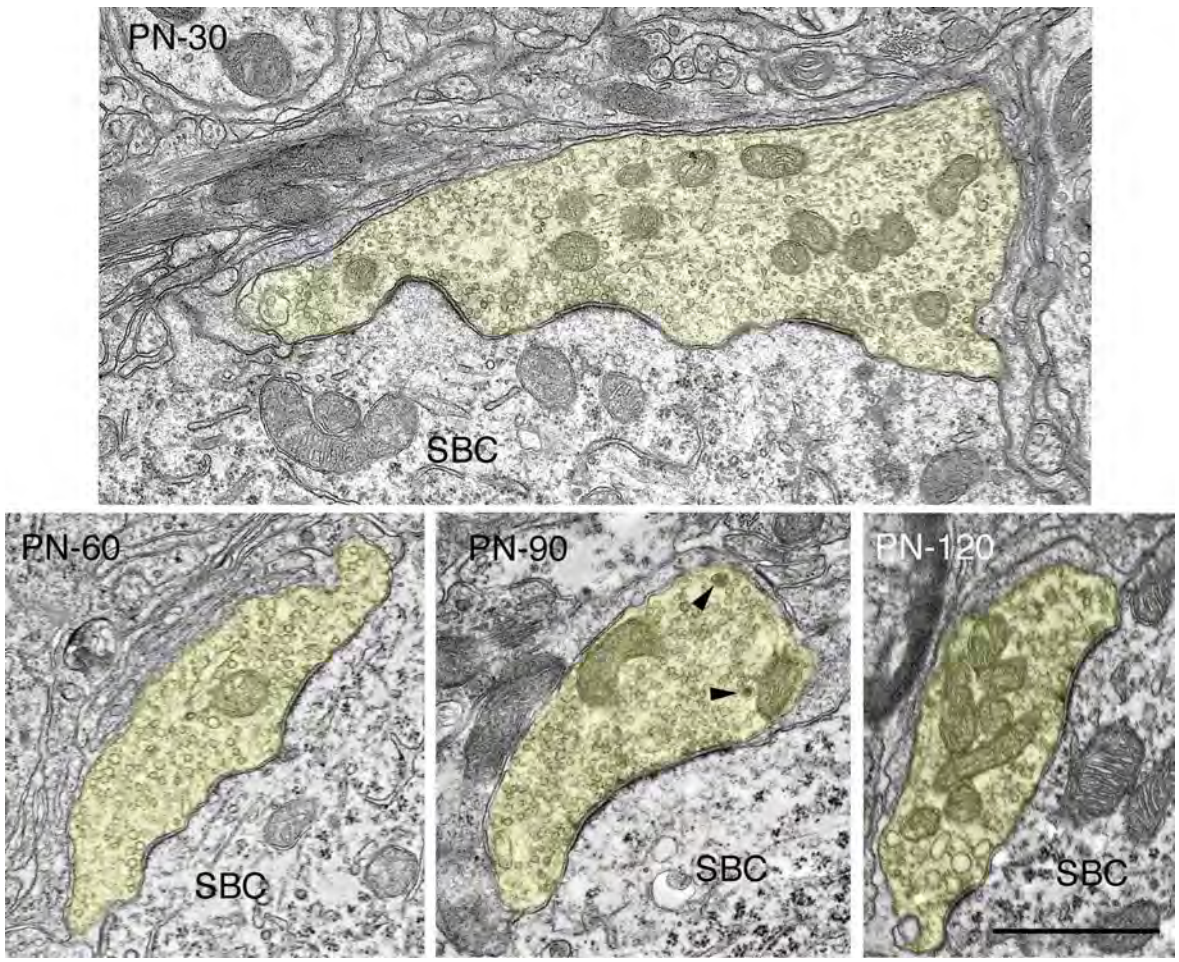

FIGURE 8 | Electron micrographs highlighting maturational changes in endbulbs from 30-, 60-, 90-, and 120-day-old deaf white kittens. The endbulb profiles (yellow) have been reduced in size due to the repeated branching during maturation. The endbulb membrane apposition with the SBC has also reorganized from a highly corrugated surface to a smooth interface. The number of PSDs has decreased, whereas the lengths of the PSDs have increased. Large dense-core vesicles (arrowheads) are still present though their numbers have decreased. Scale bar equals 1 μm.

DISCUSSION

This study describes the structural maturation of the endbulbs of Held of white cats raised from a colony with a history of family deafness. In order to have confidence that these white cats were indeed deaf, we used a light microscope to verify that the cochlear duct was collapsed and that there was no organ of Corti for all cats over five postnatal days of age. Moreover, for cats older than 30 days of age, we also used ABR testing to determine that these cats had no response to clicks or tones up to 100 dB SPL. In cats younger than 5 days of age, prior to the collapse of the cochlear duct and before we could use ABR methods, we selected kittens from a breeding pair that only produced deaf offspring. Because the morphological features of endbulbs of Held from these newborn kittens were virtually identical to those of one newborn kitten with bilateral spongiform pathology of its inner ear and different from those of newborn pigmented kittens, we infer that the newborn white cats in this study were deaf.

Endbulbs of deaf cats exhibit a smaller profile area, flattened and elongated PSDs, and increased synaptic vesicle density as compared to endbulbs from normal hearing cats (see **Figure 14** for summary). These differences are present at birth despite the seemingly intact cochlear structure in both cohorts. Before the onset of hearing, endings from deaf animals have only about half the number of PSDs of normal animals, but by PN-20 both groups show an equal number. One of the most remarkable features of endbulbs in young (<30 days) kittens is the degree of interdigitation with the SBC, as marked by the presence of SBC inclusions and complex endbulb-SBC membrane appositions. In deaf kittens of the same ages, there are fewer inclusions and the membranes are less convoluted. Intermembraneous cisternae begin forming at about PN-10 in normal kittens and by the onset of hearing average one to two per endbulb profile, whereas they are much more rare in deaf kittens. These results show that at birth the endbulbs of Held manifest morphological abnormalities related to deafness despite the normal appearance of the cochlea. In addition, the results also suggest that the development of intermembraneous cisternae is dependent on sound-evoked activity.

COCHLEAR PATHOLOGY

Deafness in our cat colony is evidenced by two principal types of cochlear pathology, which sometimes combine to produce a third (Ryugo et al., 2003). The first type, involving a spongiform

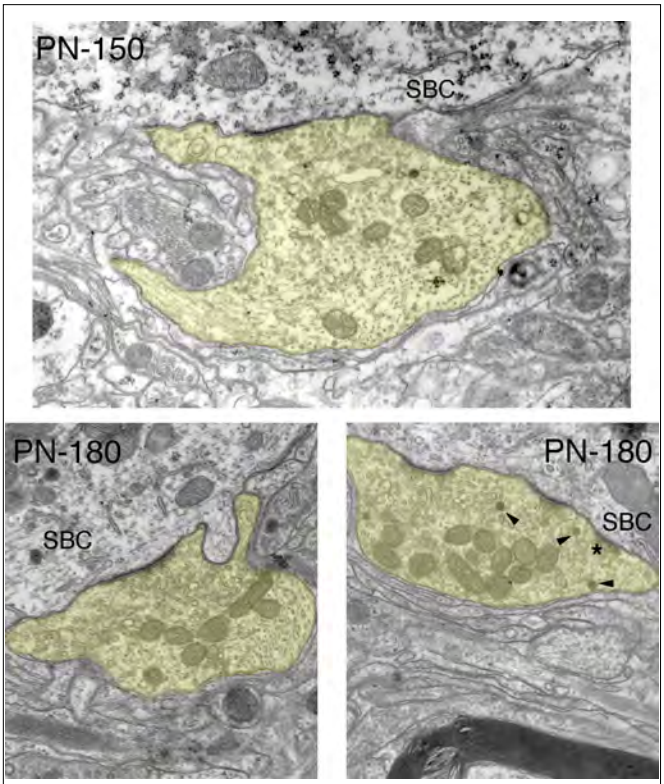

FIGURE 9 | Electron micrographs of endbulbs from 150-day and 180-day deaf white cats. The most prominent and stable morphological features are flattening and lengthening of PSDs, accumulation of synaptic vesicles near the synapses, and increased mitochondrial volume fraction. Smaller, normal looking PSDs (*) are not uncommon in mature deaf animals but they are far outweighed by long flat synapses. Occasionally large dense-core vesicles (arrowheads) can be seen. Scale bar equals 1 μm.

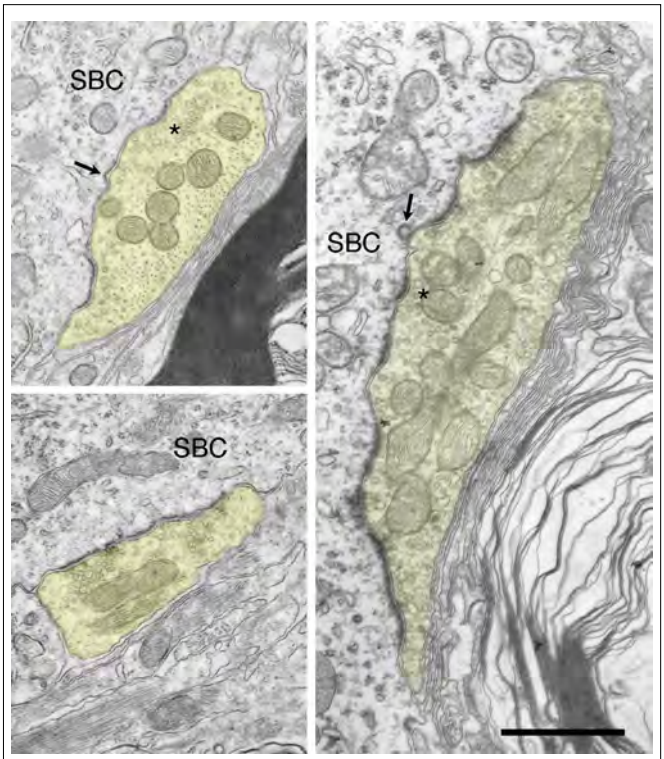

FIGURE 10 | Electron micrographs of endbulbs from adult deaf cats. These endbulbs typically exhibit a mixture of abnormal synapses characterized by long, flat PSDs and normal (*) ones. Postsynaptic coated vesicles (arrows) at varying stages of endocytosis can infrequently be seen at the SBC-endbulb interface. Scale bar equals 1 μm.

overgrowth of epithelial tissue, appears to be present at birth. The second, more common cochlear abnormality involves progressive cochlear degeneration and results in the collapse of the scala media and obliteration of the organ of Corti. The scala media collapses between postnatal day 5 and 10 in our deaf white cats, and the development of deafness features of the endbulb do not seem related to this drastic change in the cochlea.

The cochleae of white kittens do not appear different from those of normal pigmented kittens at birth, with inner and outer hair cells intact in both groups. However, endbulbs of animals destined to be deaf exhibit morphological differences on the first day of life. Compared to those of pigmented kittens, endings from deaf white newborn kittens have a smaller endbulb profile area, a shorter and less complex membrane apposition with the SBC, fewer SBC inclusions, and fewer than half the number of PSDs. The PSDs that are present are considerably longer and have a higher concentration of associated synaptic vesicles when compared to normal newborn endings. Endbulb morphology is similar for deaf animals with both types of cochlear deformation. Therefore, the abnormal endbulb morphology in deaf kittens must be caused by some irregularity independent of cochlear structure.

Cochleae of *deafness* (*dn*/*dn*) mice also appear normal at birth until degeneration starts around postnatal day 10 and progresses until about day 21 (Pujol et al., 1983). Slice recordings revealed abnormally large excitatory postsynaptic currents at the SBC-endbulb synapse in *deafness* mice both before and after hearing onset (Oleskevich and Walmsley, 2002; McKay and Oleskevich, 2007). These authors infer that the difference in synaptic strength between *dn/dn* and wild type mice is related to the lack of spontaneous activity in the auditory nerve of *dn/dn* mice. Moreover, an electron microscopic study of newborn cochleae in these mice found abnormal vacuolization in inner hair cells, a swelling of IHC afferent dendrites, and abnormal smooth endoplasmic reticulum in spiral ganglion neurons (Pujol et al., 1983). It is possible that cochleae of newborn deaf white cats also have abnormalities but that they may not be resolvable even at the electron microscope level.

ACTIVITY-DEPENDENCE OF CISTERNAE DEVELOPMENT

The development of intermembraneous cisternae appears to be dependent on sound-evoked activity. Cisternae start forming in animals destined to develop normal hearing at around PN-10. At this age, the middle ear is opening after having been filled with mesenchyme and occluded by internal ridges since birth (Olmstead and Villablanca, 1980). From this date on, the external ear canal continues to open until about PN-26 (Olmstead and

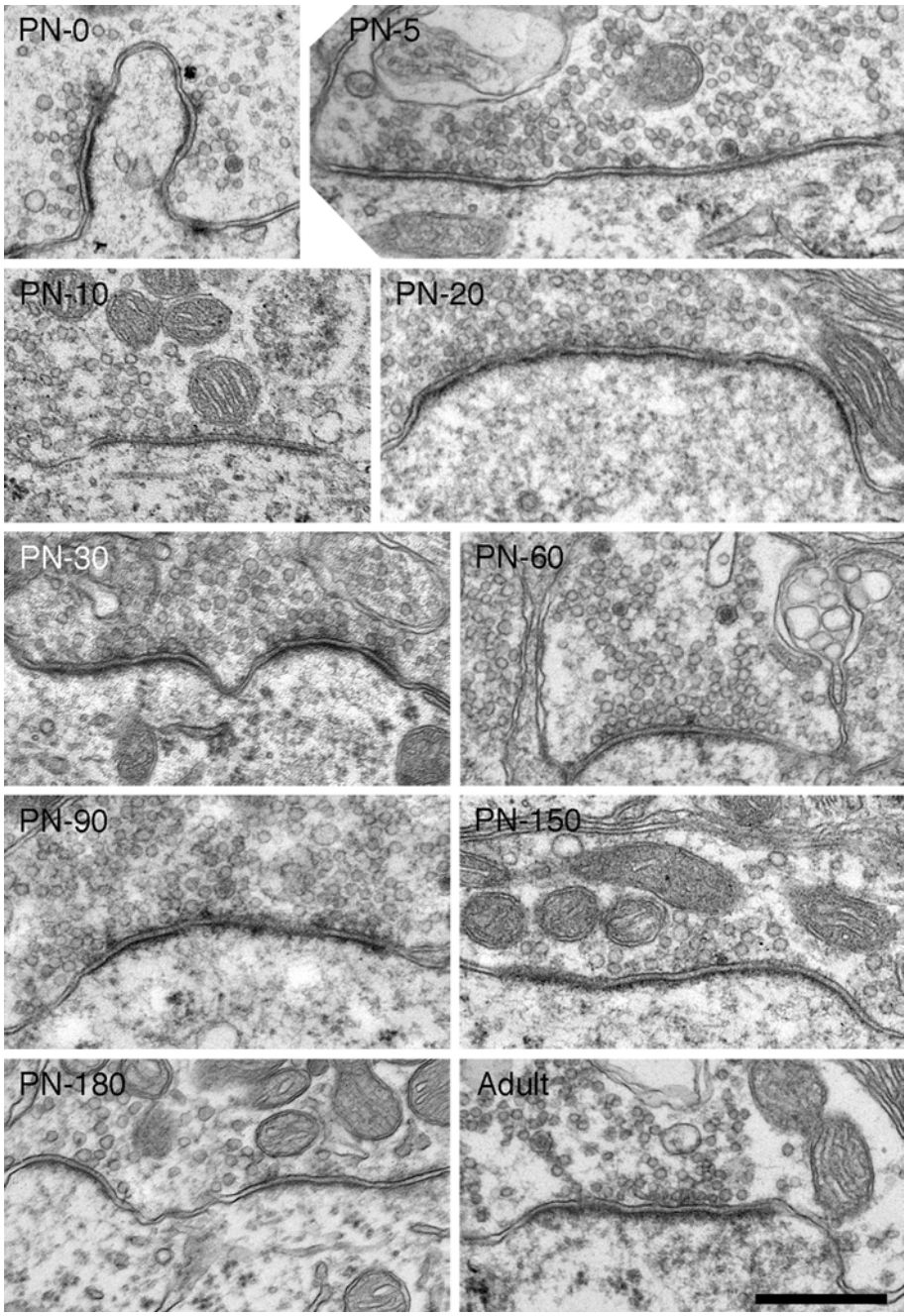

FIGURE 11 | Electron micrographs of synapses from deaf cats. Synapses in deaf animals are marked by long, flat asymmetric membrane thickenings. The presence of small, dome-shaped PSDs is not uncommon in deaf animals, but a large portion of synapses are hypertrophied. From birth, synapses of deaf animals are considerably longer than normals. In fact, PSDs of newborn deaf cats are nearly as large those in mature hearing cats. At all ages, synapses of deaf cats are substantially elongated and flattened compared to those of age-matched hearing animals, including those of hearing littermates. As endbulbs mature, average PSD length grows as does the number of synaptic vesicles associated with synapses. Scale bar equals 0.5 μm.

Villablanca, 1980; Ryugo et al., 2003). At PN-30, reliable ABRs can be recorded with thresholds that are stable into adulthood (Ryugo et al., 2003). By this age, endbulbs of normal hearing kittens exhibit an average of one to two cisternae per profile. Though cisternae can occasionally be seen in deaf endings, their appearance is rare.

While the exact function of these cisternae is not known, it is speculated that they play a role in transmitter uptake and/or recycling (Ryugo et al., 2006). Often glia, which are known to have high concentrations of glutamate transporters (Gegelashvili and Schousboe, 1997), can be found sending filopodial "fingers" into the cisternae of normal hearing cats. A study of the calyces

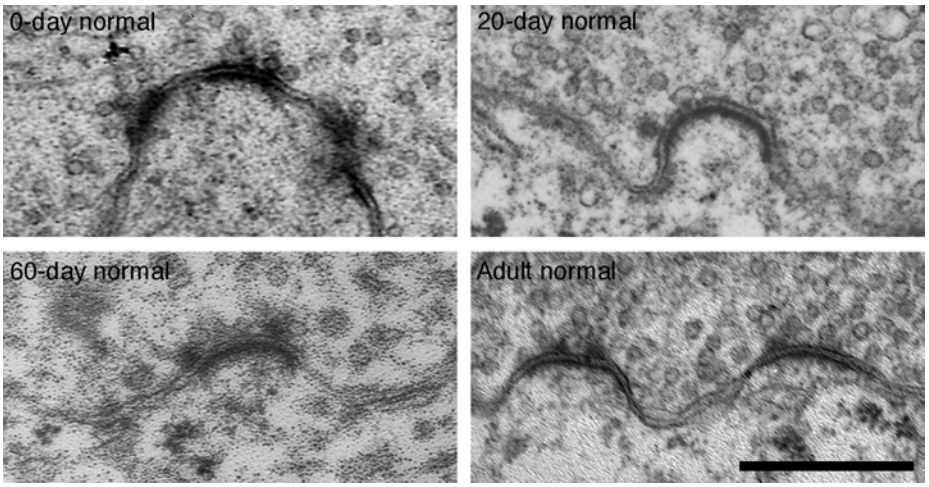

FIGURE 12 | Electron micrographs of 0-day, 20-day, 60-day, and adult synapses of normal hearing cats. PSDs are on average shorter in length and more dome-shaped than those of age-matched deaf animals. Additionally, fewer synaptic vesicles are seen in close proximity to normal synapses. Scale bar equals 0.5 μm.

of Held in the gerbil found that the calyceal fenestration process allowed glial access to the somata of principal neurons of the medial nucleus of the trapezoid body (MNTB, Ford et al., 2009). In addition, the MNTB neurons having more highly branched calyces, and thus more somatic contact with glia, exhibited a faster decay time and lower residual current in response to a stimulus train. These findings are consistent the idea that glia are involved in transmitter clearance. Therefore, the cisternae that we see between the endbulb and SBC membranes could be extracellular spaces left for glia to enter.

SYNAPSE HYPERTROPHY AND SYNAPTIC VESICLE UPREGULATION

An increase in PSD size in the endbulbs of deaf animals has been reported in cats (Ryugo et al., 1997, 2005, 2010), *Shaker-2* mice (Lee et al., 2003), and rats reared in quiet (Rees et al., 1985).

Slice recordings from congenitally deaf (*dn*/*dn*) mice just after hearing onset revealed enhanced synaptic transmission at the endbulb of Held-SBC synapse due to an increase in transmitter release probability (Oleskevich and Walmsley, 2002). The number of independent release sites and the average amplitude of the postsynaptic response to a vesicle of transmitter were no different between deaf and wildtype mice. These findings are consistent with the results presented here. Around the time of hearing onset, endbulbs from deaf kittens have the same number but larger PSDs and a greater accumulation of synaptic vesicles, which may be correlated to a greater glutamate release probability, than normal hearing kittens.

An increase in synaptic strength was also found in *deafness* (*dn/dn*) mice before the onset of hearing (McKay and Oleskevich, 2007). In contrast to the presynaptic mechanisms found to underlie these differences in older mice, a postsynaptic mechanism was concluded to be responsible for the increase in synaptic strength in deaf mice before the onset of hearing (i.e., the amplitude of the miniature excitatory postsynaptic currents was larger in deaf mice). The estimated number of release sites and the probability of release were similar in deaf and wildtype mice. Interestingly, there was a trend for the number of release sites in deaf animals to be higher than that of wildtype. It is not clear to what degree morphology can be used to predict synaptic function as measured by quantal analysis, and vice versa, but the physiological results in mice seem to suggest that deafness features of endbulbs may exert varying degrees of effects before and after the age of normal hearing onset.

Cochlear implantation of congenitally deaf white cats resulted in decreased synaptic vesicle density and PSDs that were statistically similar in size to those of normal hearing cats (Ryugo et al., 2005; O'Neil et al., 2010). The finding in the present study that PSDs are larger from birth in kittens destined to become deaf shows that electrical stimulation has a restorative rather than a preventative effect on the endbulb of Held synapse. The determination that these synapses can be rescued by electrical stimulation strongly suggests that their hypertrophy in deaf animals is caused by a lack of auditory nerve activity.

The implication of our analysis is that at birth, synapses of auditory nerve fibers in the cochlear nucleus have already been signaled that they are destined to be abnormal, and that this information is not in the form of obvious cochlear pathology. It is possible that the perinatal harbinger for deafness involves the spontaneous bursting of auditory nerve fibers (Jones et al., 2007; Tritsch et al., 2007). In normal hearing cats and rats, prior to auditory nerve responsiveness to environmental sounds, spontaneous spike discharges occur in repetitive bursting patterns. Because such rhythmic discharges before the onset of vision have been shown to be important for the development of retinotopic projections and binocular vision (McLaughlin and O'Leary, 2005), it is tempting to speculate that spontaneous activity in the auditory nerve serves a similar function. If congenital deafness disrupts and/or prevents the occurrence of such spontaneous discharges, then the absence of auditory nerve spikes would indicate a hearing abnormality that precipitates pathologic change in endbulb synapses.

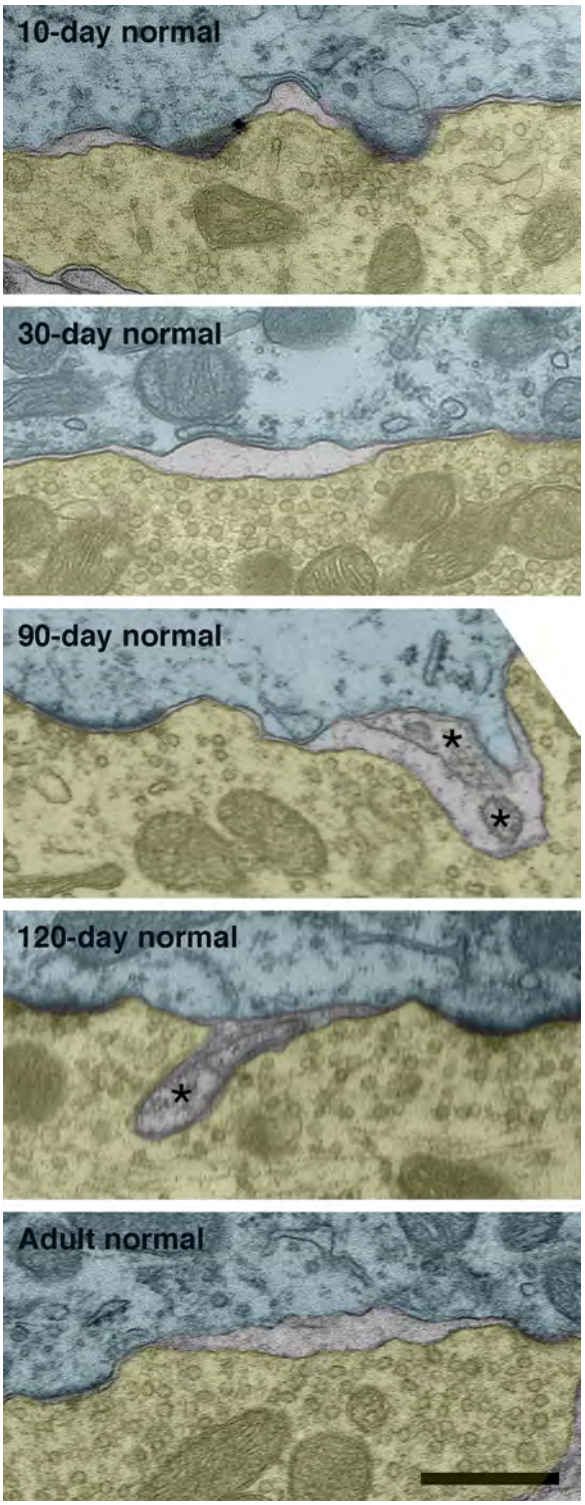

FIGURE 13 | Intermembraneous cisternae in 10-day, 30-day, 90-day, 120-day, and adult normal hearing cats. At around 10-days postnatal, endings of normal hearing kittens start developing spaces between the membranes of SBCs (green) and endbulbs (yellow). These spaces are not artifacts of fixation as surrounding structures are well preserved. Note that cisternae are often found in proximity to PSDs. Occasionally structures (asterisks) can be found occupying the intermembraneous spaces. Scale bar equals 0.5 μm.

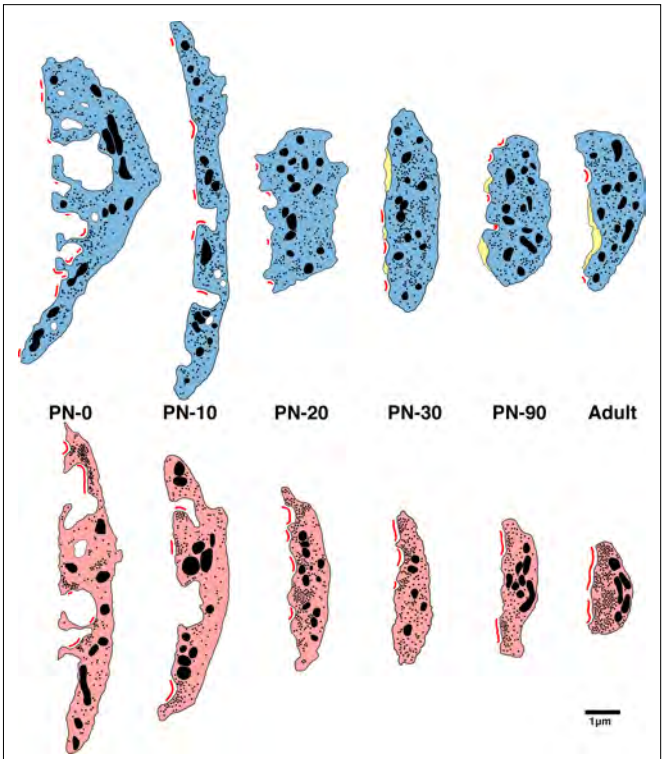

FIGURE 14 | Schematic of endbulb development in deaf (bottom) and normal hearing (top) cats. At birth in both cohorts, endbulb profiles have a convoluted membrane abutting the SBC which becomes less complex into adulthood. Endbulbs of deaf animals are in general smaller than normal. The number of PSDs (red) at birth in deaf animals is less than half that of normal. While mature endbulbs of both deaf and normal animals have the same number of PSDs, the PSDs of deaf animals are longer and flatter than the normal convex PSDs. Deaf endbulbs exhibit an increase in synaptic vesicle (black dots) density near the PSDs. No remarkable differences were seen with respect to mitochondria (large black) size or volume fraction between the two groups. Endbulbs of normal cats begin to develop cisternae (yellow) around postnatal day 10 while deaf endbulbs never develop them to any notable degree.

CLINICAL IMPLICATIONS

We show striking morphological abnormalities at birth in the brain of an animal with hereditary deafness. Cochlear implantation of young (3 months of age) deaf kittens resulted in the restoration of endbulb structure, whereas implantation of older (6 months of age) deaf kittens did not (O'Neil et al., 2010). Endbulb pathology, if not corrected early, becomes exacerbated with age. These findings underscore the importance of early intervention in deafness.

ACKNOWLEDGMENTS

Portions of this work were presented in preliminary form at the 32nd annual MidWinter Meeting of the Association for Research in Otolaryngology, Baltimore, MD, February 14–19, 2009. This work was supported by NIH/NIDCD grants DC000232, DC005211, EY01765; The Emma Liepmann Endowment Fund; and a grant from the Advanced Bionics Corporation.

REFERENCES

Bosher, S. K., and Hallpike, C. S. (1965). Observations on the histological features, development, and pathogenesis of the inner ear degeneration of the deaf white cat. *Proc. R. Soc. Lond., B, Biol. Sci.* 162, 147–170.

Bosher, S. K., and Hallpike, C. S. (1967). Observations on the histogenesis of the inner ear degeneration of the deaf white cat and its possible relationship to the aetiology of certain unexplained varieties of human congenital deafness. *J. Laryngol. Otol.* 80, 222–235.

Brighton, P., Ramesar, R., and Winship, I. (1991). Hearing impairment and pigmentary disturbance. *Ann. N. Y. Acad. Sci.* 630, 152–166.

Carr, C. E., and Konishi, M. (1990). A circuit for detection of interaural time differences in the brain stem of the barn owl. *J. Neurosci.* 10, 3227–3246.

Deol, M. S. (1970). The relationship between abnormalities of pigmentation and of the inner ear. *Proc. R. Soc. Lond., B, Biol. Sci.* 175, 201–217.

Ford, M. C., Grothe, B., and Klug, A. (2009). Fenestration of the calyx of Held occurs sequentially along the tonotopic axis, is influenced by afferent activity, and facilitates glutamate clearance. *J. Comp. Neurol.* 514, 92–106.

Gegelashvili, G., and Schousboe, A. (1997). High affinity glutamate transporters: regulation of expression and activity. *Mol. Pharmacol.* 52, 6–15.

Jones, T. A., Leake, P. A., Snyder, R. L., Stakhovskaya, O., and Bonham, B. (2007). Spontaneous discharge patterns in cochlear spiral ganglion cells before the onset of hearing in cats. *J. Neurophysiol.* 98, 1898–1908.

Koppl, C. (1994). Auditory nerve terminals in the cochlear nucleus magnocellularis: differences between low and high frequencies. *J. Comp. Neurol.* 339, 438–446.

Koppl, C., and Carr, C. E. (1997). Low-frequency pathway in the barn owl's auditory brainstem. *J. Comp. Neurol.* 378, 265–282.

Lee, D. J., Cahill, H. B., and Ryugo, D. K. (2003). Effects of congenital deafness in the cochlear nuclei of Shaker-2 mice: an ultrastructural analysis of synapse morphology in the endbulbs of Held. *J. Neurocytol.* 32, 229–243.

Limb, C. J., and Ryugo, D. K. (2000). Development of primary axosomatic endings in the anteroventral cochlear nucleus of mice. *J. Assoc. Res. Otolaryngol.* 1, 103–119.

Mair, I. W. (1973). Hereditary deafness in the white cat. *Acta Otolaryngol. Suppl.* 314, 1–48.

McKay, S. M., and Oleskevich, S. (2007). The role of spontaneous activity in development of the endbulb of Held synapse. *Hear. Res.* 230, 53–63.

McLaughlin, T., and O'Leary, D. D. (2005). Molecular gradients and development of retinotopic maps. *Annu. Rev. Neurosci.* 28, 327–355.

Molnar, C. E., and Pfeiffer, R. R. (1968). Interpretation of spontaneous spike discharge patterns of neurons in the cochlear nucleus. *Proc. IEEE* 56, 993–1004.

Murthy, V. N., Schikorski, T., Stevens, C. F., and Zhu, Y. (2001). Inactivity produces increases in neurotransmitter release and synapse size. *Neuron* 32, 673–682.

Oleskevich, S., and Walmsley, B. (2002). Synaptic transmission in the auditory brainstem of normal and congenitally deaf mice. *J. Physiol. (Lond.)* 540, 447–455.

Olmstead, C. E., and Villablanca, J. R. (1980). Development of behavioral audition in the kitten. *Physiol. Behav.* 24, 705–712.

O'Neil, J. N., Limb, C. J., Baker, C. A., and Ryugo, D. K. (2010). Bilateral effects of unilateral cochlear implantation in congenitally deaf cats. *J. Comp. Neurol.* (in press)

Pfeiffer, R. R. (1966a). Anteroventral cochlear nucleus: wave forms of extracellularly recorded spike potentials. *Science* 154, 667–668.

Pfeiffer, R. R. (1966b). Classification of response patterns of spike discharges for units in the cochlear nucleus: tone-burst stimulation. *Exp. Brain Res.* 1, 220–235.

Pujol, R., Shnerson, A., Lenoir, M., and Deol, M. S. (1983). Early degeneration of sensory and ganglion cells in the inner ear of mice with uncomplicated genetic deafness (dn): preliminary observations. *Hear. Res.* 12, 57–63.

Rees, S., Galdner, F. H., and Aitkin, L. (1985). Activity dependent plasticity of postsynaptic density structure in the ventral cochlear nucleus of the rat. *Brain Res.* 325, 370–374.

Ryugo, D. K., Baker, C. A., Montey, K. L., Chang, L. Y., Coco, A., Fallon, J. B., Shepherd, R. K. (2010). Synaptic plasticity after chemical deafening and electrical stimulation of the auditory nerve in cats. *J. Comp. Neurol.* in press.

Ryugo, D. K., Cahill, H. B., Rose, L. S., Rosenbaum, B. T., Schroeder, M. E., and Wright, A. L. (2003). Separate forms of pathology in the cochlea of congenitally deaf white cats. *Hear. Res.* 181, 73–84.

Ryugo, D. K., and Fekete, D. M. (1982). Morphology of primary axosomatic endings in the anteroventral cochlear nucleus of the cat: a study of the endbulbs of Held. *J. Comp. Neurol.* 210, 239–257.

Ryugo, D. K., Kretzmer, E. A., and Niparko, J. K. (2005). Restoration of auditory nerve synapses in cats by cochlear implants. *Science* 310, 1490–1492.

Ryugo, D. K., Montey, K. L., Wright, A. L., Bennett, M. L., and Pongstaporn, T. (2006). Postnatal development of a large auditory nerve terminal: the endbulb of Held in cats. *Hear. Res.* 216-217, 100–115.

Ryugo, D. K., Pongstaporn, T., Huchton, D. M., and Niparko, J. K. (1997). Ultrastructural analysis of primary endings in deaf white cats: morphologic alterations in endbulbs of Held. *J. Comp. Neurol.* 385, 230–244.

Ryugo, D. K., Rosenbaum, B. T., Kim, P. J., Niparko, J. K., and Saada, A. A. (1998). Single unit recordings in the auditory nerve of congenitally deaf white cats: morphological correlates in the cochlea and cochlear nucleus. *J. Comp. Neurol.* 397, 532–548.

Scheibe, A. (1892). A case of deaf-mutism, with auditory atrophy and anomalies of development in the membranous labyrinth of both ears. *J. Comp. Neurol.* 397, 532–548.

Scheibe, A. (1895). Bildungsanomalien im hautigen Labyrinth bei Taubstummheit. *Z Ohrenheilkd* 27, 95–99.

Smith, P. H., Joris, P. X., and Yin, T. C. (1993). Projections of the physiologically characterized spherical bushy cell axons from the cochlear nucleus of the cat: evidence for delay lines to the medial superior olive. *J. Comp. Neurol.* 331, 245–260.

Suga, F., and Hattler, K. W. (1970). Physiological and histopathological correlates of hereditary deafness in animals. *Laryngoscope* 80, 81–104.

Tritsch, N. X., Yi, E., Gale, J. E., Glowatzki, E., and Bergles, D. E. (2007). The origin of spontaneous activity in the developing auditory system. *Nature* 450, 50–55.

Conflict of Interest Statement: The authors declare that the research was conducted in the absence of any commercial or financial relationships that could be construed as a potential conflict of interest.

Received: 14 January 2010; paper pending published: 15 February 2010; accepted: 24 April 2010; published online: 21 May 2010.

Citation: Baker CA, Montey KL, Pongstaporn T and Ryugo DK (2010) Postnatal development of the endbulb of Held in congenitally deaf cats. Front. Neuroanat. ***4****:19. doi: 10.3389/fnana.2010.00019*

frontiers in
NEUROANATOMY

ORIGINAL RESEARCH ARTICLE
published: 28 September 2010
doi: 10.3389/fnana.2010.00135

Origins of glutamatergic terminals in the inferior colliculus identified by retrograde transport and expression of VGLUT1 and VGLUT2 genes

Tetsufumi Ito[1,2] and Douglas L. Oliver[2]*

[1] *Department of Anatomy, Faculty of Medical Sciences, University of Fukui, Fukui, Japan*
[2] *Department of Neuroscience, University of Connecticut Health Center, Farmington, CT, USA*

Edited by:
Miguel A. Merchán, Universidad de Salamanca, Spain

Reviewed by:
Adrian Rees, Newcastle University, UK
Nell B. Cant, Duke University, USA

****Correspondence:***
Douglas L. Oliver, Department of Neuroscience, University of Connecticut Health Center, Farmington, CT 06030-3401, USA.
e-mail: doliver@neuron.uchc.edu

Terminals containing vesicular glutamate transporter (VGLUT) 2 make dense axosomatic synapses on tectothalamic GABAergic neurons. These are one of the three types of glutamatergic synapses in the inferior colliculus (IC) identified by one of three combinations of transporter protein: VGLUT1 only, VGLUT2 only, or both VGLUT1 and 2. To identify the source(s) of these three classes of glutamatergic terminals, we employed the injection of Fluorogold (FG) into the IC and retrograde transport in combination with *in situ* hybridization for VGLUT1 and VGLUT2 mRNA. The distribution of FG-positive soma was consistent with previous reports. In the auditory cortex, all FG-positive cells expressed only VGLUT1. In the IC, the majority of FG-positive cells expressed only VGLUT2. In the intermediate nucleus of the lateral lemniscus, most FG-positive cells expressed VGLUT2, and a few FG-positive cells expressed both VGLUT1 and 2. In the superior olivary complex (SOC), the majority of FG-positive cells expressing VGLUT2 were in the lateral superior olive, medial superior olive, and some periolivary nuclei. Fewer FG-positive cells expressed VGLUT1&2. In the ventral cochlear nucleus, almost all FG-positive cells expressed VGLUT1&2. On the other hand in the dorsal cochlear nucleus, the vast majority of FG-positive cells expressed only VGLUT2. Our data suggest that (1) the most likely sources of VGLUT2 terminals in the IC are the intermediate nucleus of the lateral lemniscus, the dorsal cochlear nucleus, the medial and lateral superior olive, and the IC itself, (2) VGLUT1 terminals in the IC originate only in the ipsilateral auditory cortex, and (3) VGLUT1&2 terminals in IC originate mainly from the VCN with minor contributions from the SOC and the lateral lemniscal nuclei.

Keywords: vesicular glutamate transporter, *in situ* hybridization, retrograde transport, auditory system

INTRODUCTION

The inferior colliculus (IC) receives ascending inputs from many lower auditory nuclei (Whitley and Henkel, 1984; Oliver, 1985, 1987; Saint Marie et al., 1989; Saint Marie and Baker, 1990; Oliver et al., 1995; Gonzalez-Hernandez et al., 1996; Alibardi, 1998; Cant and Benson, 2006) and descending inputs from the auditory cortex (Winer et al., 1998). In spite of the number of studies about neurotransmitters used in these pathways (Saint Marie et al., 1989; Saint Marie and Baker, 1990; Gonzalez-Hernandez et al., 1996; Alibardi, 1998), the expression of neurotransmitters, especially glutamate, in the auditory nuclei is not well defined because of the lack of reliable markers. The lack of information about neurotransmitters, as well as the complexity of the inputs, has retarded progress in understanding the synaptic organization of the IC (Oliver et al., 1999; Loftus et al., 2004).

Vesicular glutamate transporters (VGLUT) are reliable markers for glutamatergic terminals (Kaneko and Fujiyama, 2002), and currently three subtypes of VGLUT are known (Takamori, 2006). In the IC, both VGLUT1 and VGLUT2 are found in synaptic terminals (Kaneko et al., 2002; Altschuler et al., 2008; Ito et al., 2009), but VGLUT3 is not (Ito et al., 2009). Indeed, three types of glutamatergic terminals have been identified in the IC; terminals containing only VGLUT1, those containing only VGLUT2, and those containing both molecules (VGLUT1&2) (Ito et al., 2009). Certain VGLUT molecules in terminals seems to associate with specific patterns of synaptic organization: For example, the large terminals in IC tend to contain VGLUT1 and terminate on distal dendrites (Altschuler et al., 2008). In contrast, numerous, smaller VGLUT2-positive axosomatic terminals encircle somata of GABAergic tectothalamic cells (Ito et al., 2009). Therefore, elucidating the combination of VGLUT molecules in glutamatergic neurons which project to the IC will help to identify the origin of these VGLUT1- and VGLUT2-containing glutamatergic terminals. To identify the source of these inputs, we employed *in situ* hybridization (ISH) for VGLUT molecules

Abbreviations: AVCN, anteroventral cochlear nucleus; CNC, cochlear nuclei complex; DCN, dorsal cochlear nucleus; DIG, digoxigenin; DNLL, dorsal nucleus of the lateral lemniscus; DPO, dorsal periolivary nucleus; Fast Red, 4-chloro-2-methylbenzenediazonium hemi-zinc chloride; FG, Fluorogold; FL, fluorescein; IC, inferior colliculus; ICC, central nucleus of the IC; DC, dorsal cortex of the IC; LC, lateral cortex of the IC; INLL, intermediate nucleus of the lateral lemniscus; LSO, lateral superior olive; LVPO, lateroventral periolivary nucleus; MNTB, medial nucleus of the trapezoid body; MSO, medial superior olive; MVPO, medioventral periolivary nucleus; NLL, nuclei of lateral lemniscus; PBS-X, 0.3% Triton X-100 in 0.05 M phosphate-buffered saline; PBS-XG, 0.3% Triton X-100 with 1% normal goat serum in 0.05 M phosphate-buffered saline; PVCN, posteroventral cochlear nucleus; RPO, rostral periolivary nucleus; SOC, superior olivary complex; SPO, superior paraolivary nucleus; TS7.5, Tris–HCl (pH 7.5) and 0.15 M NaCl; VGLUT1, vesicular glutamate transporter 1; VGLUT2, vesicular glutamate transporter 2; VGLUT3, vesicular glutamate transporter 3; VMPO, ventromedial periolivary nucleus; VNLL, ventral nucleus of the lateral lemniscus.

combined with the retrograde transport and immunohistochemical detection of Fluorogold (FG) after the large injection of FG into the IC. Neurons expressing VGLUT mRNA exhibit whole population of glutamatergic neurons and large FG injection into the IC reveals neural population making projection to the IC. Therefore, this approach is useful to show the sources of IC VGLUT terminals.

MATERIALS AND METHODS

SUBJECTS

Fourteen adult Long-Evans rats were used for this study. All experiments were done in accordance with institutional guidelines at the University of Connecticut Health Center and in accordance with NIH guidelines for the care and use of laboratory animals. All efforts were made to minimize the number of animals used and their suffering.

SURVIVAL SURGERY

Rats were anesthetized with ketamine (97.5 mg/kg i.m.) and xylazine (2.4 mg/kg i.m.), and maintained in an areflexive state with isoflurane mixed with oxygen for the duration of the surgery and recording. Surgery and recording were done in a double-walled sound attenuating chamber (IAC, Bronx, NY, USA). Acoustic stimuli were generated by a TDT System 2 (Tucker Davis Technologies, Gainesville, FL, USA) under the control of a PC computer and custom software. All sounds were delivered by Beyer earphones (DT-48, Hicksville, NY, USA) via sealed enclosures. Animals were fixed in a stereotaxic apparatus that incorporated hollow ear bars to deliver sound stimuli. The sound delivery system was calibrated from 60 to 40,000 Hz, and the calibration was performed at the end of the ear bar with a 1/8″ microphone (Brüel & Kjær, Nærum, Denmark). A craniotomy opened the right parietal bone over the visual cortex. Glass micropipettes (4–7 μm tip, 0.5–5 MΩ) were filled with 3% FG (Fluorochrome, Denver, CO, USA) diluted in saline. These glass electrodes were advanced with a microdrive (Burleigh Inchworm, Fishers, NY, USA) mounted on the stereotaxic manipulator through the cortex after the dura was opened. Recordings of activity evoked by sounds in the contralateral ear were used to locate the IC. Acoustically driven responses of single or multiple units were amplified with a Dagan 2400 amplifier (Minneapolis, MN, USA) and a low noise amplifier (Princeton Applied Research, model 5113 amplifiers). Neurons in the central nucleus of the IC (ICC) were identified by short latency responses to white noise bursts or pure tones. At locations in the IC with brisk responses, FG was iontophoretically injected from the recording pipette with a 2–5 μA current for durations of 2–5 min with a 50% duty cycle (7 s on/7 s off).

Four to seven days after the surgery, the rats were deeply anesthetized with ketamine (97.5 mg/kg i.m.) and xylazine (2.4 mg/kg i.m.), and perfused transcardially with 4% paraformaldehyde in 0.1 M phosphate buffer (PB, pH 7.4). After cryoprotection in 30% sucrose in PB for 2 days, serial, 40 μm-thick, coronal sections were cut with a freezing microtome. A series of every fifth section was used for histology.

IMMUNOHISTOCHEMISTRY FOR FG

We used a rabbit polyclonal antibody to detect FG (AB153, Millipore). Specificity of the antibody was confirmed by absence of staining in tissues which did not contain FG. Sections were incubated with the rabbit anti-FG antibody (1:8000) diluted in 0.3% Triton X-100 with 1% normal goat serum in 0.05 M phosphate-buffered saline (PBS-XG), followed by an incubation in a biotinylated goat anti-rabbit secondary antibody (1:200; Vector Laboratories, Burlingame, CA, USA) diluted in PBS-XG. After an incubation in avidin-biotinylated peroxidase complex (1:50; ABC-Elite, Vector) in PBS containing 0.3% Triton X-100 (PBS-X), sections were processed for a Nickel-diaminobenzidine (DAB) reaction. Sections were mounted on coated glass slides, counterstained with Neutral Red (Fisher Scientific, Fair Lawn, NJ, USA), dehydrated through graded alcohols, cleared with Histoclear (National Diagnostics, Atlanta, GA, USA), and coverslipped with Permount (Fisher Scientific, Waltham, MA, USA).

BRIGHTFIELD ISH COMBINED WITH IMMUNOHISTOCHEMISTRY FOR FG

Both digoxigenin (DIG)- and fluorescein (FL)-labeled antisense riboprobes were made from cDNAs of mouse VGLUT1 (nucleotides of 152–1085, GenBank accession number NM_182993.2) and mouse VGLUT2 (nucleotides of 848–2044, GenBank accession number NM_080853.2). The specificity of the riboprobes for VGLUT1 and VGLUT2 was established in previous studies (Watakabe et al., 2006; Nakamura et al., 2007). Furthermore, the sequences of VGLUT1, VGLUT2 probes have very high similarities with corresponding regions of the rat cDNAs (96 and 94%, respectively). On the other hand, similarities of these riboprobes with other members of the family of molecules are low: The mouse VGLUT1 riboprobe shares only 74 and 71% identity with the corresponding regions of the rat VGLUT2 and VGLUT3 mRNA; and the mouse VGLUT2 riboprobe has only 74 and 76% homology with the rat VGLUT1 and VGLUT3 mRNA.

All 14 animals were processed for non-radioactive ISH. The procedure for non-radioactive ISH was described previously (Liang et al., 2000; Ito et al., 2007, 2008). Free-floating sections were washed in 0.1 M PB (pH 7.0) for 5 min twice, immersed in PB containing 0.3% Triton X-100, and rinsed in 0.1 M PB. Then, sections were acetylated for 10 min at room temperature with 0.003% acetic acid anhydrate, 1.3% (v/v) triethanolamine, and 6.5% (w/v) HCl diluted in DEPC-treated water. After being rinsed in 0.1 M PB twice, the sections were incubated for 1 h at 70°C in a prehybridization buffer containing 50% (v/v) formamide, 5 × SSC buffer (a 5× concentration of SSC buffer containing 16.65 mM sodium chloride and 16.65 mM sodium citrate buffer, pH 7.0), 2% blocking reagents (Roche Diagnostics, Mannheim, Germany), 0.1% N-lauroylsarcosine (NLS), and 0.1% sodium dodecyl sulfate. Then, the sections were hybridized with 1 μg/ml DIG-labeled sense or antisense RNA probe for VGLUT1 or VGLUT2 in freshly prepared prehybridization buffer for 20 h at 70°C. After two washes in 2× SSC, 50% formamide, and 0.1% NLS for 20 min at 70°C, the sections were rinsed in 2× SSC with 0.1% NLS for 20 min twice at 37°C, and in 0.2× SSC with 0.1% NLS for 20 min twice at 37°C. These sections were incubated with 1% blocking reagent (Roche) diluted in Tris–HCl (pH 7.5) and 0.15 M NaCl (TS7.5) for 1 h at room temperature, and then with alkaline phosphatase-conjugated anti-DIG antibody Fab fragment (1:2000; Roche) and rabbit anti-FG antibody (1:8000) in 1% blocking reagent (Roche) diluted in TS7.5 at room temperature overnight. After the secondary and ABC reactions described above, FG was visualized by a DAB

reaction. Subsequently, the bound phosphatase was visualized by a reaction with nitro blue tetrazolium chloride/5-bromo-4-chloro-3-indolyl phosphate toluidine salt (Roche) for 4 h at 37°C in Tris–HCl (pH 9.5), 0.15 M NaCl, and 10 mM $MgCl_2$. Finally, the sections were mounted on coated glass slides, dehydrated, cleared with Histoclear (National Diagnostics, Atlanta, GA, USA), and coverslipped.

DOUBLE FLUORESCENT ISH COMBINED WITH IMMUNOHISTOCHEMISTRY FOR FG

In three rats that showed the strongest signals in brightfield ISH, brainstem sections were also processed for a combination of fluorescent ISH and FG immunohistochemistry. For fluorescent ISH to detect VGLUT1 and VGLUT2 expression, the FL-labeled riboprobe for VGLUT1 and DIG-labeled riboprobe for VGLUT2 were diluted in hybridization buffer at a final concentration of 1 μg/ml. The hybridization temperature was set at 70°C. After the incubation and washing described above, these sections were incubated with alkaline phosphatase-conjugated sheep anti-FL antibody Fab fragment (1:2000; Roche), peroxidase-conjugated sheep anti-DIG antibody Fab fragment (1:2000; Roche), and rabbit anti-FG (1:1000) in 1% blocking reagent (Roche) diluted in TS7.5 at room temperature overnight. The sections were rinsed three times, and then the bound peroxidase was reacted with dinitrophenol-tyramide signal amplification (Perkin-Elmer, Waltham, MA, USA). After three more washes, the sections were incubated with AlexaFluor 488-conjugated goat anti-rabbit IgG (1:100; Invitrogen, Carlsbad, CA, USA), blocked by 10% normal rabbit serum, and then incubated with AlexaFluor 647-conjugated rabbit anti-dinitrophenol (1:50; Invitrogen) diluted in 1% normal rabbit serum/TS7.5. To visualize bound alkaline phosphatase by fluorescent microscopy, sections were developed with 0.005% (w/v) 4-chloro-2-methylbenzenediazonium hemi-zinc chloride (Fast Red TR, Roche), 1% (v/v) 2-hydroxy-3-naphthoic acid-2′-phenylanilide phosphate (HNPP, Roche) diluted in 0.1 M Tris–HCl (pH 8.0), 0.15 M NaCl, 10 mM $MgCl_2$, for 30 min at room temperature. The sections were mounted on glass slides with CC/Mount (DBS, Pleasanton, CA, USA).

IMAGE ANALYSIS

Fluorescent images were acquired with a laser scanning confocal microscope (Zeiss 510 META, Carl Zeiss Microimaging, Göttingen, Germany) or structural illuminated microscope (Zeiss Axiovert microscope with Apotome, Zeiss). For the laser scanning confocal microscopy, AlexaFluor 488 was excited by a 488 nm Ar laser, and emitted fluorescence was filtered with a 500–530 nm band-pass filter. Fast Red was excited by a 543-nm He–Ne laser, and emitted fluorescence was filtered with a 565–615 nm band-pass filter. AlexaFluor 647 was excited by a 633-nm He–Ne laser, and emitted fluorescence was filtered with a 650-nm low-pass filter. Images of each dye were taken sequentially to avoid bleed-through artifact. For structural illuminated microscopy, filter sets for FITC, rhodamine, and Cy5 were used to visualize AlexaFluor 488, FastRed, and AlexaFluor 647, respectively. Minimal adjustments of the levels were made by Photoshop CS3 (Adobe Systems, San Jose, CA, USA).

To plot FG-immunofluorescent cells, we took images of FG-positive cells with a ×10 lens (NA 0.5). Outlines of the evenly spaced (200 μm) serial sections were traced with Neurolucida (MBF Bioscience, Inc., Williston, VT, USA), and the images of FG-positive cells were assembled on the trace. The nuclei were identified by Nissl cytoarchitecture, and in accordance with Mugnaini et al. (1980) for the cochlear nuclei complex (CNC), Schofield and Cant (1991) for the superior olivary complex (SOC), Saint Marie et al. (1997) for the nuclei of the lateral lemniscus (NLL), and Loftus et al. (2008) for the IC.

RESULTS

INJECTION SITES

The injection was restricted to the IC in all 14 cases. In nine cases, the injection site was mainly in the ICC. In two cases, the injection site was in the lateral cortex of the IC (LC). In three cases, the injection was made around the border of the ICC and LC. Double fluorescent ISH combined with FG immunohistochemistry was performed in three cases, and those injection sites were in the ICC (08-110; **Figure 1A**) and the border of the ICC and LC (08-118 and 08-124; **Figures 1B,C**).

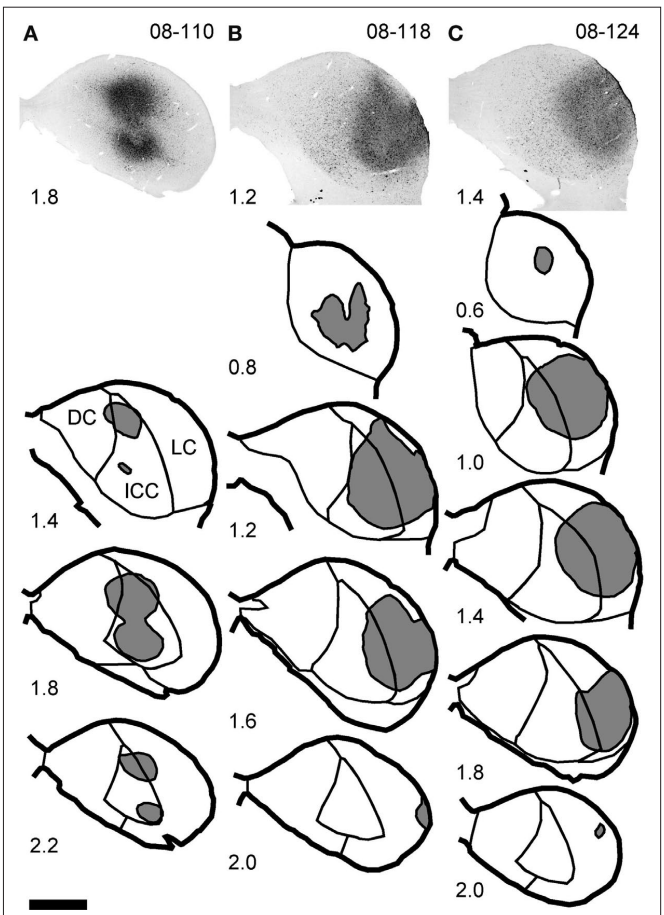

FIGURE 1 | Injection sites of FG. Top images show the center of the injection site in three animals processed for fluorescent ISH. Line drawings show the full extent of the injection sites (gray) at several rostro-caudal levels. In case 08-110 **(A)**, the injection is almost restricted to the central nucleus (ICC). In cases 08-118 **(B)** and 08-124 **(C)**, the injections are larger, and they cover both the lateral cortex (LC) and lateral part of the ICC. Numbers indicate the distance (in millimeters) from the section which contains the most rostral part of the ventral nucleus of the lateral lemniscus (VNLL). Note that in the case 08-110, two injections were made. Scale bar: 1 mm.

OVERVIEW OF RETROGRADE LABELING AND VGLUT GENE EXPRESSION

The combined analysis of retrograde FG-labeling and gene expression for VGLUT revealed four patterns of retrogradely labeled neurons. Some retrogradely FG-labeled neurons expressed the gene for VGLUT2 only (VGLUT2 in the text; FG+/V1−/V2+ in the figures and tables). Others co-expressed both VGLUT1 and VGLUT2 (VGLUT1&2 in the text; FG+/V1+/V2+ in the figures and tables). The third pattern was FG-labeling and the absence of either VGLUT1 or VGLUT2 gene expression (FG+/V1−/V2− in the figures and tables). This is most likely associated with neurons that use GABA or glycine as a neurotransmitter. These first three patterns were prevalent in the auditory midbrain, pons, and medulla. FG-labeling with gene expression of VGLUT1 alone was not seen in these regions. However, in the auditory cortex the only pattern observed was FG-labeled neurons that expressed only VGLUT1 (VGLUT1 in the text). In all cases, FG-retrogradely labeled cells were found in the contralateral IC, bilaterally in the dorsal NLL (DNLL), ipsilaterally in the intermediate and ventral NLL (INLL and VNLL), bilaterally in the SOC, and contralaterally in the CNC. Four cases had bilateral FG retrograde label in the auditory cortex. The general pattern of retrograde labeling was consistent with previous studies (Beyerl, 1978; Coleman and Clerici, 1987; Herbert et al., 1991; Saldana and Merchan, 1992; Gonzalez-Hernandez et al., 1996; Oliver et al., 1999).

MIDBRAIN

The main source of VGLUT2 inputs to the IC from the midbrain was the contralateral IC and the ipsilateral INLL. The majority of the retrogradely labeled cells in the IC were located in the contralateral central nucleus (**Figure 2A**). We found numerous neurons expressing VGLUT2 but none that expressed VGLUT1. VGLUT2 was expressed in around 90% of FG-positive cells in the central nucleus and lateral cortex (**Table 2**) and in over 70% of FG-positive neurons in dorsal cortex (**Table 2**). No neurons expressed VGLUT1 or VGLUT1&2 (**Figures 2B,3A1–4**; **Tables 1,2**). The FG-labeled cells without VGLUT expression are likely the GABAergic neurons. So, both glutamatergic and GABAergic neurons have projections through the commissure of the IC.

The INLL also had significant numbers of FG-labeled, VGLUT2-expressing cells. Fewer FG-labeled cells expressed VGLUT1&2. Both patterns were found throughout the nucleus (**Figure 2B**, sections 0.4–1.4). Over 50% of FG-positive cells in the ipsilateral INLL expressed VGLUT2 (white arrows in **Figure 3C**). Around 20% of retrogradely labeled cells co-expressed VGLUT1&2 (black arrows in **Figure 3C**). The morphology was very similar for the FG-positive cells that expressed VGLUT1&2 or VGLUT2 alone (**Figure 3C**) and project to the IC.

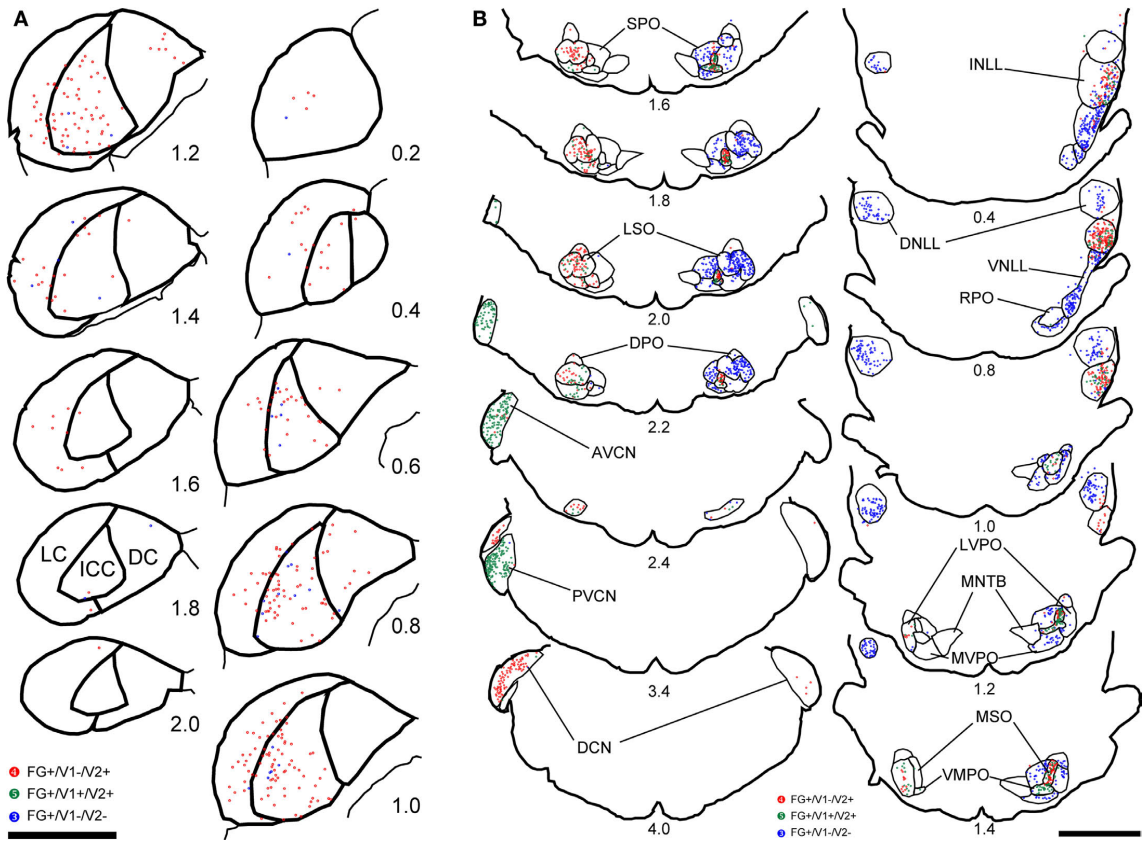

FIGURE 2 | Plots of retrogradely labeled cells in the IC (A), NLL, SOC, and CNC (B) of the case 08-118. In the IC **(A)**, contralateral side to the injection site was presented. Red dots indicate cells positive for both FG and VGLUT2 but negative for VGLUT1 (FG+/V1−/V2+). Green dots indicate cells positive for all three molecules (FG+/V1+/V2+). Blue dots indicate cells positive for FG but negative for VGLUT1 and VGLUT2 (FG+/V1−/V2−). Numbers indicate the distance (in millimeter) from the section which contains the most rostral part of the VNLL. Scale bar: 2 mm.

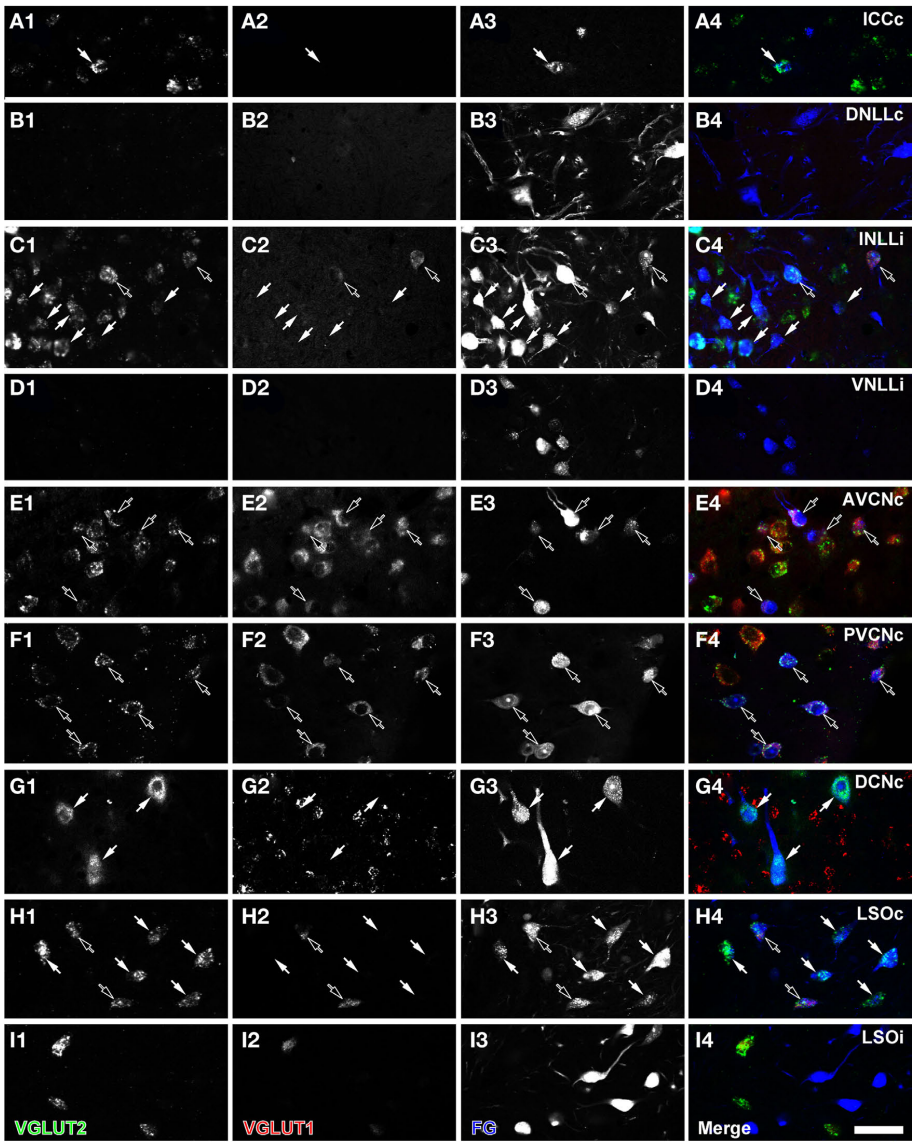

FIGURE 3 | Fluorescent micrographs of retrogradely labeled cells in the IC (A), NLL (B–D), CNC (E–G), and SOC (H–Q). Some retrogradely labeled cells expressed only VGLUT2 (white arrows) or both VGLUT1 and VGLUT2 (black arrows). The "**c**" and "**i**" after the abbreviation of the nuclei mean contralateral and ipsilateral to the injection site. Green: VGLUT2; red: VGLUT1; blue: FG. Scale bar: 50 μm.

In the DNLL, expression of either VGLUT was rare (**Figure 2B**, sections 0.4–1.4; **Figure 3B**). We found that VGLUT negative neurons comprised over 90% of FG-labeled neurons in the contralateral and ipsilateral side, respectively (**Table 2**). Most likely, these are GABAergic neurons. A similar pattern was seen in the ventral part of the lateral lemniscus where the expression of VGLUT was rare. Over 90% of VNLL retrogradely labeled cells were not positive for VGLUT1 or VGLUT2 (**Figure 2B**, sections 0.4 and 0.8; **Figure 3D**). These are likely GABAergic and/or glycinergic neurons with projections to the IC.

COCHLEAR NUCLEUS

Most FG-labeled neurons in the cochlear nucleus were found on the contralateral side, but the patterns in AVCN and PVCN were different from the DCN (**Figure 2B**, sections 2.0–4.0). Almost all the FG-positive cells (99%) co-expressed VGLUT1&2 in the AVCN (**Figure 3E**) and PVCN (**Figure 3F**). These were likely to be T-stellate cells with projections to the IC (Oliver, 1987; Oertel et al., 1990; Oliver et al., 1999). In contrast, the large cells in the DCN mainly found in layer 2 expressed only VGLUT2, and only these, presumably fusiform cells, were labeled with FG (**Figure 3G**). This is consistent with presumed glutamatergic inputs to the IC from these cells (Adams, 1979; Oliver, 1984a). No other neurons were FG-labeled including the small granule cells that were positive for only VGLUT1 (**Figure 3G2**).

SUPERIOR OLIVARY COMPLEX

In general, the IC projections from the SOC followed either the LSO pattern, the MSO pattern, or the SPO pattern. The LSO pattern was a mixture of VGLUT expression on the contralateral side and

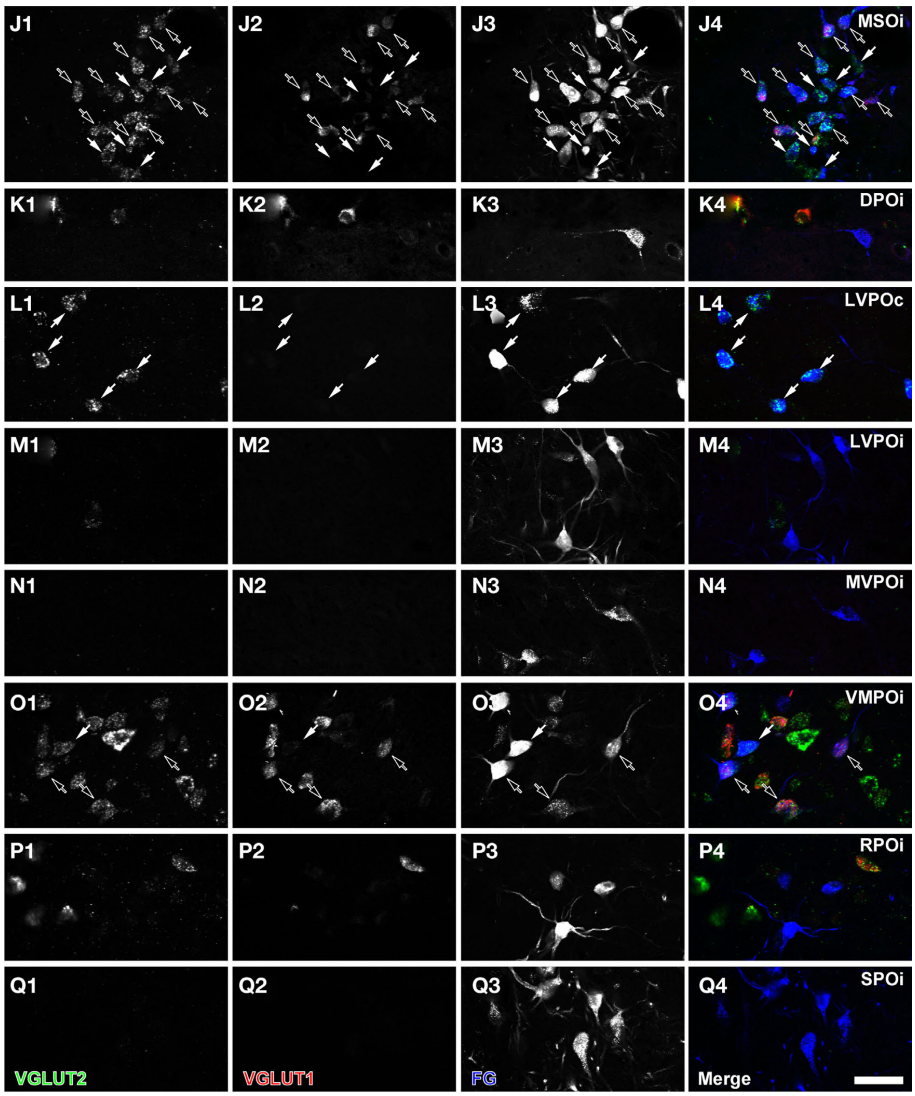

FIGURE 3 | Continued

non-VGLUT expression on the ipsilateral side. The MSO pattern was predominantly an ipsilateral projection that was exclusively VGLUT-positive. The SPO pattern was also an ipsilateral projection, but it was exclusively non-glutamatergic (**Table 2**).

In the contralateral LSO, all FG-positive cells expressed VGLUT2 (**Table 2**; white arrows in **Figure 3H**). About 20% co-expressed VGLUT1&2. The morphology of these two types of FG-positive cells was similar (**Figure 3I**). Cells expressing both molecules were located throughout the nucleus (**Figure 2B**, sections 1.6–2.2) and represent an exclusively glutamatergic contralateral LSO projection. In the ipsilateral LSO, to the contrary, 99% of the hundreds of FG-positive cells were negative for both VGLUT1 and VGLUT2 (**Table 2**; **Figure 3I**). Thus, the ipsilateral LSO projection is probably exclusively glycinergic, and a glutamatergic input to the ipsilateral IC from LSO appears to be absent in the rat.

In the LSO pattern, VGLUT2 or VGLUT1&2 expression in FG-labeled neurons was seen on the contralateral side, and a lack of VGLUT expression was seen on the ipsilateral side. The DPO (**Figure 2B**, sections 1.0–2.2; **Figure 3K**), the LVPO (**Figure 2B**, sections 1.0–2.2; **Figures 3L,M**), and the RPO (**Figure 2B**, sections 0.4–1.0; **Figure 3P**) followed the general LSO pattern. However, they tended to have fewer FG-labeled VGLUT2 or VGLUT1&2 expressing neurons on the contralateral side (**Table 1**) and FG-positive cells expressed neither VGLUT gene on the ipsilateral side (**Table 2**). Thus, this pattern provides mixed glutamatergic and non-glutamatergic inputs to the IC with a predominant inhibitory input from the ipsilateral side.

In the MSO, almost all FG-positive cells expressed VGLUT2 on the ipsilateral side. About half of these co-expressed VGLUT1&2 (**Table 2**; black arrowheads in **Figure 3J**). Both types of neurons were located throughout the nucleus (**Figure 2B**, sections 1.2–2.2)

Table 1 | The percentage and number of FG-positive neurons that express VGLUT1 (V1) and/or VGLUT2 (V2).

	Percentage FG+ neurons											
Case #	**08-110**				**08-118**				**08-124**			
Nucleus	**V1–/V2+**	**V1+/V2+**	**V1–/V2–**	**N**	**V1–/V2+**	**V1+/V2+**	**V1–/V2–**	**N**	**V1–/V2+**	**V1+/V2+**	**V1–/V2–**	**N**
IC												
LCc	86.1		13.9	36	94.8		5.2	97	86.7		13.3	165
ICCc	90.7		9.3	129	89.4		10.6	216	93.2		6.8	414
DCc	62.5		37.5	8	90.9		9.1	22	77.8		22.2	63
NLL												
DNLLc	6.3		93.8	16	0.4		99.6	228	1.0	0.3	98.6	296
DNLLi	7.7		92.3	26	9.3	1.4	89.3	140	1.1	4.3	94.7	188
INLLi	67.0	9.4	23.6	106	58.2	19.9	22.0	428	53.7	31.8	14.4	471
VNLLi	2.3	1.5	96.1	389	6.4	1.7	91.9	470	4.2	2.1	93.6	1083
SOC												
DPOc		100.0		3	90.9	9.1		11	80.0	10.0	10.0	10
DPOi			100.0	3	10.5		89.5	19	16.0	4.0	80.0	25
LSOc	78.8	21.2		52	74.4	25.6		195	83.7	16.3		166
LSOi			100.0	4	1.6		98.4	306	0.3	0.3	99.3	293
LVPOc		100.0		2	51.3	46.2	2.6	78	70.7	28.0	1.3	75
LVPOi		12.5	87.5	16	5.0	2.8	92.2	141	10.0	13.0	77.0	200
MNTBi			100.0	1			100.0	1			100.0	4
MSOc				0	60.0	20.0	20.0	5	42.9	57.1		7
MSOi	30.8	61.5	7.7	13	66.4	33.6		223	52.3	46.5	1.2	172
MVPOc				0			100.0	1	100.0			1
MVPOi			100.0	11			100.0	75			100.0	84
RPOc				0				0	60.0	20.0	20.0	5
RPOi		9.1	90.9	11	12.8	35.9	51.3	39	12.2	4.9	82.9	41
SPOc			100.0	1			100.0	2	20.0		80.0	5
SPOi	3.4	3.4	93.1	29	4.6	0.6	94.9	175			100.0	151
VMPOc				0	60.0	30.0	10.0	10	60.0	20.0	20.0	5
VMPOi	33.3	66.7		3	24.7	67.4	7.9	89	25.0	67.9	7.1	28
CNC												
AVCNc		100.0		312	1.8	98.2		541	0.8	99.2		485
AVCNi		100.0		1		100.0		8		100.0		3
DCNc	98.4	1.6		245	99.1	0.6	0.3	344	97.9	1.1	1.1	285
DCNi	100.0			1	84.6	15.4		13	77.8		22.2	9
PVCNc	0.7	99.3		140	1.9	97.7	0.4	258		100.0		262
PVCNi				0				0		100.0		7
All nuclei	34.0	33.8	32.2	1558	39.5	33.0	27.4	4135	47.4	30.2	22.4	5003

c, contralateral; i, ipsilateral. See list of abbreviations.

and were flat-shaped and densely packed in the dorso-ventral axis. Thus, at least 97% of the ipsilateral MSO projection to IC is glutamatergic.

The MSO pattern emphasizes the ipsilateral glutamatergic input to IC. The VMPO follows the MSO pattern (**Figure 2B**, sections 1.2–2.2). FG-positive cells were mainly found on the ipsilateral side, and most of them colocalized VGLUT2. The majority of FG-positive cells co-expressed VGLUT1&2 (**Table 2**). Both VGLUT2 and VGLUT1&2 cells had similar morphology (**Figure 3O**).

In the SPO pattern, VGLUT expression was rare and most projections to IC were ipsilateral.

This pattern was seen in the SPO (**Figure 2B**, sections 1.0–2.2) and the MVPO (**Figure 2B**, sections 0.8–2.2). In SPO, over 96% of FG-positive cells were negative for VGLUT1 and/or VGLUT2 (**Table 2**; **Figure 3Q**). Likewise, in the MVPO there were almost no VGLUT-expressing, FG-positive neurons found on the ipsilateral side (**Table 1**; **Figure 3N**). These data suggest both SPO and MVPO function exclusively as ipsilateral inhibitory inputs to IC. Interestingly, this is similar to the pattern seen for the VNLL, non-glutamatergic inputs to ipsilateral IC. Both VNLL and these periolivary nuclei may receive excitatory inputs from the contralateral cochlear nucleus.

Table 2 | Mean percentage and standard deviation of all FG-positive cells that express VGLUT1 (V1) and VGLUT2 (V2) calculated from the three cases in Table 1.

	Mean of FG+ neurons (% ± SD)		
Nucleus	**V1–/V2+**	**V1+/V2+**	**V1–/V2–**
IC			
LCc	89.2 ± 4.9	0.0 ± 0.0	10.8 ± 4.9
ICCc	91.1 ± 2.0	0.0 ± 0.0	8.9 ± 2.0
DCc	77.1 ± 14.2	0.0 ± 0.0	22.9 ± 14.2
NLL			
DNLLc	2.6 ± 3.2	0.1 ± 0.2	97.3 ± 3.1
DNLLi	6.0 ± 4.4	1.9 ± 2.2	92.1 ± 2.7
INLLi	59.6 ± 6.8	20.4 ± 11.2	20.0 ± 4.9
VNLLi	4.3 ± 2.0	1.8 ± 0.3	93.9 ± 2.1
SOC			
DPOi	8.8 ± 8.1	1.3 ± 2.3	89.8 ± 10.0
LSOc	79.0 ± 4.7	21.0 ± 4.7	0.0 ± 0.0
LSOi	0.7 ± 0.9	0.1 ± 0.2	99.2 ± 0.8
LVPOc	40.6 ± 36.5	58.1 ± 37.4	1.3 ± 1.3
LVPOi	5.0 ± 5.0	9.4 ± 5.7	85.6 ± 7.8
MSOi	49.8 ± 17.9	47.2 ± 14.0	3.0 ± 4.1
MVPOi	0.0 ± 0.0	0.0 ± 0.0	100.0 ± 0.0
RPOi	8.3 ± 7.2	16.6 ± 16.8	75.0 ± 21.0
SPOi	2.7 ± 2.4	1.3 ± 1.8	96.0 ± 3.6
VMPOi	27.7 ± 4.9	67.3 ± 0.6	5.0 ± 4.3
CNC			
AVCNc	0.9 ± 0.9	99.1 ± 0.9	0.0 ± 0.0
DCNc	98.5 ± 0.6	1.1 ± 0.5	0.4 ± 0.5
PVCNc	0.9 ± 1.0	99.0 ± 1.2	0.1 ± 0.2
All nuclei	32.3 ± 1.9	27.4 ± 4.9	40.3 ± 6.7

Nuclei that have more than 10 mean cell counts are presented.

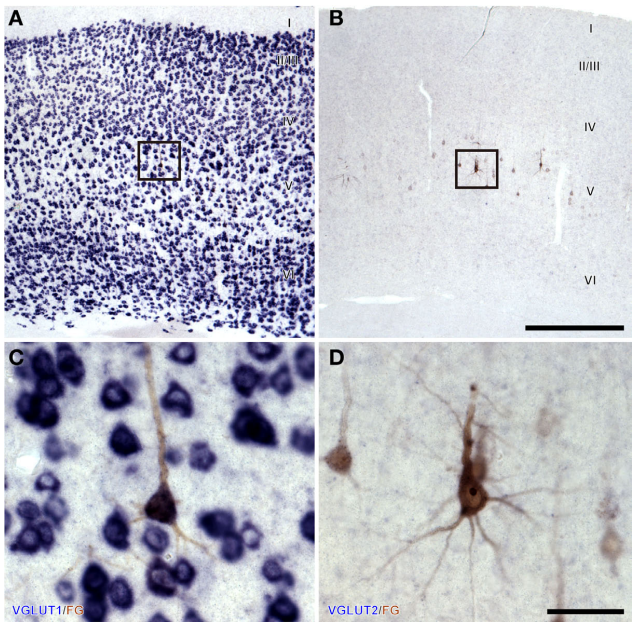

FIGURE 4 | Corticofugal neurons in layer 5 (V) express only VGLUT1. Brightfield ISH for VGLUT1 **(A,C)** or VGLUT2 **(B,D)** combined with immunohistochemistry for FG showed that retrogradely labeled pyramidal neurons express VGLUT1 but not VGLUT2. **(C,D)** Are the higher magnification of boxes in **(A,B)**, respectively. Scale bars: 500 μm **(A,B)**, and 50 μm **(C,D)**.

AUDITORY CORTEX

In the ipsilateral AC, numerous neurons were retrogradely labeled with FG and expressed VGLUT1 (**Figure 4A**). We examined the cortex in four cases that underwent non-florescent ISH and found that most retrogradely labeled cells were in layer 5 and expressed only VGLUT1 (**Figure 4C**). In contrast, FG-labeled cells did not express VGLUT2 (**Figures 4B,D**). VGLUT2 expression in the cortex was slightly above the background level in layer 2–4 and moderate in layer 6 in the rostral AC (**Figures 5A,B**), which is consistent with previous studies (Hisano et al., 2000; De Gois et al., 2005). This weak expression of VGLUT2 in the cortex was in contrast to the strong expression in the thalamus seen in the same section (**Figure 5C**). Since all FG-positive cells expressed only VGLUT1, we did not count the FG-labeled cells or calculate the percentage of VGLUT in FG-labeled cells.

DISCUSSION

These results suggest the origins of both excitatory and inhibitory terminals in the IC. In the IC, putative glutamatergic terminals contain VGLUT1 and/or VGLUT2 (Altschuler et al., 2008; Ito et al., 2009). Three kinds of glutamatergic terminals are seen in the IC, those with only the VGLUT2 protein, those with only the VGLUT1 protein, and those with both proteins (Ito et al., 2009). Neither terminals nor soma positive for VGLUT3 were found in the IC (Ito et al., 2009). The present data offer new information about the origins of these terminals. The VGLUT1 terminals in the IC most likely arise from pyramidal cells in the auditory cortex since that is the predominant gene expressed in cortex. The IC terminals that contain GABA or glycine are highly likely to come from the FG-positive cells that lack VGLUT1 and VGLUT2 expression. The IC terminals that contain VGLUT1 and VGLUT2 proteins most likely come from the neurons that express both genes, and this pattern is most prevalent in the ventral cochlear nucleus. The VGLUT2 terminals constitute the largest number of terminals in the IC. It is of interest because it is the only type of terminal that makes dense axosomatic and axodendritic terminals on the large GABAergic tectothalamic neurons (Ito et al., 2009). However, there are multiple inputs that could be the source of these terminals.

POSSIBLE SOURCES OF AXOSOMATIC VGLUT2 TERMINALS IN IC

Our data demonstrate that possible sources of VGLUT2 terminals in the IC are the contralateral LSO and DCN and the ipsilateral INLL, MSO, and VMPO. Each of these sources is also a potential source for the axosomatic VGLUT2 terminals on the large GABAergic neurons in the IC. In addition, the local axons of IC neurons from the both the ipsilateral and contralateral sides are possible sources of VGLUT2 axosomatic terminals. Most IC neurons make local axonal collaterals (Oliver et al., 1991) and many project contralaterally through the commissure to the opposite side (Saldana and Merchan, 1992). These multiple sources of VGLUT2 may make

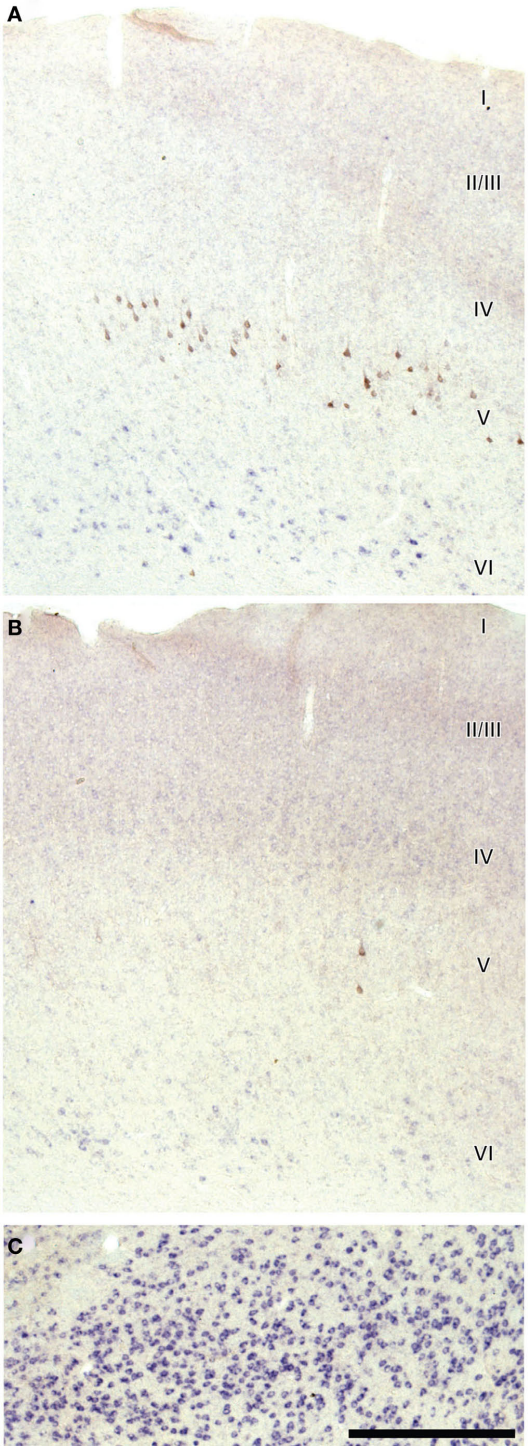

FIGURE 5 | Weak expression of VGLUT2 in layer 6 (VI) of rostral auditory cortex in same case as Figure 4. Compared to **Figure 4B**, this section is developed to show weak expression and consequently some background labeling. Modest VGLUT2 expression is in layer 6 of ipsilateral cortex **(A)** and contralateral cortex **(B)**, but it is weak compared to the thalamus of the same section **(C)**. Labeling in layers 2/3 and 4 (II/III and IV) is slightly above background and less intense than layer 6. Lack of above background label in layer 5 suggests no FG+ neurons are VGLUT2 positive. Scale bar: 500 μm.

different types of terminals in the IC. For example, some VGLUT2 terminals synapse on small, distal dendrites (Altschuler et al., 2008; Ito et al., 2009), and these may not be from the same source as the dense VGLUT2 axosomatic terminals. Some DCN terminals with round synaptic vesicles make asymmetric axosomatic synapses on large IC cells in the cat (Oliver, 1984a, 1985). So, DCN neurons expressing VGLUT2 may be the source of some of the VGLUT2 axosomatic terminals on the large GABAergic IC neurons. Indeed, the GABAergic neurons are the largest IC cells in the cat (Oliver et al., 1994) similar to the rat (Ito et al., 2009).

It is unlikely that a single axon forms all of the axosomatic VGLUT2 terminals that surround the soma of the large GABAergic IC cells in the IC (Ito et al., 2009). Calyx- or endbulb-like terminals have not been seen in the IC in Golgi preparations or in anterograde transport experiments (Morest and Oliver, 1984; Oliver, 1984b; Oliver et al., 1991, 1999). These endings may come from a single brainstem nucleus or multiple nuclei.

Cells with axosomatic VGLUT2-positive terminals are distributed in all parts of the IC (Ito et al., 2009). This suggests that if a single nucleus supplies all the axosomatic VGLUT2 endings, the most likely source is a nucleus where retrogradely FG-labeled cells are always numerous regardless of the location of the injection site in the IC. Using this logic, our data suggest that the MSO and LSO are unlikely candidates for a single source since the number of retrogradely labeled cells in those nuclei varied dramatically between cases, while the number of retrogradely labeled cells in the other nuclei was consistently high. Only 4/14 cases (including 08-118 and 08-124) in which injections were made in lateral ICC have large numbers of retrogradely labeled cells in the LSO and MSO. These results are consistent with the findings in the gerbil (Cant and Benson, 2006) where the number of retrogradely labeled cells in the LSO and MSO were few when injections were made into the medial central nucleus. On the other hand, if the VGLUT2 axosomatic endings are formed by terminals from multiple sources, we cannot exclude any of the nuclei.

One population of IC terminals contained both VGLUT1 and VGLUT2 proteins, and this suggests one or more source expressing both genes. Since axosomatic endings on large IC GABAergic neurons express only VGLUT2 (Altschuler et al., 2008; Ito et al., 2009), it is unlikely that nuclei with neurons expressing VGLUT1&2 will be the sources of the dense axosomatic synapse. The percentage of neurons expressing VGLUT1&2 was larger than VGLUT2 alone in the AVCN, PVCN, LVPO, and VMPO. Since AVCN and PVCN exclusively expressed VGLUT1&2, they can be ruled out completely as a source for the VGLUT2 terminals in IC. Most presumed terminals from the AVCN in the SOC contain both VGLUT1 and VGLUT2 proteins (e.g., Billups, 2005).

FUNCTIONAL CONSIDERATIONS

The present results demonstrate that different combinations of VGLUT gene expression are present in the auditory brainstem nuclei that project to the IC. This may be related to functional differences in the pathways to the IC. The properties of the vesicular transporters of glutamate are very similar (Schafer et al., 2002; Varoqui et al., 2002); however, the vesicles that use VGLUT1 have two pathways for recycling vesicles, while those using VGLUT2 or VGLUT3 only have one (Voglmaier et al., 2006). This suggests

that vesicles using VGLUT1 may recycle faster under prolonged, high-frequency stimuli. This ability to recycle faster may explain why the VGLUT1 synapses on hippocampal neurons depress more slowly than VGLUT2 synapses in response to high-frequency stimulation and recover more quickly (Fremeau Jr. et al., 2004). This resistance to depression and faster recycling may be related to the prevalence of VGLUT1&2 expression in the AVCN, MSO, VMPO, and LVPO pathways. The VGLUT1-expression pattern was also found in the MGV and auditory cortex where phase locking is not commonly expected, and it raises the possibility that VGLUT1 may be associated fast spiking neurons or other synaptic functions. In contrast, the pure VGLUT2 synapses from the DCN and local IC axons may have a different function unrelated to rapid firing and rapid vesicle recycling.

ACKNOWLEDGMENTS

We gratefully acknowledge the gift of the VGLUT1 and VGLUT2 riboprobes from Drs. Tetsuo Yamamori and Akiya Watakabe (National Institute for Basic Biology, Japan) and Phillip Polychoniou (Duke University) for his help with the data analysis. This work is supported by grants from Uehara Memorial Research Scholarship (Tetsufumi Ito) and NIH DC00189 (Douglas L. Oliver).

REFERENCES

Adams, J. C. (1979). Ascending projections to the inferior colliculus. *J. Comp. Neurol.* 183, 519–538.

Alibardi, L. (1998). Ultrastructural and immunocytochemical characterization of neurons in the rat ventral cochlear nucleus projecting to the inferior colliculus. *Ann. Anat.* 180, 415–426.

Altschuler, R. A., Tong, L., Holt, A. G., and Oliver, D. L. (2008). Immunolocalization of vesicular glutamate transporters 1 and 2 in the rat inferior colliculus. *Neuroscience* 154, 226–232.

Beyerl, B. D. (1978). Afferent projections to the central nucleus of the inferior colliculus in the rat. *Brain Res.* 145, 209–223.

Billups, B. (2005). Colocalization of vesicular glutamate transporters in the rat superior olivary complex. *Neurosci. Lett.* 382, 66–70.

Cant, N. B., and Benson, C. G. (2006). Organization of the inferior colliculus of the gerbil (*Meriones unguiculatus*): differences in distribution of projections from the cochlear nuclei and the superior olivary complex. *J. Comp. Neurol.* 495, 511–528.

Coleman, J. R., and Clerici, W. J. (1987). Sources of projections to subdivisions of the inferior colliculus in the rat. *J. Comp. Neurol.* 262, 215–226.

De Gois, S., Schafer, M. K., Defamie, N., Chen, C., Ricci, A., Weihe, E., Varoqui, H., and Erickson, J. D. (2005). Homeostatic scaling of vesicular glutamate and GABA transporter expression in rat neocortical circuits. *J. Neurosci.* 25, 7121–7133.

Fremeau, R. T. Jr., Kam, K., Qureshi, T., Johnson, J., Copenhagen, D. R., Storm-Mathisen, J., Chaudhry, F. A., Nicoll, R. A., and Edwards, R. H. (2004). Vesicular glutamate transporters 1 and 2 target to functionally distinct synaptic release sites. *Science* 304, 1815–1819.

Gonzalez-Hernandez, T., Mantolan-Sarmiento, B., Gonzalez-Gonzalez, B., and Perez-Gonzalez, H. (1996). Sources of GABAergic input to the inferior colliculus of the rat. *J. Comp. Neurol.* 372, 309–326.

Herbert, H., Aschoff, A., and Ostwald, J. (1991). Topography of projections from the auditory cortex to the inferior colliculus in the rat. *J. Comp. Neurol.* 304, 103–122.

Hisano, S., Hoshi, K., Ikeda, Y., Maruyama, D., Kanemoto, M., Ichijo, H., Kojima, I., Takeda, J., and Nogami, H. (2000). Regional expression of a gene encoding a neuron-specific Na(+)-dependent inorganic phosphate cotransporter (DNPI) in the rat forebrain. *Brain Res. Mol. Brain Res.* 83, 34–43.

Ito, T., Bishop, D. C., and Oliver, D. L. (2009). Two classes of GABAergic neurons in the inferior colliculus. *J. Neurosci.* 29, 13860–13869.

Ito, T., Hioki, H., Nakamura, K., Kaneko, T., Iino, S., and Nojyo, Y. (2008). Some gamma-motoneurons contain gamma-aminobutyric acid in the rat cervical spinal cord. *Brain Res.* 1201, 78–87.

Ito, T., Hioki, H., Nakamura, K., Tanaka, Y., Nakade, H., Kaneko, T., Iino, S., and Nojyo, Y. (2007). Gamma-aminobutyric acid-containing sympathetic preganglionic neurons in rat thoracic spinal cord send their axons to the superior cervical ganglion. *J. Comp. Neurol.* 502, 113–125.

Kaneko, T., and Fujiyama, F. (2002). Complementary distribution of vesicular glutamate transporters in the central nervous system. *Neurosci. Res.* 42, 243–250.

Kaneko, T., Fujiyama, F., and Hioki, H. (2002). Immunohistochemical localization of candidates for vesicular glutamate transporters in the rat brain. *J. Comp. Neurol.* 444, 39–62.

Liang, F., Hatanaka, Y., Saito, H., Yamamori, T., and Hashikawa, T. (2000). Differential expression of gamma-aminobutyric acid type B receptor-1a and -1b mRNA variants in GABA and non-GABAergic neurons of the rat brain. *J. Comp. Neurol.* 416, 475–495.

Loftus, W. C., Bishop, D. C., Saint Marie, R. L., and Oliver, D. L. (2004). Organization of binaural excitatory and inhibitory inputs to the inferior colliculus from the superior olive. *J. Comp. Neurol.* 472, 330–344.

Loftus, W. C., Malmierca, M. S., Bishop, D. C., and Oliver, D. L. (2008). The cytoarchitecture of the inferior colliculus revisited: a common organization of the lateral cortex in rat and cat. *Neuroscience* 154, 196–205.

Morest, D. K., and Oliver, D. L. (1984). The neuronal architecture of the inferior colliculus in the cat: defining the functional anatomy of the auditory midbrain. *J. Comp. Neurol.* 222, 209–236.

Mugnaini, E., Warr, W. B., and Osen, K. K. (1980). Distribution and light microscopic features of granule cells in the cochlear nuclei of cat, rat, and mouse. *J. Comp. Neurol.* 191, 581–606.

Nakamura, K., Watakabe, A., Hioki, H., Fujiyama, F., Tanaka, Y., Yamamori, T., and Kaneko, T. (2007). Transiently increased colocalization of vesicular glutamate transporters 1 and 2 at single axon terminals during postnatal development of mouse neocortex: a quantitative analysis with correlation coefficient. *Eur. J. Neurosci.* 26, 3054–3067.

Oertel, D., Wu, S. H., Garb, M. W., and Dizack, C. (1990). Morphology and physiology of cells in slice preparations of the posteroventral cochlear nucleus of mice. *J. Comp. Neurol.* 295, 136–154.

Oliver, D. L. (1984a). Dorsal cochlear nucleus projections to the inferior colliculus in the cat: a light and electron microscopic study. *J. Comp. Neurol.* 224, 155–172.

Oliver, D. L. (1984b). Neuron types in the central nucleus of the inferior colliculus that project to the medial geniculate body. *Neuroscience* 11, 409–424.

Oliver, D. L. (1985). Quantitative analyses of axonal endings in the central nucleus of the inferior colliculus and distribution of 3H-labeling after injections in the dorsal cochlear nucleus. *J. Comp. Neurol.* 237, 343–359.

Oliver, D. L. (1987). Projections to the inferior colliculus from the anteroventral cochlear nucleus in the cat: possible substrates for binaural interaction. *J. Comp. Neurol.* 264, 24–46.

Oliver, D. L., Beckius, G. E., and Shneiderman, A. (1995). Axonal projections from the lateral and medial superior olive to the inferior colliculus of the cat: a study using electron microscopic autoradiography. *J. Comp. Neurol.* 360, 17–32.

Oliver, D. L., Ostapoff, E. M., and Beckius, G. E. (1999). Direct innervation of identified tectothalamic neurons in the inferior colliculus by axons from the cochlear nucleus. *Neuroscience* 93, 643–658.

Oliver, D. L., Winer, J. A., Beckius, G. E., and Saint Marie, R. L. (1994). Morphology of GABAergic neurons in the inferior colliculus of the cat. *J. Comp. Neurol.* 340, 27–42.

Oliver, D. L., Kuwada, S., Yin, T. C., Haberly, L. B., and Henkel, C. K. (1991). Dendritic and axonal morphology of HRP-injected neurons in the inferior colliculus of the cat. *J. Comp. Neurol.* 303, 75–100.

Saint Marie, R. L., and Baker, R. A. (1990). Neurotransmitter-specific uptake and retrograde transport of [3H]glycine from the inferior colliculus by ipsilateral projections of the superior olivary complex and nuclei of the lateral lemniscus. *Brain Res.* 524, 244–253.

Saint Marie, R. L., Shneiderman, A., and Stanforth, D. A. (1997). Patterns of gamma-aminobutyric acid and glycine immunoreactivities reflect structural and functional differences of the cat lateral lemniscal nuclei. *J. Comp. Neurol.* 389, 264–276.

Saint Marie, R. L., Ostapoff, E. M., Morest, D. K., and Wenthold, R. J. (1989). Glycine-immunoreactive projection of the cat lateral superior olive: possible role in midbrain ear dominance. *J. Comp. Neurol.* 279, 382–396.

Saldana, E., and Merchan, M. A. (1992). Intrinsic and commissural connections of the rat inferior colliculus. *J. Comp. Neurol.* 319, 417–437.

Schafer, M. K., Varoqui, H., Defamie, N., Weihe, E., and Erickson, J. D. (2002). Molecular cloning and functional identification of mouse vesicular glutamate transporter 3 and its expression in subsets of novel excitatory neurons. *J. Biol. Chem.* 277, 50734–50748.

Schofield, B. R., and Cant, N. B. (1991). Organization of the superior olivary complex in the guinea pig. I. Cytoarchitecture, cytochrome oxidase histochemistry, and dendritic morphology. *J. Comp. Neurol.* 314, 645–670.

Takamori, S. (2006). VGLUTs: 'exciting' times for glutamatergic research? *Neurosci. Res.* 55, 343–351.

Varoqui, H., Schafer, M. K., Zhu, H., Weihe, E., and Erickson, J. D. (2002). Identification of the differentiation-associated Na+/PI transporter as a novel vesicular glutamate transporter expressed in a distinct set of glutamatergic synapses. *J. Neurosci.* 22, 142–155.

Voglmaier, S. M., Kam, K., Yang, H., Fortin, D. L., Hua, Z., Nicoll, R. A., and Edwards, R. H. (2006). Distinct endocytic pathways control the rate and extent of synaptic vesicle protein recycling. *Neuron.* 51, 71–84.

Watakabe, A., Ohsawa, S., Hashikawa, T., and Yamamori, T. (2006). Binding and complementary expression patterns of semaphorin 3E and plexin D1 in the mature neocortices of mice and monkeys. *J. Comp. Neurol.* 499, 258–273.

Whitley, J. M., and Henkel, C. K. (1984). Topographical organization of the inferior collicular projection and other connections of the ventral nucleus of the lateral lemniscus in the cat. *J. Comp. Neurol.* 229, 257–270.

Winer, J. A., Larue, D. T., Diehl, J. J., and Hefti, B. J. (1998). Auditory cortical projections to the cat inferior colliculus. *J. Comp. Neurol.* 400, 147–174.

Conflict of Interest Statement: The authors declare that the research was conducted in the absence of any commercial or financial relationships that could be construed as a potential conflict of interest.

Received: 08 April 2010; paper pending published: 21 May 2010; accepted: 07 September 2010; published online: 28 September 2010.

Citation: Ito T and Oliver DL (2010) Origins of glutamatergic terminals in the inferior colliculus identified by retrograde transport and expression of VGLUT1 and VGLUT2 genes. Front. Neuroanat. ***4****:135. doi: 10.3389/fnana.2010.00135*

frontiers in
NEUROANATOMY

ORIGINAL RESEARCH ARTICLE
published: 22 February 2011
doi: 10.3389/fnana.2011.00001

Connections of the superior paraolivary nucleus of the rat: II. Reciprocal connections with the tectal longitudinal column

Antonio Viñuela[1,2], M.-Auxiliadora Aparicio[1,3], Albert S. Berrebi[4] and Enrique Saldaña[1,2]*

[1] *Laboratory for the Neurobiology of Hearing, Neuroscience Institute of Castilla y León, University of Salamanca, Salamanca, Spain*
[2] *Department of Cell Biology and Pathology, Medical School, University of Salamanca, Salamanca, Spain*
[3] *Department of Pathology, Clinical University Hospital of Salamanca, Salamanca, Spain*
[4] *Department of Otolaryngology, The Sensory Neuroscience Research Center, West Virginia University School of Medicine, Morgantown, WV, USA*

Edited by:
Enrico Mugnaini, Northwestern University, USA

Reviewed by:
Marina Bentivoglio, University of Verona, Italy
Douglas L. Oliver, University of Connecticut Health Center, USA
Donata Oertel, University of Wisconsin, USA
Joe Adams, Massachusetts Eye and Ear Infirmary, USA

***Correspondence:**
Enrique Saldaña, Laboratory for the Neurobiology of Hearing, Neuroscience Institute of Castilla y León, University of Salamanca, Salamanca 37007, Spain.
e-mail: saldana@usal.es

The superior paraolivary nucleus (SPON), a prominent GABAergic center of the mammalian auditory brainstem, projects to the ipsilateral inferior colliculus (IC) and sends axons through the commissure of the IC (CoIC). Herein we demonstrate that the SPON is reciprocally connected with the recently discovered tectal longitudinal column (TLC). The TLC is a long and narrow structure that spans nearly the entire midbrain tectum longitudinally, immediately above the periaqueductal gray matter (PAG) and very close to the midline. Unilateral injections of biotinylated dextran into the SPON of the rat label abundant terminal fibers in the TLC of both sides, with an ipsilateral predominance. The SPON provides a dense innervation of the entire rostrocaudal extent of the ipsilateral TLC, and a relatively sparser innervation of the caudal and rostral portions of the contralateral TLC. SPON fibers reach the TLC by two routes: as collaterals of axons of the CoIC, and as axons that circumvent the ipsilateral IC before traveling in the deep layers of the superior colliculus (SC). The density of these projections identifies SPON as a significant source of input to the TLC. Other targets of the SPON discovered in this study include the deep layers of the SC and the PAG. The same experiments reveal numerous labeled cell bodies in the TLC, interspersed among the labeled SPON fibers. This observation suggests that the SPON is a significant target of TLC projections. The discovery of novel reciprocal connections between the SPON and the TLC opens unexpected avenues for investigation of sound processing in mammalian brainstem circuits.

Keywords: auditory brainstem, commissure of the inferior colliculus, superior colliculus, periaqueductal gray matter, superior olivary complex, biotinylated dextran amine, tract-tracing

INTRODUCTION

The tectal longitudinal column (TLC) spans the midbrain tectum longitudinally, immediately above the periaqueductal gray matter (PAG) and very close to the midline. In the rat, the TLC extends approximately 3.5 mm, from the caudal end of the commissure of the inferior colliculus (CoIC) to the rostral end of the commissure of the superior colliculus (CoSC), and occupies what has traditionally been considered the medial-most region of the deep superior colliculus (SC) and the medial-most region of the inferior colliculus (IC). Despite measuring only 250–350 μm in diameter, more than 11,500 neurons are packed within this long and narrow structure (Saldaña et al., 2007).

The caudal and rostral thirds of the TLC are crossed by the CoIC and by the CoSC (Saldaña et al., 2007), respectively, suggesting that these fiber tracts are a preferred pathway of entry for afferent inputs to the TLC. The CoIC contains mostly commissural axons of the IC, as well as axons from other sources or destined for other targets (reviewed by Saldaña and Merchán, 2005). These include axons from various subcollicular auditory nuclei, namely the sagulum and nuclei of the lateral lemniscus (González-Hernández et al., 1987; Henkel and Shneiderman 1988; Hutson et al., 1991; Bajo et al., 1993). Recently, it has been demonstrated that the superior paraolivary nucleus (SPON), a prominent cell group of the superior olivary complex (SOC), also projects axons across the CoIC (Saldaña et al., 2009). Thus, we set forth to investigate whether the SPON, which is likely the caudal-most auditory center sending projections across the CoIC, innervates the TLC. We chose to carry out this investigation in rats because the TLC has been best characterized in this species (Saldaña et al., 2007; Marshall et al., 2008; Aparicio et al., 2010); moreover, abundant information is available concerning the structure, connections and physiology of the rat SPON (Kulesza Jr. and Berrebi, 2000; Saldaña and Berrebi, 2000; Kulesza Jr. et al., 2003, 2007; Kadner et al., 2006; Kadner and Berrebi, 2008; Saldaña et al., 2009).

MATERIALS AND METHODS

Thirteen female albino rats (body weight 190–210 g) with clean ear canals and no sign of middle ear infection were used in this study. These specimens were also used for the study of SPON projections to the IC described in a previous article (Saldaña et al., 2009). All animals were cared for and used in compliance with European Union regulations concerning the use of animals in biomedical research, and the experimental procedures were approved and supervised by the Animal Care and Use Committee of the University of Salamanca.

For surgical procedures, including the transcardial perfusion of fixatives, all animals were deeply anesthetized with a mixture of ketamine HCl (80 mg/kg body weight) and xylazine (6 mg/kg body weight) administered intramuscularly. Animal suffering was minimized by monitoring the depth of anesthesia often, carefully attending to physiological cues such as rate and depth of respiration and reflex activity. Supplemental doses of anesthetics were given as needed to maintain deep anesthesia throughout all procedures.

Glass micropipettes loaded with the neuroanatomical tracer biotinylated dextran amine (BDA, 10,000 MW, Molecular Probes, Eugene, OR, USA; 10% in 0.1 M sodium phosphate buffer, pH 7.4) were lowered into the SPON of deeply anesthetized rats using stereotaxic coordinates (Paxinos and Watson, 2007). To avoid damage to the prominent transverse sinus, the pipettes were lowered into the brain *via* a dorsocaudal to ventrorostral approach, so that their trajectory formed a 16° angle with the coronal plane. The tracer was delivered by iontophoresis using a pulsed 5 μA DC positive current (7 s on/7 s off) for 5–15 min. The current was then stopped and the pipette left in place for an additional 15–20 min prior to withdrawal in order to minimize leakage of the tracer along the injection tract.

Following 7–10 days survival, the rats were anesthetized deeply and their brains fixed by transcardial perfusion of buffered 4% formaldehyde (prepared from freshly depolymerized paraformaldehyde) and 0.1% glutaraldehyde. After cryoprotection in 30% sucrose in phosphate buffer, the brains were cut coronally on a freezing microtome at a thickness of 40 μm. To visualize the tracer, the sections were first processed by the avidin–biotin–peroxidase complex procedure following the manufacturer's specifications (ABC, Vectastain, Vector Labs, Burlingame, CA, USA), and then by standard histochemistry for peroxidase, with or without heavy-metal intensification (Vetter et al., 1993). For cytoarchitectural reference, every fourth section was counterstained with cresyl violet.

Sections were photographed at high resolution using a Zeiss Axioskop 40 microscope equipped with a Zeiss AxioCam MRc 5 digital camera and 2.5× (NA 0.075), 5× (NA 0.15), 10× (NA 0.30), 20× (NA 0.50), and 40× (NA 0.75) plan semi-apochromatic objective lenses. Image brightness and contrast were adjusted with Adobe Photoshop software (Adobe Systems Incorporated, San Jose, CA, USA), and the illustrations were arranged into plates using Canvas software (ACD Systems of America, Inc., Miami, FL, USA).

To generate the drawings of **Figure 2**, the sections were first photographed at high resolution with the 5× objective lens. At this magnification, several micrographs were needed to photograph every section. These photographs were then arranged and fitted using Adobe Photoshop software to create a large mosaic image of the section. The resulting digital image was imported into Canvas software. To increase the resolution of the final image, a new layer was created over the digital image and each labeled fiber contained within the original micrograph was redrawn digitally using Canvas' freehand drawing tool. This digital procedure allowed us to subsequently adjust the thickness of the lines. The new digital layer, without the underlying micrograph, was finally saved as a TIFF file.

A similar procedure was used to produce the plots showing the distribution of presumed labeled synaptic boutons in **Figures 6 and 7**. To convey a clear impression of synaptic bouton density, each plot of **Figure 7** was subsequently transferred to a Photoshop document and blurred using a Gaussian filter with a 20-pixel square matrix.

RESULTS

The present results are based on 13 cases with single injections of BDA into the SPON. In 12 cases, the injection sites were localized within the SPON, without encroaching upon neighboring structures (e.g., **Figure 1A**). In the other case (case 99014), the injection site encroached upon the medial superior olive. The mediolateral diameter of the center of the injection sites ranged from 150 to 380 μm. **Figure 1B** shows schematically the injection site of seven representative cases.

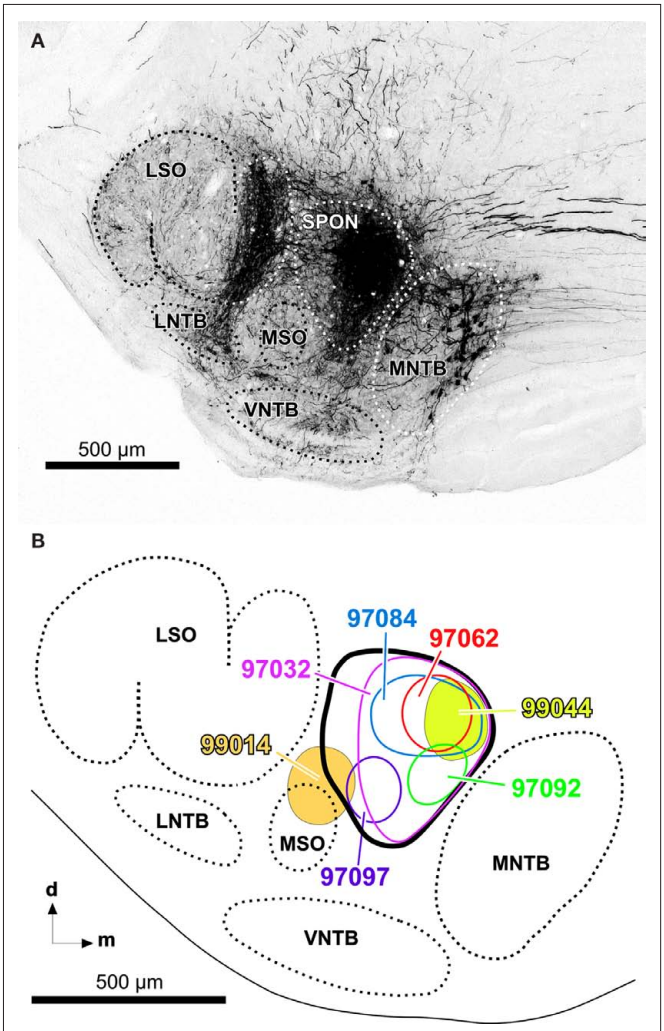

FIGURE 1 | (A) Representative injection site of BDA into the SPON of the rat. Digital photomicrograph of a coronal section through the central rostrocaudal third of the left superior olivary complex from a case whose injection site is wholly contained within the limits of the SPON (case 97062). Retrogradely labeled neuronal cell bodies in the medial nucleus of the trapezoid body (MNTB) and their fibers and terminals in the lateral superior olive (LSO) are evident. For more information on the interpretation of the neurons and fibers labeled following injections of BDA into the SPON, see Saldaña et al. (2009). **(B)** Schematic representation of the sizes and locations of the injection sites of various representative cases. Other abbreviations: d, dorsal; LNTB, lateral nucleus of the trapezoid body; m, medial; MSO, medial superior olive; VNTB, ventral nucleus of the trapezoid body.

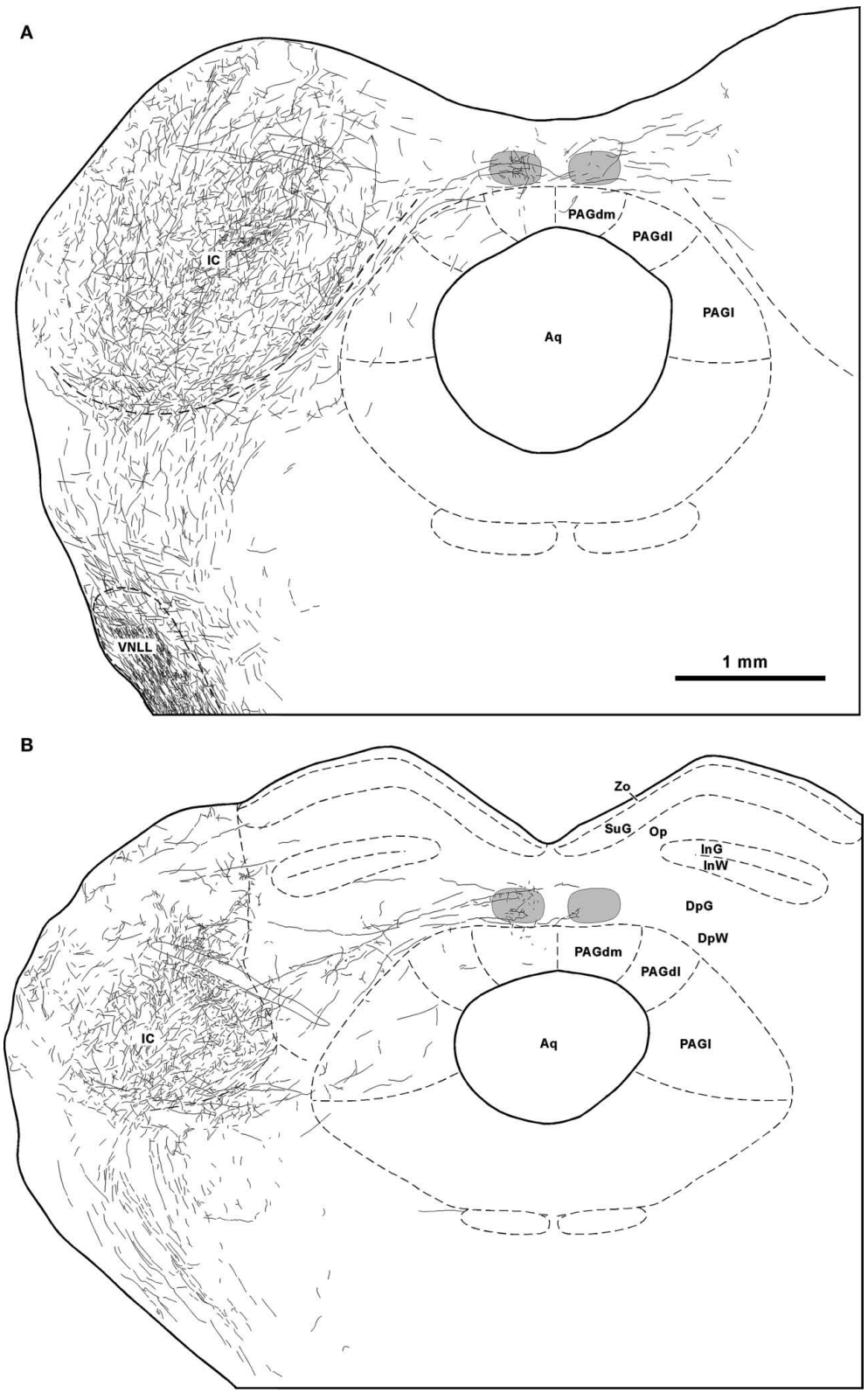

FIGURE 2 | ***(Continued)***

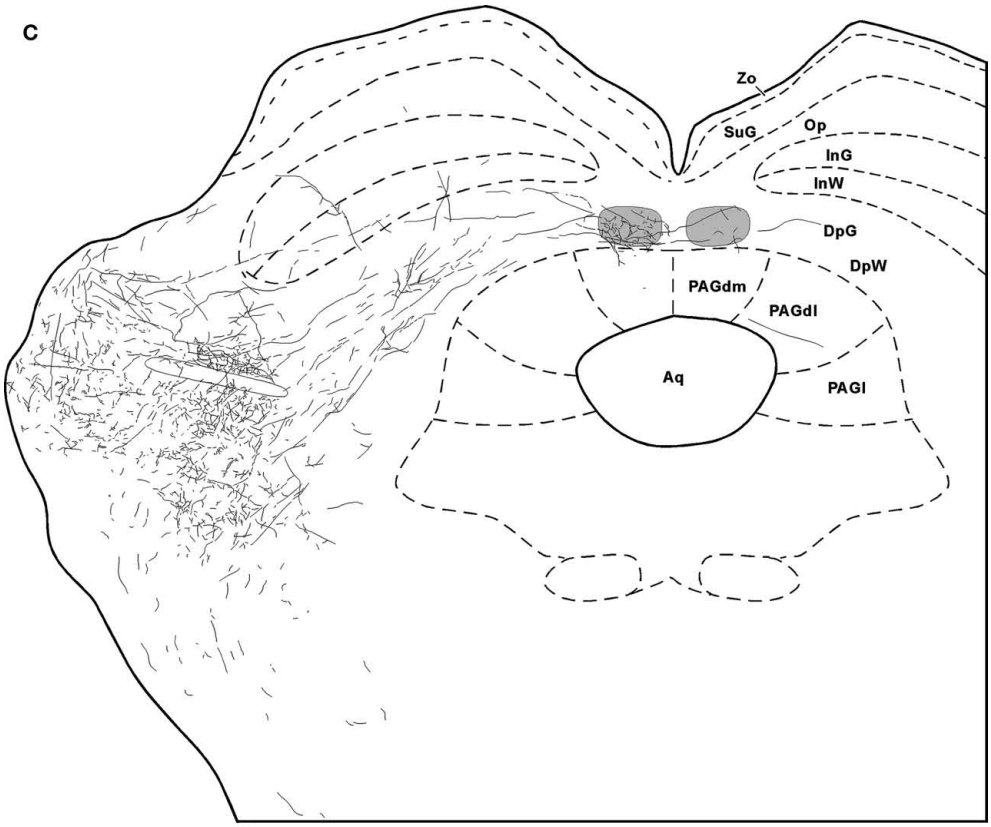

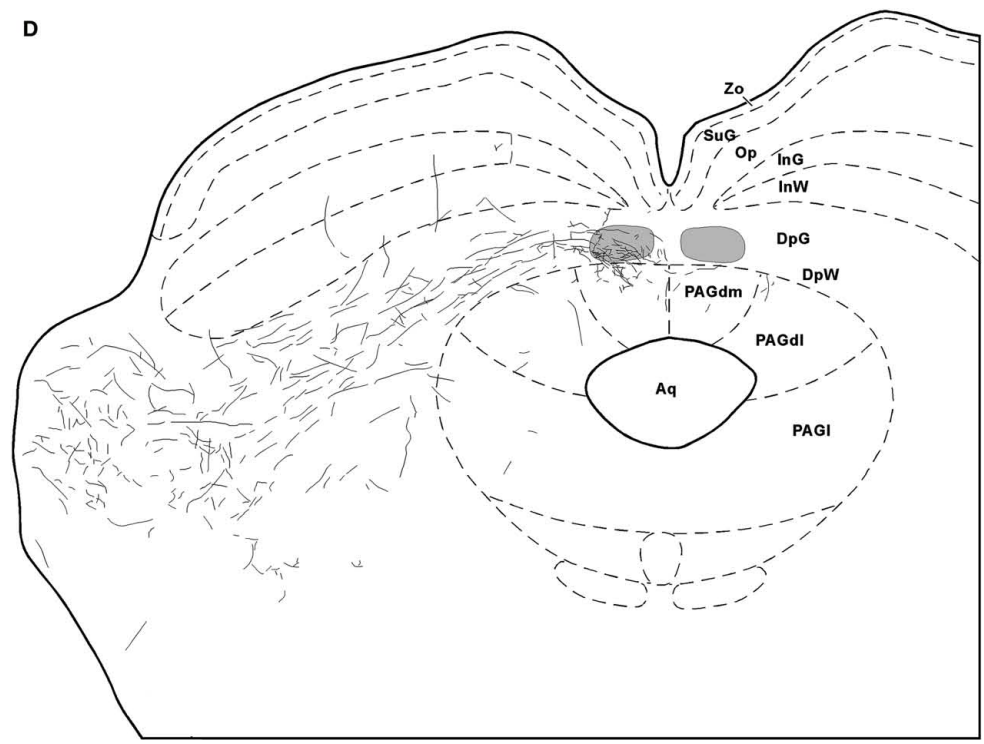

FIGURE 2 | ***(Continued)***

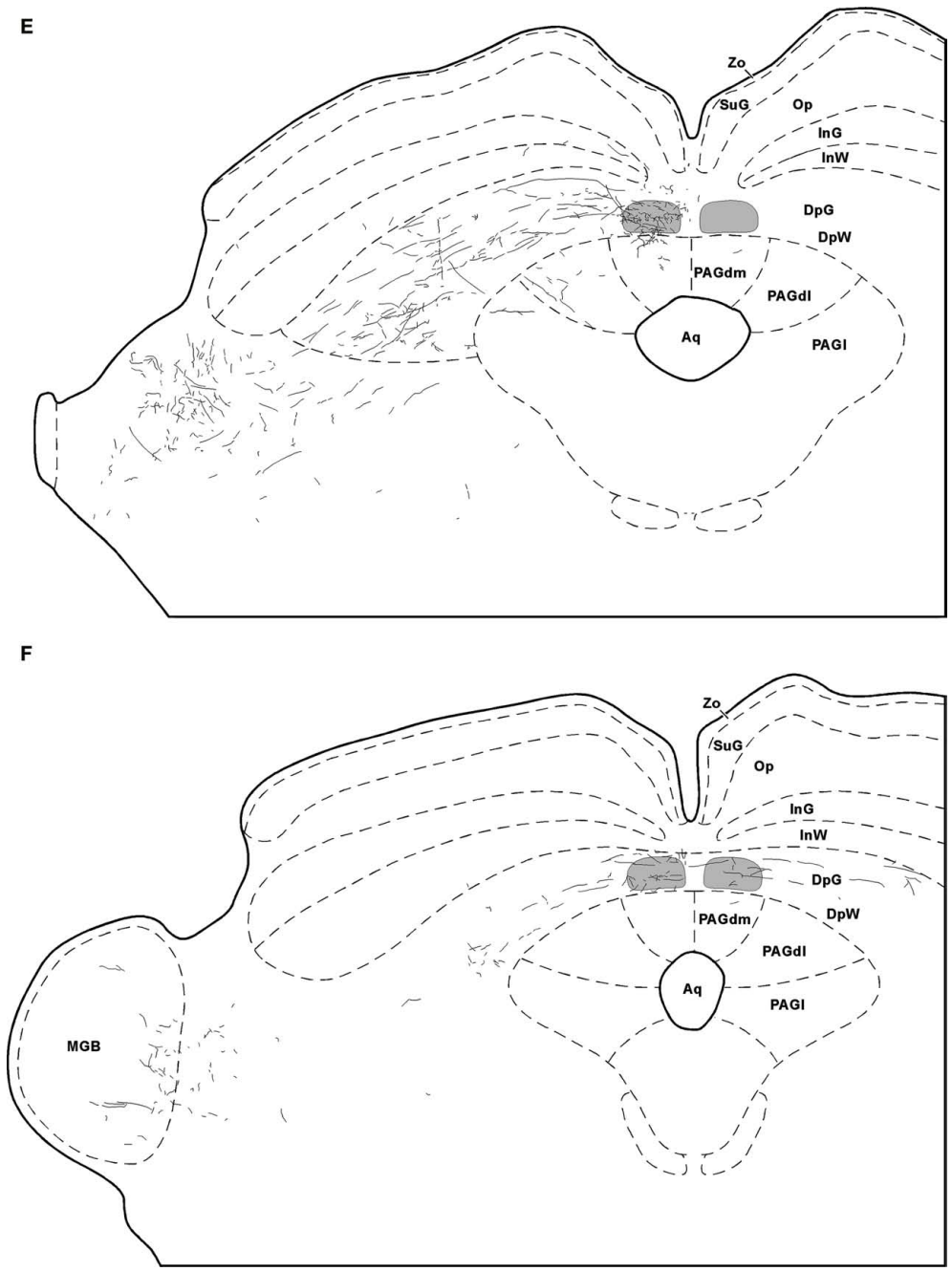

FIGURE 2 | Trajectory and distribution of SPON axons. (A–F) Drawings of coronal sections of the midbrain illustrating axons labeled following a single injection of BDA into the left SPON. Case 97084, whose injection site is depicted in **Figure 1B**. The sections have been ordered from caudal to rostral and illustrate levels similar to those shown in **Figure 3**. The TLC is represented in light gray and the scale bar in **(A)** applies to all six drawings. Abbreviations of SC layers: DpG, deep gray; DpW, deep white; InG, intermediate gray; InW, intermediate white; Op, stratum opticum; SuG, superficial gray; Zo, stratum zonale. Abbreviations of periaqueductal gray matter (PAG) columns: PAGl, lateral column; PAGdl, dorsolateral column; PAGdm, dorsomedial column. Other abbreviations: Aq, cerebral aqueduct; IC, inferior colliculus; MGB, medial geniculate body; VNLL, ventral nucleus of the lateral lemniscus.

PROJECTION FROM THE SPON TO THE TLC

Labeled SPON axons, easily recognizable by their large caliber (>1.2 μm), exit the injection site and travel rostrally, dorsally, and laterally to join the medial-most aspect of the ipsilateral lateral lemniscus, through which they ascend toward the midbrain tectum without entering the nuclei of the lateral lemniscus. Most SPON axons then penetrate into the IC, where they create dense terminal fields in all IC subdivisions. Some SPON axons that reach the dorsal cortex

of the IC extend dorsomedially and cross the CoIC, to innervate the dorsal cortex of the contralateral IC. The distribution of labeled fibers in the nuclei of the lateral lemniscus and the IC following injections of BDA into the SPON has been described previously (Saldaña et al., 2009) and will therefore not be considered further in this account.

Those SPON axons destined to innervate the TLC do so by two different routes. The first route is taken by some of the axons traveling in the CoIC (**Figures 2A,B, 3A,B, and 4A**). These fibers give off one or more collaterals within the ipsilateral TLC and/or, less frequently, within the contralateral TLC. Occasionally individual labeled SPON fibers give off collaterals to both the ipsilateral and contralateral TLCs (**Figure 4A**). All of these collaterals are usually thin and tend to run either vertically within the CoIC or rostrally, so that the latter course caudorostrally within the TLC.

The second, more prominent pathway of entry into the TLC is formed by SPON axons that circumvent the ipsilateral IC ventromedially or ventrorostrally to reach the SC. These fibers then run dorsomedially through the deep layers of the SC to reach the

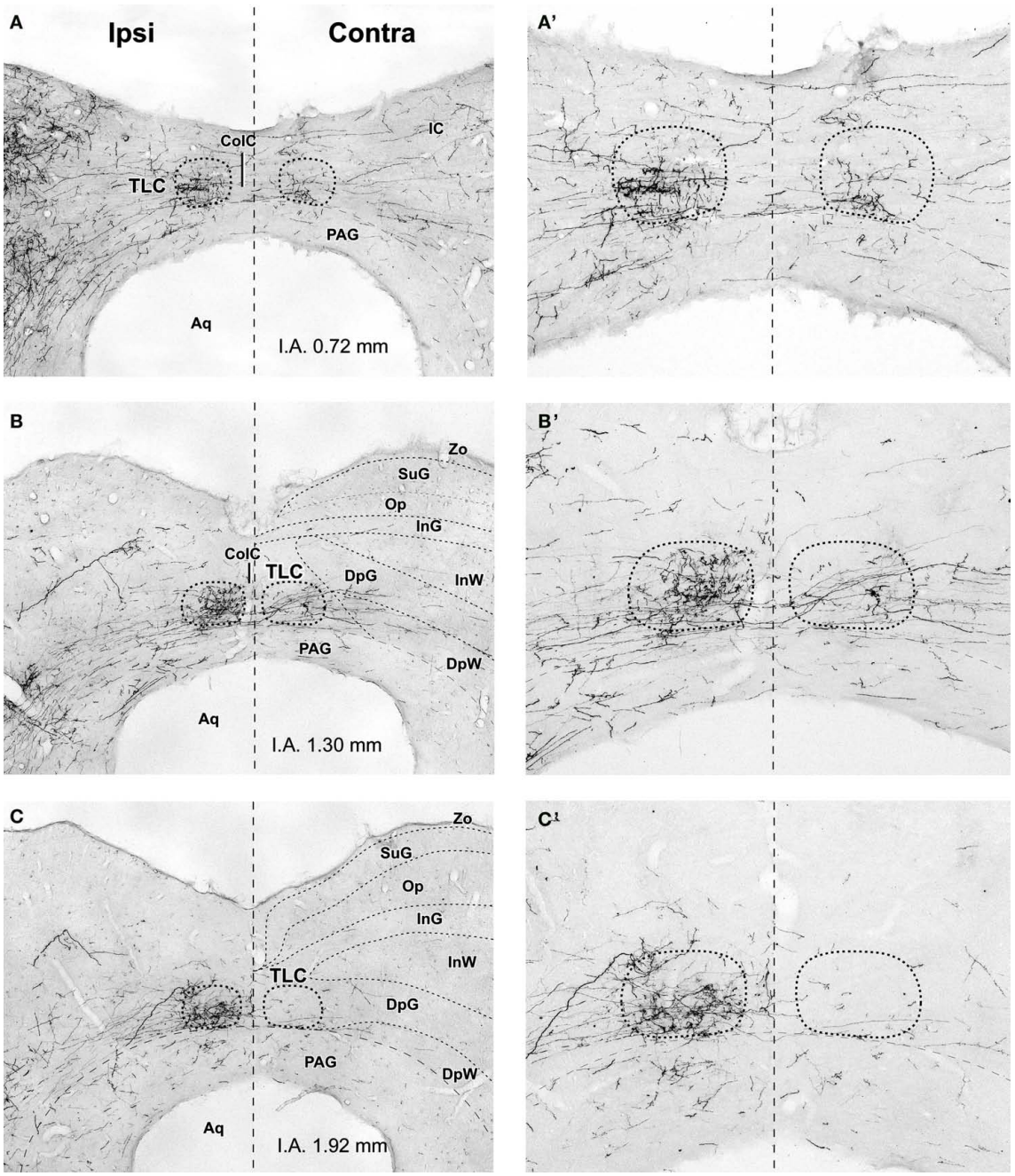

FIGURE 3 | ***(Continued)***

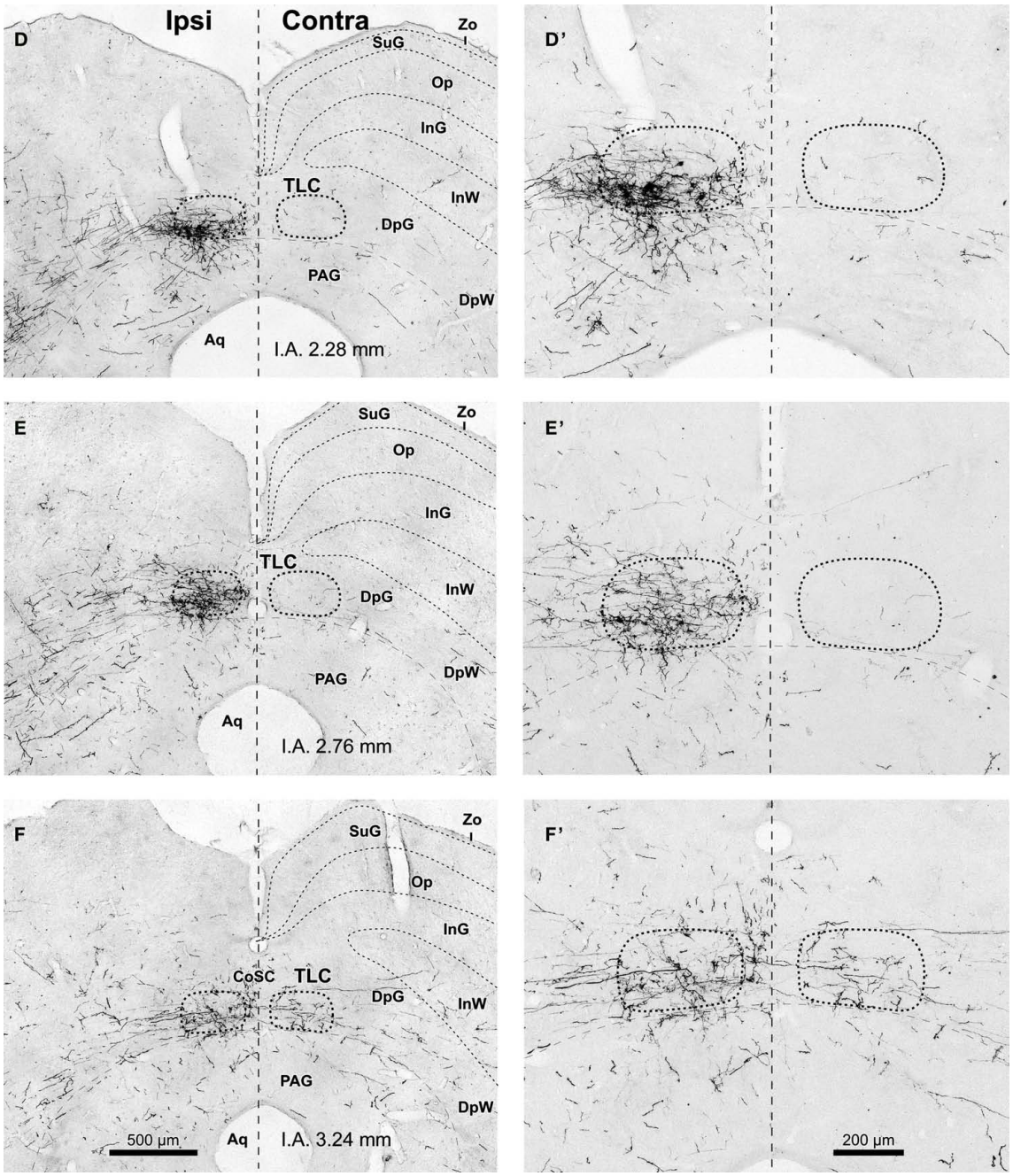

FIGURE 3 | Labeled SPON axons in the TLC. (A–F, A′–F′) Digital micrographs of six coronal sections taken from different rostrocaudal levels of the midbrain tectum of case 97084, whose injection site is depicted in **Figure 1B**. Sections have been ordered from caudal to rostral. The number at the bottom of each panel indicates the distance in millimeters between the depicted plane and the interaural coronal plane (I.A.). Micrographs in the right column show higher magnification views of the corresponding micrograph in the left column. Vertical dashed lines indicate the midline. Scale bars in **(F,F′)** apply to all six micrographs within the corresponding column. Abbreviations of SC layers as in **Figure 2**. Other abbreviations: CoIC, commissure of the IC; CoSC, commissure of the SC; PAG, periaqueductal gray matter.

ipsilateral TLC, which they enter at different rostrocaudal levels (**Figures 2C–F and 3C–F**). Upon entering the TLC by this route, SPON axons usually turn caudally and/or rostrally to span the nucleus longitudinally. Most of these axons seem to end within the ipsilateral TLC. However, some of them, particularly those traveling in the CoSC, give off collaterals for the ipsilateral TLC before crossing the midline to innervate the contralateral TLC or even proceeding into the contralateral SC (**Figures 2F and 3F**). The two routes taken by SPON axons that innervate the TLC are depicted schematically in **Figure 5**.

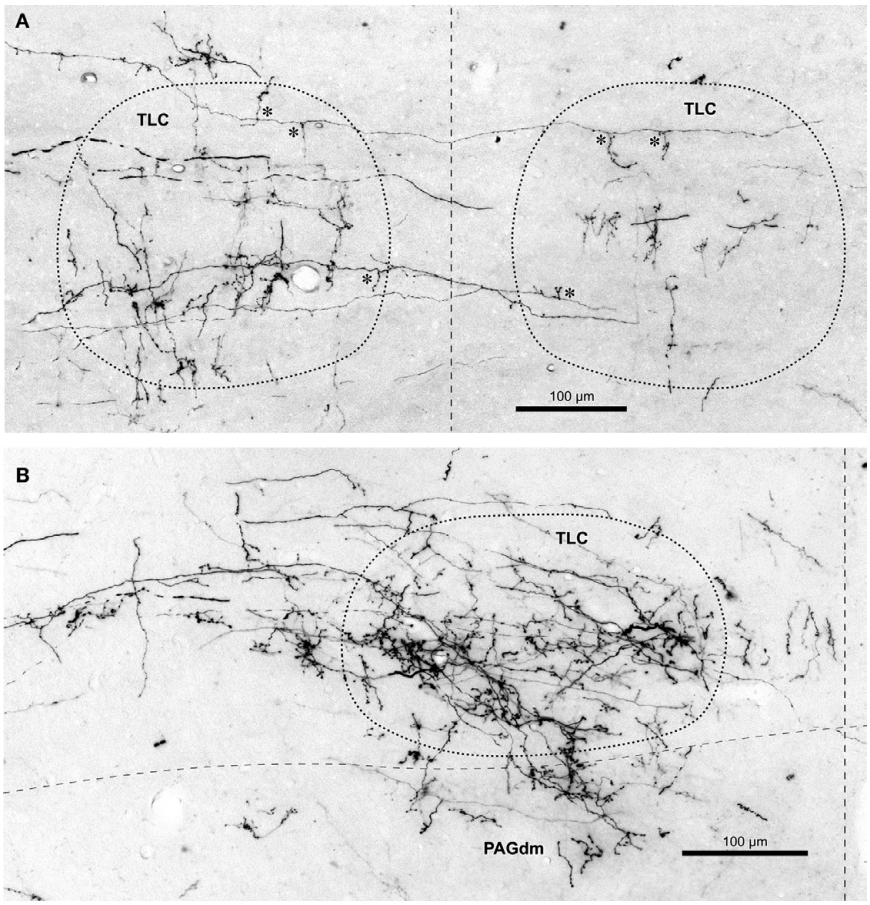

FIGURE 4 | Labeled terminal SPON fibers in the TLC. (A) Micrograph of a coronal section through the caudal portion of the left and right TLC after BDA was injected into the left SPON. Case 97097, whose injection site is depicted in **Figure 1B**. Several labeled SPON axons give off collateral branches (asterisks) within the ipsilateral and the contralateral TLC. Note the predominantly vertical orientation of the terminal axonal branches. **(B)** Micrograph of a coronal section through the central third of the TLC, Case 97084, whose injection site is depicted in **Figure 1B**. Numerous labeled fibers from the ipsilateral SPON enter the TLC from the SC and branch into thin collateral bearing abundant en passant and terminal boutons. Note terminal fibers entering the dorsomedial column of the PAG (PAGdm) from the overlying TLC. In both **(A,B)** the TLC has been delimited by dotted lines and the dashed vertical line indicates the midline.

It is evident from these observations that the projections from SPON to the ipsilateral and contralateral TLC are asymmetric. SPON fibers innervate densely the entire rostrocaudal length of the ipsilateral TLC, but only the caudal and rostral ends of the contralateral TLC (**Figures 2 and 3**).

The caudal third of the ipsilateral TLC is innervated preferentially by collaterals of axons that travel in the CoIC (**Figures 2A, B, 3A, B, 4A, and 5**), whereas the central and the rostral thirds of the nucleus are innervated mostly by axons that run through the deep layers of the SC (**Figures 2C–F, 3C–F, 4B, and 5**). The density of terminal SPON fibers is maximal in the central rostrocaudal third and decreases toward the caudal and the rostral ends of the TLC (**Figures 3 and 6**).

The caudal and the rostral portions of the contralateral TLC receive relatively sparse projections from the SPON by way of collaterals of axons that travel in the CoIC (**Figures 3A,B**) and the CoSC (**Figure 3F**), respectively. At every rostrocaudal level, the projection from SPON to the contralateral TLC is considerably less dense than the uncrossed projection (**Figure 6**).

The terminal branches of SPON axons within the TLC are variously oriented, although vertically oriented terminal fibers predominate at caudal levels on both sides (**Figures 3A′ and 4A**). Despite these varying orientations, the morphology of SPON axons is essentially similar on the two sides and remains rather constant at all rostrocaudal levels. Many terminal branches give off multiple short collaterals with one to three swellings, whereas others end in beaded branches bearing numerous small (<1.5 μm) *en passant* swellings and a terminal bouton (**Figure 4B**); all these varicosities and boutons are presumed to represent synaptic specializations.

TOPOGRAPHY OF PROJECTIONS FROM THE SPON TO THE TLC

Despite the fact that the projections from the SPON to the IC are clearly topographic and presumably tonotopic (Saldaña et al., 2009), no topographic organization is readily apparent in the projections from the SPON to the TLC. In all cases, regardless of the location of the injection site within SPON, labeled terminal fibers are widely distributed along the rostrocaudal

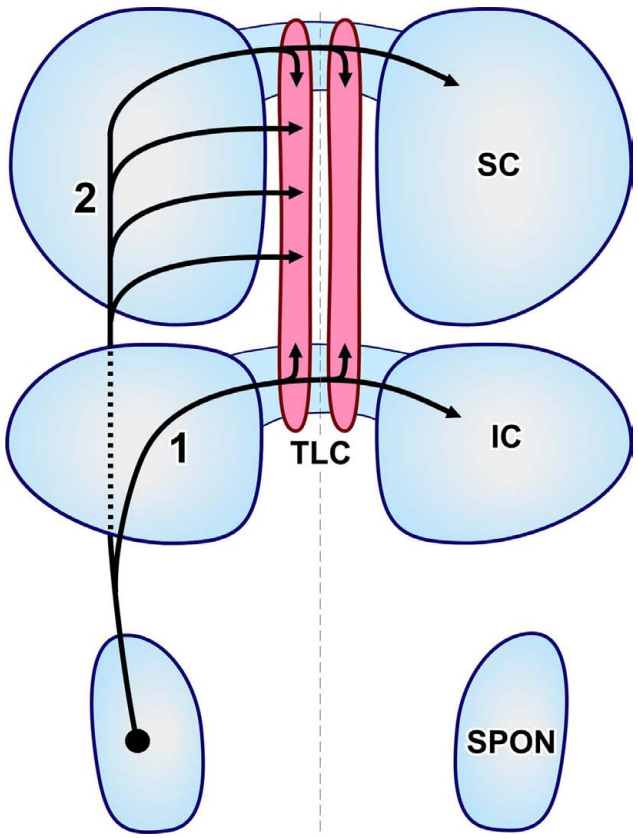

FIGURE 5 | Schematic representation of the routes followed by SPON axons that innervate the TLC. The projections have been superimposed on an idealized, dorsal view of the brainstem. The left and right TLC are shown in pink. The thin, vertical dashed line indicates the midline. Rostral is to the top. **(1)** Collaterals of axons that travel in the commissure of the IC. **(2)** Axons that reach the TLC by circumventing the IC (discontinuous line) and traveling through the deep layers of the SC.

and mediolateral axes of the TLC (**Figure 3**). The distribution of terminal fibers along the dorsoventral axis shows variations among different sections in a given case (for instance, in **Figures 3B,E** the labeled terminal fibers cover the entire dorsoventral diameter of the TLC, whereas in **Figures 3C,D** terminal fibers are concentrated in the ventral half of the nucleus; see also **Figure 6**).

Despite the above considerations, a subtle dorsoventral topography is appreciated at caudal levels. The terminal fields of SPON fibers tend to shift their dorsoventral position within the TLC as a function of the position of the injection site along the tonotopic (i.e., mediolateral) axis of the SPON (**Figures 7A1–A3,B1–B3**). Thus, in cases with tracer deposits in the medial (high characteristic frequency) region of the SPON, labeled terminal fibers are distributed mostly throughout the ventral half of the TLC; conversely, after injections in more lateral (lower characteristic frequency) regions of the SPON, labeled terminal fibers predominate dorsally within the TLC. This slight topographic tendency observed at caudal levels becomes gradually more difficult to discern rostrally (**Figures 7A4,A5,B4,B5**).

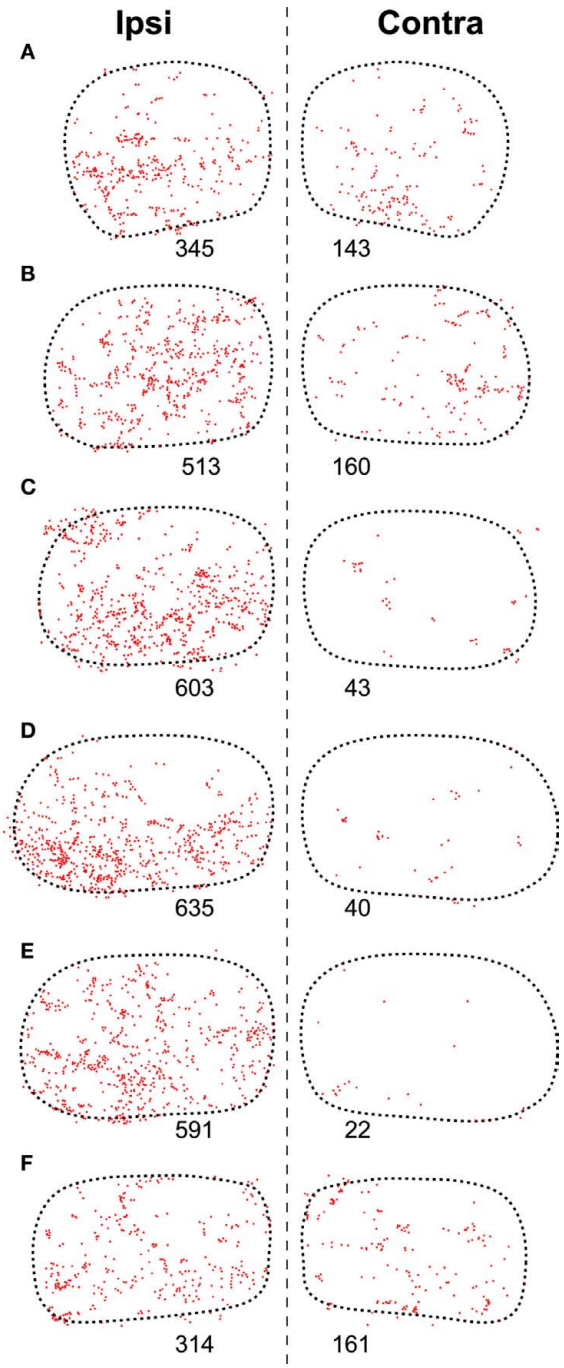

FIGURE 6 | Distribution of presumed synaptic boutons of SPON fibers in the TLC. (A–F) Plots of the location of all swellings and varicosities of SPON fibers labeled in the same sections of the TLC shown in **Figure 3** (Case 97084). Each dot represents one presumed bouton. The number below each TLC indicates the number of labeled boutons.

OTHER TARGETS OF SPON PROJECTIONS

Superior paraolivary nucleus neurons send projections to other targets besides the IC and the TLC. For example, even though many SPON axons that circumvent the IC appear to traverse the deep layers of the SC without branching, others give off collaterals that innervate the SC or the PAG (**Figures 2, 3, 4B, and 8**).

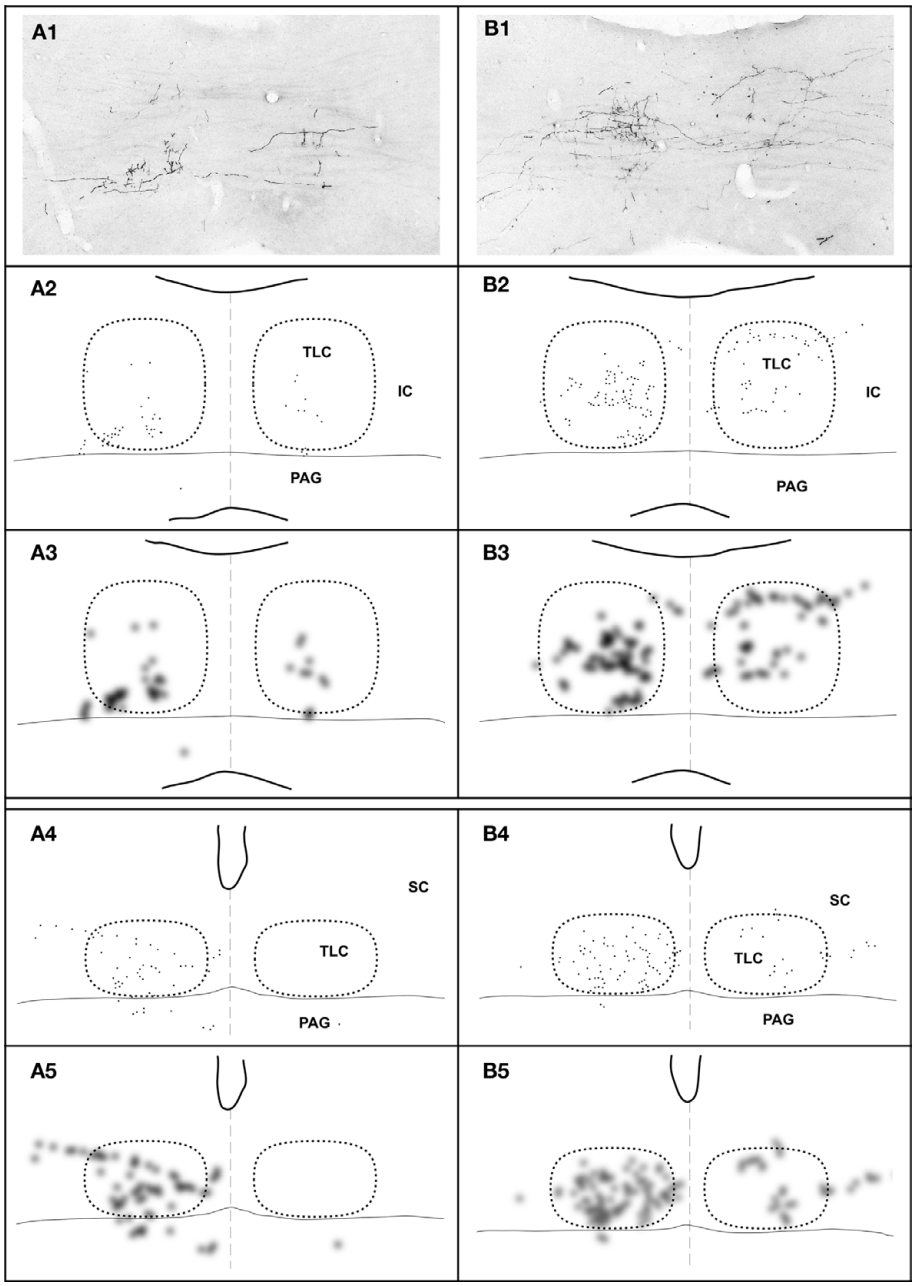

FIGURE 7 | Topography of the projection from the SPON to the TLC in two cases, whose injections of BDA were located in different positions along the mediolateral, tonotopic axis of the SPON. In case 97092 (left column) the injection site was located close to the medial border of the SPON (**Figure 1B**), whereas in case 97097 (right column) it was located in the lateral half of the SPON (**Figure 1B**). In each column, the image at the top **(A1,B1)** is a digital photomicrograph of a coronal section through the commissure of the IC (caudal third of the TLC). The second row **(A2,B2)** depicts a plot of the location of all labeled axonal swellings or varicosities (presumed to represent synaptic boutons) found in the microscopic field illustrated above. Each dot represents one axonal swelling or varicosity. The third row **(A3,B3)** shows a blurred image of the plots of the second row, in which the areas with the highest density of presumed synaptic boutons appear darkest. The fourth **(A4,B4)** and the fifth **(A5,B5)** rows show plots and blurred images of the distribution of the presumed synaptic boutons in a coronal section through the central rostrocaudal third of the TLC. In all panels, the right and the left TLC are delimited by dotted lines. Notice that the dorsoventral topography observed in caudal sections **(A3–B3)** becomes virtually lost at more rostral levels **(A5–B5)**.

In the SC ipsilateral to the injection site, labeled terminal fibers seem to concentrate in the caudal, ventral, and lateral region of the deep layers, not far from the rostral pole of the IC (**Figures 8A,B**). A few labeled collaterals ascend radially toward the intermediate and superficial layers, where terminal labeling is very sparse (**Figures 8A,C**). Very few labeled fibers are observed in layers of the ipsilateral SC more superficial than the intermediate gray layer (**Figures 2 and 8**).

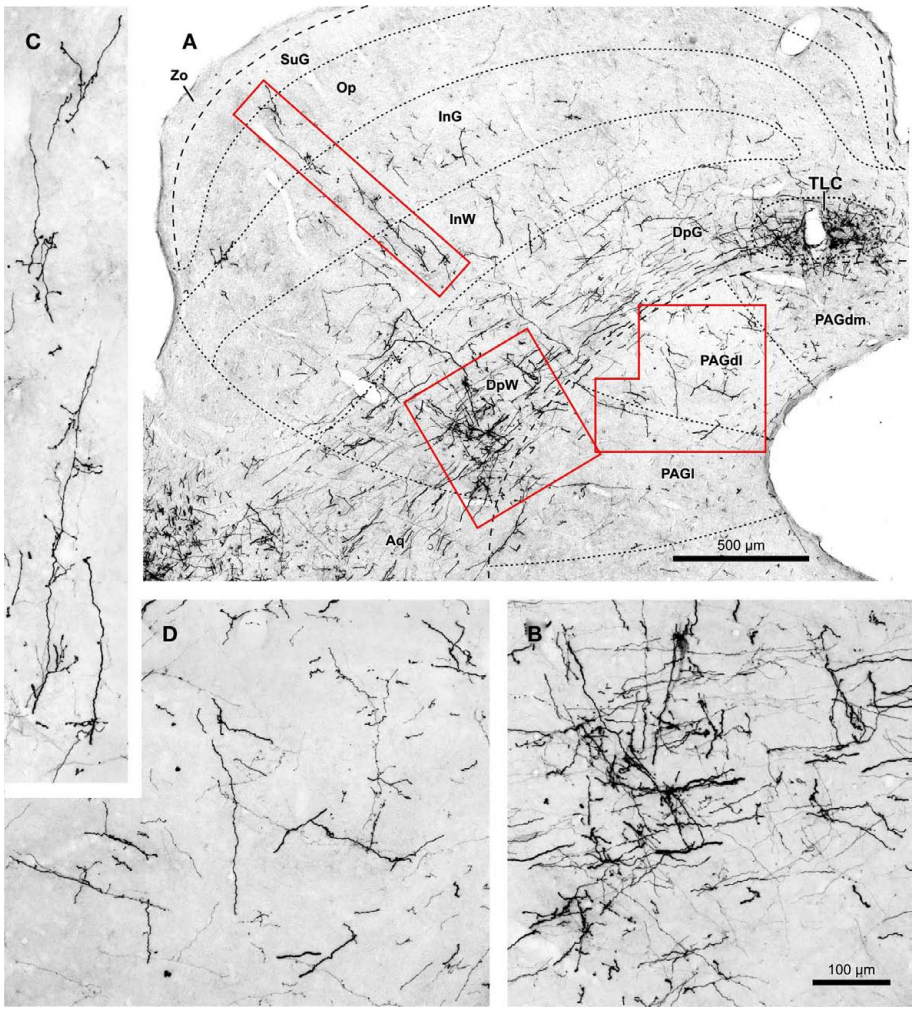

FIGURE 8 | (A) Micrograph of a coronal section of the midbrain tectum from a case that received an injection of BDA confined to the ipsilateral SPON. Case 97084, whose injection site is depicted in **Figure 1B**. The boxed areas are shown at higher magnification in **(B–D)**. **(B)** Terminal labeling in the ventrolateral part of the deep layers of the SC. **(C)** Labeled fibers that ascend radially toward the superficial layers of the SC. **(D)** Details of terminal fibers in the dorsolateral column of the PAG (PAGdl). Calibration bar in **(B)** applies also to **(C,D)**. Abbreviations of SC layers and PAG columns as in **Figure 2**.

Terminal labeling in the PAG ipsilateral to the injection site is sparse and widely distributed throughout the lateral, dorsolateral, and dorsomedial columns (**Figures 2, 3, and 8A,D**). In all cases, a few labeled fibers enter the dorsomedial column of the PAG from the overlying TLC (**Figure 4B**).

Terminal labeling is observed also in the SC and PAG contralateral to the injection site (**Figures 2 and 3**). These crossed projections are considerably less dense, however, than their ipsilateral counterparts.

Lastly, we also noted labeled terminal axons in the medial geniculate body ipsilateral to the injection site (**Figure 2F**). This novel projection from the SPON will be described in detail in a separate account.

RETROGRADELY LABELED NEURONS IN THE TLC

In most of our cases, retrogradely labeled cell bodies are found in the ipsilateral TLC (**Figure 9**), whereas neurons labeled in the contralateral TLC are very scarce (**Figure 9E**). The number of retrogradely labeled neurons varied from case to case and is apparently not related to the position of the injection site within the SPON. It is noteworthy that such retrogradely labeled neurons are always located within the territory occupied by SPON labeled terminal fibers (**Figure 9**), suggesting that the SPON and the TLC are reciprocally connected.

Most labeled TLC neurons display a punctate reaction product restricted to the cell body and, sometimes, the proximal dendritic segments; their axons are not labeled (**Figures 9A–E**). In the rare instances of neurons with diffuse labeling whose axons are labeled for hundreds of micrometers, no axonal collaterals are observed within the TLC (**Figure 9F**), suggesting that tectobulbar TLC neurons do not possess local recurrent collaterals.

Whereas close appositions between anterogradely labeled axonal swellings of SPON fibers and labeled cell bodies or dendrites in the TLC are occasionally observed, most axonal swellings are seen at a distance from retrogradely labeled neurons (**Figure 9**). This result suggests that SPON fibers preferentially target TLC neurons that do not innervate the SPON. However, we cannot rule out the

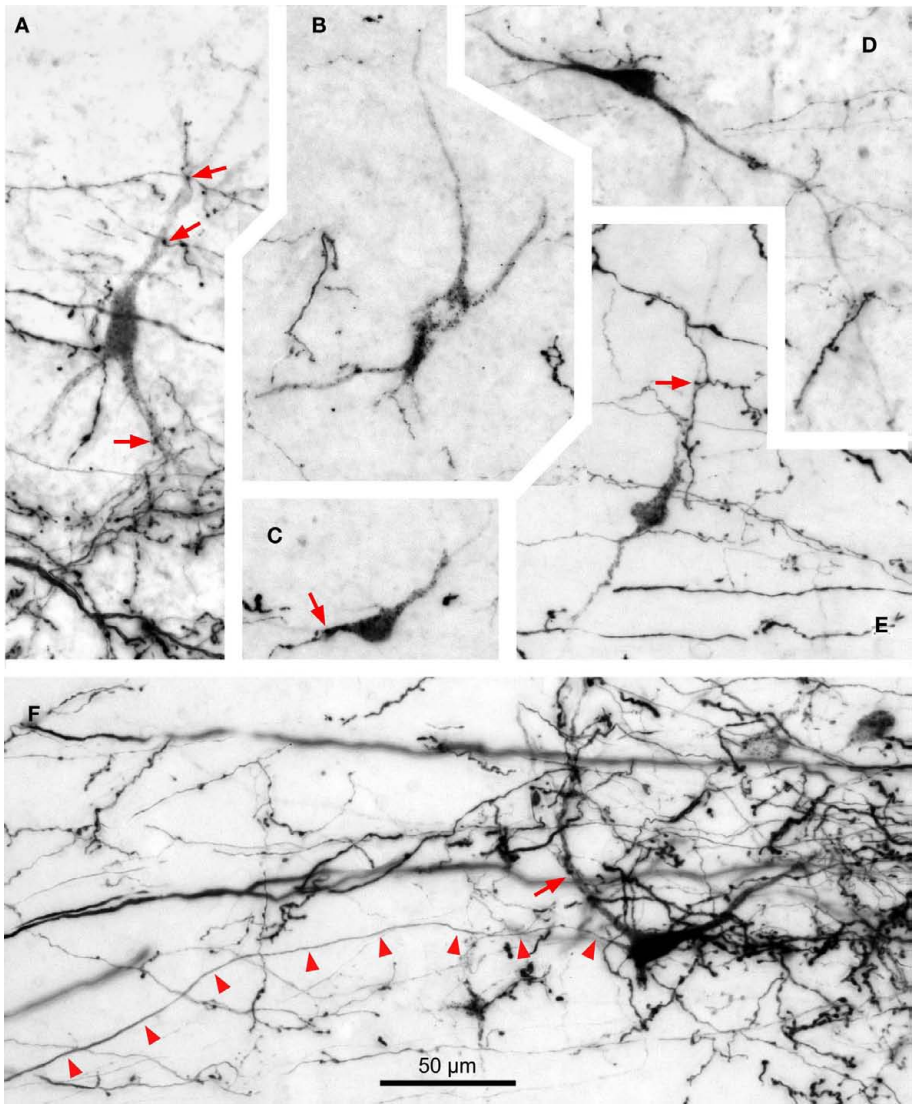

FIGURE 9 | Digital micrographs of TLC neurons retrogradely labeled following an injection of BDA into the SPON. Coronal sections. With the exception of **(E)**, all fields depict labeling in the TLC ipsilateral to the injection site. Note the multipolar morphology of the neurons, which are always intermingled with the terminal fiber fields formed by SPON axons. Red arrows indicate close appositions between boutons of labeled SPON axons and retrogradely labeled TLC neurons. Arrowheads in **(F)** point to the unbranched axon of a retrogradely labeled TLC neuron. **(A)** to **(D)** are from case 99044, and **(E,F)** from case 97084. Calibration bar in **(F)** applies to all micrographs.

possibility that SPON axons also innervate distal-most portions of the dendrites of tectobulbar TLC neurons that remained unlabeled in our experiments.

DISCUSSION

Our experiments have disclosed hitherto unknown projections from the SPON to the TLC of the rat, which constitute a major, novel auditory pathway through the lower brainstem to the midbrain. The SPON targets the entire ipsilateral TLC and, less densely, the caudal and rostral regions of the contralateral TLC. Our study also demonstrates that the SPON and the TLC are reciprocally connected, as the TLC contains abundant neurons that project back to the ipsilateral SPON.

TECHNICAL CONSIDERATIONS

In all our cases with injections of BDA into the SPON, numerous fibers were labeled in both the ipsilateral and contralateral TLC. This tracer is capable of giving rise to so-called collateral transport, whereby it labels anterogradely the collaterals of the axons through which it is transported retrogradely (i.e., Merchán et al., 1994; Warr et al., 1997; Doucet and Ryugo, 2003; Saldaña et al., 2009). Therefore, in principle, axons labeled with BDA may originate from neurons at the injection site (genuine anterograde transport) or may belong to neurons that innervate or cross the injection site (collateral transport). In our cases, numerous neurons were labeled in the ipsilateral medial nucleus of the trapezoid body (MNTB), and to a lesser extent in the contralateral ventral

cochlear nucleus and ipsilateral lateral nucleus of the trapezoid body (see also Saldaña et al., 2009). It is very unlikely, however, that the axons labeled in the TLC originated from these nuclei for two reasons: first, because labeled neurons are never found in any of these brainstem nuclei following deposits of the sensitive retrograde tracer FluoroGold into the paramedian region of the midbrain tectum that include large portions of the TLC within the injection site; and second, because labeled fibers are never found in the TLC following injections of BDA into the MNTB or the cochlear nuclei (unpublished observations).

In many of our cases, numerous neurons were retrogradely labeled within the TLC, but their axons were not visible (**Figure 9**). Moreover, the few retrogradely labeled neurons whose axons were labeled did not give off local collaterals (**Figure 9F**). Furthermore, labeled axons were systematically observed in the contralateral TLC, where retrogradely labeled neurons were extremely scarce. Finally, labeled axons in the TLC were observed in all cases with BDA injection into the SPON, including those that did not exhibit retrogradely labeled TLC neurons. Our interpretation, therefore, is that *all* BDA-labeled fibers in the TLC originate from the SPON.

THE SPON TO TLC PROJECTION

Our results demonstrate that the SPON sends direct projections to the TLC. These projections are predominantly ipsilateral, and seem to be dense. Given that the number of SPON neurons is relatively modest (approximately 2,500 neurons; Kulesza Jr. et al., 2002), the density of the projections revealed in this study indicates that the TLC is a main target of the SPON.

It has been known for decades that the main target of SPON projections is the ipsilateral IC (for references, see Saldaña et al., 2009). Given that virtually all SPON neurons participate in this projection (Saldaña and Berrebi, 2000), it is highly probable that SPON neurons that innervate the TLC also contribute to the innervation of the IC.

Recently, electrophysiological studies have demonstrated that, unlike neurons in the gerbil SPON, which exhibit considerable heterogeneity in their response properties (Behrend et al., 2002; Dehmel et al., 2002), neurons of the rat SPON are remarkably homogeneous. These cells are driven by input from the contralateral ear and strongly suppressed during acoustic stimulation by tonically active glycinergic inhibition that originates in the adjacent MNTB (Banks and Smith, 1992; Sommer et al., 1993; Smith et al., 1998; Kulesza Jr. et al., 2003; Kadner et al., 2006; Kadner and Berrebi, 2008). When the acoustic stimulus is terminated, SPON neurons are released from this inhibition and fire brief trains of discharges which constitute their characteristic offset response (Kulesza Jr. et al., 2003, 2007; Kadner and Berrebi, 2008). Because these offset spikes are triggered by episodes of low stimulus energy, i.e., gaps in ongoing stimuli and the troughs of amplitude modulated tones, Kadner and Berrebi (2008) proposed that the functional relevance of the brainstem MNTB/SPON circuit lies mainly in the encoding of *stimulus discontinuities*. The precisely timed output of the SPON is then relayed to its synaptic targets in the midbrain, including the TLC.

To understand the contribution of SPON projections to TLC function will require knowledge of the neuroactive substances released by SPON axons and the receptors expressed on the membranes of TLC neurons. Nothing is currently known regarding the latter issue, but several studies indicate that SPON neurons utilize GABA as their neurotransmitter (Mugnaini and Oertel, 1985; González-Hernández et al., 1996; Kulesza Jr. and Berrebi, 2000), so it is reasonable to assume that the projections described in this study are inhibitory. In the only detailed study to record the sound-evoked responses of TLC neurons, Marshall et al. (2008) reported no evidence for tonotopy in the nucleus, relatively broad frequency tuning and very limited sensitivity to amplitude modulation, even within the range of modulation frequencies that trigger highly synchronous action potentials from SPON neurons. Thus, it is difficult at this time to reconcile the physiological response properties of TLC neurons with the precisely timed offset spiking activity of SPON neurons. However, one must keep in mind that TLC neurons integrate their synaptic inputs from multiple sources, only a few of which are identified at this time, namely the auditory cortex (Morest and Oliver, 1984; Saldaña et al., 1996), the IC (Morest and Oliver, 1984; Saldaña and Merchán, 1992, 2005; Aparicio et al., 2010) and the SPON, as shown herein.

PROJECTION FROM THE TLC TO THE SPON

Based on the relatively high response thresholds and broad frequency tuning, as well as long first spike latencies, a prevalence for sustained firing patterns and poor phase-locking of TLC neurons, Marshall et al. (2008) concluded that the nucleus functions mainly in the descending modulation of lower auditory centers. This notion is supported by the fact that a large proportion of TLC neurons are immunolabeled by antisera directed against the inhibitory neurotransmitter GABA (our own unpublished immunohistochemical results) or its synthetic enzyme glutamic acid decarboxylase (Mugnaini and Oertel, 1985).

The present demonstration of TLC neurons retrogradely labeled from SPON injection sites confirms the existence of a descending projection and extends and refines previous studies that reported neurons labeled in the TLC following large deposits of retrograde tracers into the SOC (Faye-Lund, 1986; Mulders and Robertson, 2001; Saldaña et al., 2007). Thus, the SPON becomes the first identified target of TLC neurons.

It is also noteworthy that the TLC is the only documented source of descending inputs to the SPON of the rat, as this nucleus seems to be spared by other descending projections to the SOC (but see Thompson and Thompson, 1993; Coomes and Schofield, 2004, for results in the guinea pig). Indeed, descending IC fibers target preferentially the ventral nucleus of the trapezoid body (Faye-Lund, 1986; Caicedo and Herbert, 1993; Vetter et al., 1993; Mulders and Robertson, 2002). Likewise, the projections from the auditory cerebral cortex to the SOC terminate mainly in the ventral nucleus of the trapezoid body and, to a lesser extent, in the lateral superior olive and the so-called dorsal ribbon of the SOC (Feliciano et al., 1995; Mulders and Robertson, 2000).

CONCLUSION

The present tract-tracing investigation revealed two hitherto unknown connections in the rat auditory system: ascending projections from the SPON to the TLC and descending projections from the TLC to the SPON. Both the TLC and SPON have been identified in postmortem human brainstem (Saldaña et al., 2007; Kulesza Jr., 2008; Kulesza Jr. et al., 2011), leading us to believe that

the circuits discovered in the rat may also be present in humans. In any event, given our current level of understanding of the function of either nucleus, it is not possible at this time to formulate specific testable hypotheses of the biological significance of these reciprocal circuits. Electrophysiological recordings from the TLC while reversibly inactivating the SPON, or *vice versa*, would provide considerable insight into the impact of these reciprocal projections on auditory processing in the brainstem.

AUTHOR CONTRIBUTION

Enrique Saldaña designed the experiments and supervised the project. Antonio Viñuela and M.-Auxiliadora Aparicio performed the experiments and prepared the illustrations. Antonio Viñuela, M.-Auxiliadora Aparicio, Albert S. Berrebi, and Enrique Saldaña analyzed and interpreted the results. Enrique Saldaña and Albert S. Berrebi wrote the manuscript. Antonio Viñuela and M.-Auxiliadora Aparicio contributed equally to the work.

ACKNOWLEDGMENTS

This work was supported by the Spanish Ministries of Education and Science and Innovation grants PB95-1129, BFI2000/1358, BFU2004-05909, and BFU2008-04197 (to Enrique Saldaña), by the Junta de Castilla y León grants SA15/97, SA097/01, SA007C05, GR221, and Biomedicina 2009 (to Enrique Saldaña) and by the National Institute on Deafness and Other Communication Disorders Grant RO1 DC-002266 (to Albert S. Berrebi). The authors are thankful to Dr. Verónica Fuentes-Santamaría, who performed many of the tracing experiments.

REFERENCES

Aparicio, M. A., Viñuela, A., and Saldaña, E. (2010). Projections from the inferior colliculus to the tectal longitudinal column in the rat. *Neuroscience* 166, 653–664.

Bajo, V. M., Merchán, M. A., López, D. E., and Rouiller, E. M. (1993). Neuronal morphology and efferent projections of the dorsal nucleus of the lateral lemniscus in the rat. *J. Comp. Neurol.* 334, 241–262.

Banks, M. I., and Smith, P. H. (1992). Intracellular recordings from neurobiotin-labeled cells in brain slices of the rat medial nucleus of the trapezoid body. *J. Neurosci.* 12, 2819–2837.

Behrend, O., Brand, A., Kapfer, C., and Grothe, B. (2002). Auditory response properties in the superior paraolivary nucleus of the gerbil. *J. Neurophysiol.* 87, 2915–2928.

Caicedo, A., and Herbert, H. (1993). Topography of descending projections from the inferior colliculus to auditory brainstem nuclei in the rat. *J. Comp. Neurol.* 328, 377–392.

Coomes, D. L., and Schofield, B. R. (2004). Projections from the auditory cortex to the superior olivary complex in guinea pigs. *Eur. J. Neurosci.* 19, 2188–2200.

Dehmel, S., Doerrscheidt, G., and Reubsamen, R. (2002). Electrophysiological characterization of neurons in the superior paraolivary nucleus of the gerbil (*Meriones unguiculatus*). *Hear. Res.* 172, 18–36.

Doucet, J. R., and Ryugo, D. K. (2003). Axonal pathways to the lateral superior olive labeled with biotinylated dextran amine injections in the dorsal cochlear nucleus of rats. *J. Comp. Neurol.* 461, 452–465.

Faye-Lund, H. (1986). Projection from the inferior colliculus to the superior olivary complex in the albino rat. *Anat. Embryol.* 175, 35–52.

Feliciano, M., Saldaña, E., and Mugnaini, E. (1995). Direct projections from the rat primary auditory neocortex to nucleus sagulum, paralemniscal regions, superior olivary complex and cochlear nuclei. *Aud. Neurosci.* 1, 287–308.

González-Hernández, T., Mantolán-Sarmiento, B., González-González, B., and Pérez-González, H. (1996). Sources of GABAergic input to the inferior colliculus of the rat. *J. Comp. Neurol.* 372, 309–326.

González-Hernández, T. H., Meyer, G., Ferres-Torres, R., Castañeyra-Perdomo, A., and Pérez-Delgado, M. M. (1987). Afferent connections of the inferior colliculus in the albino mouse. *J. Hirnforsch.* 28, 315–323.

Henkel, C. K., and Shneiderman, A. (1988). Nucleus sagulum: projections of a lateral tegmental area to the inferior colliculus in the cat. *J. Comp. Neurol.* 271, 577–588.

Hutson, K. A., Glendenning, K. K., and Masterton, R. B. (1991). Acoustic chiasm. IV: eight midbrain decussations of the auditory system in the cat. *J. Comp. Neurol.* 312, 105–131.

Kadner, A., and Berrebi, A. S. (2008). Encoding of temporal features of auditory stimuli in the medial nucleus of the trapezoid body and superior paraolivary nucleus of the rat. *Neuroscience* 151, 868–687.

Kadner, A., Kulesza, R. J. Jr., and Berrebi, A. S. (2006). Neurons in the medial nucleus of the trapezoid body and superior paraolivary nucleus of the rat may play a role in sound duration coding. *J. Neurophysiol.* 95, 1499–1508.

Kulesza, R. J. Jr. (2008). Cytoarchitecture of the human superior olivary complex: nuclei of the trapezoid body and posterior tier. *Hear. Res.* 241, 52–63.

Kulesza, R. J. Jr., and Berrebi, A. S. (2000). The superior paraolivary nucleus of the rat is a GABAergic nucleus. *J. Assoc. Res. Otolaryngol.* 1, 255–269.

Kulesza, R. J. Jr., Kadner, A., and Berrebi, A. S. (2007). Distinct roles for glycine and GABA in shaping the response properties of neurons in the superior paraolivary nucleus of the rat. *J. Neurophysiol.* 97, 1610–1620.

Kulesza, R. J. Jr., Lukose, R., and Stevens, L. V. (2011). Malformation of the human superior olive in autistic spectrum disorders. *Brain Res.* 1367, 360–371.

Kulesza, R. J. Jr., Spirou, G. A., and Berrebi, A. S. (2003). Physiological response properties of neurons in the superior paraolivary nucleus of the rat. *J. Neurophysiol.* 89, 2299–2312.

Kulesza, R. J. Jr., Viñuela, A., Saldaña, E., and Berrebi, A. S. (2002). Unbiased stereological estimates of neuron number in subcortical auditory nuclei of the rat. *Hear. Res.* 168, 12–24.

Marshall, A. F., Pearson, J. M., Falk, S. E., Skaggs, J. D., Crocker, W. D., Saldaña, E., and Fitzpatrick, D. C. (2008). Auditory response properties of neurons in the tectal longitudinal column of the rat. *Hear. Res.* 244, 35–44.

Merchán, M. A., Saldaña, E., and Plaza, I. (1994). Dorsal nucleus of the lateral lemniscus in the rat: concentric organization and tonotopic projection to the inferior colliculus. *J. Comp. Neurol.* 342, 259–278.

Morest, D. K., and Oliver, D. L. (1984). The neuronal architecture of the inferior colliculus in the cat: defining the functional anatomy of the auditory midbrain. *J. Comp. Neurol.* 222, 209–236.

Mugnaini, E., and Oertel, W. H. (1985). "An atlas of the distribution of GABAergic neurons and terminals in the rat CNS as revealed by GAD immunohistochemistry," in *Handbook of Chemical Neuroanatomy*, Vol. 4, *GABA and Neuropeptides in the CNS*, Part I, eds A. Bjorklund and T. Hokfelt (Amsterdam: Elsevier Science Publishers), 436–608.

Mulders, W. H., and Robertson, D. (2000). Evidence for direct cortical innervation of medial olivocochlear neurones in rats. *Hear. Res.* 144, 65–72.

Mulders, W. H., and Robertson, D. (2001). Origin of the noradrenergic innervation of the superior olivary complex in the rat. *J. Chem. Neuroanat.* 21, 313–322.

Mulders, W. H., and Robertson, D. (2002). Inputs from the cochlea and the inferior colliculus converge on olivocochlear neurones. *Hear. Res.* 167, 206–213.

Paxinos, G., and Watson, C. (2007). *The Rat Brain in Stereotaxic Coordinates*, 6th Edn. San Diego: Academic Press.

Saldaña, E., Aparicio, M. A., Fuentes-Santamaría, V., and Berrebi, A. S. (2009). Connections of the superior paraolivary nucleus of the rat: projections to the inferior colliculus. *Neuroscience* 163, 372–387.

Saldaña, E., and Berrebi, A. S. (2000). Anisotropic organization of the rat superior paraolivary nucleus. *Anat. Embryol.* 202, 265–279.

Saldaña, E., Feliciano, M., and Mugnaini, E. (1996). Distribution of descending projections from primary auditory neocortex to inferior colliculus mimics the topography of intracollicular projections. *J. Comp. Neurol.* 371, 15–40.

Saldaña, E., and Merchán, M. A. (1992). Intrinsic and commissural connections of the rat inferior colliculus. *J. Comp. Neurol.* 319, 417–437.

Saldaña, E., and Merchán, M. A. (2005). "Intrinsic and commissural connections of the inferior colliculus," in *The Inferior Colliculus*, eds J. A. Winer and C. E. Schreiner (New York: Springer), 155–181.

Saldaña, E., Viñuela, A., Marshall, A. F., Fitzpatrick, D. C., and Aparicio, M. A. (2007). The TLC: a novel auditory nucleus of the mammalian brain. *J. Neurosci.* 27, 13108–13116.

Smith, P. H., Joris, P. X., and Yin, T. C. (1998). Anatomy and physiology of principal cells of the medial nucleus of the trapezoid body (MNTB) of the cat. *J. Neurophysiol.* 79, 3127–3142.

Sommer, I., Lingenhohl, K., and Friauf, E. (1993). Principal cells of the rat

medial nucleus of the trapezoid body: an intracellular in vivo study of their physiology and morphology. *Exp. Brain Res.* 95, 223–239.

Thompson, A. M., and Thompson, G. C. (1993). Relationship of descending inferior colliculus projections to olivocochlear neurons. *J. Comp. Neurol.* 335, 402–312.

Vetter, D. E., Saldaña, E., and Mugnaini, E. (1993). Input form the inferior colliculus to medial olivocochlear neurons in the rat: a double label study with PHA-L and cholera toxin. *Hear. Res.* 70, 173–186.

Warr, W. B., Boche, J. B., and Neely, S. T. (1997). Efferent innervation of the inner hair cell region: origins and terminations of two lateral olivocochlear systems. *Hear. Res.* 108, 89–111.

Conflict of Interest Statement: The authors declare that the research was conducted in the absence of any commercial or financial relationships that could be construed as a potential conflict of interest.

Received: 23 July 2010; paper pending published: 06 September 2010; accepted: 05 January 2011; published online: 22 February 2011.

Citation: Viñuela A, Aparicio M-A, Berrebi AS and Saldaña E (2011) Connections of the superior paraolivary nucleus of the rat: II. Reciprocal connections with the tectal longitudinal column. Front. Neuroanat. ***5****:1. doi: 10.3389/fnana.2011.00001*

frontiers in
NEUROANATOMY

ORIGINAL RESEARCH ARTICLE
published: 20 October 2010
doi: 10.3389/fnana.2010.00141

Transient down-regulation of sound-induced c-Fos protein expression in the inferior colliculus after ablation of the auditory cortex

Cheryl Clarkson[1], José M. Juíz[2] and Miguel A. Merchán[1]*

[1] *Instituto de Neurociencias de Castilla y León, Salamanca, Spain*
[2] *Instituto de Investigación en Discapacidades Neurológicas, Medical School, University of Castilla-La Mancha, Albacete, Spain*

Edited by:
Douglas L. Oliver, University of Connecticut Health Center, USA

Reviewed by:
Maria E. Rubio, University of Pittsburgh, USA
Avril Genene Holt, Wayne State University, USA

****Correspondence:***
Miguel A. Merchán, Laboratory for the Neurobiology of Hearing, Instituto de Neurociencias de Castilla y León, Pintor Fernando Gallego Street, 1, Salamanca 37007, Spain.
e-mail: merchan@usal.es

We tested whether lesions of the excitatory glutamatergic projection from the auditory cortex (AC) to the inferior colliculus (IC) induce plastic changes in neurons of this nucleus. Changes in neuronal activation in the IC deprived unilaterally of the cortico-collicular projection were assessed by quantitative c-Fos immunocytochemistry. Densitometry and stereology measures of sound-induced c-Fos immunoreactivity in the IC showed diminished labeling at 1, 15, 90, and 180 days after lesions to the AC suggesting protein down-regulation, at least up to 15 days post-lesion. Between 15 and 90 days after the lesion, c-Fos labeling recovers, approaching control values at 180 days. Thus, glutamatergic excitation from the cortex maintains sound-induced activity in neurons of the IC. Subdivisions of this nucleus receiving a higher density of cortical innervation such as the dorsal cortex showed greater changes in c-Fos immunoreactivity, suggesting that the anatomical strength of the projection correlates with effect strength. Therefore, after damage of the corticofugal projection, neurons of the IC down-regulate and further recover sound-induced c-Fos protein expression. This may be part of cellular mechanisms aimed at balancing or adapting neuronal responses to altered synaptic inputs.

Keywords: rat, immediate early gene, homeostatic plasticity, auditory descending projection

INTRODUCTION

The inferior colliculus (IC) is a major center of acoustic integration in the midbrain. It receives convergent ascending projections from multiple auditory brainstem nuclei, as well as intrinsic and commissural connections along with descending projections from the auditory cortex (AC). This cortico-collicular projection is direct, excitatory and bilateral, although stronger toward the ipsilateral side (Feliciano and Potashner, 1995; Saldaña et al., 1996). Excitation seems to be mediated by glutamate (Helfert et al., 1991; Wenthold, 1991; Wenthold et al., 1993; Feliciano and Potashner, 1995). The specific role of this descending projection from the AC to the IC in auditory processing is still unknown, although it is clearly involved in modulating IC neuronal responses to sound. Electrophysiological studies suggest that the cortico-collicular projection has either positive or negative feedback effects in neuronal firing properties of IC neurons. After blocking auditory cortical activity with tetrodotoxin, a majority of IC neurons either increase or decrease firing rates (Nwabueze-Ogbo et al., 2002; Popelar et al., 2003). Overactivation of the AC following local infusion of the GABAA antagonist bicuculline increases neuronal activity in the IC (Sun et al., 2007, 2009).

Modulatory effects of the AC projection on IC neuronal responses may involve ongoing changes in the activity level of IC neurons. Sun et al. (2007, 2009) found that the transcription factor c-Fos, an immediate early expression gene that is a well-known marker of neuronal activity, is overexpressed in sound-stimulated IC neurons shortly after pharmacological activation of the AC. These authors found that neurons in IC subdivisions with a higher innervation density from the cortico-collicular projection have higher levels of c-Fos protein expression (Sun et al., 2007, 2009), thus suggesting a direct correlation between the anatomical strength of the cortico-collicular projection and modulatory effects on the activity of IC neurons. On the other hand, we reported (Clarkson et al., 2010a) that after unilateral lesions of the AC, auditory brainstem response (ABR) thresholds were elevated 15 days after the lesion, returning to near normal values at 90 days post-lesion. Startle reflex and prepulse inhibition tests also showed diminished responses 15 days after lesions of the AC, followed by recovery 90 and 180 days after the lesion (Clarkson et al., 2010a). These findings stress the fact that damage of the cortico-collicular projection results in altered processing in IC neurons, due to loss of cortical modulation. Interestingly, however, IC function seems to return to normal 90–180 days after AC ablation (Clarkson et al., 2010a). Thus, connections from the AC to the IC may be involved in reparative or adaptive mechanisms after auditory damage. In this regard, it would be relevant to assess spatial and temporal changes in sound-evoked activity of IC neurons, measured by changes in the expression of c-Fos, at different times after silencing the cortico-collicular projection.

Abbreviations: ABR, auditory brainstem response; AC, auditory cortex; Au1, primary auditory cortex; AuD, secondary auditory cortex, dorsal; AuV, secondary auditory cortex, ventral; c-Fos Ir, immunoreactive for c-Fos; CNIC, central nucleus inferior colliculus; DAB, 3,3′-diamino-benzidine; DCIC, dorsal cortex inferior colliculus; IC, inferior colliculus; IEG, immediate early gene; LCIC, lateral cortex inferior colliculus; PB, phospate buffer; SD, standard deviation; TBS, Tris buffered saline

Therefore, we tested whether descending excitatory deafferentation of the IC after cortical ablation induces changes in activity of IC neurons, measured by patterns of sound-induced c-Fos activity. We also addressed whether such changes revert back with time, suggesting compensatory and/or reparative events in the adult animal. Toward this goal, we analyzed across IC subdivisions the effects of short- and long-term unilateral lesions of the AC on sound-activated expression of the transcription regulator protein c-Fos.

MATERIALS AND METHODS

EXPERIMENTAL ANIMALS AND GROUPS

Twenty-four male Wistar albino rats were used, with a weight of 230 g and 12 weeks of age (**Table 1**). Animals were provided by the Animal House facility of the University of Salamanca. The use and care of the animals as well as the surgical procedures were approved and supervised by institutional committees, following national (R.D. 1201/2005) and EU regulations (DOCE L 222; 24-08-1999) for the use and care of animals in research.

LESIONS OF THE AUDITORY CORTEX

Animals (groups 3–6, $n = 16$, **Table 1**) were anesthetized with ketamine chlorhydrate (30 mg/kg, Imalgene® 1000, Rhone Méreuse, Lyon, France) and xylazine chlorhydrate (5 mg/kg Rompun®, Bayer, Leverkusen, Germany). Unilateral ablation by aspiration of the left auditory cortices (primary – Au1, dorsal – AuD, and ventral – AuV areas), including cortical layers V and VI, was carried out under stereotaxic control using a stereotaxic frame (#900, David Kopf Ins., Tujunga, CA, USA) following a procedure described in detail elsewhere (Clarkson et al., 2010a).

SOUND STIMULATION

Twenty animals distributed in five groups (2–6, **Table 1**) were acoustically stimulated to analyze c-Fos expression in the IC. Seventy-two hours before the stimulation protocol, animals including non-stimulated controls (group 1, $n = 4$, **Table 1**), were housed individually in an acoustically isolated area of the animal house. Animals at 1, 15, 90, and 180 days post-lesion and corresponding stimulated controls were anesthetized with 20% urethane (1.5 g/kg, i.p.) and placed in a purposely made acoustic stimulation chamber, built according to the specifications of Yoshida et al. (2000). Open field stimulus consisted of 5.0 kHz, 80 dB pure tones presented at 300 ms on/500 ms off cycles, with a rise time of 10 ms for a total duration of 60 min. Sound was amplified and delivered through four open field speakers (Mac Audio Electronic GmbH & Co. KG, Germany).

Sound exposure levels were measured inside the chamber, before and after each experiment, using a 1/2-inch condenser microphone (Brüel and Kjær 4191, Nærum, Denmark), placed in a position equivalent to that of the animal's head. After stimulation delivery, animals were allowed to rest in a quiet environment for 100 min. After this, animals still under the effects of urethane anesthesia were perfusion-fixed following standard protocols described below.

HISTOLOGICAL METHODS

Two hundred fifty microliters of Ringer buffer (pH 6.9, 36°C) with 0.01% heparin were perfused transcardially, followed by 1000 ml of fixative, consisting of 4% *p*-formaldehyde and 0.025% glutaraldehyde, at room temperature. After fixation, the brains were dissected out, sectioned and postfixed by immersion in the same fixative solution for 2 h before being cryoprotected by immersion in 30% sucrose in 0.1 M phosphate buffer (PB), pH 7.4 at 4°C for 48 h. The brains were then serially sectioned in the coronal plane at 40 μ using a sliding freezing microtome.

c-Fos immunocytochemistry

Alternate serial sections of the brain including the IC were labeled for c-Fos with immunocytochemistry. Sections floating in a beaker were sequentially washed with 0.05 M Tris buffered saline (TBS), pH 7.6, followed by inhibition of endogenous peroxidase by incubating with 10% methanol + H_2O_2 3% in 0.1 M PB for 10 min. Sections were then washed with TBS–Triton X100 0.3% (0.05 M, pH 7.6, 3 × 15 min on a shaker) and non-specific labeling was blocked using 10% fetal calf serum. Sections were incubated with a polyclonal anti c-Fos Ab-5 antibody made in rabbit (Oncogene Research Products; catalog No. PC38, San Diego, CA, USA). It was raised against a synthetic peptide (SGFNADYEASSSRC) corresponding to amino acid residues 4–17 of human c-Fos [1:7,500]. Sections were incubated in a secondary antibody, a biotinylated anti-rabbit IgG (H + L) (BA-1000, Vector Laboratories, Burlingame, CA, USA), at a dilution of 1:200 in TBS 0.05 M + Triton X100 0.3% for 120 min at room temperature. After this, sections were washed again with TBS–Triton X100 and incubated in avidin–biotinylated peroxidase complex in TBS–Triton X100 for 90 min. The peroxidase reaction was revealed with 3,3′-diamino-benzidine (DAB) and nickel-ammonium sulfate (0.16%) + H_2O_2 (0.006%) for 5 min in all sections. Immunostained sections were mounted on slides, dried, dehydrated, cover slipped, and sealed. To test the specificity of the detection system, incubation with primary antibodies was omitted. No specific staining was observed.

STEREOLOGY COUNTS, DENSITOMETRY, AND MORPHOMETRY OF c-Fos IMMUNOREACTIVE NUCLEI

Nuclei immunoreactive for c-Fos (c-Fos Ir) were counted as particles in each of the three divisions of the IC, dorsal cortex (DCIC), lateral cortex (LCIC), and central nucleus (CNIC). To determine particle counting parameters, Preliminary Population Estimates, and Optical Fractionator tests (West et al., 1991) were applied by using Stereo Investigator 8.0 software (Micro Bright Field, Inc, VT, USA).

c-Fos Ir neuronal nuclei, displaying a clear-cut border was counted as positive particles. They were clearly differentiated from glial cells based on size. Limited section depth and adequate immunoreactions' intensity allowed clear distinction of c-Fos Ir nuclei. A minimum of 250 c-Fos Ir nuclei was counted for each study case, including unlesioned controls, either stimulated or non-stimulated, or lesioned, stimulated animals. Counts were made in each IC division bilaterally, obtaining final values by the Estimated Total by Optical Fractionator. Gundersen's error coefficient $m = 1$ (Gundersen et al., 1999) was calculated, with values ranging from 0.4 to 0.6.

For image analysis four selected sections were picked from equivalent interaural levels in the rostro-caudal axis. Images were captured with a digital camera, using a 20× dry objective (Leica-PlanFluotar/0.80). Mosaic fields of the entire IC were assembled

with the individual images (Neurolucida Vs 8.0, MicroBrightField, Inc, Williston, VT, USA). Image analysis was carried out with Scion ImageJ 1.42q software (National Institutes of Health – NIH), adjusting the microscope illumination source before each image capture to obtain similar light intensities in all cases.

After selecting one section per case at the same rostro-caudal level (interaural level: 0.12 mm, Paxinos and Watson, 2005) two trained observers separately marked the contours and segmented a minimum of 300 particles from each section. Particles were analyzed to obtain average gray levels and standard deviation (SD), using Scion ImageJ. Average values were analyzed statistically. Based on this data, a threshold of the average gray level ± SD, equivalent to levels 0–88 of the gray scale, was set as segmentation range for densitometry and morphometry measurements. Using this threshold, image mosaics from experimental cases were segmented and sections analyzed at four equivalent interaural levels of the rostro-caudal axis.

For each particle segmented between 0 and 88, gray level average values and SD, nuclear perimeter, and coordinate values of two-dimensional placement in the image were obtained. Positional values were fed into MATLAB (The MathWorks, Inc, Natick, MA, USA) along with gray value average and SD of segmented immunoreactive nuclei to build topographic densitometry maps of the IC.

RESULTS

LESION LOCALIZATION IN THE AC

All ablations specifically encroached the major subdivisions of the AC: primary, dorsal and ventral cortices. Lesion depth reached layers Vc and VI, leaving the white matter unaffected. Lesions affected between 65.47 and 84.89% of the cortices.

c-Fos IMMUNOCYTOCHEMISTRY

The c-Fos antibody, sharply labeled structures identifiable on the basis of size and shape as neuronal nuclei. Non-stimulated control animals showed moderately labeled nuclei (see c-Fos Densitometry and Morphometry), which were more concentrated in the dorsal two-thirds of the IC (**Figure 1A**). Control animals stimulated for 60 min with the 5.0 kHz, 80 dB test tone (group 2, $n = 4$, **Table 1**) showed much more abundant c-Fos Ir nuclei, with a higher concentration in the dorsalmost regions of the three IC subdivisions (**Figure 1B**). The highest density of c-Fos Ir nuclei was seen in layer 1 of the DCIC and in the dorsal portions of the CNIC.

One day after the cortical lesion, identically stimulated animals (group 3, $n = 4$, **Table 1**) showed a moderate decrease in the density of c-Fos Ir neuronal nuclei in all subdivisions, although mainly in the middle zone of the DCIC (**Figure 1C**), when compared with stimulated controls. In animals 15 days after the lesion (group 4, $n = 4$, **Table 1**), acoustic stimulation induced very low densities of c-Fos Ir, in the DCIC and in the CNIC (**Figure 1D**), although accumulations of c-Fos Ir neuronal nuclei were seen in its ventral portions. After 90 or 180 days of cortical lesion, sound-stimulated animals (groups 5 and 6, $n = 4$, **Table 1**) did not show visible differences with controls in the density or distribution of c-Fos Ir neuronal nuclei (**Figures 1E,F**).

c-Fos densitometry and morphometry

Comparisons of average gray levels of c-Fos Ir neuronal nuclei (range: 0–88, 0 corresponding to the darkest particles and 88 to the lightest particles, see Materials and Methods) showed that c-Fos immunoreactivity was, on average, 31.75% more intense in stimulated than in non-stimulated controls (**Figure 2**). Comparison of stimulated controls and experimental groups 1 day and 15 days after the cortical lesion, showed a shift in gray level values of 25.43 and 23.76%, respectively toward the upper (white) end of the gray level range, whereas there were no significant differences at 90 days post-lesion. After 180 days post-lesion the gray average levels were higher than those in the control group (**Figure 2**). Comparisons between stimulated controls, and lesioned animals in the sides ipsi- and contralateral to the lesion, showed significant differences only in the 15 days post-lesion group (data not shown).

In the non-stimulated control cases, density plots of c-Fos Ir gray values showed less c-Fos Ir neuronal nuclei than in stimulated controls with a random distribution of dark and light particles in the three subdivisions of the IC (**Figures 3A,B**), although higher densities were found in medial and lateral regions (**Figure 3A**). The stimulated controls showed abundant c-Fos Ir nuclei in the darker range of the gray spectrum in the three subdivisions of the IC, mainly in the cortices (**Figure 3B**). In animals stimulated 1 day after the AC lesion there was a slight decrease in c-Fos Ir particle number and density in all IC subdivisions (**Figure 3C**). Also, we show in figure 3D-3F, the distribution of all the nuclei c-Fos positives between 0-88 (gray values) in the control groups (non-stimulated and stimulated) and animals after one day post-lesion. After 15 days we observed overall diminished numbers and densities of c-Fos Ir neuronal nuclei, although a band of particles with the highest labeling density was detectable in ventro-medial portions of the CNIC (**Figure 4A**). Ninety days after the lesion, sound-stimulated animals showed a distribution of c-Fos Ir particles similar to controls, along with increased neuronal nuclei density (**Figure 4B**). In animals stimulated 180 days after the lesion, the distribution of c-Fos Ir neuronal nuclei in the IC was similar to the 90 day post-lesion and control groups, with just a slight decrease in the density of immunoreactive particles (**Figure 4C**). Also, we analyze in the figure 4D-F the distribution of c-Fos immunoreactive nuclei in the range between 0-88 (gray levels) to find differences among lesioned groups at different times of survival post-lesion, and we found in the histograms a recovery of the gray values arrangement, in animals stimulated after long-term post-lesion.

Perimeter of c-Fos Ir neuronal nuclei in the IC was, on average, 9.08% significantly larger in stimulated controls than in non-stimulated controls (**Figure 5**). Animals lesioned for 90 days showed a statistically significant increase of 9.18% in the average perimeter ± SD of c-Fos immunoreactive neuronal nuclei (**Figure 5**), relative to stimulated controls. Comparisons in all animals between c-Fos Ir nuclei perimeter in the sides ipsi- and contralateral to the lesion showed that the perimeter only was significantly increased in the contralateral IC from animals stimulated with sound 90 days after the AC lesion (data not shown).

c-Fos stereology counts

Stereology counts of c-Fos Ir neuronal nuclei in animals from the control non-stimulated cases (group 1, $n = 4$, **Table 1**) showed a total average number of 133985 ± 5330 immunoreactive particles in both ICs. In stimulated controls (group 2, $n = 4$, **Table 1**) the average number of c-Fos Ir nuclei was 155326 ± 5324, an increase of 15.92% (**Figure 6A**)

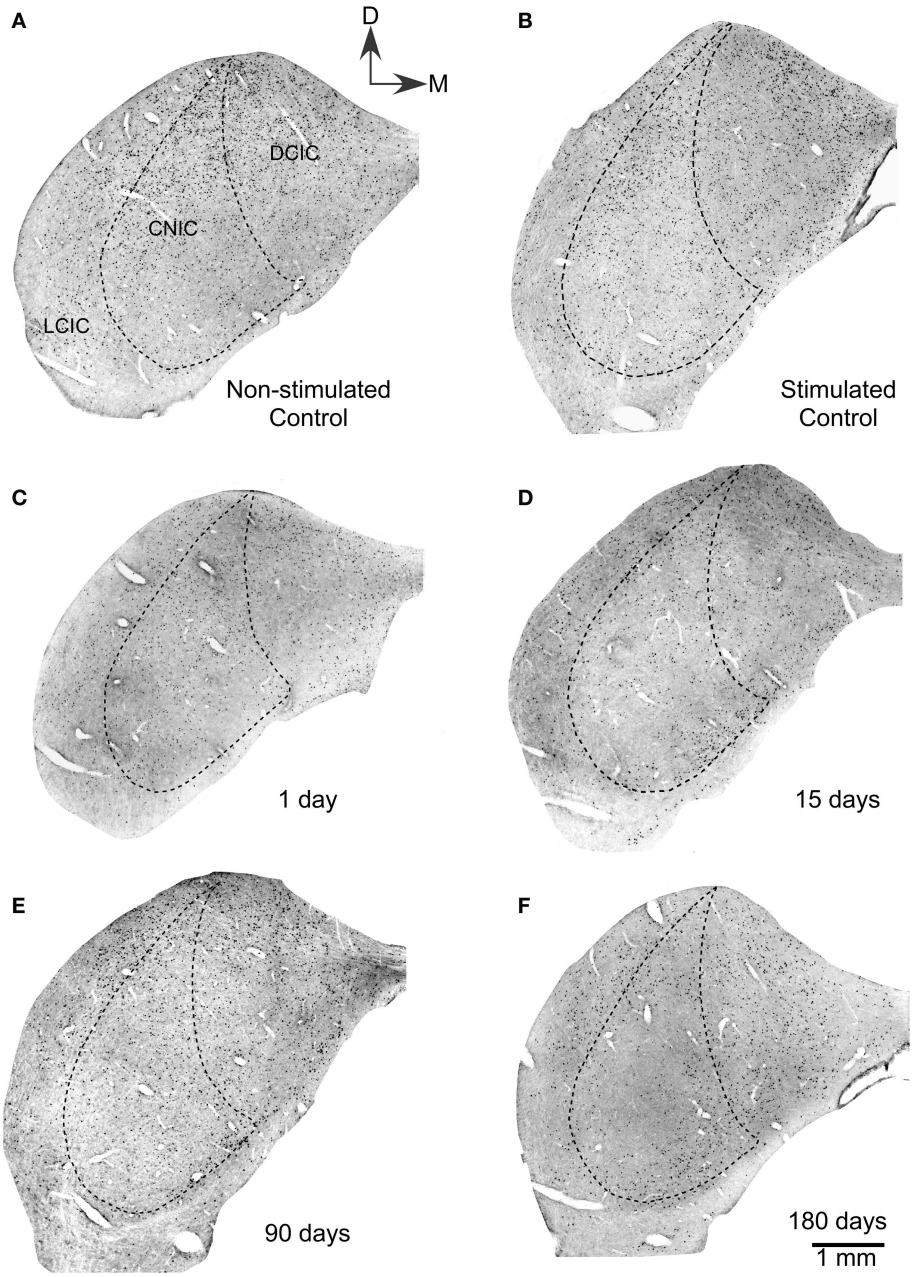

FIGURE 1 | Low power magnification photomicrograph showing sections of the ipsilateral inferior colliculus immunostained for c-Fos after lesions of the auditory cortex. (A) Non-stimulated control groups showed neuronal nuclei c-Fos Ir in all subdivisions of the IC. Also, in stimulated controls **(B)**, a large number of c-Fos immunoreactive nuclei are seen in all three subdivisions of control inferior colliculi after sound stimulation. **(C)** One day after the cortical lesion, sound stimulation induces lower numbers of c-Fos immunoreactive neuronal nuclei. **(D)** Fifteen days after cortical ablation, sound-evoked c-Fos immunoreactivity is even lower than at 1 day after the lesion. **(E)** Ninety days after the cortical lesion, sound stimulation induces c-Fos immunoreactivity in neuronal nuclei, with numbers higher than at 15 days, but still lower than in stimulated controls. **(F)** Hundred eighty days after the cortical ablation, sound-evoked c-Fos immunoreactivity is close to control values.

relative to non-stimulated controls. Comparisons between stimulated controls and animals exposed to sound at different times after lesions of the AC, showed an overall decrease in average numbers of c-Fos Ir neuronal nuclei (**Figure 6A**). Thus, after 1 day post-lesion there was an average of 88809 ± 3670 labeled nuclei in the IC. In animals stimulated 15 days after the lesion, the average was 61810 ± 10045, the largest decrease detected. In animals surviving 90 days after the lesion, there was an average of 99978 ± 6159 c-Fos Ir neuronal nuclei after sound stimulation. At 180 days after the lesion, the average number was larger, with 115262 ± 8359 neuronal nuclei. Therefore, 1 day after the lesion of the AC, there is a 42% decrease in c-Fos Ir neuronal nuclei in the IC after sound stimulation relative to identically stimulated controls. After 15 days post-lesion, the decrease reaches 55%. Ninety days after the lesion, the decrease is 33% and it goes down to

Table 1 | Experimental groups.

Group	*n* = 24	Lesion	Post-lesion survival time	Methodology
1	4	–	Control	Stereology
2	4	–	Control	Sound stimulation and stereology
3	4	Left ACs	1 day	Sound stimulation and stereology
4	4	Left ACs	15 days	Sound stimulation and stereology
5	4	Left ACs	90 days	Sound stimulation and stereology
6	4	Left ACs	180 days	Sound stimulation and stereology

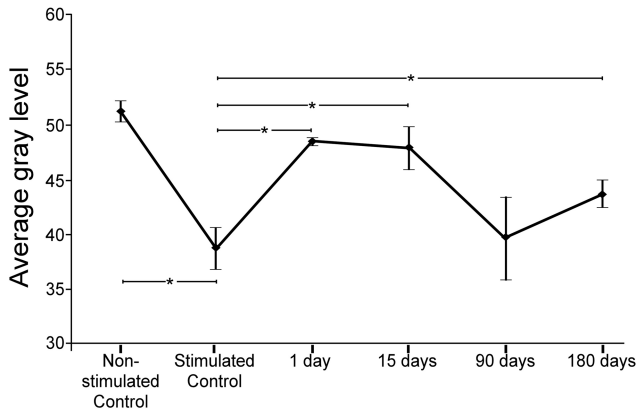

FIGURE 2 | Average gray levels of sound-induced c-Fos immunoreactivity in nuclei of the inferior colliculus at different times after a unilateral cortical lesion. In control non-stimulated groups, means were higher (i.e., shifted toward lighter gray levels) than in the stimulated control. Comparisons between stimulated controls and lesioned stimulated groups shows that the average levels shift toward values closer to the white side of the gray range at 1 and 15 days after the lesion. Ninety and 180 days after the lesion, gray values return to levels comparable to controls. The asterisks show the significant differences (average ± 2SD) between both, the non-stimulated control and the group of stimulated control, and the stimulated control group and lesioned groups.

23% 180 days after the lesion (**Figure 6A**). Average decreases in c-Fos immunoreactive neuronal nuclei between the sides ipsi- and contralateral to the lesion, were found to be significantly different in the IC only in animals stimulated 1 day after ablation of the AC (mean ± SD), with a larger decrease in the ipsilateral side (**Figure 6B**).

In addition, each of the three major IC subdivisions was analyzed separately in acoustically stimulated animals, pooling quantitative results from both ICs (**Figure 7**). The largest variation in c-Fos Ir neuronal nuclei was seen in the DCIC. One day after the lesion, the number of c-Fos Ir neuronal nuclei was 54% lower than in stimulated controls, whereas at 15 days post-lesion it had dropped to 68%, the lowest value recorded. After 90 days of the AC lesion, the average number of c-Fos Ir neuronal nuclei after sound stimulation in the IC was 42.25% lower than in controls. After 180 days of the lesion of the AC, the average number of c-Fos Ir neurons after sound stimulation was still 30% lower relative to values in control ICs (**Figure 7A**). Comparisons between the DCIC from the sides ipsi- and contralateral to the lesion, showed significant differences only in the 1 day post-lesion group, with a larger decrease in the side ipsilateral to the cortical lesion (**Figure 7B**).

In the LCIC, there were also significant percent variations in the number of c-Fos Ir neuronal nuclei after sound stimulation between the ICs (bilateral) of lesioned and stimulated control animals, with a 49% decrease 1 day after the lesion, 65% 15 days after the lesion, 31.7% at 90 days and 29% after 180 days post-lesion (**Figure 7C**). Comparisons between the LCIC from the sides ipsi- and contralateral to the lesion, showed, similar to the DCIC, significant differences only in the 1 day post-lesion group, with a higher decrease in the side ipsilateral to the lesion region (**Figure 7D**).

Changes in sound-stimulated c-Fos Ir neurons in the CNIC after cortical lesions were notably less dramatic than in the other two subdivisions, with values 10% lower than in stimulated controls in the case of the 1 day post-lesion group. Fifteen days after the lesion of the AC, the number of c-Fos Ir nuclei was 36% lower that in controls and 90 days after the lesion it was 25.91% lower. After 180 days of the AC lesion, the drop in the number of c-Fos Ir neuronal nuclei returned to values near 11% (**Figure 7E**). When the sides ipsi- and contralateral to the AC lesion were compared, significant differences were seen at 1 day, 90 and 180 days after the lesion, with the ipsilateral side showing a comparatively largest decrease in the average number of c-Fos Ir neuronal nuclei after sound stimulation (**Figure 7F**). However, no significant differences were found between both sides in the 15 days post-lesion group.

DISCUSSION

We show that unilateral lesions in the AC induce short- and long-term changes in the IC affecting c-Fos protein production. One day after unilateral ablation of the ACs, c-Fos expression in IC neurons induced by acoustic stimulation, is diminished. Fifteen days after the cortical lesion, c-Fos expression subsequent to acoustic stimulation is further diminished. Ninety days after the lesion we find recovery of c-Fos activity relative to stimulated controls. After 180 days of lesion-induced changes, all c-Fos values tested histologically, i.e., neuron number, average gray values and nuclear perimeter had returned to values comparable to those of the stimulated control group. Also, stereology counts of the number of c-Fos immunoreactive neuronal nuclei in the three major subdivisions of the IC showed that the most significant changes in c-Fos expression affected both IC cortical divisions, DCIC and LCIC. The number of c-Fos immunoreactive collicular neurons was comparable in both sides at all survival times, with the exception of the 1 day survival group, in which the side ipsilateral to the lesion showed fewer immunoreactive neurons than the contralateral side.

The induction of the expression of protein products of immediate early genes (IEG), notably c-Fos (Greenberg and Ziff, 1984; Ceccatelli et al., 1989; Bullitt, 1990), is a widely used tool for the anatomical identification and mapping of cells and neuronal circuits activated in response to different stimuli. *c-fos* is an IEG that does not require "*de novo*" protein synthesis (Herrera and Robertson, 1996) and therefore can be quickly activated as part of primary

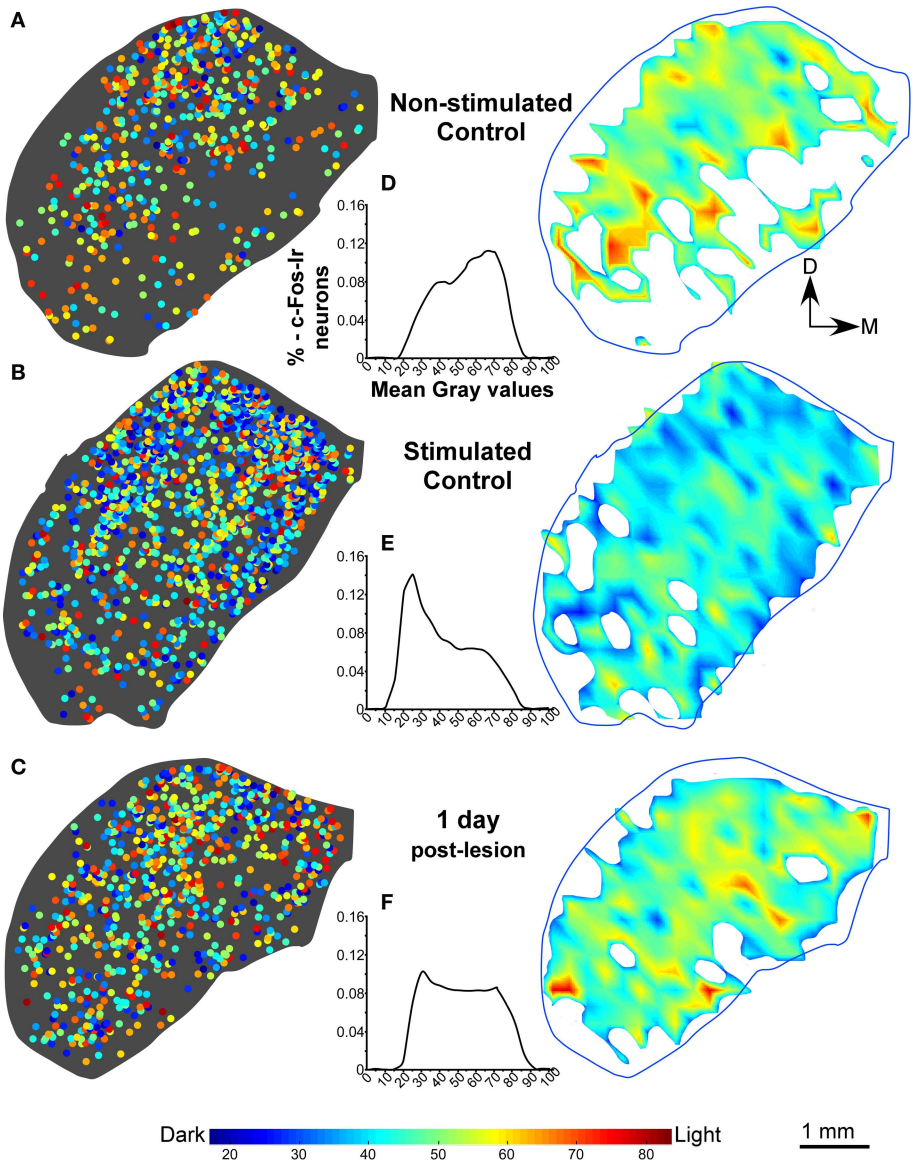

FIGURE 3 | (A,B) Distribution density, gray value plots, and histograms of c-Fos immunoreactive neuronal nuclei, in representative sections of the inferior colliculus in non-stimulated control groups and control groups after sound stimulation. In stimulated control animals, the sound stimulation protocol utilized (see text), induces a higher density of c-Fos labeling, than in non-stimulated controls **(A,B)**, in particular in the dorsal two-thirds of the nucleus including the dorsal cortex (DCIC). **(C)** c-Fos labeling density diminishes after stimulation at 1 day post-lesion. As shown in the interval histograms in **(D,E)**, gray intensity values of individual c-Fos immunoreactive nuclei shift toward more intense (higher numerical) values between non-stimulated and stimulated controls. After 1 day post-lesion, values are lower than in stimulated controls and the histogram curve **(F)** is more flat than in stimulated control group.

nuclear responses to intracellular signaling cascades (Soloaga et al., 2003). In the auditory pathway c-Fos is highly expressed after acoustic stimulation (Friauf 1992, 1995; Zhang et al., 1996). Also, c-Fos expression patterns have been used to study central auditory activity after lesions to the auditory receptor or ascending auditory pathways followed by electrical stimulation (Saito et al., 1999; Nagase et al., 2000, 2003; Nakamura et al., 2003, 2005; Reisch et al., 2007). Here we have used c-Fos expression to test how the lack of descending activity after disruption of pathways originating in the AC to the IC affects sound-induced activation of neurons in this nucleus.

One day after the cortical lesion, the largest drops in c-Fos Ir neuronal nuclei relative to control-stimulated animals are seen in the IC ipsilateral to the lesion and in the contralateral DCIC. These regions correspond to those more affected by preterminal degeneration after ablation of the AC, as described by Feliciano and Potashner (1995). Therefore, loss of excitatory endings in the IC originating in the AC may lead to diminished activity in IC neurons. In this regard, Sun et al. (2007) showed that blocking inhibition in the AC with bicuculline, increased c-Fos immunoreactivity in the IC, mainly in its cortical regions, although this increase it was concentrated in the side ipsilateral to the injection. Our results indicate that

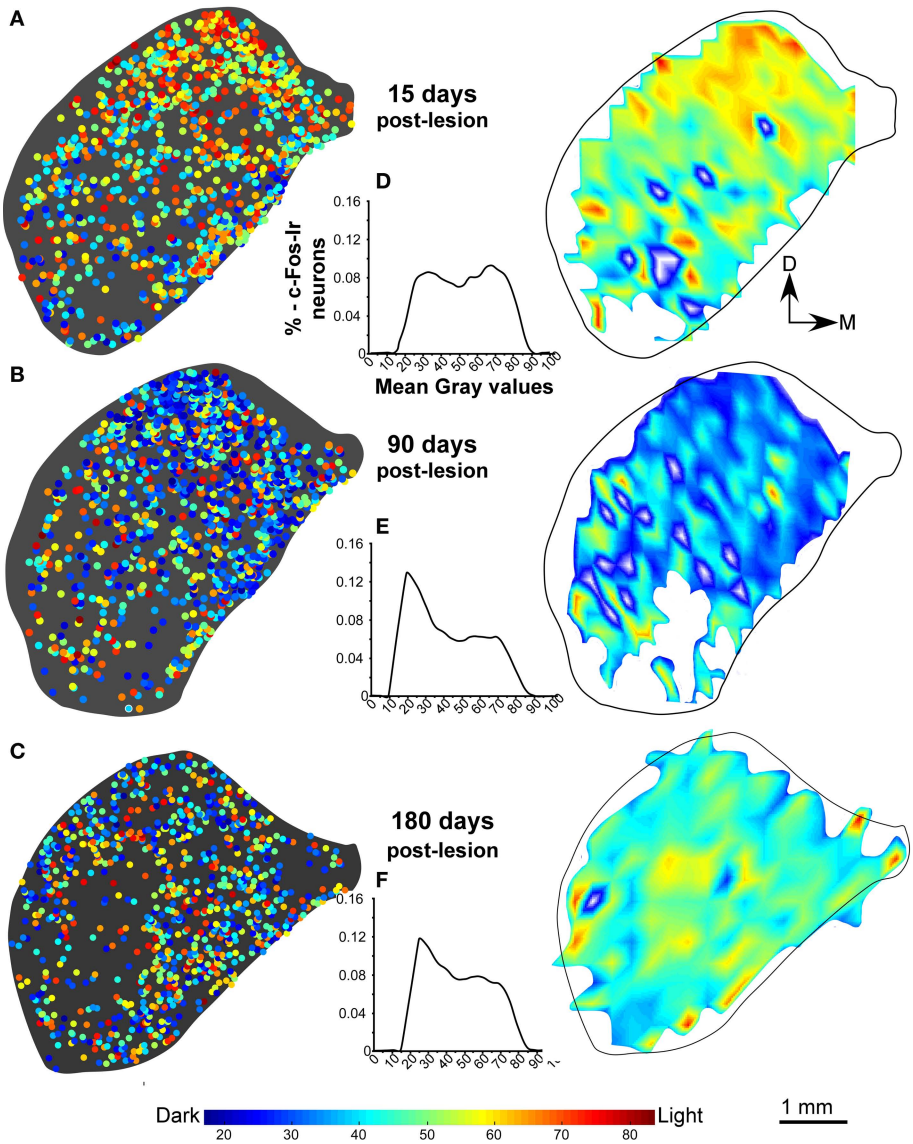

FIGURE 4 | Distribution density and gray value plots of c-Fos immunoreactive nuclei in representative sections of the inferior colliculus after sound stimulation. (A) After 15 days post-lesion, values continue to be lower than the in the stimulated control group **(B,C)** c-Fos labeling densities are comparable to those in controls after sound stimulation 90 days **(B)** and 180 days **(C)** post-lesion. The interval histograms in **(D)** shows two slight peaks in values more close to 88, whereas the histograms in **(E,F)**, show that gray intensity values of individual c-Fos immunoreactive nuclei at 90 and 180 days after the cortical lesion are comparable to controls, suggesting recovery of neuronal activity.

diminished neuronal activity of IC neurons after deafferentation of descending projection is evidenced by a decreased sound-induced c-Fos expression, being more intense in those IC subdivisions that receiving more dense descending (AC) projections.

To the best of our knowledge, this is the first time that labeling intensity measured as average gray levels and nuclear perimeter are used as metrics to quantify c-Fos immunoreactivity levels after induced activation. Average gray levels may be an indicator of the amount of chromogen deposited in immunoreactive nuclei, which in turn is a function of the amount of antigen detected, when reaction times are carefully controlled. On the other hand, *c-fos* transcriptional control involves histone phosphorylation and acetylation which may vary chromatin condensation state, likely leading to changes in nuclear mass, translated into perimeter variations of immunoreactive nuclei (Clayton et al., 2000; Brami-Cherrier et al., 2009). One day after AC lesion, overall c-Fos immunostaining intensity decreases, as shown by a significant shift in average gray levels toward higher, or "less dark" values. In addition, the perimeter of c-Fos Ir nuclei also decreases. These two quantitative changes, along with diminished of total number of c-Fos Ir nuclei, strengthens the notion that lesions to the cortico-collicular pathway reduce, in the short range, not only the number of nuclei, but also protein production rates in neurons of the IC.

Fifteen days after cortical lesion, there is a further significant decrease of c-Fos immunoreactivity in both ICs after sound stimulation (**Figures 4A and 6A**). These findings support diminished

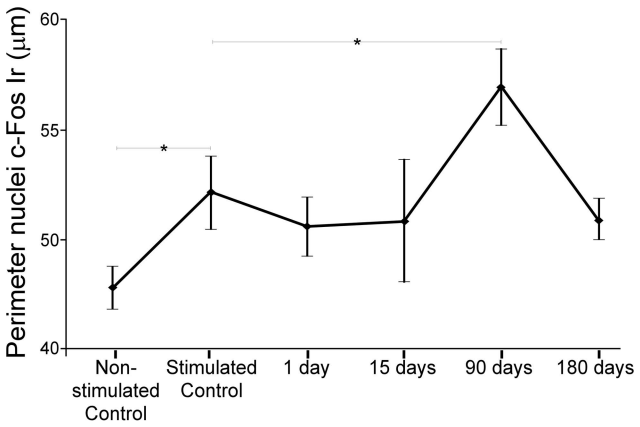

FIGURE 5 | Charts showing average perimeter of c-Fos immunoreactive neuronal nuclei. Perimeter increases significantly (*mean ± 2SD) between non-stimulated and stimulated controls, also after 90 days post-lesion (see text for details).

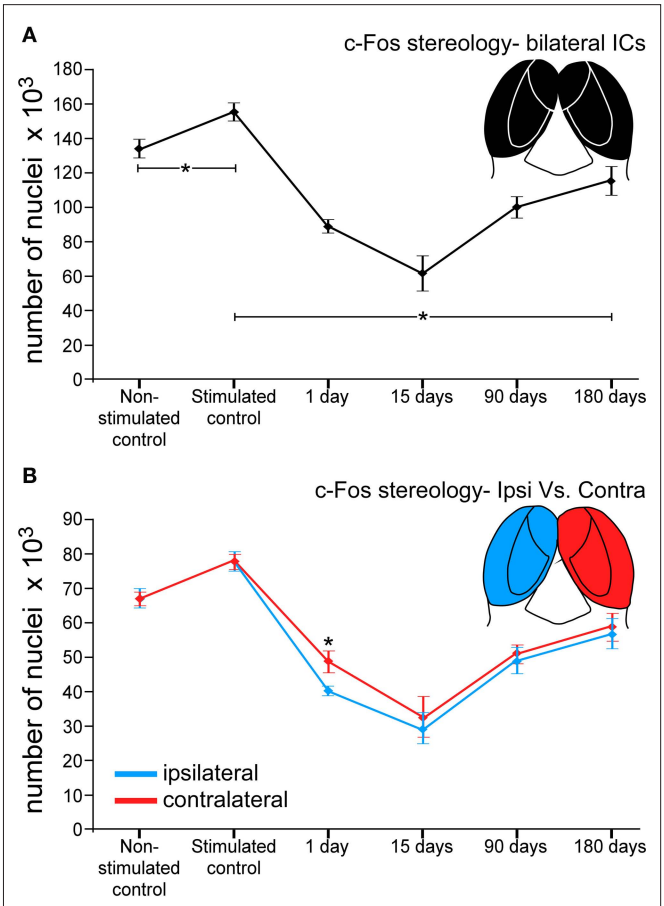

FIGURE 6 | Graphs showing number of c-Fos immunoreactive neuronal nuclei in the IC after sound stimulation at different times after lesions of the auditory cortex. (A) The number of c-Fos immunoreactive neuronal nuclei significantly drops at 1 day (42%) and 15 days (55%) after the cortical lesion. Ninety and 180 days post-lesion, the number of immunoreactive neurons following sound stimulation recovers, but still remains below control values (33% at 90 days and 23% at 180 days). *Asterisks denote the significant differences between the control groups and the stimulated control and each lesioned group, and means the average value ± 2SD (error bars). **(B)** The number of c-Fos immunoreactive neurons differs between the sides ipsi- and contralateral to the cortical lesion. At 1 day after the lesion, the number of c-Fos immunoreactive neurons is significantly lower in the ipsilateral side. At 15, 90, and 180 days the number of immunoreactive neurons is comparable, although slightly lower in the ipsilateral side.

c-Fos production in IC neurons 15 days after ablation, which may bear correlation with a significant drop in acoustic activity found previously by us with ABRs (Clarkson et al., 2010a). We have shown that 15 days after AC lesions, ABR amplitudes are diminished; particularly wave V (Clarkson et al., 2010a), which hypothetically originates in the IC (Biacabe et al., 2001). The correlation between strongly diminished c-Fos production and IC activity 15 days post-lesion is also supported by the finding that the acoustic startle reflex/prepulse inhibition was also attenuated after an identical post-lesion period (Clarkson et al., 2010a). Feliciano and Potashner (1995) found that 7 days after unilateral lesions to the AC, GABA inhibition might be altered in the IC as a consequence of a drop in GABA release. Therefore, both excitation and inhibition are likely to become affected in the IC by lesions to the descending projection, leading to, at least, a partial activity block (Clarkson et al., 2010a) which is seen at this time post-lesion in continuing c-Fos down-regulation.

In the experimental group analyzed 90 days after cortical ablation, the number of c-Fos immunoreactive neuronal nuclei in the IC tends to increase relative to shorter post-lesion times (1 and 15 days), but it is still lower than in sound-stimulated controls. Interestingly, however, average gray values in nuclei approached those of control animals. We previously reported that 90 days after AC ablation, ABRs recover in amplitude and thresholds, relative to those recorded in animals 15 days post-lesion (Clarkson et al., 2010a). These findings support a trend toward a long-range recovery of neuronal activity patterns. Also, at 90 days post-lesion, the average nuclei perimeter of c-Fos immunoreactive collicular neurons was even larger than in stimulated controls and more so in the side contralateral to the lesion. If changes in nuclear perimeter do reflect changes in synthesis activity (see above), such an increase may be interpreted as a rebound c-Fos activity above normal values, being higher in the contralateral region less affected by the loss of the corticofugal projection. Recovery suggested by the increase in c-Fos activity in the IC 90 days after lesioning the corticofugal projection may reflect structural and functional plasticity mechanism (see Butz et al., 2009). Such mechanisms are still unknown in the IC, including the possibility of collateral sprouting from the intact cerebral cortex or other sources.

After 180 days of the lesion to the AC, c-Fos immunoreactivity after sound stimulation, approached control values, as seen by gray levels and number of c-Fos Ir neuronal nuclei. This supports recovery of normal production of c-Fos and correlates with functional recovery, as measured by auditory startle response/prepulse inhibition after 180 days post-lesion (Clarkson et al., 2010a). Also previous studies from our lab show that under identical experimental conditions, calretinin immunoreactive neurons increase in number in the IC up to 180 days after the lesion to the AC, further returning to control values 240 days after the lesion (Clarkson et al.,

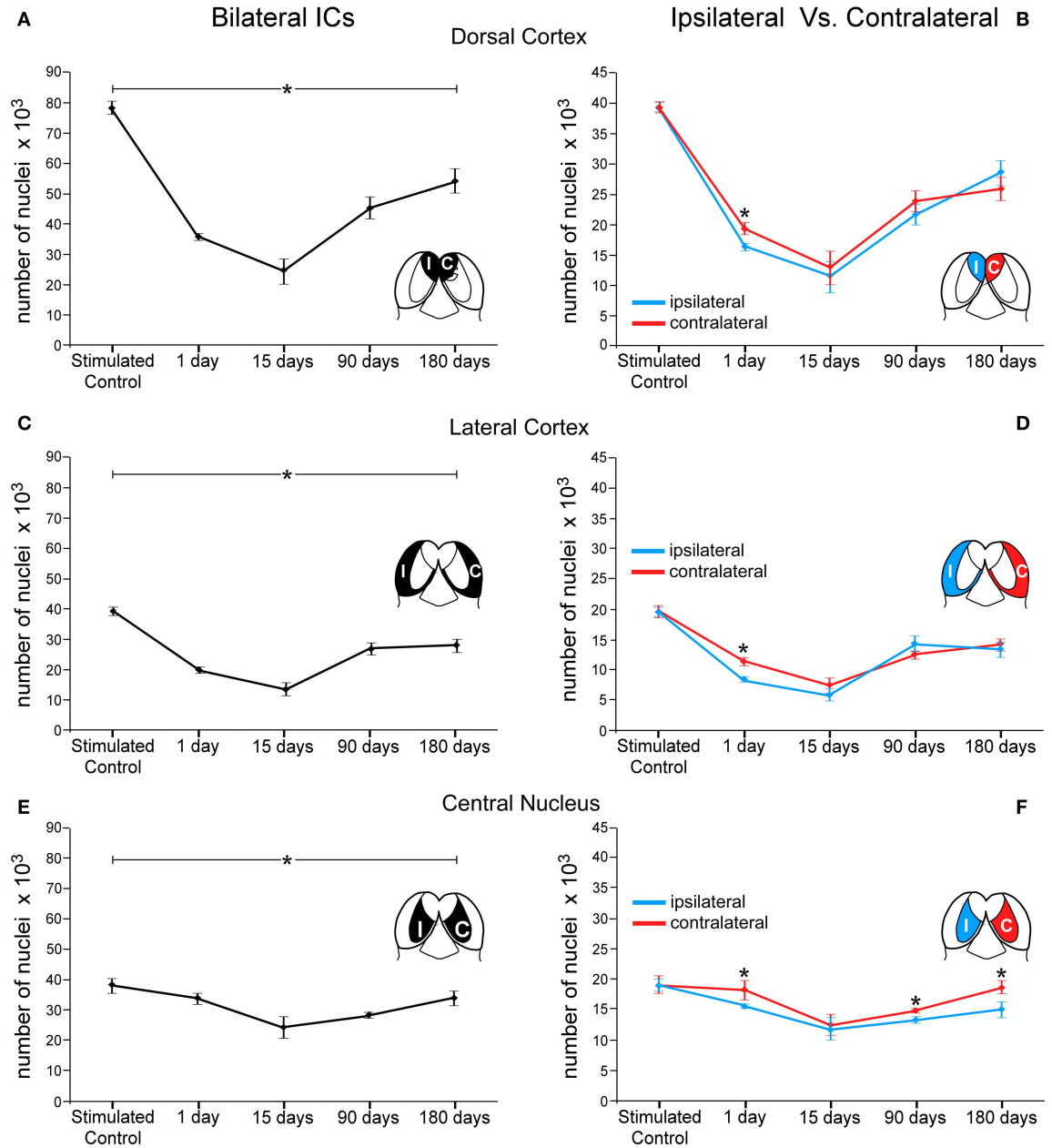

FIGURE 7 | Graphs showing number of c-Fos immunoreactive neuronal nuclei by cytoarchitectural subdivisions of the IC after sound stimulation at different times after lesions of the auditory cortex. The asterisks denote changes (average ± 2SD, with a $p < 0.005$) in numbers of immunoreactive nuclei at different times after the cortical lesion. These changes are larger in the dorsal cortex **(A)** and lateral cortex **(C)** and less so in the central nucleus **(E)** although following similar temporal patterns (compare with **Figure 6**). In **(B,D,F)** the asterisks show significant differences in c-Fos immunoreactive nuclei between the sides ipsi- and contralateral to the lesion. In animals stimulated 1 day after the cortical lesion, the number of c-Fos immunoreactive nuclei is significantly lower in the ipsilateral side in the three IC subdivisions (*DC: 15%, EC: 27%, and CN: 14%). In the central nucleus **(F)**, the contralateral side shows significantly higher numbers of immunoreactive nuclei after 90 and 180 days of the cortical lesion (*10% and 20%, respectively).

2010b). It is known that *c-fos* accumulation in nuclei depends on intracellular Ca^{2+} and second messenger increases as a consequence of changes in neuronal activity (Morgan and Curran, 1988; Sheng and Greenberg, 1990). Turrigiano (1999) suggested that balanced intracellular Ca^{2+} concentrations are needed to reach a "set point level" in neurons, needed to keep excitability and firing within adequate ranges. Changes in the concentration of this ion may lead to a global imbalance of inward and outward currents, thus altering excitability. In this regard, our data indicate that c-Fos recovery and return to control values coincides with the highest level of calretinin up-regulation (Clarkson et al., 2010b) 180 days after lesioning the AC. This temporal correlation may be explained by stabilization of Ca^{2+} entry produced after recovery of the homeostatic balance of activity in the IC.

All these findings indicate that, in adult animals, after ablation of the corticofugal projection to the IC, neurons in this midbrain auditory nucleus and the functional circuits in which they assemble have the capacity of progressively recovering, on the long range, the loss of activity subsequent to AC ablation. Although more experiments will be needed to determine which structures and mechanisms are involved in "compensating" this loss of activity, our results suggest that long-range repair or adaptation in the IC is successful, as there seems to be functional recovery.

ACKNOWLEDGMENTS

The authors would like to thank Ignacio Plaza for excellent technical assistance and Dr. Marco Izquierdo and Dr. Manuel Malmierca for assistance with sound stimulation, and Dr. Enrique López-Poveda for developing the morphometry, densitometry and numerical analysis methods employed in the study. This work was supported by grants from the Ministry of Science and Innovation of the Government of Spain, #BFU2009-13754-C02 and #BFU2006-13974, and by Proyecto de Excelencia JCyL #GR221 to Miguel A. Merchán).

REFERENCES

Biacabe, B., Chevallier, J. M., Avan, P., and Bonfils, P. (2001). Functional anatomy of auditory brainstem nuclei: application to the anatomical basis of brainstem auditory evoked potentials. *Auris Nasus Larynx* 28, 85–94.

Brami-Cherrier, K., Roze, E., Girault, J. A., Betuing, S., and Caboche, J. (2009). Role of the ERK/MSK1 signalling pathway in chromatin remodelling and brain responses to drugs of abuse. *J. Neurochem.* 108, 1323–1335.

Bullitt, E. (1990). Expression of c-fos-like protein as a marker for neuronal activity following noxious stimulation in the rat. *J. Comp. Neurol.* 296, 517–530.

Butz, M., van Ooyen, A., and Worgotter, F. (2009). A model for cortical rewiring following deafferentation and focal stroke. *Front. Comput. Neurosci.* 3:10. doi: 10.3389/neuro.10.010.2009.

Ceccatelli, S., Villar, M. J., Goldstein, M., and Hokfelt, T. (1989). Expression of c-Fos immunoreactivity in transmitter-characterized neurons after stress. *Proc. Natl. Acad. Sci. U.S.A.* 86, 9569–9573.

Clarkson, C., Lòpez, D. E., and Merchán, M. A. (2010a). Long-term functional recovery in the rat auditory system after unilateral auditory cortex ablation. *Acta Otolaryngol.* 130, 326–332.

Clarkson, C., Juìz, J. M., and Merchán, M. A. (2010b). Long-term regulation in calretinin staining in the rat inferior colliculus after unilateral auditory cortical ablation. *J. Comp. Neurol.* 518, 4261–4276.

Clayton, A. L., Rose, S., Barratt, M. J., and Mahadevan, L. C. (2000). Phosphoacetylation of histone H3 on c-fos- and c-jun-associated nucleosomes upon gene activation. *EMBO J.* 19, 3714–3726.

Feliciano, M., and Potashner, S. J. (1995). Evidence for a glutamatergic pathway from the guinea pig auditory cortex to the inferior colliculus. *J. Neurochem.* 65, 1348–1357.

Friauf, E. (1992). Tonotopic order in the adult and developing auditory system of the rat as shown by c-fos immunocytochemistry. *Eur. J. Neurosci.* 4, 798–812.

Friauf E. (1995). C-fos immunocytochemical evidence for acoustic pathway mapping in rats. *Behav. Brain Res.* 66, 217–224.

Greenberg, M. E., and Ziff, E. B. (1984). Stimulation of 3T3 cells induces transcription of the c-fos proto-oncogene. *Nature* 311, 433–438.

Gundersen, H. J., Jensen, E. B., Kieu, K., and Nielsen, J. (1999). The efficiency of systematic sampling in stereology – reconsidered. *J. Microsc.* 193(Pt 3), 199–211.

Helfert, R. H., Snead, C. R., and Altschuler, R. A. (1991). "The ascending auditory pathways," in *Neurobiology of Hearing: The Central Auditory System*, eds R. A. Altschuler, R. P. Bobbin, B. M. Clopton, and D. W. Hoffman (New York: Raven Press), 1–25.

Herrera, D. G., and Robertson, H. A. (1996). Activation of c-fos in the brain. *Prog. Neurobiol.* 50, 83–107.

Morgan, J. I., and Curran, T. (1988). Calcium as a modulator of the immediate-early gene cascade in neurons. *Cell Calcium* 9, 303–311.

Nagase, S., Miller, J. M., Dupont. J., Lim, H. H., Sato, K., and Altschuler, R. A. (2000). Changes in cochlear electrical stimulation induced Fos expression in the rat inferior colliculus following deafness. *Hear. Res.* 147, 242–250.

Nagase, S., Mukaida, M., Miller, J. M., and Altschuler, R. A. (2003). Neonatal deafening causes changes in Fos protein induced by cochlear electrical stimulation. *J. Neurocytol.* 32, 353–361.

Nakamura, M., Rosahl, S. K., Alkahlout, E., Gharabaghi, A., Walter, G. F., and Samii, M. (2003). C-Fos immunoreactivity mapping of the auditory system after electrical stimulation of the cochlear nerve in rats. *Hear. Res.* 184, 75–81.

Nakamura, M., Rosahl, S. K., Alkahlout, E., Walter, G. F., and Samii, M. M. (2005). Electrical stimulation of the cochlear nerve in rats: analysis of c-Fos expression in auditory brainstem nuclei. *Brain Res.* 1031, 39–55.

Nwabueze-Ogbo, F. C., Popelar, J., and Syka, J. (2002). Changes in the acoustically evoked activity in the inferior colliculus of the rat after functional ablation of the auditory cortex. *Physiol. Res.* 51(Suppl. 1), S95–S104.

Paxinos, G., and Watson, C. (2005). *The Rat Brain in Stereotaxic Coordinates*, 5th Edn. Burlington: Elsevier Academic Press.

Popelar, J., Nwabueze-Ogbo, F. C., and Syka, J. (2003). Changes in neuronal activity of the inferior colliculus in rat after temporal inactivation of the auditory cortex. *Physiol. Res.* 52, 615–628.

Reisch, A., Illing, R. B., and Laszig, R. (2007). Immediate early gene expression invoked by electrical intracochlear stimulation in some but not all types of neurons in the rat auditory brainstem. *Exp. Neurol.* 208, 193–206.

Saito, H., Miller, J. M., Pfingst, B. E., and Altschuler, R. A. (1999). Fos-like immunoreactivity in the auditory brainstem evoked by bipolar intracochlear electrical stimulation: effects of current level and pulse duration. *Neuroscience* 91, 139–161.

Saldaña, E., Feliciano, M., and Mugnaini, E. (1996). Distribution of descending projections from primary auditory neocortex to inferior colliculus mimics the topography of intracollicular projections. *J. Comp. Neurol.* 371, 15–40.

Sheng, M., and Greenberg, M. E. (1990). The regulation and function of c-fos and other immediate early genes in the nervous system. *Neuron* 4, 477–485.

Soloaga, A., Thomson, S., Wiggin, G. R., Rampersaud, N., Dyson, M. H., Hazzalin, C. A., Mahadevan, L. C., and Arthur, J. S. (2003). MSK2 and MSK1 mediate the mitogen- and stress-induced phosphorylation of histone H3 and HMG-14. *EMBO J.* 22, 2788–2797.

Sun, X., Guo, Y. P., Shum, D. K., Chan, Y. S., and He, J. (2009). Time course of cortically induced fos expression in auditory thalamus and midbrain after bilateral cochlear ablation. *Neuroscience* 160, 186–197.

Sun, X., Xia, Q., Lai, C. H., Shum, D. K., Chan, Y. S., and He, J. (2007). Corticofugal modulation of acoustically induced Fos expression in the rat auditory pathway. *J. Comp. Neurol.* 501, 509–525.

Turrigiano, G. G. (1999). Homeostatic plasticity in neuronal networks: the more things change, the more they stay the same. *Trends Neurosci.* 22, 221–227.

Wenthold, R. J. (1991). "Neurotransmitters of brainstem auditory nuclei," in *Neurobiology of Hearing: The Central Auditory System*, eds R. A. Altschuler, R. P. Bobbin, B. M. Clopton, D. W. Hoffmann (New York: Raven Press), 121–139.

Wenthold, R. J., Hunter, C., and Petralia, R. S. (1993). "Excitatory amino acid in the rat cochlear nucleus," in *The Mammalian Cochlear Nuclei: Organization and Function*, eds M. A. Merchan, J. M. Juiz, D. A. Godfrey, and E. Mugnaini (New York: Plenum Press), 179–194.

West, M. J., Slomianka, L., and Gundersen, H. J. (1991). Unbiased stereological estimation of the total number of neurons in the subdivisions of the rat hippocampus using the optical fractionator. *Anat. Rec.* 231, 482–497.

Yoshida, N., Hequembourg, S. J., Atencio, C. A., Rosowski, J. J., and Liberman, M. C. (2000). Acoustic injury in mice: 129/SvEv is exceptionally resistant to noise-induced hearing loss. *Hear. Res.* 141, 97–106.

Zhang, J. S., Haenggeli, C. A., Tempini, A., Vischer, M. W., Moret, V., and Rouiller, E. M. (1996). Electrically induced fos-like immunoreactivity in the auditory pathway of the rat: effects of survival time, duration, and intensity of stimulation. *Brain Res. Bull.* 39, 75–82.

Conflict of Interest Statement: The authors declare that the research was conducted in the absence of any commercial or financial relationships that could be construed as a potential conflict of interest.

Received: 03 March 2010; paper pending published: 04 March 2010; accepted: 27 September 2010; published online: 20 October 2010.

Citation: Clarkson C, Juíz JM and Merchán MA (2010) Transient down-regulation of sound-induced c-Fos protein expression in the inferior colliculus after ablation of the auditory cortex. Front. Neuroanat. 4:141. doi: 10.3389/fnana.2010.00141

frontiers in
NEUROANATOMY

ORIGINAL RESEARCH ARTICLE
published: 19 October 2010
doi: 10.3389/fnana.2010.00137

Cholinergic and non-cholinergic projections from the pedunculopontine and laterodorsal tegmental nuclei to the medial geniculate body in guinea pigs

Susan D. Motts[1,2] and Brett R. Schofield[1,2]*

[1] *Department of Anatomy and Neurobiology, Northeastern Ohio Universities Colleges of Medicine and Pharmacy, Rootstown, OH, USA*
[2] *School of Biomedical Sciences, Kent State University, Kent, OH, USA*

Edited by:
Enrique Saldaña, Universidad de Salamanca, Spain

Reviewed by:
Dolores E. López García, Universidad de Salamanca, Spain
Marisela Morales, National Institutes of Health, USA

***Correspondence:**
Brett R. Schofield, Department of Anatomy and Neurobiology, Northeastern Ohio Universities Colleges of Medicine and Pharmacy, PO Box 95, Rootstown, OH 44272, USA.
e-mail: bschofie@neoucom.edu

The midbrain tegmentum is the source of cholinergic innervation of the thalamus and has been associated with arousal and control of the sleep/wake cycle. In general, the innervation arises bilaterally from the pedunculopontine tegmental nucleus (PPT) and the laterodorsal tegmental nucleus (LDT). While this pattern has been observed for many thalamic nuclei, a projection from the LDT to the medial geniculate body (MG) has been questioned in some species. We combined retrograde tracing with immunohistochemistry for choline acetyltransferase (ChAT) to identify cholinergic projections from the brainstem to the MG in guinea pigs. Double-labeled cells (retrograde and immunoreactive for ChAT) were found in both the PPT (74%) and the LDT (26%). In both nuclei, double-labeled cells were more numerous on the ipsilateral side. About half of the retrogradely labeled cells were immunonegative, suggesting they are non-cholinergic. The distribution of these immunonegative cells was similar to that of the immunopositive ones: more were in the PPT than the LDT and more were on the ipsilateral than the contralateral side. The results indicate that both the PPT and the LDT project to the MG, and suggest that both cholinergic and non-cholinergic cells contribute substantially to these projections.

Keywords: acetylcholine, arousal, auditory, GABA, glutamate, thalamus, sleep

INTRODUCTION

The medial geniculate body (MG) is part of the auditory thalamus and serves as the primary source of ascending input to the auditory cortex. The MG, like other thalamic nuclei, is under the influence of projections from the brainstem cholinergic nuclei (Mesulam et al., 1983; Steriade et al., 1988; Oakman et al., 1999). These projections arise from the pedunculopontine tegmental nucleus (PPT) and the laterodorsal tegmental nucleus (LDT), collectively referred to as the pontomesencephalic tegmentum (PMT). The cholinergic projections form part of the ascending arousal system and, as such, control the firing mode of thalamic cells through both nicotinic and muscarinic effects (Tebecis, 1972; McCormick and Prince, 1987; Steriade et al., 1988; Jones, 2005). These effects control the flow of information to the cortex and underlie changes in thalamic responsiveness during the sleep-wake cycle and at varying levels of arousal during wakefulness (Edeline, 2003; Steriade, 2004; Hennevin et al., 2007).

There have been numerous studies of cholinergic innervation of the thalamus and a general pattern of projections has emerged (Shute and Lewis, 1967; Hallanger et al., 1987; Steriade et al., 1988). The PPT contributes more cells than the LDT to the thalamic projections. Both nuclei project bilaterally with an ipsilateral dominance (Steriade et al., 1988). It has been reported that up to 85% of the PMT projection to thalamic relay nuclei is cholinergic (Steriade et al., 1988). None of the studies have focused exclusively on the MG, but Steriade et al. (1988) reported that the projection to the MG in cats follows the general pattern described above. In contrast, results from both retrograde and anterograde tracing experiments have reported that there is no projection to the MG from the LDT in rats (Satoh and Fibiger, 1986; Hallanger et al., 1987; Cornwall et al., 1990). The extent to which projections from the LDT and the PPT have distinct functions is unclear; nonetheless, the similarities in their projection patterns to most thalamic nuclei suggest that the contributions are similar across the many systems represented by those thalamic nuclei. The possible lack of a projection from the LDT to the MG suggests that the auditory thalamus may be exceptional in receiving a unique pattern of cholinergic inputs from the brainstem.

Another question concerns the types of cells in the PMT that project to the thalamus. The PPT and the LDT are known as cholinergic nuclei, but contain a variety of cell types, including distinct populations of cholinergic, glutamatergic, and GABAergic neurons (Boucetta and Jones, 2009; Wang and Morales, 2009). Recently there has been increasing interest in the contribution of non-cholinergic cells to the functions ascribed to the PMT. For example, Boucetta and Jones (2009) have recorded the physiological activity of cholinergic, glutamatergic, and GABAergic cells in the PMT and have suggested that all three cell types act in concert to control behavioral states across the sleep-wake cycle. Previous studies have acknowledged a non-cholinergic PMT projection to the thalamus (Steriade et al., 1988), but the relative number of cholinergic and non-cholinergic cells contributing to the projection is unknown for the MG and for most thalamic targets.

We used a combination of retrograde tracers and immunohistochemistry to examine the projection from the PMT to the MG. We describe the relative contributions of the PPT and the LDT to the projection, the proportions of ipsilateral and contralateral projections, and the proportions of cholinergic and non-cholinergic components.

MATERIALS AND METHODS

During all experiments, efforts were made to minimize suffering and the number of animals used. All procedures were performed in accordance with the Institutional Animal Care and Use Committee and the National Institutes of Health guidelines on the ethical use of animals. Twelve pigmented guinea pigs (Elm Hill; Chelmsford, MA, USA) of either gender weighing 250–500 g were used.

SURGERY

Sterile instruments and aseptic technique were used for all surgical procedures. Each animal was anesthetized with isoflurane (4% for induction, 1.5–2.5% for maintenance) in oxygen. The animal's head was shaved and cleansed with Betadine (Purdue Products L.P., Stamford, CT, Rochester, NY, USA). Ophthalmic ointment (Moisture Eyes PM, Bausch & Lomb, Rochester, NY, USA) was applied to each eye. Atropine sulfate (0.05 mg/kg, i.m.) was administered to decrease respiratory secretions during surgery, and Ketofen (ketoprofen 3 mg/kg, i.m.; Henry Schein, Melville, NY, USA) was given for post-operative pain control. The animal was positioned with its head in a stereotaxic frame. A feedback-controlled heating pad was used for maintaining the animal's body temperature.

An incision was made in the scalp and the wound edges were injected with Marcaine (0.25% bupivacaine with epinephrine 1:200,000; Hospira, Inc., Lake Forest, IL, USA). A dental drill was used to make a small hole in the skull. Details about the tracers used and the injection parameters for each case are provided in **Table 1**. After the tracer injection, the opening in the skull was covered with Gelfoam (Harvard Apparatus, Holliston, MA, USA). The scalp was sutured. Anesthesia was then discontinued and the animal was removed from the stereotaxic frame and placed in a clean cage. The animal was monitored in its cage until it was ambulatory and able to eat and drink.

PERFUSION AND SECTIONING

After surgery, the animal remained in the animal care facility for 4–25 days to allow for transport of the tracers. The animal was given an overdose of either sodium pentobarbital (440 mg/kg, i.p.) or isoflurane (5% in oxygen, inhaled). After cessation of breathing and loss of the withdrawal reflex, the animal was perfused through the vascular system with Tyrode's solution, then 250 ml of 4% paraformaldehyde in 0.1 M phosphate buffer, pH 7.4, followed by 250 ml of the same fixative with 10% sucrose added. The brain was removed and placed in fixative with 25 or 30% sucrose and stored at 4°C. The following day the cerebellum was removed. In some cases the cortex was also removed. The brainstem or brainstem and cortex were frozen and cut in the transverse or sagittal plane on a sliding microtome into 40–50 μm thick sections. The sections were collected serially into six sets.

HISTOLOGY

For most cases, in one tissue set (containing every sixth section), the tissue sections containing the MG were reacted with cytochrome oxidase (CO) for the identification of MG subdivisions (Anderson et al., 2007). In some cases, one set was stained with thionin for identification of cytoarchitectural borders and landmarks. The remaining sets of tissue were used for immunohistochemistry.

Choline aceyltransferase (ChAT) immunohistochemistry was used to identify putative cholinergic cells as previously reported (Motts et al., 2008) except that primary antibody concentrations were increased two- to eight-fold for fluorescence imaging. Briefly, sections were incubated (1 day at 4°C) with goat anti-ChAT antibody (Chemicon AB 144P, [Millipore, Billerica, MA, USA]) diluted 1:25–1:100. The sections were then treated with 1% biotinylated rabbit anti-goat antibody (BA-5000, Vector Laboratories, Burlingame,

Table 1 | Summary of experimental parameters.

Case	Side	Tracer	Inj. type	Volume	Survival time (days)	Plane of section	No. of sections quantified	Weight (g)	Section thickness (μm)
GP471	L	FG	ms	0.05 μl	13	s	–	310	40
GP473	L	FG	ms	0.03 μl	11	s	–	415	40
GP480	R	FG	ms	0.05 μl	10	t	–	468	40
GP481	R	GB	ms	0.4 μl	6	t	–	317	50
GP482	L	FG	ms	0.05 μl	6	t	8	300	50
GP484	R	GB	ms	0.2 μl	9	t	5	393	50
GP579	L	FG	mp	13.8 nl	4	t	8	316	50
GP585	L	GB	mp	69 nl	25	t	9	439	40
	R	RB	mp	69 nl	25	t	9		
GP586	R	RB	mp	69 nl	25	t	6	419	40
GP587	L	GB	mp	69 nl	5	t	6	258	40
GP595	L	GB	mp	69 nl	7	t	8	401	50
	R	RB	mp	69 nl	7	t	8		
GP604	L	FG	ms	0.05 μl	11	t	10	367	50

Red beads (RB; Luma-Fluor, Inc., Naples, FL, USA), green beads (GB; Luma-Fluor, Inc.), and FluoroGold (FG; FluoroChrome, Inc., Englewood, CO, USA) were used as retrograde fluorescent tracers. Injection type was either by a 1-μl Hamilton microsyringe (ms) or by a Nanoliter Injector (World Precision Instruments), with a glass micropipette (mp) with an inside tip diameter of 25–35 μm. For the FG mp injection (GP579), one pulse was used to inject the tracer, and the micropipette was left in place for 5 min before it was withdrawn. For the remaining mp injections, 5 pulses of 13.8 nl were given, with a 1–5 min pause after each pulse. Each microsyringe was used only for a single tracer. In some animals, a different tracer was placed into left and right MG to obtain two experiments from each animal. Plane of section was either sagittal (s) or transverse (t). Number of sections quantified indicates the number of sections in the series that were quantified (and contained PMT).

CA, USA) and labeled with streptavidin conjugated to a fluorescent marker (AlexaFluor 488 [green] or AlexaFluor 647 [near-infrared]; Invitrogen, Carlsbad, CA, USA) that could be distinguished from the tracers used in the case. The sections were mounted on gelatin-coated slides, air dried, and coverslipped with DPX (Sigma).

DATA ANALYSIS

A Neurolucida reconstruction system (version 8; MBF Bioscience, Williston, VT, USA) attached to a Zeiss Axioplan II microscope (Carl Zeiss, Inc., Thornwood, NY, USA) was used to plot labeled cells, nuclear borders, and injection sites. Plots were exported to Adobe Illustrator CS2 (Adobe Systems, Inc., San Jose, CA, USA) for final figure construction.

The brainstem cholinergic nuclei (PPT and LDT) in guinea pigs have been described in detail previously (Leonard et al., 1995; Motts et al., 2008). Some of the borders of the PPT and the LDT are indistinct in a thionin stain, so the distribution of ChAT-immunopositive cells was used to define the extent of the nuclei.

A Zeiss AxioImager Z1 fluorescence microscope with AxioCam HRm (monochrome) and HRc (color) cameras (Zeiss) was used to take photomicrographs. Monochrome images, including all images of AlexaFluor 647, which fluoresces at near infrared wavelengths, were pseudocolored either with the camera software (AxioVision 4.6, Zeiss) or with Photoshop CS2. Adobe Photoshop CS2 was used to add scale bars and labels, scale, and crop images, erase background around tissue sections, and adjust intensity levels in photomicrographs.

Three criteria were used to select cases for quantitative summary. First, sections had to be free from tissue damage that would prevent assessment of injection sites and areas of retrogradely labeled cells. Second, the ChAT immunostain had to be bright and even across sections. Third, there had to be at least 50 retrogradely labeled PMT cells in a bin (every sixth section). Of the 12 animals used for this study, results from 8 animals met the criteria to be included in the quantitative summary. All of the cases used for quantitative analysis and illustration were cut in the transverse plane. **Table 1** shows the experimental parameters for each case.

RESULTS

We combined retrograde tracing and immunohistochemistry to identify the cholinergic and non-cholinergic PMT inputs to the MG. The patterns of labeled cells were similar qualitatively for the different tracers and different survival times used in this study. Our experiments included both large injections that involved several MG subdivisions, and smaller injections, which were largely confined to one or two subdivisions (**Figure 1**).

A large injection labeled many cells in the PMT and in numerous areas associated with the brainstem auditory pathways. The latter areas included the cochlear nucleus, superior olivary complex, ventral nucleus of the lateral lemniscus and adjacent paralemniscal area, nucleus sagulum, and a region dorsal to the dorsal nucleus of the lateral lemniscus (where a collection of cholinergic cells stretches from the PPT to the laterally placed nucleus sagulum). Among all these regions, only the nuclei of the PMT contained retrogradely labeled cells that were also immunopositive for ChAT (**Figure 2**). The remainder of this paper focuses on the retrogradely labeled cells within the PMT.

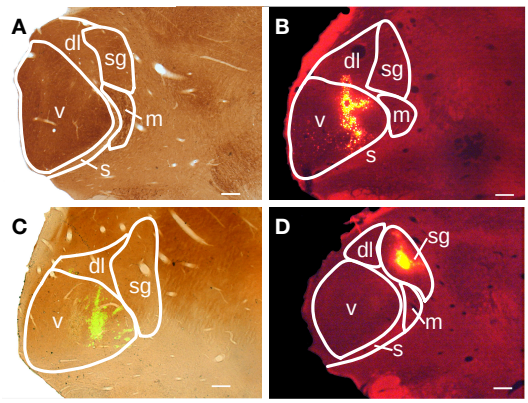

FIGURE 1 | Photomicrographs of medial geniculate body (MG) subdivisions and representative tracer injection sites in transverse sections. (A) Section stained with cytochrome oxidase (CO) showing the subdivisions of MG: dl, dorsolateral; m, medial; s, shell; sg, suprageniculate; v, ventral. **(B)** Injection of red beads that is centered in the ventral MG (v) and extends into the dorsolateral subdivision (dl). This photomicrograph is of the right MG, but was flipped to make comparisons between the cases easier. GP 595R. **(C)** Injection of green beads confined to the ventral subdivision. The image is an overlay of a fluorescence image to visualize the GB and a brightfield image to show the CO counterstain. GP 587L. **(D)** An injection of red beads within the suprageniculate subdivision (sg). This photomicrograph is of the right MG, but was flipped to make comparisons between the cases easier. GP 586R. Scale bars = 0.5 mm for **A**–**D**.

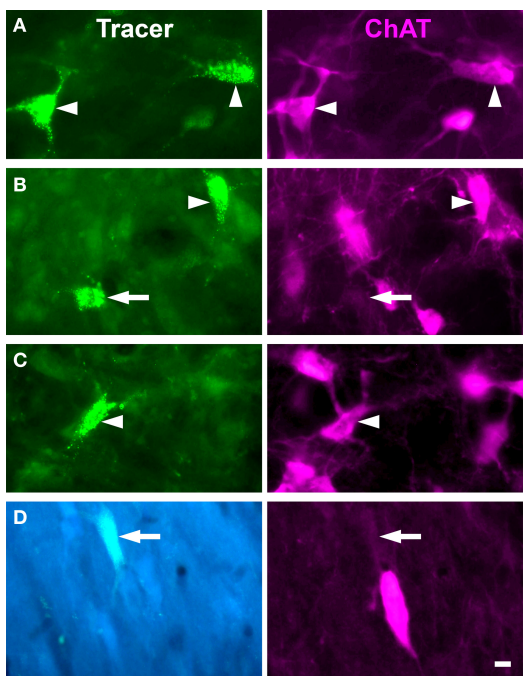

FIGURE 2 | Photomicrographs of labeled cells in the PMT after injections in MG. In each panel the left image shows cells labeled with retrograde tracer [green beads for **A**–**C** (GP 585L), FluoroGold for D (GP 484L)]. The right image shows the same field of view filtered for ChAT immunolabel. Arrowheads indicate cells labeled with both tracer and immunolabel; arrows indicate cells labeled with tracer only. **(A,B)** PPT cells projecting to the ipsilateral MG. **(C)** PPT cell projecting to the contralateral MG. **(D)** LDT cell projecting to contralateral MG. All photomicrographs are taken from transverse sections. Scale bar = 10 μm.

The distribution of labeled cells in the PMT after a large FG injection is illustrated in **Figure 3A**. This case (GP 604L) had a large injection in the left MG that almost completely filled the dorsolateral subdivision and included significant portions of the medial, suprageniculate, and ventral subdivisions. A small part of the shell region was included in the injection as well. The injection spread dorsally and rostrally beyond MG to include the dorsal lateral geniculate and lateral posterior nuclei. We found retrogradely labeled cells in the PPT and the LDT on both sides. More labeled cells were present on the ipsilateral side and, on each side, more were present in the PPT than the LDT. In each of the nuclei, some of the retrogradely labeled cells were ChAT immunopositive; overall, these constituted 53% of the retrogradely labeled cells in PMT (**Table 2**). In each nucleus, immunonegative cells were located near immunopositive cells, suggesting that the immunostain was effective in the area and that the tracer-labeled, immunonegative cells were non-cholinergic (**Figure 2**). Together, these data indicate that both cholinergic and non-cholinergic PMT cells contribute to the projection to the MG.

Interpretation of the results just described is complicated by spread of the injection into areas surrounding the MG, which also receive inputs from the PMT nuclei (Steriade et al., 1988). We now describe results from smaller injections; two of these were confined entirely to the MG and the remainder had only slight spread outside the MG (**Table 2**). **Figure 3B** shows an injection in the MGv and resulting label in PMT. **Figure 3C** shows an injection in the suprageniculate subdivision of the MG and resulting label. In both cases, the results were qualitatively similar to large injections. Quantitative analysis revealed some additional points (**Table 2**; **Figure 4**). The LDT contained double-labeled cells in every case, although they were relatively few and not always present bilaterally. While the percentage of ChAT-immunopositive cells varied (11–65%), it was not possible to relate the variation to the location of the injection; e.g., the 3 highest percentages for ChAT+ cells were associated with injections in the MGv, but so was the lowest value. The reasons for the variation are not clear. Across the nine experiments with small injections, 44% of the retrogradely labeled cells in the PMT were ChAT immunopositive (compared to 53% after the large injection). In fact, the ipsilateral PPT was the only nucleus in which the retrogradely labeled ChAT-immunopositive cells outnumbered the retrogradely labeled ChAT-immunonegative cells on average. This suggests that non-cholinergic cells may be more prominent in the PMT projections to the MG than to other thalamic nuclei.

DISCUSSION

Our results show that both the PPT and the LDT are sources of cholinergic input to the MG in guinea pigs. In addition, a sizable non-cholinergic projection to the MG also arises in the PPT and the LDT. We first address the technical issues of our experiments. We then discuss our data in the context of previous studies and the functional significance of the projections.

TECHNICAL CONSIDERATIONS

We used an antibody against ChAT as a marker for cholinergic cells. ChAT is considered a specific marker for cholinergic cells (Levey and Wainer, 1982; Armstrong et al., 1983; German et al., 1985; Maley et al., 1988). The antibody has been validated previously in guinea pigs (Motts et al., 2008), and we used the same fixation and tissue processing parameters as in the previous study. We see clearly labeled cells in the expected areas, such as the cranial nerve motor nuclei. We conclude that the immunolabeled cells are cholinergic.

It is always possible that an immunohistochemical assay will fail to label every cell that contains the antigen. However, we obtained immunopositive and immunonegative retrogradely labeled cells within the same focal plane (**Figure 2**), suggesting that the immunolabeling reagents penetrated the tissue and that the immunonegative cells are likely to be non-cholinergic. In addition to cholinergic cells, the PPT and the LDT contain GABAergic and glutamatergic cells (Vincent et al., 1986; Lavoie and Parent, 1994; Ford et al., 1995; Leonard et al., 1995; Jia et al., 2003; Wang and Morales, 2009). It is likely that cells of either or both of these types were among our immunonegative cells. Future studies are necessary to identify the non-cholinergic cell types and determine their contributions to the PMT projections. This information will help in understanding the effects of the PMT projection to the MG across the sleep-wake cycle.

Two final issues relate to the injections. First, some injections spread beyond the MG. Other thalamic nuclei are innervated by the PMT, and we would expect that some of the cells labeled in these cases terminate outside the MG. However, small injections confined to the MG produce a distribution of retrogradely labeled cells that was similar to that after the larger injections. We conclude that the quantitative differences between our cases with small injections versus the large injection reflect specifics of the PMT projection to the MG. More meaningful comparison will require future experiments with small injections confined to other thalamic nuclei.

A related issue concerns the possibility of labeling axons of passage whereby injections in the caudal thalamus, where the MG is located, could label PMT cells that project to more rostral thalamic (or extrathalamic) targets. We have used red beads and green beads in many of our experiments. These tracers are less likely than other tracers to be taken up by axons of passage (Katz and Iarovici, 1990). In addition, we have used micropipettes for some of our injections. Micropipettes cause less damage than syringes, thus decreasing the likelihood of tracer uptake by axons of passage. While we cannot rule out the possibility of labeling PMT cells that project outside the MG, we believe that such cells were in the minority and are unlikely to alter the main conclusions.

FUNCTIONAL IMPLICATIONS

Our results are generally consistent with previous studies that the MG is a target of brainstem cholinergic cells (Hallanger et al., 1987; Steriade et al., 1988). These results are very similar to those in cats (Steriade et al., 1988) but differ from those in rats, where both anterograde and retrograde experiments failed to label a projection from the LDT to the MG (Satoh and Fibiger, 1986; Hallanger et al., 1987; Cornwall et al., 1990). Our results demonstrate both cholinergic and non-cholinergic projections from the LDT to the MG in guinea pigs. The LDT projections are bilateral with an ipsilateral dominance, and involve fewer cells than the projections from the PPT. Additional experiments will be needed to determine whether the apparent differences in rats are due to the species or to differences in methods.

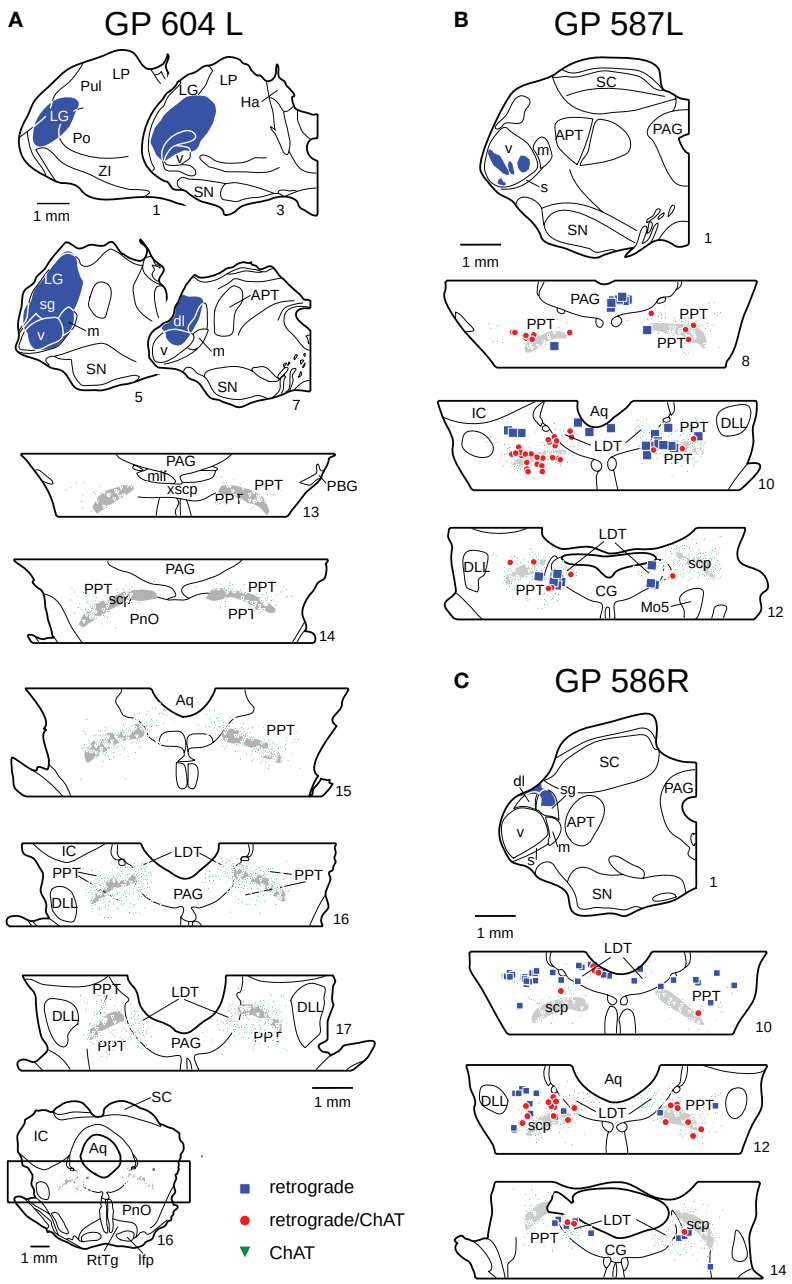

FIGURE 3 | Plots of labeled cells in the PMT after large (A) or small **(B,C)** injections in the thalamus. **(A)** Drawings of transverse sections showing a large FluoroGold injection (blue shading, sections 1–7 [left side of section only]) in the left thalamus and labeled cells in the PMT nuclei (sections 13–17). An entire midbrain section is shown (bottom of column) for orientation of brainstem sections. Only the portion of tegmentum that included the PPT and the LDT (indicated by box) are shown in the remaining sections. The legend indicates the type of label in all panels; each symbol represents at least one labeled cell. GP 604L. **(B)** Drawing through the center of a green bead injection site confined to the ventral subdivision of the MG. Labeled cells are shown in the PMT at 3 rostro-caudal levels. GP 587L. **(C)** Drawing through the center of a red bead injection in the MG suprageniculate subdivision, and resulting label in the PMT. The drawings were flipped to make comparisons between the cases easier. GP 586R. In all panels, the sections are numbered from rostral to caudal with each whole number representing a 300-μm spacing. The extent of the PPT and LDT nuclei are indicated by the distribution of the ChAT immunopositive cells (green triangles). The ChAT immunopositive cells within the periaqueductal gray (PAG) are in the LDT; the ChAT immunopositive cells outside the PAG are in the PPT. The superior cerebellar peduncle is shown in gray as it is a helpful landmark for the PPT. APT, anterior pretectal nucleus; Aq, aqueduct; CG, central gray; dl, dorsolateral subdivision of MG; DLL, dorsal nucleus of lateral lemniscus; Ha, habenula; IC, inferior colliculus; LDT, laterodorsal tegmental nucleus; lfp; longitudinal fasciculus of the pons; LG, lateral geniculate body; LP, lateral posterior nucleus; m, medial subdivision of MG; mlf, medial longitudinal fasciculus; Mo5, motor nucleus of 5th nerve; PAG, periaqueductal gray; PBG, parabigeminal nucleus; PnO, pontine reticular nucleus, oral part; Po, posterior nucleus of the thalamus; PPT, pedunculopontine tegmental nucleus; Pul, pulvinar nucleus; RtTg, reticulotegmental nucleus of the pons; s, shell subdivision of MG; SC, superior colliculus; scp, superior cerebellar peduncle; sg, suprageniculate subdivision of MG; SN, substantia nigra; v, ventral subdivision of MG; xscp, decussation of scp; Zl, zona incerta.

Table 2 | Description of the injection sites and resultant PMT label in cases used for quantitative analysis.

Case		Injection site						# Retro cells	% ChAT immunopositive					% ChAT immunonegative				
	Tracer	MGv	MGm	MGsg	MGdl	MGs	Other		iPPT	iLDT	cPPT	cLDT	All PMT	iPPT	iLDT	cPPT	cLDT	All PMT
GP604L	FG	X	X	X	X	X	X	105	39	9	3	2	**53**	25	7	11	5	**48**
GP595R	RB	X			+			195	43	16	5	1	**65**	11	9	8	7	**35**
GP587L	GB	X						206	43	9	9	1	**62**	9	7	15	6	**37**
GP579L	FG	X					+	50	30	0	26	2	**58**	20	4	16	2	**42**
GP482L	FG	X				+	+	53	30	11	2	0	**43**	40	11	4	2	**57**
GP484R	GB	X	+				+	114	1	4	2	4	**11**	21	48	10	10	**89**
GP586R	RB			X			+	280	22	13	6	2	**43**	32	11	11	3	**57**
GP595L	GB	+			X		+	415	23	7	5	4	**39**	20	19	14	7	**60**
GP585R	RB	+			X		+	60	8	13	8	0	**29**	20	20	18	12	**70**
GP585L	GB				X		+	96	33	8	4	2	**47**	19	18	9	6	**53**
Mean									26	9	7	2	**44**	21	16	12	6	**56**

Results from a large injection are indicated in the top row; smaller injections and the mean from those smaller injections ("Mean"), are also indicated. Injection sites are characterized by indicating the MG subdivisions included in the injection: X indicates the subdivision with the most tracer, + indicates MG subdivisions that contain tracer. The "other" column indicates minor spread outside the MG. "# retro cells" is the number of retrogradely labeled cells in PMT (bilaterally, every 6th section). The "%ChAT immunopositive" and "%ChAT immunonegative" columns describe the indicated cells as a percentage of "# retro cells". FG, FluoroGold. GB, green beads. RB, red beads.

Another quantitative difference relates to the percentage of the PMT projection that is cholinergic. Previous reports have described the PMT projection to MG as up to 85% cholinergic in cats (Steriade et al., 1988), and PMT projections to the thalamus in general as 91% cholinergic (Sofroniew et al., 1985). However, our data in guinea pigs show only 44% of the projection is cholinergic (**Table 2**). It is possible that our immunostaining did not label every cholinergic cell. Another issue here is how one defines the borders of the PMT nuclei. Many of these borders, especially for the PPT, are difficult to identify. We use an operational definition based on the distribution of the presumptive cholinergic cells (Leonard et al., 1995). Small differences between species in the distribution of different cell types could lead to inclusion of more or fewer non-cholinergic cells within the PPT border. As mentioned above, there is growing evidence for important roles of the non-cholinergic projections from these areas (e.g., Boucetta and Jones, 2009). Future experiments designed to identify the neurotransmitters used by presumptive non-cholinergic cells will be necessary both to provide insight into functions and to clarify the relative contributions of different transmitters to the PMT projection.

It is likely that all MG subdivisions receive both cholinergic and non-cholinergic inputs from PMT. All subdivisions of the MG contain nicotinic and muscarinic receptors (Schwartz, 1986). However, there are reports that principle sensory nuclei can have a non-uniform distribution of ChAT immunopositive axons (e.g., Fitzpatrick et al., 1989). All of our injections, regardless of subdivisions involved, labeled cholinergic and non-cholinergic cells. We do not have sufficient numbers of cases with injections restricted to single subdivisions to make conclusions about the types of PMT cells (cholinergic or non-cholinergic) that contribute to the projection to each MG subdivision. Even with such data, this issue will benefit from examination of cholinergic axons in the MG.

The PMT projections to the thalamus have long been recognized as important for the generation of the REM component of sleep (Rye, 1997). While the cholinergic component has received the most attention, recently the non-cholinergic PPT and LDT contributions to the sleep-wake cycle have been considered (Boucetta and Jones, 2009). The authors suggested that the cholinergic, GABAergic, and glutamatergic cells act in concert to modulate sleep-wake cycles. These projections presumably control the flow of information through the thalamus in relation to the various stages of the sleep wake cycle as well as different levels of vigilance during waking. Our data show that cholinergic and non-cholinergic cells project to the MG, suggesting that multiple transmitters could modulate the MG during the sleep-wake cycle. This suggestion is consistent with physiological studies of MG activity during different phases of the sleep-wake cycle (Edeline, 2003; Hennevin et al., 2007).

It is possible that the PMT projections serve additional functions as well. Approximately half of the cells in both the PPT and LDT respond to sound (Reese et al., 1995a,b), suggesting a substantial auditory role for these nuclei. In addition to their projections to the MG, the PPT and LDT also project to the inferior colliculus (Motts and Schofield, 2009) and the cochlear nucleus (Motts and Schofield, 2005). The PPT and LDT are also the targets of descending projections from the auditory cortex (Schofield and Motts, 2009). The cortical projections appear to contact cholinergic PMT cells that project to the IC (Schofield, 2010), suggesting that the

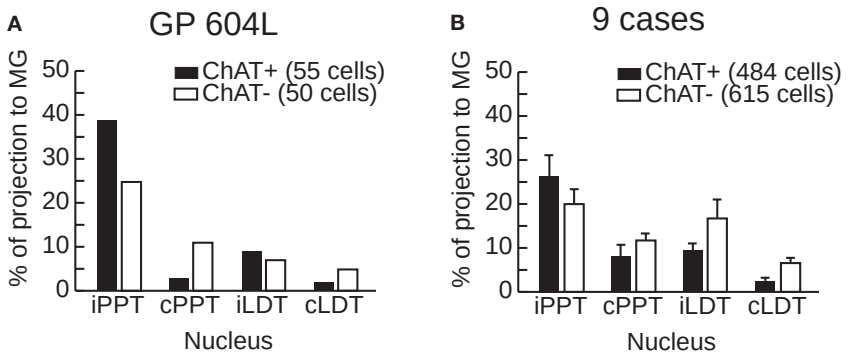

FIGURE 4 | Graphs to illustrate the contribution of ipsilateral and contralateral PPT and LDT to the overall projection to MG. Tracer-labeled cells were counted in every sixth section and tallied according to whether they were ChAT+ or ChAT–. The results are expressed as a percentage of the total number of tracer-labeled cells. **(A)** Results from a very large injection (GP604L). **(B)** Aggregate results from nine cases with small injections located almost entirely within the MG. Error bars indicate standard error of the mean. cLDT, contralateral laterodorsal tegmental nucleus; cPPT, contralateral pedunculopontine tegmental nucleus; iLDT, ipsilateral laterodorsal tegmental nucleus; iPPT, ipsilateral pedunculopontine tegmental nucleus.

cortex can modify the level of cholinergic input to some subcortical auditory centers. Such projections might allow the cortex to modulate activity in subcortical centers according to the salience of a recent acoustic stimulus. In this regard, it would be interesting to determine whether the cortical projections also contact PMT cells (cholinergic or otherwise) that project to the MG.

Pontomesencephalic tegmentum cells are also involved in prepulse inhibition of startle via cholinergic projections to the caudal pontine nuclei (Koch et al., 1993). Prepulse inhibition has been viewed as a form of gating that allows the auditory system to continue processing acoustic information without the interruption that would be induced by a startle response. It will be of particular interest to know if the same PMT cells project to the caudal pontine nuclei and to the MG or another auditory nucleus. Such projections may serve to enhance processing (increase gain?) in the auditory nuclei while suppressing the motor response to an otherwise startling stimulus.

ACKNOWLEDGMENTS

We gratefully acknowledge Colleen Sowick and Megan Storey-Workley for their expert technical assistance. We thank Dr. Jeffrey G. Mellott and Dr. Kyle Nakamoto for comments on an earlier draft. Supported by National Institutes of Health DC04391 and DC08463.

REFERENCES

Anderson, L. A, Wallace, M. N, and Palmer, A. R. (2007). Identification of subdivisions in the medial geniculate body of the guinea pig. *Hear. Res.* 228, 156–167.

Armstrong, D. M., Saper, C. B., Levey, A. I., Wainer, B. H., and Terry, R. D. (1983). Distribution of cholinergic neurons in rat brain: demonstrated by the immunocytochemical localization of choline acetyltransferase. *J. Comp. Neurol.* 216, 53–68.

Boucetta, S., and Jones, B. E. (2009). Activity profiles of cholinergic and intermingled GABAergic and putative glutamatergic neurons in the pontomesencephalic tegmentum of urethane-anesthetized rats. *J. Neurosci.* 29, 4664–4674.

Cornwall, J., Cooper, J. D., and Phillipson, O. T. (1990). Afferent and efferent connections of the laterodorsal tegmental nucleus in the rat. *Brain Res. Bull.* 25, 271–284.

Edeline, J. M. (2003). The thalamo-cortical auditory receptive fields: regulation by the states of vigilance, learning and the neuromodulatory systems. *Exp. Brain Res.* 153, 554–572.

Fitzpatrick, D., Diamond, I. T., and Raczkowski, D. (1989). Cholinergic and monoaminergic innervation of the cat's thalamus: comparison of the lateral geniculate nucleus with other principal sensory nuclei. *J. Comp. Neurol.* 288, 647–675.

Ford, B., Holmes, C. J., Mainville, L., and Jones, B. E. (1995). GABAergic neurons in the rat pontomesencephalic tegmentum: codistribution with cholinergic and other tegmental neurons projecting to the posterior lateral hypothalamus. *J. Comp. Neurol.* 363, 177–196.

German, D. C., Bruce, G., and Hersh, L. B. (1985). Immunohistochemical staining of cholinergic neurons in the human brain using a polyclonal antibody to human choline acetyltransferase. *Neurosci. Lett.* 61, 1–5.

Hallanger, A. E., Levey, A. I., Lee, H. J., Rye, D. B., and Wainer, B. H. (1987). The origins of cholinergic and other subcortical afferents to the thalamus in the rat. *J. Comp. Neurol.* 262, 105–124.

Hennevin, E., Huetz, C., and Edeline, J. M. (2007). Neural representations during sleep: from sensory processing to memory traces. *Neurobiol. Learn. Mem.* 87, 416–440.

Jia, H. G., Yamuy, J., Sampogna, S., Morales, F. R., and Chase, M. H. (2003). Colocalization of gamma-aminobutyric acid and acetylcholine in neurons in the laterodorsal and pedunculopontine tegmental nuclei in the cat: a light and electron microscopic study. *Brain Res.* 992, 205–219.

Jones, B. E. (2005). From waking to sleeping: neuronal and chemical substrates. *Trends Pharmacol. Sci.* 26, 578–586.

Katz, L. C., and Iarovici, D. M. (1990). Green fluorescent latex microspheres: a new retrograde tracer. *Neuroscience* 34, 511–520.

Koch, M., Kungel, M., and Herbert, H. (1993). Cholinergic neurons in the pedunculopontine tegmental nucleus are involved in the mediation of prepulse inhibition of the acoustic startle response in the rat. *Exp. Brain Res.* 97, 71–82.

Lavoie, B., and Parent, A. (1994). Pedunculopontine nucleus in the squirrel monkey: distribution of cholinergic and monoaminergic neurons in the mesopontine tegmentum with evidence for the presence of glutamate in cholinergic neurons. *J. Comp. Neurol.* 344, 190–209.

Leonard, C. S., Kerman, I., Blaha, G., Taveras, E., and Taylor, B. (1995). Interdigitation of nitric oxide synthase-, tyrosine hydroxylase-, and serotonin-containing neurons in and around the laterodorsal and pedunculopontine tegmental nuclei of the guinea pig. *J. Comp. Neurol.* 362, 411–432.

Levey, A. I., and Wainer, B. H. (1982). Cross-species and intraspecies reactivities of monoclonal antibodies against choline acetyltransferase. *Brain Res.* 234, 469–473.

Maley, B. E., Frick, M. L., Levey, A. I., Wainer, B. H., and Elde, R. P. (1988). Immunohistochemistry of choline acetyltransferase in the guinea pig brain. *Neurosci. Lett.* 84, 137–142.

McCormick, D. A., and Prince, D. A. (1987). Actions of acetylcholine in the guinea-pig and cat medial and lateral geniculate nuclei, in vitro. *J. Physiol.* 392, 147–165.

Mesulam, M. M., Mufson, E. J, Wainer, B. H., and Levey, A. I. (1983). Central

cholinergic pathways in the rat: an overview based on an alternative nomenclature (Ch1-Ch6). *Neuroscience* 10, 1185–1201.

Motts, S. D., and Schofield, B. R. (2005). Olivary and extra-olivary sources of cholinergic input to the cochlear nucleus. *Assoc. Res. Otolaryngol. Abs.* 27, 242.

Motts, S. D., and Schofield, B. R. (2009). Sources of cholinergic input to the inferior colliculus. *Neuroscience* 160, 103–114.

Motts, S. D., Slusarczyk, A. S., Sowick, C. S., and Schofield, B. R. (2008). Distribution of cholinergic cells in guinea pig brainstem. *Neuroscience* 154, 186–195.

Oakman, S. A., Faris, P. L., Cozzari, C., and Hartman, B. K. (1999). Characterization of the extent of pontomesencephalic cholinergic neurons' projections to the thalamus: comparison with projections to midbrain dopaminergic groups. *Neuroscience* 94, 529–547.

Reese, N. B., Garcia-Rill, E., and Skinner, R. D. (1995a). Auditory input to the pedunculopontine nucleus: I. Evoked potentials. *Brain Res. Bull.* 37, 257–264.

Reese, N. B., Garcia-Rill, E., and Skinner, R. D. (1995b). Auditory input to the pedunculopontine nucleus: II. Unit responses. *Brain Res. Bull.* 37, 265–273.

Rye, D. B. (1997). Contributions of the pedunculopontine region to normal and altered REM sleep. *Sleep* 20, 757–788.

Satoh, K., and Fibiger, H. C. (1986). Cholinergic neurons of the laterodorsal tegmental nucleus: efferent and afferent connections. *J. Comp. Neurol.* 253, 277–302.

Schofield, B. R. (2010). Projections from auditory cortex to midbrain cholinergic neurons that project to the inferior colliculus. *Neuroscience* 166, 231–240.

Schofield, B. R., and Motts, S. D. (2009). Projections from auditory cortex to cholinergic cells in the midbrain tegmentum of guinea pigs. *Brain Res. Bull.* 80, 163–170.

Schwartz, R. D. (1986). Autoradiographic distribution of high affinity muscarinic and nicotinic cholinergic receptors labeled with [3H]acetylcholine in rat brain. *Life Sci.* 38, 2111–2119.

Shute, C. C., and Lewis, P. R. (1967). The ascending cholinergic reticular system: neocortical, olfactory and subcortical projections. *Brain* 90, 497–520.

Sofroniew, M. V., Priestley, J. V., Consolazione, A., Eckenstein, F., and Cuello, A. C. (1985). Cholinergic projections from the midbrain and pons to the thalamus in the rat, identified by combined retrograde tracing and choline acetyltransferase immunohistochemistry. *Brain Res.* 329, 213–223.

Steriade, M. (2004). Acetylcholine systems and rhythmic activities during the waking-sleep cycle. *Prog. Brain Res.* 145, 179–196.

Steriade, M., Paré, D., Parent, A., and Smith, Y. (1988). Projections of cholinergic and non-cholinergic neurons of the brainstem core to relay and associational thalamic nuclei in the cat and macaque monkey. *Neuroscience* 25, 47–67.

Tebecis, A. K. (1972). Cholinergic and non-cholinergic transmission in the medial geniculate nucleus of the cat. *J. Physiol.* 226, 153–172.

Vincent, S. R., Satoh, K., and Fibiger, H. C. (1986). The localization of central cholinergic neurons. *Prog. Neuropsychopharmacol. Biol. Psychiatry* 10, 637–656.

Wang, H. L., and Morales, M. (2009). Pedunculopontine and laterodorsal tegmental nuclei contain distinct populations of cholinergic, glutamatergic and GABAergic neurons in the rat. *Eur. J. Neurosci.* 29, 340–358.

Conflict of Interest Statement: The authors declare that the research was conducted in the absence of any commercial or financial relationships that could be construed as a potential conflict of interest.

Received: 12 March 2010; accepted: 19 September 2010; published online: 19 October 2010.

*Citation: Motts SD and Schofield BR (2010) Cholinergic and non-cholinergic projections from the pedunculopontine and laterodorsal tegmental nuclei to the medial geniculate body in guinea pigs. Front. Neuroanat. **4**:137. doi: 10.3389/fnana.2010.00137*

frontiers in
NEUROANATOMY

ORIGINAL RESEARCH ARTICLE
published: 21 May 2010
doi: 10.3389/fnana.2010.00018

The non-lemniscal auditory cortex in ferrets: convergence of corticotectal inputs in the superior colliculus

Victoria M. Bajo*, Fernando R. Nodal, Jennifer K. Bizley and Andrew J. King

Department of Physiology, Anatomy and Genetics, University of Oxford, Oxford, UK

Edited by:
Miguel A. Merchán, Universidad de Salamanca, Spain

Reviewed by:
M. Alex Meredith, Virginia Commonwealth University, USA
Craig K. Henkel, Wake Forest University School of Medicine, USA

****Correspondence:***
Victoria M. Bajo, Department of Physiology, Anatomy and Genetics, University of Oxford, Sherrington Building, Parks Road, Oxford OX1 3PT, UK.
e-mail: victoria.bajo@dpag.ox.ac.uk

Descending cortical inputs to the superior colliculus (SC) contribute to the unisensory response properties of the neurons found there and are critical for multisensory integration. However, little is known about the relative contribution of different auditory cortical areas to this projection or the distribution of their terminals in the SC. We characterized this projection in the ferret by injecting tracers in the SC and auditory cortex. Large pyramidal neurons were labeled in layer V of different parts of the ectosylvian gyrus after tracer injections in the SC. Those cells were most numerous in the anterior ectosylvian gyrus (AEG), and particularly in the anterior ventral field, which receives both auditory and visual inputs. Labeling was also found in the posterior ectosylvian gyrus (PEG), predominantly in the tonotopically organized posterior suprasylvian field. Profuse anterograde labeling was present in the SC following tracer injections at the site of acoustically responsive neurons in the AEG or PEG, with terminal fields being both more prominent and clustered for inputs originating from the AEG. Terminals from both cortical areas were located throughout the intermediate and deep layers, but were most concentrated in the posterior half of the SC, where peripheral stimulus locations are represented. No inputs were identified from primary auditory cortical areas, although some labeling was found in the surrounding sulci. Our findings suggest that higher level auditory cortical areas, including those involved in multisensory processing, may modulate SC function via their projections into its deeper layers.

Keywords: sound localization, multisensory integration, orientation behavior, auditory cortical fields, neural tracers, corticofugal input

INTRODUCTION

The superior colliculus (SC) is a multisensory integration center located in the midbrain (reviewed in Stein, 1998; King, 2004), which is responsible for directing behavioral responses toward specific points in space (Sprague and Meikle, 1965). The SC is the only structure in the mammalian brain where a two-dimensional auditory spatial map has been described (Palmer and King, 1982; Middlebrooks and Knudsen, 1984; King and Hutchings, 1987). This auditory spatial representation, found in the deeper layers, is topographically aligned with the visual and somatosensory maps that are also present in the SC. Ascending auditory input to the SC comes from the inferior colliculus (IC), particularly the external cortex and the nucleus of the brachium (King et al., 1998; Nodal et al., 2005), where coarse topographic representations of sound azimuth have been described (Binns et al., 1992; Schnupp and King, 1997).

It is well established that the cortex can modulate signal processing in the SC via descending corticofugal connections (e.g. Diamond et al., 1969; Wallace et al., 1993). Early work in the cat suggested that cortical influences have a much greater influence on the visual responses of SC neurons than on their responses to other sensory modalities (Stein, 1978). However, subsequent studies showed that cortical deactivation can greatly reduce the responses of SC neurons to both somatosensory (Clemo and Stein, 1986) and auditory stimulation (Meredith and Clemo, 1989) too. The cortical areas in the cat that have been the focus of these studies are the anterior ectosylvian sulcus (AES) and the rostral aspect of the lateral suprasylvian sulcus (rLS), which both contain a mixture of visual, somatosensory, and auditory neurons. Deactivation of either of these cortical areas also compromises multisensory interactions at both single SC neuron (Jiang et al., 2001; Alvarado et al., 2007) and behavioral (Jiang et al., 2002) levels, even when responses to modality-specific stimuli are only slightly altered. These findings therefore suggest that the major role of descending cortical inputs to the SC is to enable different modality stimuli to be combined and integrated in a behaviorally-relevant fashion.

Abbreviations: I, II, III, IV, V, VI, cortical layers I–VI; A, anterior; A1, primary auditory cortex; AAF, anterior auditory field; ADF, anterior dorsal field; AEG, anterior ectosylvian gyrus; AES, anterior ectosylvian sulcus; AEV, anterior ectosylvian visual region; ALLS, anterolateral lateral suprasylvian area; AMLS, anteromedial lateral suprasylvian area; AVF, anterior ventral field; BDA, dextran biotin fixable; cns, coronal sulcus; CO, cytochrome oxidase; D, dorsal; DZ, dorsal auditory zone (equivalent to SF); EG, ectosylvian gyrus; FAES, anterior ectosylvian sulcal field (auditory); FR, Fluororuby (dextran tetramethylrhodamine lysine fixable); IC, inferior colliculus; L, lateral; LGN, lateral geniculate nucleus; M, medial; MEG, middle ectosylvian gyrus; MGB. medial geniculate body; P, posterior; PAF, posterior auditory field; PAG, periaqueductal gray; PEG, posterior ectosylvian gyrus; PMLS, posteromedial lateral suprasylvian area; PPF, posterior pseudosylvian field; PSF, posterior suprasylvian field; pss, pseudosylvian sulcus; rLS, rostral aspect of the lateral suprasylvian sulcus; S, section; SC, superior colliculus; SAI, stratum album intermediale; SAP, stratum album profundum; SF, suprasylvian fringe (equivalent to DZ); SGI, stratum griseum intermediale; SGP, stratum griseum profundum; SGS, stratum griseum superficiale; SO, stratum opticum; SSG, suprasylvian gyrus; sss, suprasylvian sulcus; SZ, stratum zonale; VP, ventro-posterior area.

Damage or deactivation of the SC in the cat impairs both modality-specific (Lomber et al., 2001) and multisensory (Burnett et al., 2004) orientation behavior. Similar deficits in auditory spatial orienting in this species have been described after cooling several different cortical fields, including not only AES, but also the primary auditory cortex (A1), dorsal zone (DZ), and posterior auditory field (PAF) (Malhotra and Lomber, 2007; Lomber and Malhotra, 2008). This raises the possibility that auditory cortical areas other than AES might contribute to the orientation responses mediated by the SC. However, Meredith and Clemo (1989) showed that the auditory subregion of AES (referred to as FAES) provides the only robust projection to the SC and that activation of this cortical area can drive auditory SC neurons, whereas this is not the case for other parts of auditory cortex. Although there is also anatomical evidence in cats for sparser inputs to the SC from several other parts of non-primary auditory cortex (Meredith and Clemo, 1989; Winer et al., 1998), including the secondary auditory cortex (A2) and areas of multisensory affiliation, it is unknown what role these descending projections have in SC function. The sources and terminal distribution of descending auditory cortical inputs to the SC in other species have not so far been investigated, so it is presently unclear whether an area equivalent to AES dominates corticotectal influences in the same way as it does in the cat.

In this study, we used a combination of retrograde and anterograde tracing techniques to investigate auditory corticotectal projections in the ferret, a species that is becoming increasingly popular for investigations of sensory processing and, in particular, the neural basis of hearing. Ferrets are naturally curious, intelligent animals that are well suited for behavioral and physiological studies (e.g., Fritz et al., 2003; Kacelnik et al., 2006; Allman et al., 2009; Bajo et al., 2010). However, very limited information is available on the organization of the auditory cortex (Kelly et al., 1986; Kowalski et al., 1995; Wallace et al., 1997), and only recently have auditory cortical fields outside the primary areas have been described (Nelken et al., 2004; Bizley et al., 2005). Therefore, a description of the corticotectal projection in the ferret will contribute to our understanding of the organization and functions of the different auditory cortical fields in this species. Additionally, this will facilitate comparison with existing data from the cat, an animal model in which the different auditory cortical fields and their connections are well established.

MATERIALS AND METHODS

Sixteen adult ferrets (*Mustela putorius furo*) of both sexes were used in this study. The experiments were approved by a local Ethical Review Committee at the University of Oxford, and performed under license from the UK Home Office in accordance with the Animal (Scientific Procedures) Act 1986.

Four animals received neuronal tracer injections in the SC and twelve animals at different locations within the auditory cortex. A summary of neuronal tracers and injection locations in each animal is provided in **Table 1**. To minimize the number of animals used, many of the cases with injections in the cortex were also used for studying other descending corticofugal connections (Bajo et al., 2007) and the connectivity between the auditory and visual cortices (Bizley et al., 2007).

Table 1 | Tracer injections in each animal used in this study.

Animal	Location	BF (kHz)	Tracer	Size (mm³) center (Halo)	Cutting plane (Cortex/SC)
***F0033**	SC	–	FR	0.06 (0.75)	F/C
F0034	SC	–	FR	0.04 (0.62)	F/C
F9921	SC	–	FR	0.52 (3.68)	C
F9806	SC	–	BDA	0.13 (1.52)	C
F0252	A1	15	FR	0.07 (1.02)	F/C
		1	BDA	0.18 (1.39)	
F0268	A1	7	FR	0.04 (1.2)	F/C
	AAF	7	BDA	0.05 (0.22)	
F0404	A1	7	FR	0.04 (0.2)	F/C
	AAF	7	BDA	0.037 (0.69)	
F0522	A1 (MEG)	–	FR	0.46 (22.02)	C
F0532	A1	20	FR	0.22 (3.09)	C
	AAF	20	BDA	0.04	
***F0505**	AVF	–	BDA	1.31 (7.13)	F/C
***F0523**	**AVF/ADF**	–	FR	0.71 (1.68)	C
	ADF		BDA	0.03 (0.39)	
***F0535**	ADF	10	BDA	0.01	C
	***AVF**	Noise	FR	0.14 (7.2)	
***F0504**	PPF/PSF	–	BDA	0.54 (6.09)	F/C
F0533	VP	Broad low	BDA	0.01 (0.13)	C
***F0536**	**PSF**	2	BDA	0.05 (0.39)	C
	A1	19	FR	0.12 (0.84)	
***F0717**	PSF	–	BDA	0.36 (1.2)	C

Cases in bold are those illustrated in the figures and the asterisks label the cases used for 3D reconstruction and stereological quantification of corticotectal axon terminals.

The tracers used were dextran amine conjugated with biotin (dextran biotin fixable, BDA, 10,000 MW; Molecular Probes Inc, Eugene, OR, USA) or rhodamine (dextran tetramethylrhodamine lysine fixable, 3,000 and 10,000 MW Fluororuby, FR; Molecular Probes). Both tracer solutions (diluted 10% in 0.9% saline) were injected by iontophoresis (5 μA of positive current in 7 s pulses for 15 min) through a glass micropipette with a 15–30 μm tip diameter.

SURGICAL PROTOCOL

All animals were examined otoscopically to ensure that both ears were clean and disease-free. After sedation with Domitor (0.1 mg/kg body weight i.m. medetomidine hydrochloride; Pfizer Ltd, Kent, UK), anesthesia was induced with Saffan (2 ml/kg body weight i.m. alfaxalone/alfadolone acetate; Schering-Plough Animal Health, Welwyn Garden City, UK) and maintained with an intravenous infusion of a mixture of Domitor (0.022 mg/kg/h) and Ketaset (5 mg/kg/h ketamine hydrochloride; Fort Dodge Animal Health, Southampton, UK) in saline solution. Dexadreson (0.5 mg/kg/h dexamethasone; Intervet UK Ltd, Milton Keynes, UK) and Atrocare (0.006 mg/kg/h atropine sulfate; Animalcare Ltd, York, UK) were added to the infusate to avoid cerebral edema and minimize pulmonary secretions, respectively. In each case, the animals received perioperative analgesia with Vetergesic (0.15 ml i.m. buprenorphine

hydrochloride; Alstoe Animal Health, Melton Mowbray, UK) and Metacam (0.05 ml oral meloxicam; Boehringer Ingelheim, Rhein, Germany). The animals were intubated and artificially ventilated with oxygen. End-tidal CO_2, the electrocardiogram and body temperature were monitored throughout the duration of the surgery. Temperature was maintained at 38°C using a rectal probe coupled to a heating blanket and by covering the animal with drapes during surgery.

Once these measures were stable, the animal was placed in a stereotaxic frame. A midline incision was then made in the scalp, the left temporal muscle retracted to expose the skull and the surgical wound infused with Marcain (bupivacaine hydrochloride, Astra Pharmaceuticals Ltd, Kings Langley, UK). In the cases of injections in the SC, the left occipital cortex was exposed by a craniotomy. The dura mater was removed, and the most posterior corner of the occipital cortex was carefully aspirated until the SC was visible. For injections in the auditory cortex, a craniotomy was made over the left ectosylvian gyrus, exposing the suprasylvian, and pseudosylvian sulci to provide landmarks. The animal was then transferred to a small table inside an anechoic chamber (IAC Ltd, Winchester, UK). We recorded multi-unit activity with a glass pipette in response to contralateral ear stimulation before placing tracer injections. Acoustic stimuli were generated using TDT system 3 hardware (Tucker-Davis Technologies, Alachua, FL, USA) and were presented via a closed-field electrostatic speaker (EC1, Tucker-Davis Technologies) with a flat frequency output (±5dB) to ≤30 kHz. Closed-field calibrations of the sound-delivery system were performed using a 1/8th-inch condenser microphone (Brüel and Kjær, Naerum, Denmark) placed at the end of a model ferret ear canal. Frequency-response areas of cortical neurons were constructed from the responses to pure-tone stimuli presented pseudorandomly at frequencies from 500 Hz to 30 kHz, in one-third octave steps. Tones were 100 ms in duration (5 ms cosine ramped) and intensity levels were varied between 10 and 80 dB SPL in 10 dB increments. Broadband noise bursts (40 Hz–30 kHz bandwidth and cosine ramped with a 10-ms rise/fall time, 100 ms duration from 30 to 80 dB SPL) were also used as a search stimulus.

All the animals with SC injections ($n = 4$) and some of those with cortical injections ($n = 5$) received a single injection of either BDA or FR. In addition, a further seven cases received injections of both tracers at different locations in the auditory cortex (**Table 1**). In each case, after the injection was complete, the dura mater was replaced and small pieces of Surgicel were used to cover the exposed brain before the piece of cranium was put back in its previous position and the temporal muscles and the skin were sutured independently.

HISTOLOGICAL PROCEDURES

The animals were perfused transcardially 2–5 weeks after the initial surgery under terminal anesthesia with Euthatal (2 ml of 200 mg/ml of pentobarbital sodium; Merial Animal Health Ltd, Harlow, UK). The blood vessels were flushed with 300 ml of 0.9% saline followed by 1 l of fresh 4% paraformaldehyde in 0.1 M phosphate buffer (PB), pH 7.4. Each brain was dissected from the skull, maintained in the same fixative for several hours, and immersed in a 30% sucrose solution in 0.1 M PB for 3 days.

In five cases with injections in the auditory cortex and two cases with injections in the SC, both hemispheres were dissected and gently flattened between two glass slides. In those cases, the cortex was later sectioned in a flat tangential plane and the rest of the brain cut in the coronal plane. The other brains were sectioned in the standard coronal plane (**Table 1**); 50 μm sections were cut on a freezing microtome and six sets of serial sections were collected, with one section in every three (1/150 μm) being used to analyze the tracer labeling.

Fluororuby was visualized immunocytochemically (primary anti-tetramethylrhodamine, rabbit IgG, dilution 1:6000; Molecular Probes; followed by secondary biotinylated anti-rabbit IgG H + L, made in goat, dilution 1:200; Vector Laboratories), whereas BDA was incubated in ABC (avidin biotin peroxidase, Vectastain Elite ABC Kit; Vector Laboratories, Burlingame, CA, USA) only. After washing the sections several times in 10 mM phosphate buffer saline (PBS) with 0.1% Triton X_{100} (PBS-Tx), they were incubated under gentle agitation overnight at +5°C in the primary antibody. The sections were again rinsed several times in PBS-Tx and then incubated in the biotinylated secondary antibody for 2 h. After further rinsing, the sections were incubated for 90 min in avidin biotin peroxidase (Vectastain Elite ABC kit; Vector Laboratories). Rinsing in PBS was followed by incubation in the chromogen solution with 3,3′-Diaminobenzidine (DAB; Sigma-Aldrich Company Ltd, Dorset, UK). Sections were incubated in 0.4 mM DAB and 9.14 mM H_2O_2 in 0.1 M PB until the reaction product could be seen. When BDA and FR were present in the same tissue, the BDA was first visualized using ABC followed by DAB enhanced with 2.53 mM Nickel ammonium sulfate. Immunocytochemistry to reveal FR was then performed, as described above but without nickel enhancement of the DAB. Reactions were stopped by rinsing the sections several times in 0.1 M PB. Sections were mounted on gelatinized glass slides, air dried, dehydrated, and coverslipped.

To identify the different subdivisions of SC and auditory cortex (Bajo et al., 2007), one set of serial sections (1 every 300 μm) was counterstained with 0.2% cresyl violet, another set was selected to visualize cytochrome oxidase (CO) activity, and a third set was used to stain the non-phosphorylated form of neurofilament H protein SMI_{32}. Other sections from our archive stained with AChEase and Gallyas were also used for cytoarchitectonic purposes. CO staining was obtained after 12 h incubation with 4% sucrose, 0.025% Cytochrome C (Sigma-Aldrich) and 0.05% DAB in 0.1 M PB at +37°C. Monoclonal mouse anti-SMI_{32} (Covance Research Products Inc., Emeryville, CA, USA) was used at a dilution of 1:4000. After immersion for 60 min in a blocking serum solution with 5% normal horse serum, the sections were incubated overnight at +5°C with the mouse antibody and 2% normal horse serum in 10 mM PBS. Anti-mouse biotinylated secondary antibody (mouse ABC kit, dilution 1:200 in PBS with 2% normal horse serum; Vector Laboratories) was used after brief washings in 10 mM PBS. Immunoreaction was followed by several more washings in PBS, incubation in ABC, and visualization using DAB with nickel–cobalt intensification (Adams, 1981; J. A. Winer, personal communication).

DATA ANALYSIS

Histological analysis was carried out and photomicrographs were taken with a Leica DMR microscope (Leica Microsystems, Heerbrugg, Switzerland) and a digital camera (Microfire™,

Olympus America Inc, Center Valley, PA, USA). Histological reconstructions and unbiased stereological estimates were performed using Neurolucida and StereoInvestigator software (version 8, MBF Bioscience, MicroBrightField Inc., Williston, VT, USA). Three dimensional reconstructions from the sections were performed using the 3D module in Neuroexplorer (MBF Neuroscience). One set of serial sections (1 every 300 μm) at the level of the SC or at the level of the auditory cortex was plotted in StereoInvestigator using a Cartesian coordinate system. The sections were aligned using blood vessels and outlines of adjacent sections. Statistical analysis was carried out using SPSS software (SPSS Inc., Chicago, IL, USA).

To estimate the relationship between the labeled terminals and the different layers of the SC, we reconstructed the position of the terminals and of the intermediate and deep gray layers in this nucleus using the center of the fourth ventricle at the most posterior section in which the SC is present as a reference point, i.e., the point that marks the 0,0,0 origin of our Cartesian coordinate system. We used three independent metrics to compare the distribution of the terminals in the deep SC cellular layers across animals. The first metric compared the dispersion and the clustering indexes. The dispersion index was calculated as the ratio of the area of labeling in the SC layers normalized by the area of the injection site in the cortex. Those areas (A in the following equation) were calculated by drawing a polygon around the labeled terminals, within the limits of the SGI and SGP, and around the limits of the injection sites (x, y, and z represent the three spatial coordinates):

$$A = \frac{1}{2}\left|\left(x_0 y_n - x_n y_0\right) + \sum_{i=1}^{n-1}\left(x_{i+1} y_i - x_i y_{i+1}\right)\right|$$

The clustering index (CI) is the mean distance between a terminal and its closest neighbor in the same layer

$$\left(\mathrm{CI} = \frac{\Sigma d_n}{n}\right), \text{where } d = \sqrt{\left(x_0 - x_1\right)^2 + \left(y_0 - y_1\right)^2 + \left(z_0 - z_1\right)^2}$$

Therefore, larger values in the dispersion and clustering indexes indicate greater divergence in the projection and *vice versa*.

The second metric relates the distribution of the terminals to the spatial extent of each SC layer by comparing the locations of the centroids (C_x and C_y) for each in every section examined. The centroids were defined by the intersection of all the hyperplanes of symmetry of each terminal distribution or SC layer according to the following equations. This comparison provides a measure of how homogenous the terminal labeling is within each layer.

$$C_x = \frac{1}{6A}\sum_{i=0}^{n-1}\left(x_i + x_{i+1}\right)\left(x_i y_{i+1} - x_{i+1} y_i\right)$$

$$C_y = \frac{1}{6A}\sum_{i=0}^{n-1}\left(y_i + y_{i+1}\right)\left(x_i y_{i+1} - x_{i+1} y_i\right)$$

To further analyze the distribution of the cortical terminals within the SC, the intermediate and deep layers were divided into four equal quadrants based on their centroid coordinates and the anteroposterior axis. The number of terminals in each quadrant was compared across animals. The density of terminals in the SC was calculated by dividing the total number of terminals (estimated using the fractionator after counting one in every six sections without employing counting frames) by the volume of each layer. The volumes of the SGI and SGP were calculated by the Cavalieri method (Gundersen, 1988). This involved multiplying the area of one in every six sections along the anteroposterior axis of the SC by the distance between them. The small size of the terminals relative to the thickness of the sections prevented any possible double counting.

Analysis of the morphological features of the labeled terminals was performed using optical microscopy. We considered every swelling in a labeled fiber as an "*en passant*" bouton and every swelling at the end of a labeled fiber as an end-terminal bouton. Terminals were classified according to their morphology following the same criteria used by Fuentes-Santamaria et al. (2009) in the cat SC.

NOMENCLATURE AND CRITERIA FOR SUBDIVISIONS IN THE SUPERIOR COLLICULUS AND IN THE AUDITORY CORTEX

The nomenclature and limits used for the different areas in the auditory cortex or layers in the SC are shown in **Figure 1**. The different layers of the SC were defined as in previous studies in the ferret (King and Hutchings, 1987; Meredith et al., 2001; Nodal et al., 2005), which are based on an earlier description of the SC in the cat (Kanaseki and Sprague, 1974). Briefly, the SC has a laminar structure with alternating gray and white layers formed predominantly of cells or fibers, respectively (**Figures 1C,D**). Superficial SC is primarily involved in visual functions (reviewed by Stein and Meredith, 1991), and comprises the three most superficial layers: the stratum zonale (SZ), the stratum griseum superficiale (SGS), and the stratum opticum (SO). The deeper SC layers comprise the intermediate layers, the stratum griseum intermediale (SGI) and the stratum album intermediale (SAI), and the deep layers, the stratum griseum profundum (SGP) and the stratum album profundum (SAP) (**Figure 1D**). This region is involved primarily in multisensory integration and in generating premotor commands for orientation behavior (reviewed by King, 1993).

Ferret auditory cortex is located in the ectosylvian gyrus (EG) and its middle, anterior and posterior regions (MEG, AEG, and PEG, respectively) can be distinguished according to the distribution pattern of SMI_{32} immunostaining (**Figure 1B**, dashed lines) and also by Nissl and CO staining patterns (Bajo et al., 2007). Four tonotopic areas have been described electrophysiologically (Kowalski et al., 1995; Bizley et al., 2005): A1 and the anterior auditory field (AAF) in the MEG, and the posterior suprasylvian field (PSF) and posterior pseudosylvian field (PPF) in the PEG. The tonotopic axes in A1 and AAF have a dorso-ventral orientation with low frequency areas in the most ventral part of MEG. A reversal in the tonotopic organization occurs between PPF and PSF, which share a region of low frequency sensitivity that extends up to the low frequency border of A1. High frequencies are represented in PPF and PSF close to the pss and sss, respectively. In addition, a third ventroposterior area (VP) has been described anatomically in the PEG (Pallas and Sur, 1993; Bajo et al., 2007). In the AEG, at least two non-tonotopic areas have been characterized, the anterodorsal field (ADF) and, ventral to it, the anteroventral field (AVF) (Bizley et al., 2005). AVF is the most ventral and anterior area in AEG

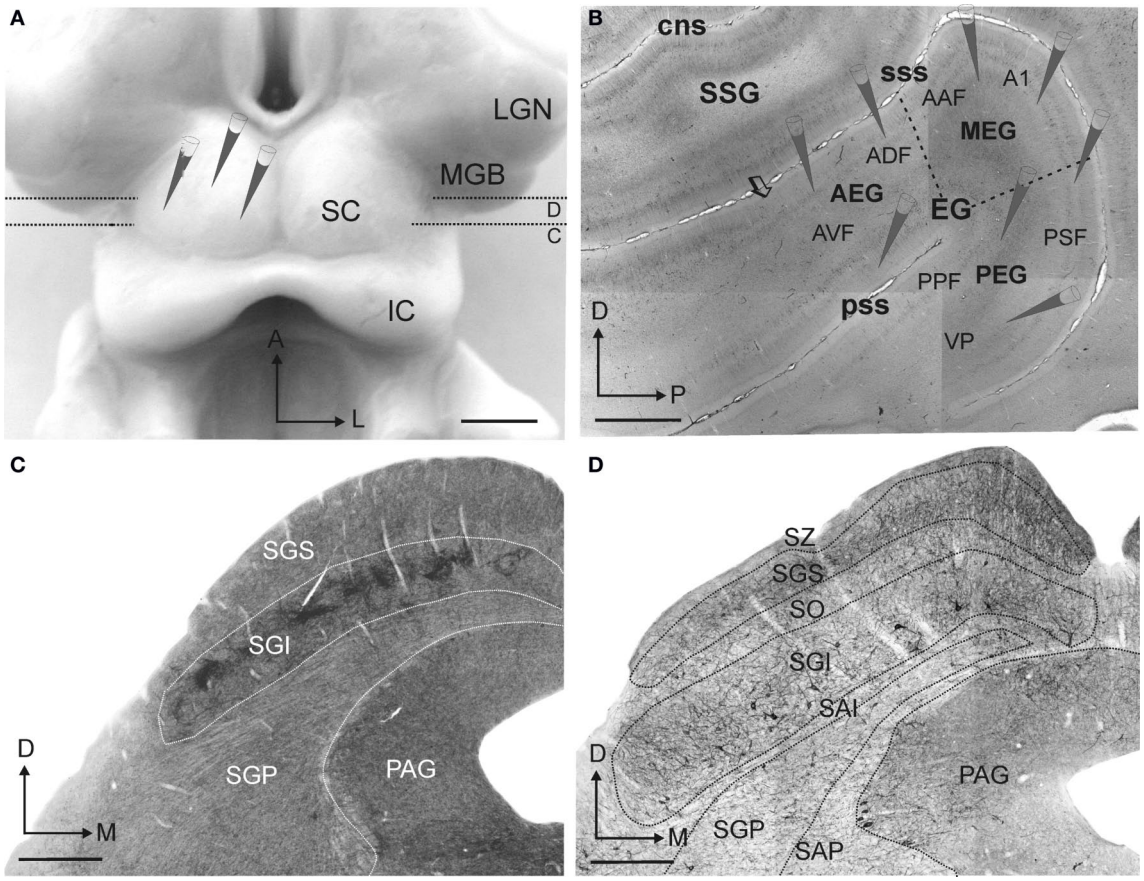

FIGURE 1 | The experimental design. Neural tracer injections in the superior colliculus (SC) and in the auditory cortex were made to label corticotectal cells retrogradely and their terminals in the SC anterogradely. **(A)** Dorsal view of the SC after the cortical hemispheres have been removed, showing the location of the tracer injections. Dotted lines and small C and D letters indicate the anteroposterior level of the coronal sections shown in panels **(C)** and **(D)**, respectively, in which the laminar organization of the SC can be observed. **(B)** Lateral view at the level of the ectosylvian gyrus taken from a flattened, tangential section stained with SMI_{32} monoclonal antibody. Tracer injections were placed in the different auditory fields (see **Table 1**), as indicated. The limits between the different layers in the SC were identified primarily on the basis of acetycholinesterase staining **(C)** and SMI_{32} immunocytochemistry **(D)**. Calibration bars are 2 mm in **(A)** and **(B)** and 0.5 mm in **(C)** and **(D)**.

defined as part of the auditory cortex on the basis of the vigorous responses of the neurons found there to broadband noise (Bizley et al., 2005). Anatomically, at the anterior limit of AVF a change in SMI_{32} pattern is observed (arrow in **Figure 1B**), with more intense staining found in layer II/III outside the auditory cortex.

RESULTS

In initial experiments, tracer injections were placed in the SC to label neurons retrogradely in the auditory cortex. The distribution of labeled cortical neurons in the EG was then used to guide tracer injections into different areas of the auditory cortex, in order to study the pattern of organization of their terminal fields in the SC.

RETROGRADE LABELING AFTER TRACER INJECTIONS IN THE SUPERIOR COLLICULUS IS FOUND IN SPECIFIC CORTICAL AREAS

Figure 2 shows an example of an injection of FR into the SC; the injection site was centered in the SGP, although its halo extended dorsally into the SGI and medially so that it just included the edge of the periaqueductal gray (PAG, **Figure 2A**). Retrogradely labeled neurons were numerous in the ipsilateral EG (**Figures 2B,C**). However, the labeling was not uniformly distributed across the gyrus. Labeling was most prominent in the AEG, particularly in the AVF and non-auditory areas located more anterior to the AVF, but was also present on the posterior EG (PEG), especially in its most posterior and dorsal part, where PSF is located. Labeled neurons in the MEG, where the primary areas A1 and AAF are located, were relatively scarce (**Figures 2B,C**). Moreover, where labeling was present in this region, it was found in peripheral locations consistent with these cells being located within the sulci. Such labeling is evident when the cortex was cut in the coronal plane (e.g., in **Figure 3**). Labeled cells were found deep in the dorsal part of suprasylvian sulcus (sss, **Figure 3C**) and also in the dorsal wall of the suprasylvian gyrus (**Figure 3C**).

The cortical cells that were labeled after tracer injections in the SC were large pyramidal neurons in layer V. Labeled neurons were always located in the ventral half of the layer V, and were often observed in clustered groups of two to three neurons (**Figure 3B**,

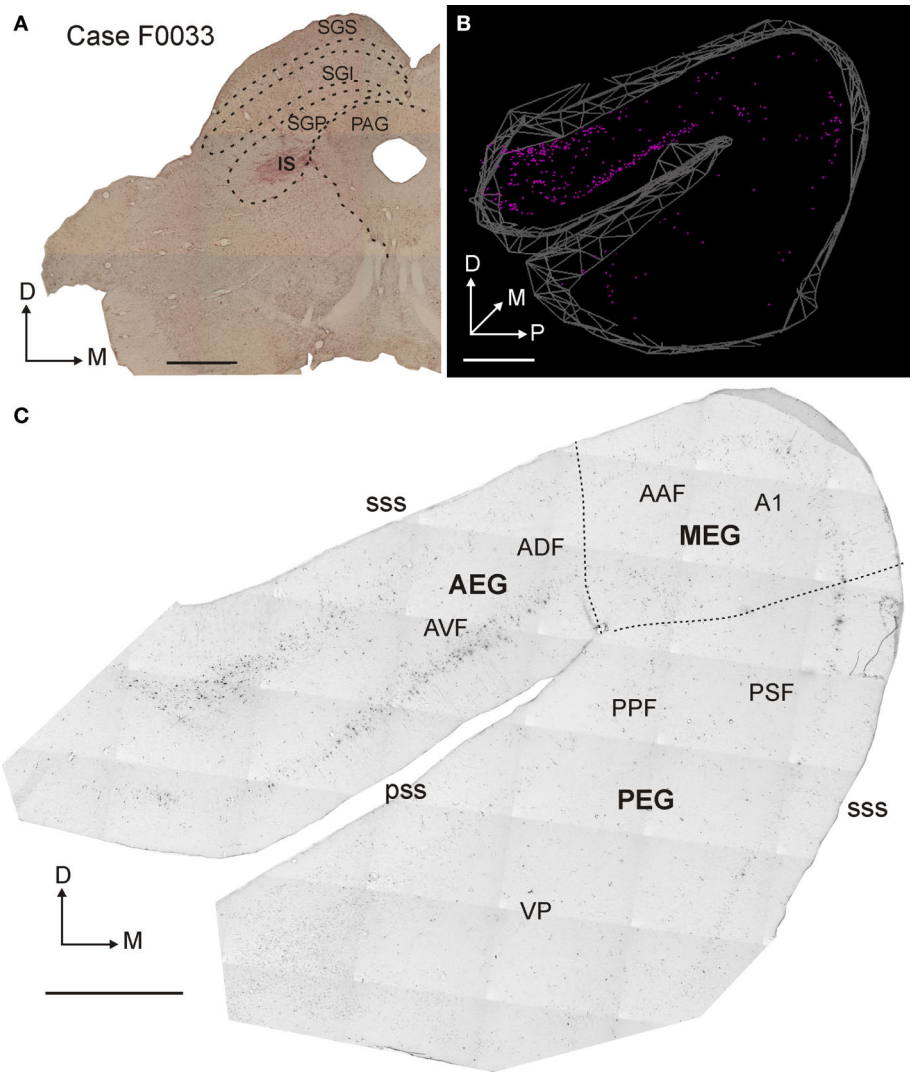

FIGURE 2 | Distribution of retrogradely labeled cells in the auditory cortex after rhodamine (FR) injection in the superior colliculus. (A) Coronal section at the level of the left SC showing the injection site in the deep SC (SGP). **(B)** 3D reconstruction of auditory cortex showing the location of retrogradely labeled neurons. (**C**) Photomicrograph of a flattened, tangential section at the level of the ipsilateral auditory cortex. The retrogradely labeled cells are numerous, especially in the anterior part of the ectosylvian gyrus (AEG). Calibration bars are 1 mm in **(A)** and 2 mm in **(B)** and **(C)**.

asterisks). Labeled neurons had a characteristic triangular cell body, a thick apical dendrite oriented toward the pial surface and perpendicular to the cortical layers, and several basal dendrites oriented parallel to the cortical lamination (**Figure 3D**).

We performed a morphometric analysis in order to explore whether labeled cells in different areas of the EG share a common morphology. To avoid bias due to the cutting plane, only the two cases with injections in the SC and cut in the coronal plane (F9921 and F9806) were analyzed. Cells were only considered if the whole cell body, as judged by the presence of the beginning of the apical dendrite or the beginning of at least two basal dendrites, was present in the same section. This selection criterion was imposed in order to avoid any bias that might result from sectioning artifacts. The size and shape of the selected cell bodies were analyzed by measuring the perimeter and form factor (4π Area/Perimeter). The mean perimeters were 64.8 ± 6.1 μm for neurons located in PEG, 67.3 ± 11.2 μm for neurons in MEG and 75.5 ± 16.6 μm for neurons in AEG, with form factors of 0.79 ± 0.07, 0.84 ± 0.05, and 0.78 ± 0.06, respectively (mean ± standard deviation). No significant differences were found either in neuronal size or shape across the different cortical regions (ANOVA, $F_{(3,63)} = 2.7, p = 0.053$) suggesting that, irrespective of cortical location, a common neuronal subtype of layer V neurons forms the corticotectal projection.

THE DISTRIBUTION OF LABELED TERMINALS WITHIN THE SUPERIOR COLLICULUS VARIES WITH INJECTION SITE LOCATION IN THE AUDITORY CORTEX

As expected from the analysis of retrogradely labeled cells in the EG after injections in the SC, the largest number of labeled terminals were found in the SC after injections of neuronal tracer into AVF in

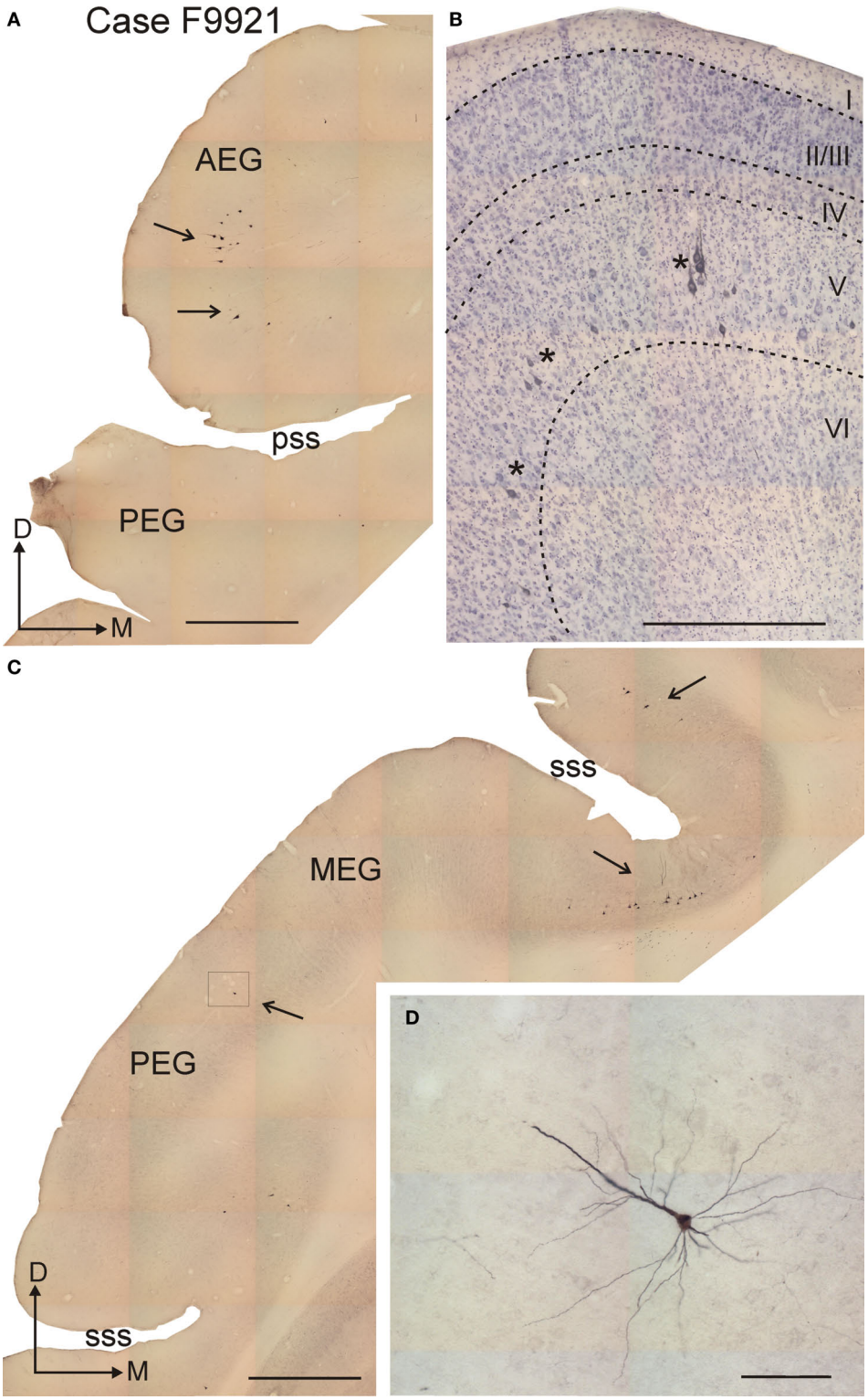

FIGURE 3 | Morphology of retrogradely labeled corticotectal neurons in layer V after rhodamine (FR) injection in the superior colliculus. **(A**,**C)** Coronal sections at the level of the anterior and middle part of the ectosylvian gyrus, respectively, showing labeled neurons that were mainly located in the AEG **(A)**, the deep part of the suprasylvian sulcus and the dorsal part of the PEG (arrows) **(C)**. **(B)** Higher-magnification photomicrograph of a Nissl-counter-stained section at the level of the AEG; sets of two to three labeled neurons can be observed in layer V (asterisks). **(D)** Higher-magnification photomicrograph showing the pyramidal morphology of a labeled neuron in layer V, whose thick apical dendrite runs orthogonal to the cortical layers. This photomicrograph was taken at the location shown by the frame in **(C)**. Calibration bars are 1 mm in **(A)** and **(C)**, 0.5 mm in **(B)** and 0.1 mm in **(D)**.

the AEG and into PSF in the PEG. **Figure 4** shows a typical example of labeling following injections into each of these two locations (Cases F0505 and F0536, **Table 1**).

Injections placed in either cortical field result in a similar pattern of labeling (**Figures 4 and 5**). Terminals were located mostly ipsilateral to the injection sites in both the intermediate and deep layers and were most numerous in the posterior-medial quadrant of the SC (**Figures 4 and 6**). Moreover, both injection locations labeled single *en passant* and terminal boutons in the SC as well as more complicated arrangements of terminals (**Figure 7**). There are, however, differences between the projections originating from these cortical fields; the density of terminals in the SC was larger and the pattern of terminals in the ipsilateral SGI was more patchy after injections in the AVF, whereas the SGI projection appears to be more targeted when the tracer was placed in the PSF (**Figure 4**).

To quantify any differences in the projections from these two cortical regions, we measured the density, clustering index and dispersion of the labeled terminals in the SC in three animals where the injection sites were located in the AEG and in three animals where injections were located in the PEG (**Table 1**, asterisks). We conservatively refer to injections centered in the AVF and PSF as being located in the AEG and PEG, respectively, because, as indicated in **Table 1**, the size of the injection sites varied and, in some cases (for example F0523 and F0504), they were not restricted to those fields. However, if the tracer injection was centered in ADF (as in animal F0535 with BDA), very little labeling was found in the SC, while injection sites centered in the VP (animal F0533) resulted in virtually no SC terminal labeling. Consequently, these data indicate that AVF and PSF are the primary sources of input to the SC from ferret auditory cortex.

The density of terminals in the SC varied with the location and the size of the injection sites in the cortex (**Figure 5A**). After normalizing for the size of the cortical injection site, there appeared to be clear differences in the terminal field labeling in the SC after injections into the AEG and PEG, with labeling being far denser in the former case (**Figure 5A**). Whilst there appears to be a clear trend in the data, as indicated by the relative height of the histogram bars, these differences were not statistically significant (ANOVA, $F_{(7,23)} = 1.01$, $p = 0.46$). Terminals from AEG tended to be more clustered and less dispersed than terminals from PEG, especially those ending in the SGI (**Figures 5B,C**). However, only differences in clustering were significant (ANOVA, $F_{(2,7)} = 5.25$, $p = 0.04$), with mean distances between terminals in the SGP being 18.5 ± 4.8 μm and 24.9 ± 9.2 μm after injections in the AEG and PEG, respectively. In the SGI distances between terminals were 15.9 ± 4.1 μm for AEG injections and 28.63 ± 12.8 μm for injections in PEG.

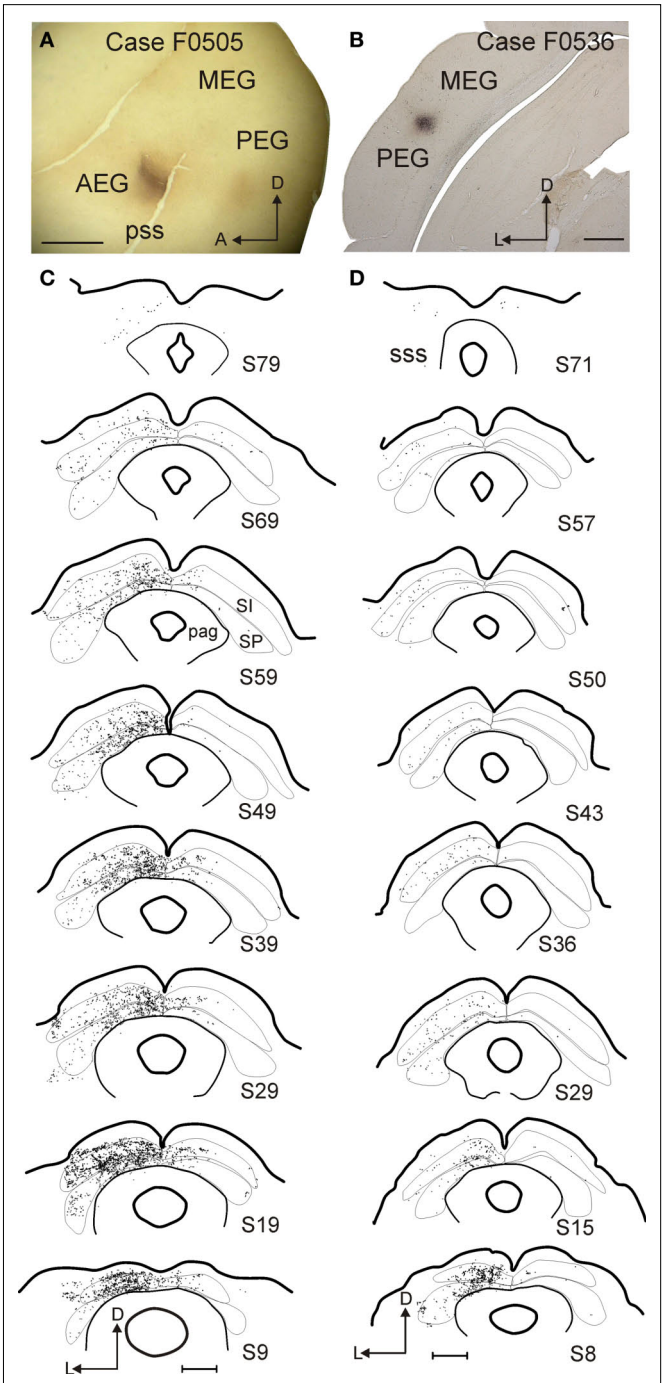

FIGURE 4 | Examples of two cases with BDA tracer injections in the auditory cortex. (A,B) Photomicrographs showing the location of the injection sites in AVF (**A**, flattened tangential section) and PEG (**B**, coronal section). **(C,D)** Drawings of coronal sections at the level of the SC with each dot representing a terminal. Gray and white layers were combined for the intermediate (stratum intermediale, SI) and deep (stratum profundum, SP) SC. The number of the section in each drawing indicates its anteroposterior position, with zero indicating the most posterior corner of the SC. Calibration bars are 2 mm for **(A)** and 1 mm for **(B–D)**.

CORTICOTECTAL TERMINAL DISTRIBUTIONS IN THE SUPERIOR COLLICULUS

Consistent with the region-specific pattern of retrograde labeling in the auditory cortex after SC tracer injections (**Figures 2B,C**), the distribution of terminal field labeling in the SC varied with injection site location in the cortex (**Figure 4**). To quantify the distribution of terminals observed within the SC, we subdivided the SGI and SGP into four quadrants (**Figure 6**). To account for the mediolateral curvature of the SC, we determined the borders of the quadrants from the position of the centroids for each layer in each section, while the anteroposterior border was defined by dividing in two the number of coronal sections that spanned the full length of the SC.

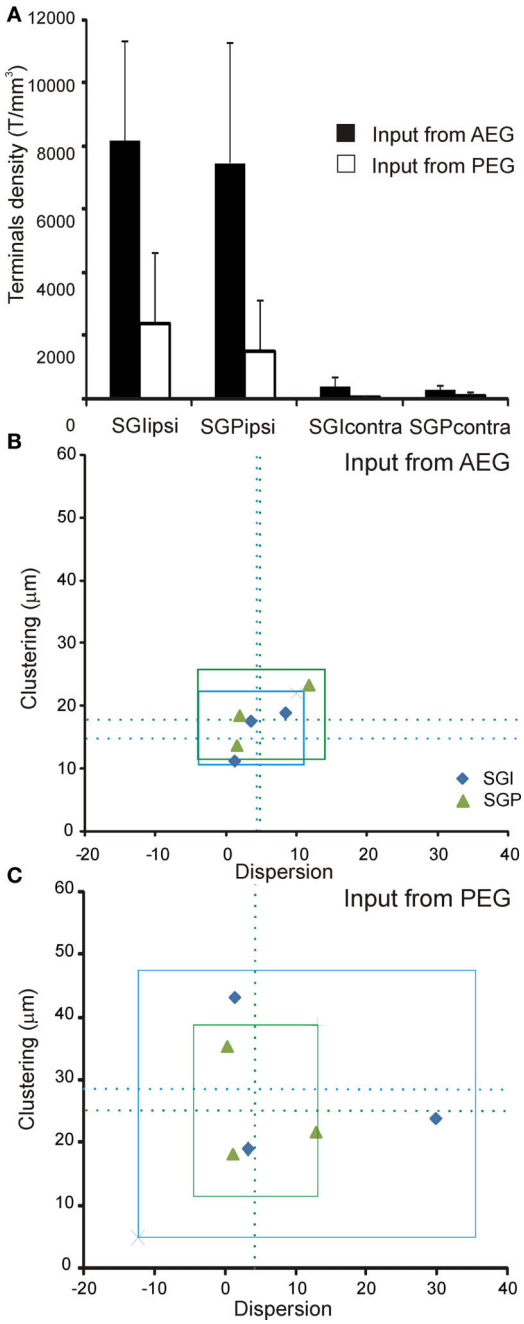

FIGURE 5 | Quantification of the corticotectal inputs to the SC. Six cases with injection sites in the AEG ($n = 3$) and PEG ($n = 3$) were used for quantification. **(A)** The normalized density of terminals (see Materials and Methods for details) is plotted in different layers of the left and right SC. The projection is predominantly uncrossed with a very minor contralateral component. No differences between the intermediate and deep layers of the SC (SGI and SGP) were found. The density of terminals was higher when input came from the AEG than from the PEG, but this difference was not significant (ANOVA, $F_{(7,23)} = 1.01$, $p = 0.46$). For each individual case, the clustering index is plotted against dispersion (measured as the ratio between the area of labeling in the SC and the area of the injection site in the cortex). These measures show that terminals from AEG **(B)** tend to be more clustered and less dispersed than terminals from PEG **(C)**. Dotted lines in **(B)** and **(C)** represent the mean and the squares represent three times the standard deviation of the mean; terminals in SGI are shown in blue and terminals in SGP in green.

The quantity of labeled terminals in each quadrant was compared across animals and quadrant locations. Examination of the labeling in **Figure 4** suggests that the terminals were not uniformly distributed along the mediolateral and anteroposterior dimensions of the SC. This is confirmed by the differences in the percentage of labeled terminals in each quadrant (**Figure 6**). The proportion of terminals was higher in the posterior half of the SC, and especially in the medial quadrant (ANOVA, $F_{(3,3)} = 9.865$, $p = 0.001$). This difference was observed irrespective of the injection site location in the auditory cortex (ANOVA, $F_{(1,3)} = 0.008$, $p = 0.93$).

Whilst the proportion of terminal labeling in the contralateral SC was much smaller, constituting only 6% of the total projection, the distribution of terminals was similar to that of the uncrossed projection, with the highest density also found in the posteromedial quadrant (**Figure 6**).

PREDOMINANCE OF *EN PASSANT* TERMINALS IN THE CORTICOTECTAL PROJECTION

The proportions of different terminal morphologies in the SC were measured in a single coronal section for each animal at the level where the densest terminal fields were observed. In all cases, the selected sections were located in the posterior half of the SC. Labeled terminals were classified as either *en passant* or end-terminal boutons, with the latter also including those described as "on short stalks" by Fuentes-Santamaria et al. (2009). Examples of labeled fibers and terminals are shown in **Figure 7**, with arrows and asterisks indicating *en passant* and end-terminal boutons, respectively (**Figures 7A,B,D,E**). We also use the term *complex terminals* to differentiate those terminals with a more intricate morphology, although in our material the number of such terminals was very small (data not shown).

No differences between AEG and PEG tracer injection groups were found in the proportion of different terminal morphologies in the SC (ANOVA, $F_{(1,11)} = 0.063$, $p = 0.0809$). In all cases, the great majority of the terminals were small *en passant* or end-terminal boutons (93–99%), with large or complex terminals representing only a small percentage of the total. *En passant* boutons were considerably more common than end-terminals, with the proportion of small boutons classified as *en passant* being 75.1 ± 6.7% and 66.8 ± 8.5% after injections in AEG and PEG, respectively (ANOVA $F_{(1,11)} = 75.162$, $p < 0.001$, **Figure 7C**). Both types of terminals were found along the length of the fibers running in the SC (**Figure 7B**). *En passant* terminals were observed as round thickenings along the axons, whereas end-terminals were typically found at the end of short thin stalks that branched out from the parent axon at small intervals (**Figure 7B**). The distribution of terminals along the axons did not result in a continuous and homogeneous terminal field within the SC layers. Rather, terminals appeared in clusters along the length of the axons in which both types of terminals were found (**Figures 7D,E**). Additionally, orthogonal branches were observed at such terminal clusters.

DISCUSSION

We have shown that inputs from non-primary and higher associative cortical areas, which form part of the non-lemniscal auditory cortex, converge in the intermediate and deep layers of the ferret SC. The cortical areas that contribute most to the corticotectal

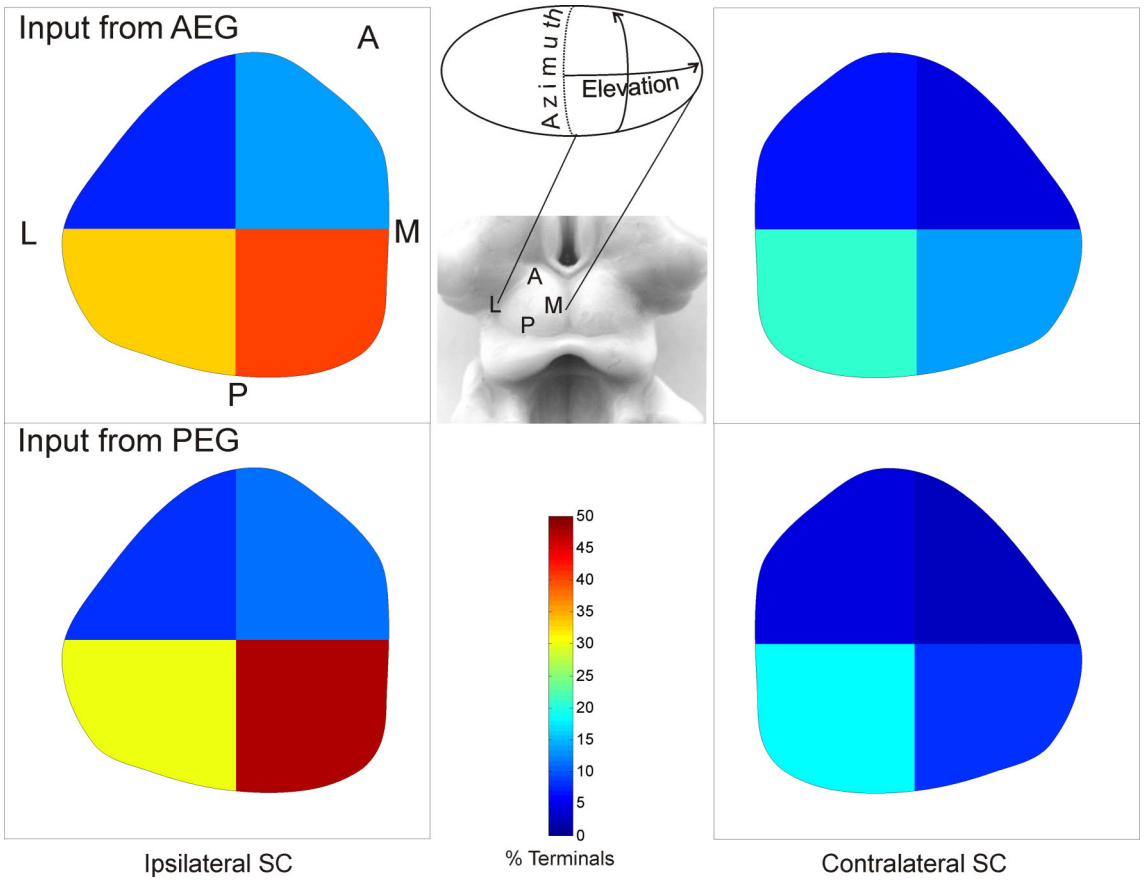

FIGURE 6 | Distribution of cortical terminals in the SC. The proportion of terminals is plotted after dividing the SC into quadrants. The highest proportion was found in the posterior half of the SC, especially in the medial quadrant (ANOVA, $F_{(3,3)} = 9.865$, $p = 0.001$), and no differences in this distribution were found with injection site location in the cortex (ANOVA, $F_{(1,3)} = 0.008$, $p = 0.93$).

input are AVF, together with the tonotopically organized PSF. Large pyramidal cells located in the lower part of layer V in each of these regions are responsible for the projections to the SC. Terminals in the SC are arranged in clusters with a high number of *en passant* boutons. Corticotectal inputs from both AVF and PSF are most extensive in the posteromedial quadrant of the SC, where lateral and posterior stimulus locations are represented.

CORTICOTECTAL PROJECTIONS IN DIFFERENT SPECIES

Previous studies of corticofugal input to the SC in different species have focused mainly on inputs from different parts of the visual cortex (e.g., Swadlow and Weyand, 1981; Tigges and Tigges, 1981; Harting et al., 1992; Serizawa et al., 1994). The organization of corticotectal inputs has been studied most extensively in the cat (e.g., Harting et al., 1992; Fuentes-Santamaria et al., 2008), where their functions have also been examined at both physiological and behavioral levels by reversible inactivation (Stein, 1978; Clemo and Stein, 1986; Meredith and Clemo, 1989; Wallace et al., 1993; Jiang et al., 2002; Alvarado et al., 2007). The presence of robust inputs from AES and rLS in this species suggests that auditory, as well as other sensory, signals can reach the SC from multisensory cortical areas. In addition, there is evidence in cats for inputs to the SC from A2 as well as from multisensory areas that are designated as part of auditory cortex (Winer et al., 1998).

Cat AES is an area of association cortex that has been shown to project heavily to the SC and to play a particularly important role in multisensory integration (reviewed by Stein, 1998). It is divided into three largely unisensory regions, the anterior ectosylvian visual region (AEV) (Mucke et al., 1982; Olson and Graybiel, 1987; Scannell et al., 1996), the fourth somatosensory cortex (S4, Clemo and Stein, 1982, 1983), and an auditory field (FAES) (Clarey and Irvine, 1986; Meredith and Clemo, 1989). Although multisensory neurons are found in cat AES, mainly at the borders of each of these areas, inputs to the SC originate from the unisensory regions (Wallace et al., 1993; Alvarado et al., 2009).

Anatomically, the ferret does not have an AES, but Ramsay and Meredith (2004) suggested that the region surrounding the pseudosylvian sulcus (pss), and named by them as pseudosylvian sulcal cortex (PSSC), might be the functional homolog of cat AES. Their proposal is based on the organization of visual and somatosensory cortical projections to the PSSC, with visual terminals being restricted to its posterior dorsal bank and somatosensory terminals having a more extensive distribution that included anterior regions of the PSSC. Ramsay and Meredith (2004) also noted that neurons responsive to auditory stimuli are found in the most posterior corner of the pss, highlighting the multisensory character of the PSSC. Manger et al. (2005) described a visually responsive area running parallel to the pss

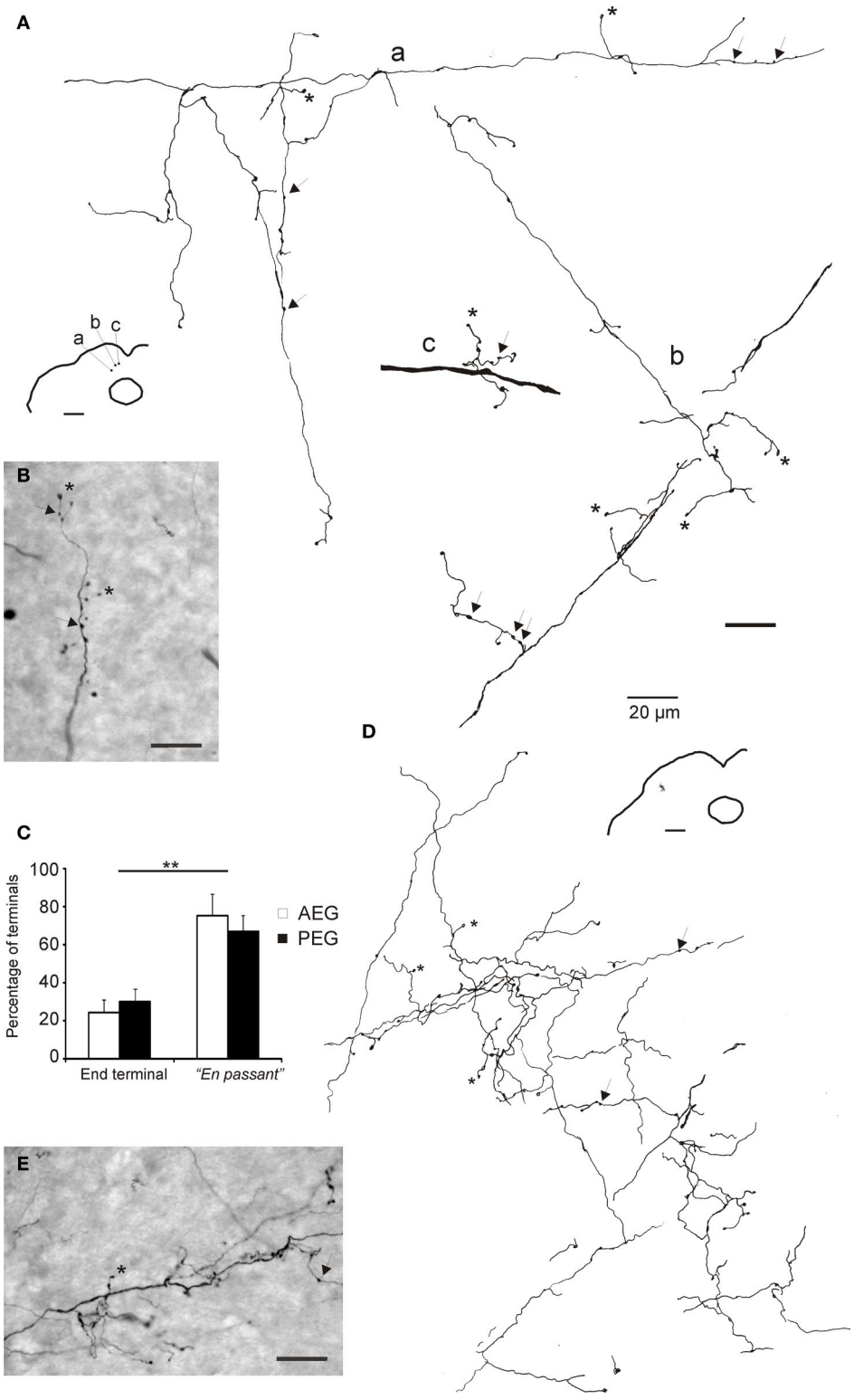

FIGURE 7 | Morphology of terminals in the superior colliculus. Camera lucida drawings **(A,D)** and photomicrographs **(B,E)** of terminal fields in the SC after tracer injections in the AEG (**A** and **B**, case F0505) and in the PEG (**D** and **E**, case 0536). Locations of the terminal fields in the SC are shown in the lower magnification drawings. Some end-terminals are labeled with asterisks and *en passant* terminals with arrows. Calibration bars are 20 µm. **(C)** Histogram showing the percentage of the different types of terminals in the SC. *En passant* terminals were significantly more numerous (** $p < 0.001$) than the end-terminals, irrespective of the location of the injection sites in the cortex.

on the postero-lateral half of the ferret AEG, which also contained bisensory neurons that were segregated according to whether they responded to both visual and tactile stimulation or to visual and auditory stimulation. They called this area AEV following the terminology used for the visual part of the cat's AES. The location of this region overlaps with the two regions on the AEG, the ADF, and AVF, which we have distinguished on the basis of the neurons' auditory response properties (Bizley et al., 2005) and sensitivity to visual stimulation (Bizley et al., 2007; Bizley and King, 2009), and now in terms of their relative contributions to the corticotectal projection.

The presence of multisensory inputs to different parts of the AEG is consistent with the possibility that this part of ferret cortex includes a region homologous to cat AES. Further evidence for this possibility is provided by our finding in the present study that the AEG is the source of a robust projection to the SC. The heaviest retrograde labeling was located in the ventral and anterior part of the AEG, which includes AVF, where many neurons respond to both auditory and visual stimulation (Bizley et al., 2007; Bizley and King, 2009), as well as non-auditory areas located anterior to the AVF. Accordingly, relative to other parts of auditory cortex, tracer injections centered in the AVF resulted in the heaviest labeling in the SC. AVF receives inputs from the dorsal division of the medial geniculate body and the suprageniculate nucleus (F. R. Nodal, V. M. Bajo, J. K. Bizley, and A. J. King, unpublished observation), and we have shown that about two-thirds of the neurons recorded there respond to broadband auditory stimuli, half of which were also visually responsive (Bizley et al., 2007). We have not, however, found any evidence for segregation of neurons according to their modality sensitivity within the area in which retrograde labeling was found in the present study. Cat AES is organized into three distinct unisensory regions, and whilst our recordings on the gyrus of the anterior bank show intermingled modality sensitivity, further mapping within the pss, along the dorsal lip and fundus, with different sensory stimuli is required to unequivocally define in ferret an area equivalent to the cat auditory region FAES.

In the cat, tracer injections in the PEG result in anterograde labeling in the IC, as well as in neighboring structures, including the deeper layers of the SC (Winer et al., 1998). The projection from the PEG to the SC originates from the dorsal part of the posterior ectosylvian gyrus (EPD), and possibly also from the intermediate part (EPI), which are multisensory in nature (Bowman and Olson, 1988a,b). We also found that the PEG projects to the SC in the ferret, but, in this species, PSF is the source of this pathway. PSF is a tonotopically organized auditory area (Bizley et al., 2005), which, like other parts of auditory cortex, contains a number of visually responsive neurons (Bizley et al., 2007). We have previously shown that PSF receives inputs from visual areas 20a and 20b (Bizley et al., 2007), which are thought to be concerned with non-spatial visual processing (Manger et al., 2004). However, relative to the other auditory cortical fields, PSF contains a particularly large number of neurons in which the presence of a spatially-coincident visual stimulus increases the amount of location-related information they convey compared to their responses to sound alone (Bizley and King, 2009).

We also observed inputs to the SC from deep sulcal regions surrounding the MEG. In the ferret, the cortical region within the dorsal edge of the suprasylvian sulcus at the level of the primary auditory fields appears to be equivalent to the anteromedial lateral suprasylvian visual area (AMLS) in the cat (Manger et al., 2008). The lateral or ventral edge of this sulcus has been referred to as a putative anterolateral lateral suprasylvian area (ALLS; Manger et al., 2008), but might also be equivalent to cat DZ, which projects to the SC (Winer et al., 1998). AMLS and the neighboring posteromedial suprasylvian visual area (PMLS, also termed the suprasylvian visual area or posterior suprasylvian area), have been implicated in visual motion (Cantone et al., 2006; Philipp et al., 2006; Manger et al., 2008), whereas DZ plays an important role in auditory spatial processing (Stecker et al., 2005). Although speculative at this time, since these sulcal areas in the ferret cortex require further anatomical and physiological investigation and their auditory and/or multisensory properties have yet to be established, the presence of a descending projection to the SC implies that this part of the cortex participates in orienting behaviors and multisensory integration.

Together, these data indicate that there are similarities between cats and ferrets in the organization of their auditory corticotectal projections, with an anterior multisensory region dominating this pathway in both cases. However, the additional projection from the PSF, as well as the concentration of corticotectal terminals in the most posteromedial quadrant of the SC in the ferret compared to the more lateral distribution in the cat (Meredith and Clemo, 1989), indicate that some differences exist between these species.

ROLE OF CORTICOTECTAL INPUT IN MODULATING AUDITORY ORIENTING BEHAVIORS

In cats, cortical deactivation of A1 (including DZ), PAF and FAES all result in sound localization deficits in the contralateral hemifield (Malhotra et al., 2004; Malhotra and Lomber, 2007). Lomber et al. (2007a) proposed that neurons in the superficial layers of A1, DZ, and PAF feed forward to AES and that neurons in AES are responsible for transmitting spatial information to the SC. While there is no doubt that AVF in the ferret auditory cortex provides the largest corticotectal projection, our results show that PSF also projects directly to the SC. Thus, parallel routes may exist for conveying signals to the SC that are important for orientation behaviors.

Deficits in auditory localization behavior have been observed following damage to or inactivation of both the auditory cortex (e.g., Jenkins and Merzenich, 1984; Kavanagh and Kelly, 1987; Heffner and Heffner, 1990; Nodal et al., 2010) and the SC (Tunkl, 1980; Lomber et al., 2001). However, it seems likely that different aspects of spatial hearing are mediated by these different brain regions. Thus, Nodal et al. (2010) found that bilateral lesions of A1 impair the localization of brief sounds in ferrets when the animals have to approach the sound source in order to receive a reward, whereas their ability to orient toward the appropriate region of space is unaffected. Deficits in acoustic orientation behavior were observed, however, if the lesions covered a more extensive region of auditory cortex, including the areas shown here to project to the SC. In keeping with this, it has been proposed that the head orienting deficits produced by cortical lesions in cats might reflect a loss of descending corticofugal neurons (Thompson and Masterton, 1978; Beitel and Kaas, 1993). Further evidence for a complex relationship between the cortex and the SC in the control of auditory localization behavior has been provided by the "auditory Sprague effect," whereby the contralateral deficits produced in cats by unilateral ablation of the auditory cortex disappear if the contralesional SC is then deactivated (Lomber et al.,

2007b). While the circuitry responsible for this recovery of function is unknown, it is possible that activity in the other SC is increased as a result of the loss of inhibition provided by the crossed nigrocollicular connection (Wallace et al., 1990) or by the commissural inputs from the inactivated SC (Behan, 1985; Jiang et al., 1997). It is also conceivable that the small crossed component of the corticotectal projection here described could be involved.

MULTISENSORY INTEGRATION IN THE SC AND CORTICOTECTAL INPUT

Inputs from the cortex are essential for multisensory integration in the SC of the cat (Stein, 1998). However, unisensory areas in different parts of AES project to the SC in this species (Wallace et al., 1993), and it is their convergence onto individual SC neurons that appears to synergistically create multisensory enhancement or depression depending on the proximity of stimuli in different sensory modalities (Alvarado et al., 2007, 2009). Axons conveying modality-specific information have been shown to terminate on the same SMI_{32}-positive SC projection neurons (Fuentes-Santamaria et al., 2009), but no differences in their terminal distribution across the SC have been reported.

Our results show that descending inputs from different parts of auditory cortex predominantly target the posterior half of the SC, where peripheral stimulus locations are represented. The influence of these cortical neurons on SC responses is therefore likely to be greatest for this region of space, where, because auditory receptive fields tend to extend beyond visual receptive fields (King and Hutchings, 1987), acoustic cues may be more relevant in guiding orienting behaviors. Although we showed that acoustically responsive neurons were present at each injection site in the cortex, we cannot, of course, rule out the possibility that the labeled axons convey non-auditory signals as well. This applies particularly to AVF, where the neurons recorded by Bizley et al. (2007) were equally likely to be unisensory visual, unisensory auditory or sensitive to both modalities. Identifying the modality specificity of individual corticotectal neurons would require the use of intracellular recording and tracer injection techniques. The significance for multisensory processing of the non-uniform innervation of the SC by these higher levels areas of the auditory cortex is unclear, but it is interesting to note that, in cats, the influence of a spatially discordant auditory stimulus on the accuracy of visual localization varies with stimulus eccentricity (Jiang et al., 2002).

Multisensory integration is a particularly prominent feature of the intermediate layers of the SC, where a patchy or honeycomb-like pattern of acetylcholinesterase staining aligns with some of the afferent and efferent connections of this region (Chevalier and Mana, 2000; Mana and Chevalier, 2001). We also saw some evidence for a patchy distribution of auditory corticotectal inputs in the SGI. This pattern of terminal labeling was not always observed, however, although that may reflect the sectioning plane used and the restricted size of the tracer injections in the cortex. It remains to be seen whether a similar modular arrangement of inputs is found for inputs from auditory subcortical structures (King et al., 1998; Nodal et al., 2005), or how this relates to the organization of afferent connections for other sensory modalities.

CONCLUDING REMARKS AND FUTURE DIRECTIONS

Previous work on the auditory corticotectal pathway in the cat has been based on the assumption that only FAES provides a direct input to the SC, and that any involvement of other auditory fields would be mediated through AES via cortico-cortical connections (Lomber et al., 2007a). The present results in the ferret show the direct contribution not only of AVF and adjoining regions on the anterior bank of the EG, but also of both the PSF on the posterior bank and of sulcal regions surrounding the primary areas on the MEG. Thus, the corticotectal projection should be seen as a convergence of information from different cortical areas, most likely conveying multisensory rather than exclusively auditory information, which are all likely to be involved in modulating orientation behavior via their inputs to the SC. In accordance with this, it has been shown that inactivation of the SC or the combined inactivation of multiple regions of auditory cortex has a far more profound impairment on orienting behavior than inactivation of any individual cortical area (Malhotra et al., 2004). In order to distinguish the role of direct corticotectal input from cortico-cortical circuits, it will be necessary to test the behavioral consequences of selectively inactivating specific descending pathways, as we have done for the projection from A1 to the IC (Bajo et al., 2010), whilst leaving intact the neurons in other cortical areas.

Elimination of the descending projection from A1 to the IC impairs learning-induced auditory plasticity in adult ferrets, without having any effect on the accuracy of sound localization behavior in the presence of normal acoustic inputs (Bajo et al., 2010). On the basis of the present results and the orienting deficits produced by large lesions of the auditory cortex (Nodal et al., 2010), we would predict that the loss of descending projections to the SC will disrupt acoustic orientation behavior. A recent study in monkeys has found that inactivation of the SC impairs the selection of which signals to use for a visual motion discrimination task, implying a role in making perceptual judgments (Lovejoy and Krauzlis, 2010), a function that is normally thought to be the preserve of the cerebral cortex. This may highlight another role of descending corticofugal projections to the SC. Similarly, the capacity of adult SC neurons to adjust their response properties following repeated exposure to particular visual–auditory cue combinations (Yu et al., 2009) may rely on descending modulatory influences. In each case, the selective inactivation of appropriate corticofugal pathways will help to identify the neural circuitry involved.

ACKNOWLEDGMENT

This work was supported by the Wellcome Trust through a Principal Research Fellowship to Andrew J. King (WT076508AIA).

REFERENCES

Adams, J. C. (1981). Heavy metal intensification of DAB-based HRP reaction product. *J. Histochem. Cytochem.* 29, 775.

Allman, B. L., Keniston, L. P., and Meredith, M. A. (2009). Adult deafness induces somatosensory conversion of ferret auditory cortex. *Proc. Natl. Acad. Sci. U.S.A.* 106, 5925–5930.

Alvarado, J. C., Stanford, T. R., Rowland, B. A., Vaughan, J. W., and Stein, B. E. (2009). Multisensory integration in the superior colliculus requires synergy among corticocollicular inputs. *J. Neurosci.* 29, 6580–6592.

Alvarado, J. C., Stanford, T. R., Vaughan, J. W., and Stein, B. E. (2007). Cortex mediates multisensory but not unisensory integration in superior colliculus. *J. Neurosci.* 27, 12775–12786.

Bajo, V. M., Nodal, F. R., Bizley, J. K., Moore, D. R., and King, A. J. (2007). The ferret auditory cortex: descending projections to the inferior colliculus. *Cereb. Cortex* 17, 475–491.

Bajo, V. M., Nodal, F. R., Moore, D. R., and King, A. J. (2010). The descending corticocollicular pathway mediates learning-induced auditory plasticity. *Nat. Neurosci.* 13, 253–260.

Behan, M. (1985). An EM-autoradiographic and EM-HRP study of the commissural projection of the superior colliculus in the cat. *J. Comp. Neurol.* 234, 105–116.

Beitel, R. E., and Kaas, J. H. (1993). Effects of bilateral and unilateral ablation of auditory cortex in cats on the unconditioned head orienting response to acoustic stimuli. *J. Neurophysiol.* 70, 351–369.

Binns, K. E., Grant, S., Withington, D. J., and Keating, M. J. (1992). A topographic representation of auditory space in the external nucleus of the inferior colliculus of the guinea-pig. *Brain Res.* 589, 231–242.

Bizley, J. K., and King, A. J. (2009). Visual influences on ferret auditory cortex. *Hear. Res.* 258, 55–63.

Bizley, J. K., Nodal, F. R., Bajo, V. M., Nelken, I., and King, A. J. (2007). Physiological and anatomical evidence for multisensory interactions in auditory cortex. *Cereb. Cortex* 17, 2172–2189.

Bizley, J. K., Nodal, F. R., Nelken, I., and King, A. J. (2005). Functional organization of ferret auditory cortex. *Cereb. Cortex* 15, 1637–1653.

Bowman, E. M., and Olson, C. R. (1988a). Visual and auditory association areas of the cat's posterior ectosylvian gyrus: thalamic afferents. *J. Comp. Neurol.* 272, 15–29.

Bowman, E. M., and Olson, C. R. (1988b). Visual and auditory association areas of the cat's posterior ectosylvian gyrus: cortical afferents. *J. Comp. Neurol.* 272, 30–42.

Burnett, L. R., Stein, B. E., Chaponis, D., and Wallace, M. T. (2004). Superior colliculus lesions preferentially disrupt multisensory orientation. *Neuroscience* 124, 535–547.

Cantone, G., Xiao, J., and Levitt, J. B. (2006). Retinotopic organization of ferret suprasylvian cortex. *Vis. Neurosci.* 23, 61–77.

Chevalier, G., and Mana, S. (2000). Honeycomb-like structure of the intermediate layers of the rat superior colliculus, with additional observations in several other mammals: AChE patterning. *J. Comp. Neurol.* 419,137–153.

Clarey, J. C., and Irvine, D. R. (1986). Auditory response properties of neurons in the anterior ectosylvian sulcus of the cat. *Brain Res.* 386, 12–19.

Clemo, H. R., and Stein, B. E. (1982). Somatosensory cortex: a 'new' somatotopic representation. *Brain Res.* 235, 162–168.

Clemo, H. R., and Stein, B. E. (1983). Organization of a fourth somatosensory area of cortex in cat. *J. Neurophysiol.* 50, 910–925.

Clemo, H. R., and Stein, B. E. (1986). Effects of cooling somatosensory cortex on response properties of tactile cells in the superior colliculus. *J. Neurophysiol.* 55, 1342–1368.

Diamond, I. T., Jones, E. G., and Powell, T. P. (1969). The projection of the auditory cortex upon the diencephalons and brain stem in the cat. *Brain Res.* 15, 305–340.

Fritz, J., Shamma, S., Elhilali, M., and Klein, D. (2003). Rapid task-related plasticity of spectrotemporal receptive fields in primary auditory cortex. *Nat. Neurosci.* 6, 1216–1223.

Fuentes-Santamaria, V., Alvarado, J. C., McHaffie, J. G., and Stein, B. E. (2009). Axon morphologies and convergence patterns of projections from different sensory-specific cortices of the anterior ectosylvian sulcus onto multisensory neurons in the cat superior colliculus. *Cereb. Cortex* 19, 2902–2915.

Fuentes-Santamaria, V., Alvarado, J. C., Stein, B. E., and McHaffie, J. G. (2008). Cortex contacts both output neurons and nitrergic interneurons in the superior colliculus: direct and indirect routes for multisensory integration. *Cereb. Cortex* 18, 1640–1652.

Gundersen, H. J. (1988). The nucleator. *J. Microsc.* 151, 3–21.

Harting, J. K., Updyke, B. V., and van Lieshout, D. P. (1992). Corticotectal projections in the cat: anterograde transport studies of twenty-five cortical areas. *J. Comp. Neurol.* 324, 379–414.

Heffner, H. E., and Heffner, R. S. (1990). Effect of bilateral auditory cortex lesions on sound localization in Japanese macaques. *J. Neurophysiol.* 64, 915–931.

Jenkins, W. M., and Merzenich, M. M. (1984). Role of cat primary auditory cortex for sound-localization behavior. *J. Neurophysiol.* 52, 819–847.

Jiang, W., Jiang, H., and Stein, B. E. (2002). Two cortical areas facilitate multisensory orientation behavior. *J. Cogn. Neurosci.* 14, 1240–1255.

Jiang, W., Wallace, M. T., Jiang, H., Vaughan, J. W., and Stein, B. E. (2001). Two cortical areas mediate multisensory integration in superior colliculus neurons. *J. Neurophysiol.* 85, 506–522.

Jiang, Z. D., Moore, D. R., and King, A. J. (1997). Sources of subcortical projections to the superior colliculus in the ferret. *Brain Res.* 755, 279–292.

Kacelnik, O., Nodal, F. R., Parsons, C. H., and King, A. J. (2006). Training-induced plasticity of auditory localization in adult mammals. *PLoS Biol.* 4, e71. doi:10.1371/journal.pbio.0040071

Kanaseki, T., and Sprague, J. M. (1974). Anatomical organization of pretectal nuclei and tectal laminae in the cat. *J. Comp. Neurol.* 158, 319–337.

Kavanagh, G. L., and Kelly, J. B. (1987). Contribution of auditory cortex to sound localization by the ferret (*Mustela putorius*). *J. Neurophysiol.* 57, 1746–1766.

Kelly, J. B., Judge, P. W., and Phillips, D. P. (1986). Representation of the cochlea in primary auditory cortex of the ferret (*Mustela putorius*). *Hear. Res.* 24, 111–115.

King, A. J. (1993). The Wellcome Prize Lecture. A map of auditory space in the mammalian brain: neural computation and development. *Exp. Physiol.* 78, 559–590.

King, A. J. (2004). The superior colliculus. *Curr. Biol.* 14, R335–R338.

King, A. J., and Hutchings, M. E. (1987). Spatial response properties of acoustically responsive neurons in the superior colliculus of the ferret: a map of auditory space. *J. Neurophysiol.* 57, 596–624.

King, A. J., Jiang, Z. D., and Moore, D. R. (1998). Auditory brainstem projections to the ferret superior colliculus: anatomical contribution to the neural coding of sound azimuth. *J. Comp. Neurol.* 390, 342–365.

Kowalski, N., Versnel, H., and Shamma, S. A. (1995). Comparison of responses in the anterior and primary auditory fields of the ferret cortex. *J. Neurophysiol.* 73, 1513–1523.

Lomber, S. G., and Malhotra, S. (2008). Double dissociation of 'what' and 'where' processing in auditory cortex. *Nat. Neurosci.* 11, 609–616.

Lomber, S. G., Malhotra, S., and Hall, A. J. (2007a). Functional specialization in non-primary auditory cortex of the cat: areal and laminar contributions to sound localization. *Hear. Res.* 229, 31–45.

Lomber, S. G., Malhotra, S., and Sprague, J. M. (2007b). Restoration of acoustic orienting into a cortically deaf hemifield by reversible deactivation of the contralesional superior colliculus: the acoustic "Sprague Effect." *J. Neurophysiol.* 97, 979–993.

Lomber, S. G., Payne, B. R., and Cornwell, P. (2001). Role of the superior colliculus in analyses of space: superficial and intermediate layer contributions to visual orienting, auditory orienting, and visuospatial discriminations during unilateral and bilateral deactivations. *J. Comp. Neurol.* 441, 44–57.

Lovejoy, L. P., and Krauzlis, R. J. (2010). Inactivation of primate superior colliculus impairs covert selection of signals for perceptual judgments. *Nat. Neurosci.* 13, 261–266.

Malhotra, S., Hall, A. J., and Lomber, S. G. (2004). Cortical control of sound localization in the cat: unilateral cooling deactivation of 19 cerebral areas. *J. Neurophysiol.* 92, 1625–1643.

Malhotra, S., and Lomber, S. G. (2007). Sound localization during homotopic and heterotopic bilateral cooling deactivation of primary and nonprimary auditory cortical areas in the cat. *J. Neurophysiol.* 97, 26–43.

Mana, S., and Chevalier, G. (2001). Honeycomb-like structure of the intermediate layers of the rat superior colliculus: afferent and efferent connections. *Neuroscience* 103, 673–693.

Manger, P. R., Engler, G., Moll, C. K., and Engel, A. K. (2005). The anterior ectosylvian visual area of the ferret: a homologue for an enigmatic visual cortical area of the cat? *Eur. J. Neurosci.* 22, 706–714.

Manger, P. R., Engler, G., Moll, C. K., and Engel, A. K. (2008). Location, architecture, and retinotopy of the anteromedial lateral suprasylvian visual area (AMLS) of the ferret (*Mustela putorius*). *Vis. Neurosci.* 25, 27–37.

Manger, P. R., Nakamura, H., Valentiniene, S., and Innocenti, G. M. (2004). Visual areas in the lateral temporal cortex of the ferret (*Mustela putorius*). *Cereb. Cortex* 14, 676–689.

Meredith, M. A., and Clemo, H. R. (1989). Auditory cortical projection from the anterior ectosylvian sulcus (Field AES) to the superior colliculus in the cat: an anatomical and electrophysiological study. *J. Comp. Neurol.* 289, 687–707.

Meredith, M. A., Miller, L. K., Ramoa, A. S., Clemo, H. R., and Behan, M. (2001). Organization of the neurons of origin of the descending pathways from the ferret superior colliculus. *Neurosci. Res.* 40, 301–313.

Middlebrooks, J. C., and Knudsen, E. I. (1984). A neural code for auditory space in the cat's superior colliculus. *J. Neurosci.* 4, 2621–2634.

Mucke, L., Norita, M., Benedek, G., and Creutzfeldt, O. (1982). Physiologic and anatomic investigation of a visual cortical area situated in the ventral bank of the anterior ectosylvian sulcus of the cat. *Exp. Brain Res.* 46, 1–11.

Nelken, I., Bizley, J. K., Nodal, F. R., Ahmed, B., Schnupp, J. W., and King, A. J. (2004). Large-scale organization of ferret auditory cortex revealed using continuous acquisition of intrinsic optical signals. *J. Neurophysiol.* 92, 2574–2588.

Nodal, F. R., Doubell, T. P., Jiang, Z. D., Thompson, I. D., and King, A. J. (2005). Development of the projection from the nucleus of the brachium of the inferior colliculus to the superior

colliculus in the ferret. *J. Comp. Neurol.* 485, 202–217.

Nodal, F. R., Kacelnik, O., Bajo, V. M., Bizley, J. K., Moore, D. R., and King, A. J. (2010). Lesions of the auditory cortex impair azimuthal sound localization and its recalibration in ferrets. *J. Neurophysiol.* 103, 1209–1225.

Olson, C. R., and Graybiel, A. M. (1987). Ectosylvian visual area of the cat: location, retinotopic organization, and connections. *J. Comp. Neurol.* 261, 277–294.

Pallas, S. L., and Sur, M. (1993). Visual projections induced into the auditory pathway of ferrets: II. Corticocortical connections of primary auditory cortex. *J. Comp. Neurol.* 337, 317–333.

Palmer, A. R., and King, A. J. (1982). The representation of auditory space in the mammalian superior colliculus. *Nature* 299, 248–249.

Philipp, R., Distler, C., and Hoffmann, K. P. (2006). A motion-sensitive area in ferret extrastriate visual cortex: an analysis in pigmented and albino animals. *Cereb. Cortex* 16, 779–790.

Ramsay, A. M., and Meredith, M. A. (2004). Multiple sensory afferents to ferret pseudosylviansulcal cortex. *Neuroreport* 15, 461–465.

Scannell, J. W., Sengpiel, F., Tovée, M. J., Benson, P. J., Blakemore, C., and Young, M. P. (1996). Visual motion processing in the anterior ectosylvian sulcus of the cat. *J. Neurophysiol.* 76, 895–907.

Schnupp, J. W. H., and King, A. J. (1997). Coding for auditory space in the nucleus of the brachium of the inferior colliculus in the ferret. *J. Neurophysiol.* 78, 2717–2731.

Serizawa, M., McHaffie, J. G., Hoshino, K., and Norita, M. (1994). Corticostriatal and corticotectal projections from visual cortical areas 17, 18 and 18a in the pigmented rat. *Arch. Histol. Cytol.* 57, 493–507.

Sprague, J. M., and Meikle, Th. Jr. (1965). The role of the superior colliculus in visually guided behavior. *Exp. Neurol.* 11, 115–146.

Stecker, G. C., Harrington, I. A., Macpherson, E. A., and Middlebrooks, J. C. (2005). Spatial sensitivity in the dorsal zone (area DZ) of cat auditory cortex. *J. Neurophysiol.* 94, 1267–1280.

Stein, B. E. (1978). Nonequivalent visual, auditory, and somatic corticotectal influences in cat. *J. Neurophysiol.* 41, 55–64.

Stein, B. E. (1998). Neural mechanisms for synthesizing sensory information and producing adaptive behaviors. *Exp. Brain Res.* 123, 124–135.

Stein, B. E., and Meredith, M. A. (1991). "Functional organization of the superior colliculus," in *The Neural Basis of Visual Function*, ed. A. G. Leventhal (Hampshire: Macmillan), 85–110.

Swadlow, H. A., and Weyand, T. G. (1981). Efferent systems of the rabbit visual cortex: laminar distribution of the cells of origin, axonal conduction velocities, and identification of axonal branches. *J. Comp. Neurol.* 203, 799–822.

Thompson, G. C., and Masterton, R. B. (1978). Brain stem auditory pathways involved in reflexive head orientation to sound. *J. Neurophysiol.* 41, 1183–1202.

Tigges, J., and Tigges, M. (1981). Distribution of retinofugal and corticofugal axon terminals in the superior colliculus of squirrel monkey. *Invest. Ophthalmol. Vis. Sci.* 20, 149–158.

Tunkl, J. E. (1980). Location of auditory and visual stimuli in cats with superior colliculus ablations. *Exp. Neurol.* 68, 395–402.

Wallace, M. N., Roeda, D., and Harper, M. S. (1997). Deoxyglucose uptake in the ferret auditory cortex. *Exp. Brain Res.* 117, 488–500.

Wallace, M. T., Meredith, M. A., and Stein, B. E. (1993). Converging influences from visual, auditory, and somatosensory cortices onto output neurons of the superior colliculus. *J. Neurophysiol.* 69, 1797–1809.

Wallace, S. F., Rosenquist, A. C., and Sprague, J. M. (1990). Ibotenic acid lesions of the lateral substantia nigra restore visual orientation behavior in the hemianopic cat. *J. Comp. Neurol.* 296, 222–252.

Winer, J. A., Larue, D. T., Diehl, J. J., and Hefti, B. J. (1998). Auditory cortical projections to the cat inferior colliculus. *J. Comp. Neurol.* 400, 147–174.

Yu, L., Stein, B. E., and Rowland, B. A. (2009). Adult plasticity in multisensory neurons: short-term experience-dependent changes in the superior colliculus. *J. Neurosci.* 29, 15910–15922.

Conflict of Interest Statement: The authors declare that the research was conducted in the absence of any commercial or financial relationship that could be construed as a potential conflict of interest.

Received: 15 January 2010; paper pending published: 15 February 2010; accepted: 23 April 2010; published online: 21 May 2010.

Citation: Bajo VM, Nodal FR, Bizley JK and King AJ (2010) The non-lemniscal auditory cortex in ferrets: convergence of corticotectal inputs in the superior colliculus. Front. Neuroanat. ***4****:18. doi: 10.3389/fnana.2010.00018*

frontiers in
NEUROANATOMY

REVIEW ARTICLE
published: 21 September 2010
doi: 10.3389/fnana.2010.00134

Development of parallel auditory thalamocortical pathways for two different behaviors

Khaleel A. Razak[1] and Zoltan M. Fuzessery[2]*

[1] *Department of Psychology, University of California, Riverside, CA, USA*
[2] *Department of Zoology and Physiology, University of Wyoming, Laramie, WY, USA*

Edited by:
Enrique Saldaña, Universidad de Salamanca, Spain

Reviewed by:
Andrew J. King, University of Oxford, UK
Douglas C. Fitzpatrick, The University of North Carolina at Chapel Hill, USA

***Correspondence:**
Zoltan M. Fuzessery, Department of Zoology and Physiology, University of Wyoming, 1000 East University Avenue, Laramie, WY 82071 USA.
e-mail: zmf@uwyo.edu

Auditory thalamocortical connections are organized as parallel pathways that originate in different divisions of the medial geniculate body (MGB). These pathways may be involved in different functions. Surprisingly little is known about the development of these connections. Here we review studies of the organization and development of auditory thalamocortical pathways in the pallid bat. The pallid bat depends primarily on passive hearing of prey-generated noise for localizing prey, while reserving echolocation for general orientation and obstacle avoidance. In the inferior colliculus (IC) and the auditory cortex, physiological studies show that noise and echolocation calls are processed in segregated regions. Injection of retrograde tracers in physiologically characterized cortical sites show that the ventral division of the MGB (MGBv) projects to the cortical region selective for noise. The cortical region selective for echolocation calls receives input from the suprageniculate (SG) nucleus in the dorsal MGB, but not from the MGBv. Taken together, these studies reveal parallel IC–MGB–cortex pathways involved in echolocation and passive listening. There is overlap of thalamocortical pathways during development. At 2-weeks postnatal, when the bat begins to exhibit adult-like hearing thresholds, the SG projects to both noise- and echolocation call-selective regions. The MGBv, as in adults, projects only to the noise-selective region. The connections become adult-like only after 2-months postnatal. These data suggest that parallel auditory thalamocortical pathways may segregate in an experience-dependent fashion, a hypothesis that remains to be tested in any species.

Keywords: auditory cortex, medial geniculate body, auditory development, plasticity, parallel pathways, echolocation, thalamocortical

PARALLEL AUDITORY THALAMOCORTICAL PATHWAYS

A hallmark of sensory system organization is parallel pathways. In the auditory system, auditory nerve fibers diverge into different divisions of the cochlear nucleus setting the stage for multiple ascending pathways. At the thalamocortical level, parallel pathways arise from three distinct divisions of the medial geniculate body (MGB; for review see Winer et al., 2005). These parallel pathways are purported to serve different functions in hearing. Thalamocortical connections include a tonotopic pathway through the MGBv (ventral division) which forms the cortical substrate for functional subregions within isofrequency contours (reviewed in Read et al., 2002). The pathway through the MGBm (medial division) is implicated in multisensory integration and learning (Wepsic, 1966; Edeline and Weinberger, 1992; Bordi and LeDoux, 1994; for review see Hu, 2003). The non-tonotopic pathway through the MGBd (dorsal division, Raczkowski et al., 1976; Andersen et al., 1980; Morel and Imig, 1987; for review see Imig and Morel, 1983; Rouiller, 1997) may be involved in representing complex sounds (Aitkin and Dunlop, 1968).

The hypothesis that parallel thalamocortical pathways are involved in different aspects of hearing is supported by studies in three species of bats from different families: the mustached bat (*Pteronotus parnellii*; Mormoopidae family), the horseshoe bat (*Rhinolophus rouxi*; Rhinolophidae family) and the pallid bat (*Antrozous pallidus*; Vespertilionidae family). The mustached bat auditory cortex contains a primary auditory cortex (A1) with a tonotopic map (reviewed in Suga, 1989). This map, as in all other species examined, receives input from the MGBv. Some specializations for echolocation, such as over-representation of dominant harmonic frequencies of the echolocation call, are present in this pathway, but within the context of tonotopic representation. Information relevant to target distance is represented by delay-tuned combination-sensitive neurons. A large delay-tuned area is located dorsal to A1. Smaller delay-tuned areas are present ventral to A1. Injections of different tracers in different delay-tuned areas label separate regions in the MGB indicating that multiple delay-tuned areas are present in the thalamus (Pearson et al., 2007; also see Wenstrup, 1999 for physiological studies with a similar conclusion) and that each thalamic delay-tuned area representation projects independently, and in parallel, to a cortical delay-tuned area (Pearson et al., 2007). Particularly, labeling was found in the rostral pole nucleus. Although it remains debated whether the rostral pole nucleus should be part of the dorsal division, the lateral part of the posterior group or an extension of the ventral division (Morel and Imig, 1987; Wenstrup et al., 1994; Lee et al., 2004; Pearson et al., 2007), it is clear there are parallel pathways conveying information from the MGB to the cortex.

In the horseshoe bat, the cortical region termed dorsal cortex contains neurons that may be involved in target ranging. These neurons receive input from the MGBd (Radtke-Schuller, 2004;

Radtke-Schuller et al., 2004). The primary auditory cortex receives input from the MGBv. In both the mustached and horseshoe bat the suprageniculate (SG) nucleus, a part of the MGBd, projects diffusely to the entire auditory cortex, with a significant input to non-primary cortical regions involved in processing echolocation calls. Taken together, these data indicate that the thalamocortical pathways that serve fine frequency analysis and target distance calculation in the mustached and horseshoe bat are mostly segregated(**Figure 1A**).

Studies on the pallid bat provide evidence that parallel auditory pathways may represent sounds used in two different behaviors. The pallid bat localizes terrestrial prey by listening to prey-generated noise while reserving echolocation calls for general orientation and obstacle avoidance (Bell, 1982; Fuzessery et al., 1993). For echolocation, it uses a downward frequency modulated (FM) sweep (60 → 30 kHz). For prey localization it depends on noise transients (5–40 kHz). Its auditory cortex and inferior colliculus (IC) are organized to process FM sweeps and noise in mostly segregated regions (Fuzessery, 1994; Razak and Fuzessery, 2002). In the auditory cortex, there is a tonotopic map with frequencies from 5 to 70 kHz. Most neurons with tuning between 5 and 30 kHz respond best to noise transients. This region has been termed the low-frequency region (LFR). Most neurons with tuning between 30 and 60 kHz respond best to downward FM sweeps. This region has been termed the high-frequency region (HFR).

The majority of inputs to the LFR and HFR in adult pallid bats arise from different divisions of the MGB (**Figure 2**, schematized in **Figure 1B**). Placement of retrograde tracers in the LFR labeled neurons predominantly in the MGBv with no label in the SG (Razak et al., 2007). Placement of tracers in the HFR labeled neurons in the SG, but not the MGBv. The MGBm and parts of MGBd outside of the SG send minor projections to both the LFR and the HFR. Thus parallel thalamocortical pathways represent sounds involved in two different behaviors, with the SG → HFR connections putatively involved in echolocation behavior and MGBv → LFR connections putatively involved with passive prey localization.

A SIGNIFICANT GAP IN KNOWLEDGE: DEVELOPMENT OF AUDITORY THALAMOCORTICAL CONNECTIONS

While the existence and functional significance of parallel thalamocortical pathways are established, very little is known about the development of these pathways. The development of these pathways between the MGB and the auditory cortex has been the subject of only one study. Gurung and Fritzsch (2004) found that the MGB innervates the auditory cortex before onset of patterned sensory input. However, whether segregation of MGB-auditory cortex inputs into parallel pathways depends on sensory experience remains unknown. Research on the development of auditory pathways has focused on connections below the thalamus. Studies of connections of the midbrain (Friauf and Kandler, 1990; Gabriele et al., 2000, 2007) and lower brainstem (Leake et al., 2002) suggest that the nucleotopic connections are mostly adult-like before hearing onset. Postnatal refinement or maintenance of connections, perhaps in an activity-dependent manner, is restricted to sharpening tonotopic organization (Kim and Kandler, 2003; Franklin et al., 2006; Leake et al., 2006) and fine tuning bilateral inputs within nuclei involved in sound localization (Kapfer et al., 2002).

DEVELOPMENT OF PARALLEL THALAMOCORTICAL CONNECTIONS IN THE PALLID BAT

The pallid bat is suited to address the development of thalamocortical connections for several reasons. First, as mentioned above, parallel pathways can be linked to representation of different behaviorally relevant sounds. Second, the ontogeny of both echolocation

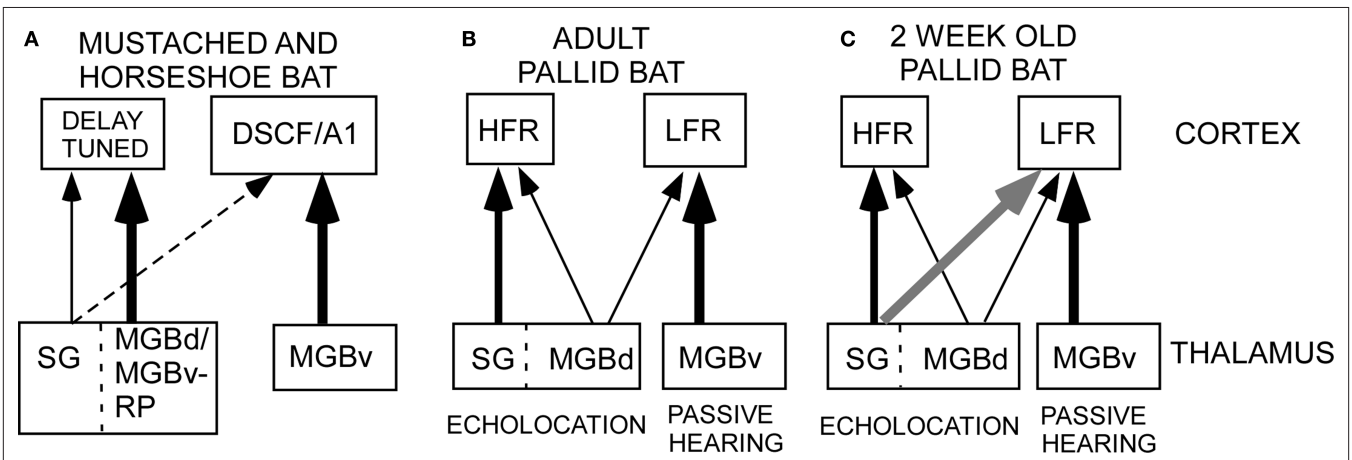

FIGURE 1 | Schematic of thalamocortical pathways in adult mustached, horseshoe and pallid bats and young pallid bat. (A) In the horseshoe bat, the MGBd projects mainly to regions dorsal to A1 that contain the combination-sensitive neurons used in target distance computation. The MGBv projects to A1. In the mustached bat, the rostral pole nucleus projects to the delay-tuned areas. It is not clear if the rostral pole nucleus should be considered a part of the ventral or dorsal MGB. Therefore, the term "MGBd/MGBv-RP" is used in this schematic. In both species, the SG, considered a part of the MGBd, projects diffusely but more to the non-primary cortex than primary cortex. **(B)** In adult pallid bats, the HFR involved in echolocation behavior receives input from the SG and the MGBd, but not the MGBv. The LFR, involved in passive localization, receives input from the MGBv, but not the SG. Based on response selectivity in the auditory cortex, the SG → HFR pathway is involved in echolocation behavior while the MGBv → LFR pathway is involved in passive localization of prey-generated noise. **(C)** In a 2-week-old pallid bat pup, however, the pathways overlap. This is because the SG projects to both the LFR and HFR. The pup MGBv, as in adults, does not project to the HFR. Thus anatomically segregated pathways arise through postnatal refinement of initially overlapping connections.

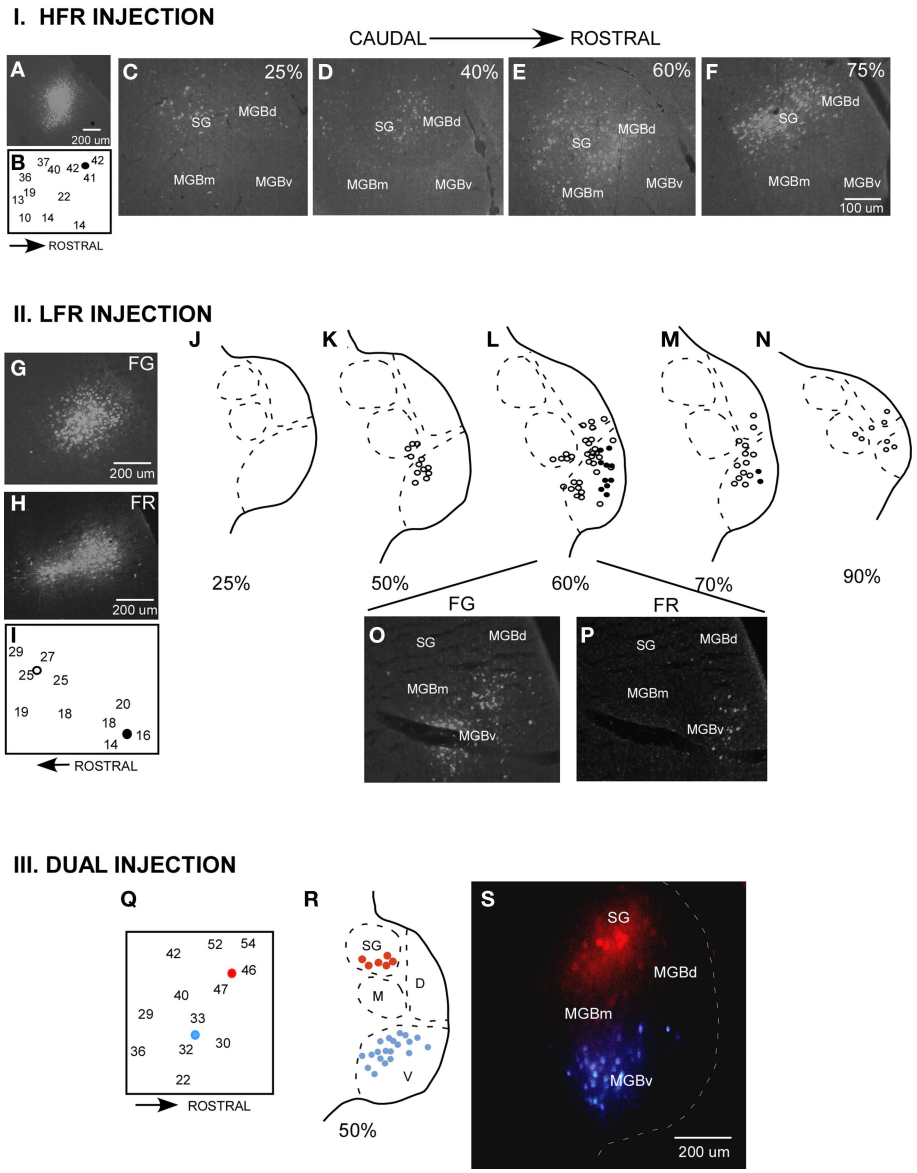

FIGURE 2 | Parallel thalamocortical pathways in the adult pallid bat auditory system. I **(A–F)** An example of injection made in the HFR. **(A)** Fluorogold (FG) injection site. **(B)** Frequency selectivity of injection site. The injection was made near neurons tuned ~42 kHz and selective for downward FM sweeps. **(C–F)** Photomicrographs of increasingly more rostral locations of the MGB show that labeled neurons were found in the SG, MGBm, and MGGd, but not in the MGBv. II **(G–P)** An example of injections made in the LFR. **(G)** FG injection site **(H)** Fluororuby (FR) injection site. **(I)** FG was injected near neurons tuned ~26 kHz. FR was injected near neurons tuned ~15 kHz. **(J–N)** Schematics of increasingly rostral sections through the MGB showing that labeled neurons were found in the MGBv, MGBm, and MGBd, but not the SG. **(O,P)** Photomicrographs showing FG and FR labeled cells near the rostrocaudal center of the MGB. III **(Q–S)** An experiment in which FG was injected in the LFR and FR was injected in the HFR. **(Q)** Schematic of injection sites. **(R)** Schematic of a section at the rostrocaudal center of the MGB showing that FG labeled neurons were present in MGBv, but not the SG, and that FR labeled cells were found in the SG, but not the MGBv. **(S)** Photomicrograph of the section shown in **(R)**.

behavior (Brown et al., 1978) and functional organization of auditory cortex (Razak and Fuzessery, 2007) has been studied. This provides a behavioral framework during development to compare anatomical and physiological data. The overall functional organization of auditory cortex, including frequency representation, is adult-like early in development (Razak and Fuzessery, 2002, 2007). An exception is the prevalence and anatomical distribution of functionally bimodal neurons (Razak et al., 1999). These neurons appear to receive input from both pathways, and have two discrete tuning curves tuned to frequencies used in echolocation and passive sound localization. In adults, these bimodal neurons are found near the interface of the LFR and HFR. In pups, however, they are

more widely distributed (Razak and Fuzessery, 2007), suggesting that projections from the MGBv and SG may show greater overlap in their cortical targets. We tested this hypothesis by retrograde tracing of MGB inputs from physiologically identified injection sites in the LFR and HFR of auditory cortex.

Details about injection method, sizes, and definition of divisions of the MGB have been addressed in detail in the original papers (Razak and Fuzessery, 2007, 2009). Although it was relatively easy to distinguish the SG from rest of the MGBd and MGBv, the boundary between MGBd and MGBv was less obvious based on Nissl or neutral red stains. However, luxol fast blue, neutral red stained sections show that MGBv stains weakly for myelin, whereas the MGBd contains fibers that run in a dorsomedial to ventrolateral direction. The boundary between the dorsal and the ventral divisions was drawn based on myelin staining. The injection sizes are noted in Razak and Fuzessery (2007). A comparison of adult and pup brain photomicrographs shows similar injection sizes for fluroruby and flurogold (**Figures 2 and 3**).

There is greater overlap in thalamocortical connections during early development (Razak et al., 2009). Injections of retrograde tracers in the LFR labeled neurons in both the MGBv and the SG (**Figure 3**, schematic in **Figure 1C**). The input from the SG to LFR was prominent from the caudal half of the MGB, and was at least as strong as the input from the MGBv to the LFR based on the number of labeled neurons. However, as in adults, there was no input from the pup MGBv to the HFR. An overlap of pathways was seen in P60 bats, but not in P150 bats, indicating that the refinement is occurring during this time period. Pallid bats obtain adult-like hearing sensitivity ~2-weeks postnatal. Pallid bats begin to fly and use echolocation in flight around 5–6 weeks (Brown et al., 1978) and are fully weaned around 12 weeks. Thus the refinement occurs a few weeks after flight onset, and more than 6 weeks after onset of adult-like hearing. These data show that the parallel thalamocortical pathways seen in adults emerge during postnatal development and may involve refinement of overlapping connections well after the bat begins to experience patterned input.

WHY PARALLEL PATHWAYS FOR NOISE AND FM SWEEPS?

We have suggested that the parallel pathways for noise and FM sweep processing observed in the IC, MGB, and cortex are an adaptation for gleaning behavior in the pallid bat (Barber et al., 2003). As the bat hunts, it receives both echoes from the flight path and prey-generated noise from the ground. The bat has to segregate these two streams of temporally overlapping inputs. The noise and FM sweeps used in prey localization and echolocation differ in spectral (low versus high frequency), temporal (noise versus sweep), and spatial (ground versus flight path) qualities. These differences should enable the bat to segregate the two sounds (Bregman, 1990). In addition, the parallel processing with strong filters (noise versus FM sweep selectivity) will provide a substrate for additional segregation of the two auditory streams. During development, the onset of adult-like hearing thresholds may not be the critical experience for initiation of segregated pathways. The experience with dual processing of echoes and terrestrial prey-generated noise may be more important in initiating segregated pathways; therefore refinement occurs when the bat begins to hunt. Such experience-dependent plasticity has been described previously in the barn owl midbrain (Bergan et al., 2005).

A NOTE ON THE SUPRAGENICULATE NUCLEUS

The SG appears to be a phylogenetically and ontogentically malleable region of the thalamus. In non-chiropterans the SG is dominated by visual input from the superior colliculus (cat: Calford and Aitkin, 1983; Katoh and Benedek, 1995; rat: Tanaka et al., 1985). Less than 15% of the neurons respond only to auditory stimuli, whereas 65% of the SG neurons respond to visual stimuli alone (Benedek et al., 1997). The entire rostrocaudal extent of the SG receives input from the superior colliculus (SC) (Katoh and Benedek, 1995). Auditory inputs to the SG may arise from the nucleus of the central acoustic tract in the brainstem and the external nucleus of the IC (Henkel, 1983; Katoh and Benedek, 1995), both of which are considered to be a part of the extralemniscal auditory pathways. The SG projects primarily to non-primary auditory cortical areas, although sparse connections to the primary auditory cortex are found in many species (owl monkey: Morel and Kaas, 1992; macaque monkey: Hackett et al., 1998; tamarin: Luethke et al., 1989; dog: Malinowska and Kosmal, 2003; rat: Roger and Arnault, 1989).

In bats, the SG is dominated by auditory inputs. The SG of the mustached bat, unlike non-chiropterans, receives inputs from all frequency bands of the central nucleus of the IC (Wenstrup et al., 1994). Like non-chiropterans, the SG also receives direct input from the nucleus of the central acoustic tract (Casseday et al., 1989; Gordon and O'Neill, 2000). In addition to broad regions of the auditory cortex, the SG of the mustached bat projects to frontal cortex, which in turn projects to the SC, suggesting a role in acoustic-motor reflexes (Kobler et al., 1987). In the horseshoe bat, the SG projects to both primary and non-primary cortical fields (Radtke-Schuller et al., 2004). There is overlap in projections from the SG and the MGBv to any given cortical region, but the dorsal cortical fields (non-primary) receive most SG inputs. In the pallid bat, the echolocation pathway is primarily routed through the SG. Taken together, these studies suggest that the SG can be taken over to increase thalamic representation of species-specific dominant sensory modalities.

The developmental plasticity of SG connections is illustrated by cross-modal plasticity in ferrets (Pallas et al., 1990). By appropriate lesions of retinal axon targets, visual input can be guided to the MGB. This rewiring leaves the MGBv-primary auditory connections similar to those of controls. However, an anomalous input to the primary auditory cortex arises from the dorsal thalamus, including the SG, in the cross-modal animals. This finding suggests that the SG typically receives and sends more exuberant connections during early development. These connections may be either stabilized or pruned by activity-dependent mechanisms. The data from the pallid bat thalamocortical development support the hypothesis that the SG sends exuberant projections during early development.

FUTURE STUDIES

1. The studies on pallid bat thalamocortical connections suggest postnatal refinement. However, it remains unclear if this is experience-dependent. It is possible to modify echolocation experience during development (Razak et al., 2008). Such modifications significantly alter response selectivity within the

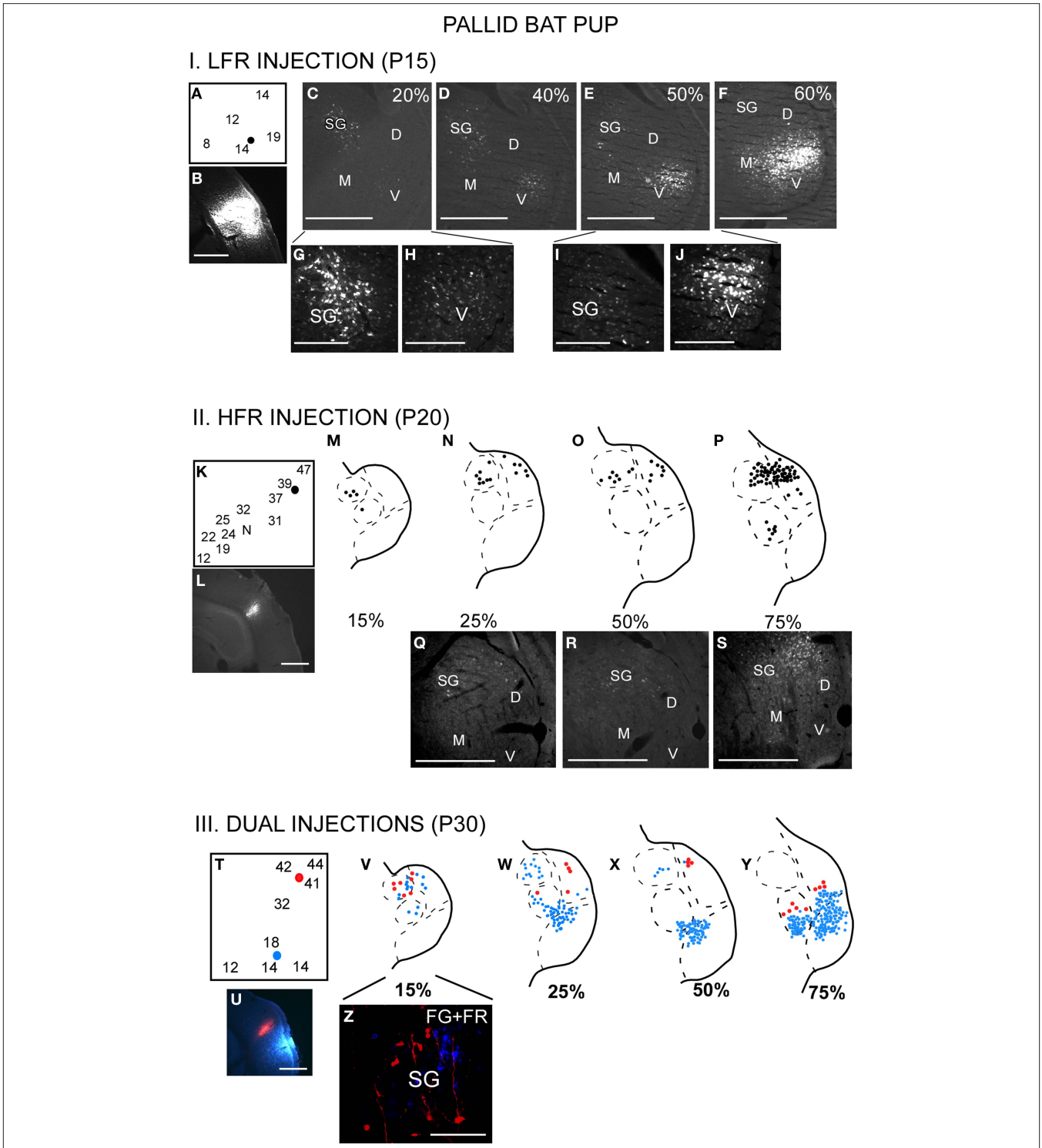

FIGURE 3 | The thalamocortical pathways overlap during early development. This occurs because the SG projects to both LFR and HFR in pups. I **(A–J)** LFR injection in a P15 pup. **(A)** FG was injected in the LFR near sites with tuning ~15 kHz. **(B)** FG injection site. **(C–F)** Photomicrographs of increasingly rostral sections through the MGB demonstrate that both the SG and MGBv show labeled cells. **(G,H)** Magnified view of the SG and **(I,J)** MGBv show strong label in both areas. It can also be noted that caudal SG sends more projections to the LFR in pups than rostral SG. II **(K–S)** HFR injection in a P20 pup. **(K)** The injection site had best frequencies near 40 kHz. **(L)** FG injection site. **(M–P)** Schematic and **(Q–S)** Photomicrographs of the MGB show that labeled cells were present in the SG and MGBd, but not the MGBv. III **(T–Z)** Injections in both LFR and HFR. **(T)** FG was injected in the LFR. FR was injected in the HFR. **(U)** Injection sites. **(V–Y)** FG and FR labeled cells were seen in the SG, while only FG labeled cells were seen in the MGBv. **(Z)** Magnified view of the SG shows FG and FR labeled cells, although no double labeled cells were seen. Scale bars: 500 μm in **B–F**; 200 μm in **G–J**.

echolocation pathway. Future studies will address how refinement of pathways proceeds in bats with altered experience with echolocation calls.

2. Although several studies have focused on development of auditory pathways below the thalamus, the pallid bat is the only animal we are aware of in which postnatal development of auditory thalamocortical connections has been examined. Therefore it remains unclear if the postnatal refinement of parallel thalamocortical pathways is a general phenomenon. In animals, such as the cat, in which the adult auditory pathways have been well characterized, studies are required on the development of these pathways. Significantly more is known about development of visual and somatosensory thalamocortical pathways.
3. A key hypothesis to emerge based on physiological and anatomical studies of the pallid bat auditory system is that in gleaning bats, parallel pathways from the IC–MGB–cortex represent different sounds used in different behaviors. This hypothesis is supported by physiological studies in the IC of *Megaderma lyra*, another gleaning bat from a different family (Rubsamen et al., 1988). Gleaning as a hunting strategy appears to have evolved independently in different families of bats. If parallel pathways are an adaptation for gleaning in the pallid bat, then a similar organization of the auditory system must be present in other gleaning bats. This hypothesis of convergent evolution of the auditory system remains to be tested. One unusual aspect of the pallid bat thalamocortical connections is that the cortical tonotopic map is composed of non-overlapping inputs from two different divisions of the MGB (Razak et al., 2007). The presence of such an organization in other gleaners will strongly suggest a modified thalamocortical plan in gleaners compared to other mammals, including obligate echolocating bats.
4. The molecular mechanisms that make the SG ontogenetically and phylogentically labile are unknown. Recent studies that compared FOXP2 expression between echolocating and non-echolocating bats identified the SG as one of the nuclei in which expression was higher in the echolocators (Berquist et al., SFN abstracts, 2009). Expression of FOXP2 in the MGB also changes in an activity-dependent manner (Horng et al., 2009). FOXP2 may therefore be a part of the molecular milieu of the SG that makes it developmentally and evolutionarily more labile. Future studies comparing the expression of FOXP2 across various divisions of the MGB will be useful in determining the mechanisms of SG malleability and to address mechanisms underlying connectional and therefore functional plasticity in the thalamocortical connections.

ACKNOWLEDGMENTS

We thank T. Zumsteg for valuable comments on the manuscript and G. McLellan for programming the software required for this study. This research was supported by an NIDCD grant DC05202 and INBRE P20 RR0 16474-04.

REFERENCES

Aitkin, L. M., and Dunlop, C. W. (1968). Interplay of excitation and inhibition in the cat medial geniculate body. *J. Neurophysiol.* 31, 44–61.

Andersen, R. A., Knight, P. J., and Merzenich, M. M. (1980). The thalamocortical and corticothalamic connections AI, AII, and the anterior auditory field (AAF) in the cat: Evidence for two largely segregated systems of connections. *J. Comp. Neurol.* 194, 663–701.

Barber, J. R., Razak, K. A., and Fuzessery, Z. M. (2003). Can two streams of auditory information be processed simultaneously? Evidence from the gleaning bat Antrozous pallidus. *J. Comp. Physiol. A* 189, 843–855.

Bell, G. P. (1982). Behavioral and ecological aspects of gleaning by the desert insectivorous bat, Antrozous pallidus (Chiroptera: Vespertilionidae). *Behav. Ecol. Sociobiol. (Print)* 10, 217–223.

Benedek, G., Pereny, J., Kovacs, G., Fischer-Szatmari, L., and Katoh, Y. Y. (1997). Visual, somatosensory, auditory and nociceptive modality properties in the feline suprageniculate nucleus. *Neuroscience* 78, 179–189.

Bergan, J. F., Ro, P., Ro, D., and Knudsen, E. I. (2005). Hunting increases adaptive auditory map plasticity in adult barn owls. *J. Neurosci.* 25, 9816–9820.

Bordi, F., and LeDoux, J. E. (1994). Response properties of single units in areas of rat auditory thalamus that project to the amygdala. II. Cells receiving convergent auditory and somatosensory inputs and cells antidromically activated by amygdala stimulation. *Exp. Brain Res.* 98, 275–286.

Bregman, A. S. (1990). *Auditory Scene Analysis*. Cambridge, MA: MIT Press.

Brown, P., Grinnell, A. D., and Harrison, J. (1978). The development of hearing in the pallid bat, *Antrozous pallidus*. *J. Comp. Physiol. A* 126, 169–182.

Calford, M. B., and Aitkin, L. M. (1983). Ascending projections to the medial geniculate body of the cat: Evidence for multiple, parallel auditory pathways through thalamus. *J. Neurosci.* 3, 2365–2380.

Casseday, J. H., Kobler, J. B., Isbey, S. F., and Covey, E. (1989). Central acoustic tract in an echolocating bat: An extralemniscal auditory pathway to the thalamus. *J. Comp. Neurol.* 287, 247–259.

Edeline, J.-M., and Weinberger, N. M. (1992). Associative retuning in the thalamic source of input to the amygdala and auditory cortex: Receptive field plasticity in the medial division of the medial geniculate body. *Behav. Neurosci.* 106, 81–105.

Franklin, S. R., Brunso-Bechtold, J. K., and Henkel, C. K. (2006). Unilateral cochlear ablation before hearing onset disrupts the maintenance of dorsal nucleus of the lateral lemniscus projection patterns in the rat inferior colliculus. *Neuroscience* 143, 105–115.

Friauf, E., and Kandler, K. (1990). Auditory projections to the inferior colliculus of the rat are present by birth. *Neurosci. Lett.* 120, 58–61.

Fuzessery, Z. M. (1994). Response selectivity for multiple dimensions of frequency sweeps in the pallid bat inferior colliculus. *J. Neurophysiol.* 72, 1061–1079.

Fuzessery, Z. M., Buttenhoff, P., Andrews, B., and Kennedy, J. M. (1993). Passive sound localization of prey by the pallid bat (Antrozous p. *pallidus*). *J. Comp Physiol. [A]* 171, 767–777.

Gabriele, M. L., Brunso-Bechtold, J. K., and Henkel, C. K. (2000). Development of afferent patterns in the inferior colliculus of the rat: Projection from the dorsal nucleus of the lateral lemniscus. *J. Comp. Neurol.* 416, 368–382.

Gabriele, M. L., Shahmoradian, S. H., French, C. C., Henkel, C. K., and McHaffie, J. G. (2007). Early segregation of layered projections from the lateral superior olivary nucleus to the central nucleus of the inferior colliculus in the neonatal cat. *Brain Res.* 1173, 66–77.

Gordon, M., and O'Neill, W. E. (2000). An extralemniscal component of the mustached bat inferior colliculus selective for direction and rate of linear frequency modulations. *J. Comp. Neurol.* 426, 165–181.

Gurung, B., and Fritzsch, B. (2004). Time course of embryonic midbrain and thalamic auditory connection development in mice as revealed by carbocyanine dye tracing. *J. Comp. Neurol.* 479, 309–327.

Hackett, T. A., Stepniewska, I., and Kaas, J. H. (1998). Thalamocortical connections of the parabelt auditory cortex in macaque monkeys. *J. Comp. Neurol.* 400, 271–286.

Henkel, C. K. (1983). Evidence of subcollicular auditory projections to the medial geniculate nucleus in the cat: An autoradiographic and horseradish peroxidase study. *Brain Res.* 259, 21–30.

Horng, S., Kreiman, G., Ellsworth, C., Page, D., Blank, M., Millen, K., and Sur, M. (2009). Differential gene expression in the developing lateral geniculate nucleus and medial geniculate nucleus reveals novel roles for Zic4 and Foxp2 in visual and auditory pathway development. *J. Neurosci.* 29, 13672–13683.

Hu, B. (2003). Functional organization of lemniscal and nonlemniscal auditory thalamus. *Exp. Brain Res.* 153, 543–549.

Imig, T. J., and Morel, A. (1983). Organization of the thalamocortical

auditory system in the cat. *Annu. Rev. Neurosci.* 6, 95–120.

Kapfer, C., Seidl, A. H., Schweizer, H., and Grothe, B. (2002). Experience-dependent refinement of inhibitory inputs to auditory coincidence-detector neurons. *Nat. Neurosci.* 5, 247–253.

Katoh, Y. Y., and Benedek, G. (1995). Organization of the colliculosuprageniculate pathway in the cat: A wheat germ agglutinin-horseradish peroxidase study. *J. Comp. Neurol.* 352, 381–397.

Kim, G., and Kandler, K. (2003). Elimination and strengthening of glycinergic/GABAergic connections during tonotopic map formation. *Nat. Neurosci.* 6, 282–290.

Kobler, J. B., Isbey, S. F., and Casseday, J. H. (1987). Auditory pathways to the frontal cortex of the mustache bat, *Pteronotus parnellii. Science* 236, 824–826.

Leake, P. A., Hradek, G. T., Chair, L., and Snyder, R. L. (2006). Neonatal deafness results in degraded topographic specificity of auditory nerve projections to the cochlear nucleus in cats. *J. Comp. Neurol.* 497, 13–31.

Leake, P. A., Snyder, R. L., and Hradek, G. T. (2002). Postnatal refinement of auditory nerve projections to the cochlear nucleus in cats. *J. Comp. Neurol.* 448, 6–27.

Lee, C. C., Imaizumi, K., Schreiner, C. E., and Winer, J. A. (2004). Concurrent tonotopic processing streams in auditory cortex. *Cereb. Cortex* 14, 441–451.

Luethke, L. E., Krubitzer, L. A., and Kaas, J. H. (1989). Connections of primary auditory cortex in the New World monkey, *Saguinus. J. Comp. Neurol.* 285, 487–513.

Malinowska, M., and Kosmal, A. (2003). Connections of the posterior thalamic region with the auditory ectosylvian cortex in the dog. *J. Comp. Neurol.* 467, 185–206.

Morel, A., and Imig, T. J. (1987). Thalamic projections to fields A, A1, P and VP in cat auditory cortex. *J. Comp. Neurol.* 265, 119–144.

Morel, A., and Kaas, J. H. (1992). Subdivisions and connections of auditory cortex in owl monkeys. *J. Comp. Neurol.* 318, 27–63.

Pallas, S. L., Roe, A. W., and Sur, M. (1990). Visual projections induced into the auditory pathway of ferrets. I. Novel inputs to primary auditory cortex (AI) from the LP/pulvinar complex and the topography of the MGN-AI projection. *J. Comp. Neurol.* 298, 50–68.

Pearson, J. M., Crocker, W. D., and Fitzpatrick, D. C. (2007). Connections of functional areas in the mustached bat's auditory cortex with the auditory thalamus. *J. Comp. Neurol.* 500, 401–418.

Raczkowski, D., Diamond, I. T., and Winer, J. A. (1976). Organization of thalamocortical auditory system in the cat studied with horseradish peroxidase. *Brain Res.* 101, 345–354.

Radtke-Schuller, S., Schuller, G., and O'Neill, W. E. (2004). Thalamic projections to the auditory cortex in the rufous horseshoe bat (*Rhinolophys rouxi*). II. Dorsal fields. *Anat. Embryol.* 209, 77–79.

Razak, K. A., and Fuzessery, Z. M. (2002). Functional organization of the pallid bat auditory cortex: Emphasis on binural organization. *J. Neurophysiol.* 87, 72–86.

Razak, K. A., and Fuzessery, Z. M. (2007). Development of functional organization of the pallid bat auditory cortex. *Hearing Res.* 228, 69–81.

Razak, K. A., Fuzessery, Z. M., and Lohuis, T. D. (1999). Single cortical neurons serve both echolocation and passive sound localization. *J. Neurophysiol.* 81, 1438–1442.

Razak, K. A., Richardson, M. D., and Fuzessery, Z. M. (2008). Experience is required for the maintenance and refinement of FM sweep selectivity in the developing auditory cortex. *Proc. Natl. Acad. Sci. U.S.A.* 105, 4465–4470.

Razak, K. A., Shen, W., Zumsteg, T., and Fuzessery, Z. M. (2007). Parallel thalamocortical pathways for echolocation and passive sound localization in a gleaning bat, Antrozous pallidus. *J. Comp. Neurol.* 500, 322–338.

Razak, K. A., Zumsteg, T., and Fuzessery, Z. M. (2009). Development of auditory thalamocortical connections in the pallid bat, *Antrozous pallidus. J. Comp. Neurol.* 515, 231–242.

Read, H. L., Winer, J. A., and Schreiner, C. E. (2002). Functional architecture of auditory cortex. *Curr. Opin. Neurobiol.* 12, 433–440.

Roger, M., and Arnault, P. (1989). Anatomical study of the connections of the primary auditory area in the rat. *J. Comp. Neurol.* 287, 339–356.

Radtke-Schuller, S. (2004). Cytoarchitecture of the medial geniculate body and thalamic projections to the auditory cortex in the rufous horseshoe bat (*Rhinolophus rouxi*). I. Temporal fields. *Anat. Embryol.* 209, 59–76.

Radtke-Schuller, S., Schuller, G., and O'Neill, W. E. (2004). Thalamic projections to the auditory cortex in the rufous horseshoe bat (*Rhinolophus rouxi*). II. Dorsal fields. *Anat. Embryol.* 209, 77–91.

Rouiller, E. M. (1997). "Functional organization of the auditory pathways," in *The Central Auditory System*, eds G. Ehret and R. Romand (New York: Oxford University Press), 3–96.

Rubsamen, R., Neuweiler, G., and Sripathi, K. (1988). Comparative collicular tonotopy in two bat species adapted to movement detection, *Hipposideros speoris* and *Megaderma lyra. J. Comp. Physiol. A* 163, 271–285.

Suga, N. (1989). Principles of auditory information-processing derived from neuroethology. *J. Exp. Biol.* 146, 277–286.

Tanaka, K., Otani, K., Tokunaga, A., and Sugita, S. (1985). The reciprocal connections of the suprageniculate nucleus and the superior colliculus in the rat. *Neurosci. Res.* 3, 79–85.

Wepsic, J. G. (1966). Multimodal sensory activation of cells in the magnocellular medial geniculate nucleus. *Exp. Neurol.* 15, 299–318.

Wenstrup, J. J. (1999). Frequency organization and responses to complex sounds in the medial geniculate body of the mustached bat. *J. Neurophysiol.* 82, 2528–2544.

Wenstrup, J. J., Larue, D. T., and Winer, J. A. (1994). Projections of physiologically defined subdivisions of the inferior colliculus in the mustached bat: Targets in the medial geniculate body and extrathalamic nuclei. *J. Comp. Neurol.* 346, 207–236.

Winer, J. A., Miller, L. M., Lee, C. C., and Schreiner, C. E. (2005). Auditory thalamocortical transformation: structure and function. *Trends Neurosci.* 28, 255–263.

Conflict of Interest Statement: The authors declare that research was conducted in the absence of any commercial or financial relationships that could be construed as potential conflict of interest.

Received: 15 January 2010; paper pending published: 03 August 2010; accepted: 29 August 2010; published online: 21 September 2010.

Citation: Razak KA and Fuzessery ZM (2010) Development of parallel auditory thalamocortical pathways for two different behaviors. Front. Neuroanat. ***4****:134. doi: 10.3389/fnana.2010.00134*

frontiers in
NEUROANATOMY

REVIEW ARTICLE
published: 08 October 2010
doi: 10.3389/fnana.2010.00129

Anatomical pathways for auditory memory in primates

Monica M. Munoz-Lopez*, Alicia Mohedano-Moriano and Ricardo Insausti

Human Neuroanatomy Laboratory, Department of Health Sciences, School of Medicine, University of Castilla-La Mancha, Albacete, Spain

Edited by:
Enrique Saldaña, Universidad de Salamanca, Spain

Reviewed by:
Jon H. Kaas, Vanderbilt University, USA
Marcello G. Rosa, Monash University, Australia

****Correspondence:***
Monica M. Munoz-Lopez, Human Neuroanatomy Laboratory, Department of Health Sciences, School of Medicine, University of Castilla-La Mancha, Ave. Almansa, 14,02006 Albacete, Spain.
e-mail: monica.munozlopez@uclm.es

Episodic memory or the ability to store context-rich information about everyday events depends on the hippocampal formation (entorhinal cortex, subiculum, presubiculum, parasubiculum, hippocampus proper, and dentate gyrus). A substantial amount of behavioral-lesion and anatomical studies have contributed to our understanding of the organization of how visual stimuli are retained in episodic memory. However, whether auditory memory is organized similarly is still unclear. One hypothesis is that, like the "visual ventral stream" for which the connections of the inferior temporal gyrus with the perirhinal cortex are necessary for visual recognition in monkeys, direct connections between the auditory association areas of the superior temporal gyrus and the hippocampal formation and with the parahippocampal region (temporal pole, perhirinal, and posterior parahippocampal cortices) might also underlie recognition memory for sounds. Alternatively, the anatomical organization of memory could be different in audition. This alternative "indirect stream" hypothesis posits that, unlike the visual association cortex, the majority of auditory information makes one or more synapses in intermediate, polymodal areas, where they may integrate information from other sensory modalities, before reaching the medial temporal memory system. This review considers anatomical studies that can support either one or both hypotheses – focusing on anatomical studies on the primate brain, primarily in macaque monkeys, that have reported not only direct auditory association connections with medial temporal areas, but, importantly, also possible indirect pathways for auditory information to reach the medial temporal lobe memory system.

Keywords: episodic memory, auditory memory, non-human primate, neuroanatomy, medial temporal cortex, cortical input, subcortical input

Abbreviations: 7a, area 7a of the inferior parietal cortex; 23, area 23 (Brodmann, 1909); 24, area 24 (Brodmann, 1909); 25, area 25 (Brodmann, 1909); 32, area 32 (Brodmann, 1909); 35, area 35 of the perirhinal cortex (Brodmann, 1909); 36r, rostral division of area 36 of the perirhinal cortex (Insausti et al., 1987a); 36c, caudal division of area 36 of the perirhinal cortex (Insausti et al., 1987a); 36pl, lateral portion of the temporal pole (Insausti et al., 1987a,b); 36pm, medial portion of the temporal pole (Insausti et al., 1987a,b) 36p-dm, dorsal division of the temporal pole (*Macaca mulatta*); 36p-vm, ventral medial divisions of the temporal pole (*Macaca mulatta*); 38DL, dorsal lateral division of the temporal pole; 38VL, ventral lateral division of the temporal pole; A, amygdala; A1, area A1 (Kaas and Hackett, 2000); AL, area AL (Kaas and Hackett, 2000); amts, anterior middle temporal sulcus; cc, corpus callosum; cis, cingulate sulcus; CA1, field CA1 of the hippocampus; CA2, field CA2 of the hippocampus; CA3, field CA3 of the hippocampus; CL, area CL (Kaas and Hackett, 2000); CM, area CM (Kaas and Hackett, 2000); DM, area DM (Kaas and Hackett, 2000); EC, entorhinal cortex; $E_{C,}$ caudal subfield of EC (Amaral et al., 1987); $E_{CL,}$ caudal limiting subfield of EC (Amaral et al., 1987); $E_{I,}$ intermediate subfield of EC (Amaral et al., 1987); $E_{LC,}$ lateral caudal subfield of EC (Amaral et al., 1987); $E_{Lr,}$ lateral rostral subfield of EC (Amaral et al., 1987); $E_{O,}$ olfactory subfield of EC (Amaral et al., 1987); $E_{R,}$ rostral subfield of EC (Amaral et al., 1987); DG, dentate gyrus; CA1, area CA1 of the hippocampus; Ia, insula; IPa, area IPa of Seltzer and Pandya (1978, 1989); Ls, lateral sulcus; MM, area MM (Kaas and Hackett, 2000); PaI, Parainsular cortex; PGa, area PGa of Seltzer and Pandya (1978, 1989); pmts, posterior medial temporal sulcus; Pul, Pulvinar; R, area R (Kaas and Hackett, 2000); RM, area RM (Kaas and Hackett, 2000); rs, rhinal sulcus; RT, area RT (Kaas and Hackett, 2000); RTL, area RTL (Kaas and Hackett, 2000); RTM, area RTM (Kaas and Hackett, 2000); STG, superior temporal gyrus; STGf, fundus of the STG (Insausti et al., 1987a); STGi, intermediate division of the STG (Insausti et al., 1987a); STGm, medial division of the STG (Insausti et al., 1987a); STGo, opercular division of the STG (Insausti et al., 1987a); STGp, posterior division of the STG (Insausti et al., 1987a); STGr, radial division of the STG (Insausti et al., 1987a); sts, superior temporal sulcus; Sub, subiculum; TAa of Seltzer and Pandya (1978, 1989); TE, area TE of Von Bonin and Bailey (1947); TF, area TF of Von Bonin and Bailey (1947); TFl, lateral division of area TF (Insausti et al., 1987a); TFm, lateral division of area TF (Insausti et al., 1987a); TH, area TH of Von Bonin and Bailey (1947); Thal, thalamus; THc, caudal division of area TH (Insausti et al., 1987a); THr, rostral division of area TH (Insausti et al., 1987a); TP, temporal pole; TPO of Seltzer and Pandya (1978, 1989); Tpt, area Tpt of Seltzer and Pandya (1978, 1989); Ts1, area Ts1 of Seltzer and Pandya (1978, 1989); Ts2, area Ts2 of Seltzer and Pandya (1978, 1989); Ts3, area Ts3 of Seltzer and Pandya (1978, 1989)

COGNITIVE NEUROSCIENCE OF EPISODIC MEMORY

The aim of this review is to consider the anatomical substrate of auditory memory. We explore two possible questions. First, in analogy with the classic view of visual processing (Mishkin and Ungerleider, 1982): *Is the flow of information in the auditory domain relatively direct and corresponds to a straightforward "auditory ventral stream" leading to memory?* Or, alternatively: *Does auditory information take a more indirect route, with additional synaptic steps, and this makes possible added features of auditory perceptual processing and the integration of auditory information with other sensory modalities, emotion, and motivation?*

Anatomical studies cannot, on their own, differentiate these two views; they do, however, reveal both opportunities and constraints on the manner by which sensory information reaches brain regions involved in memory processing (**Figure 1**).

THE NATURE OF EPISODIC MEMORY

Episodic memory refers to the ability to store information about everyday events and encompasses a complex system of hippocampo–cortical and hippocampo–subcortical connections (Aggleton and Brown, 1999; see Figure 1 in Munoz and Morris, 2009). Unlike other

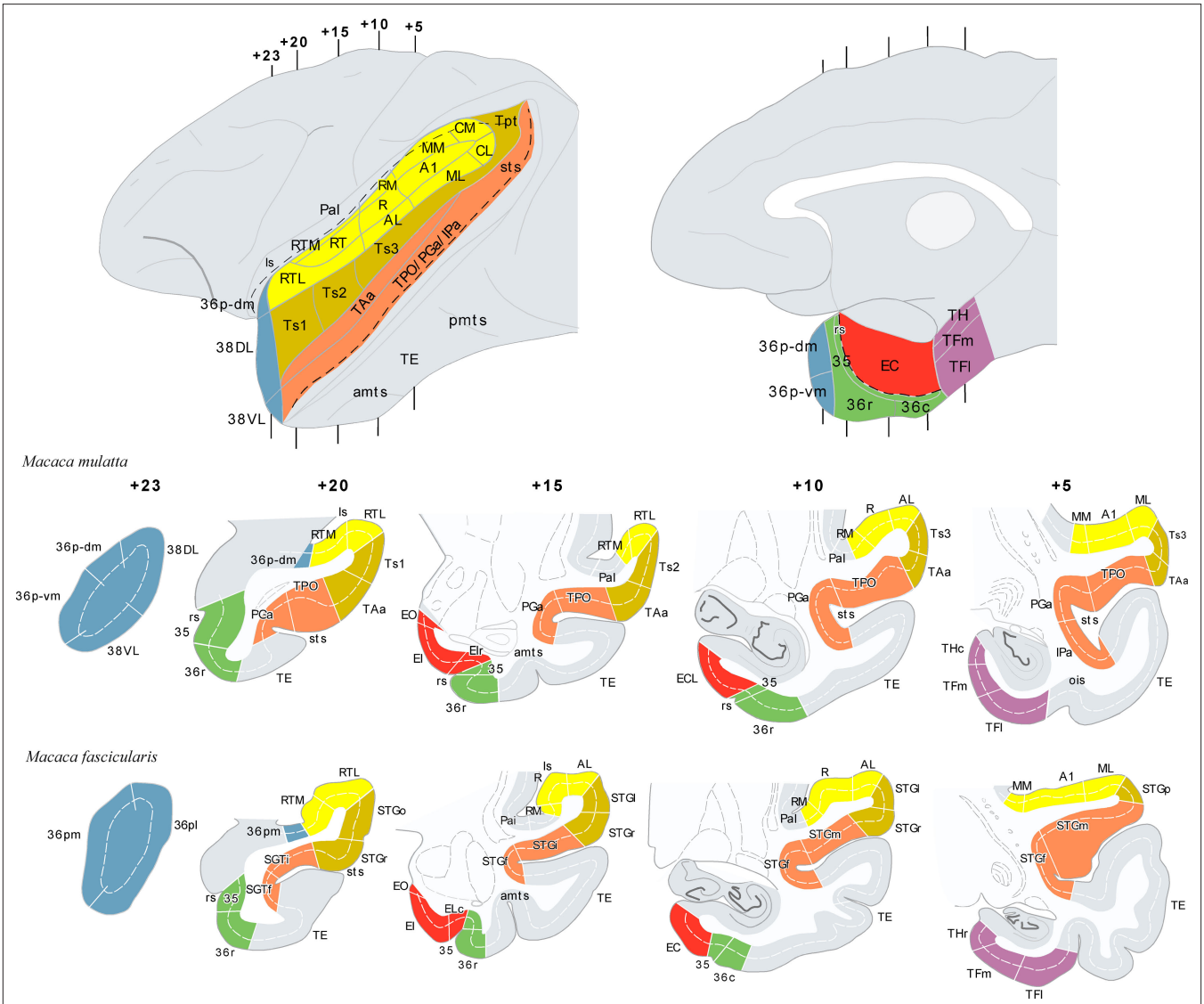

FIGURE 1 | The architectonic divisions of the STG and of the parahippocampal region are illustrated in lateral and medial views of a rhesus monkey brain template (top left and right). Architectonic areas are shown in coronal sections of the rhesus monkey (*Macaca mulatta*) and of the cynomolgus monkey (*M. fascicularis*). Numerals precede by + refer to approximate coronal levels anterior to the interaural plane. See list of abbreviations.

types of memory, as habits or motor skill learning, episodic memory involves the long-term storage, recollection, and retrieval of the "what, where, and when" of everyday events, and yet requires no training. In fact, in contrast to the effortful nature of skill learning, encoding of episodic memory is most often automatic or incidental, whereas retrieval requires conscious effort. This memory system allows us to process and remember information received via different sensory modalities, including the auditory domain. Using it, we can remember, for example, our past holidays, the flavor of our grandmother's cake, the voice of our friends when they phone us, or the sound of our own car.

Episodic memory has been attributed almost exclusively to humans (Suddendorf and Corballis, 1997; Tulving, 2004). However, as the relevant anatomical structures and their connections are shared with other animal species as old phylogenetically as the hedgehog, it is generally assumed that some features of the memory system mediated by them are also shared, even if in more rudimentary form (Insausti, 1993; Burwell et al., 1995). To stress the differences across species, however, the term "episodic-like" memory has been used for monkeys and rodents (see review in Munoz and Morris, 2009). This is relevant in the context of auditory memory, as humans are unique in having communication through language and the auditory memory system may differ significantly from the non-human primate system for this reason. It is interesting that the anatomical organization of memory in both species may tell us something about the evolution of language and communication.

DEVELOPMENT OF BEHAVIORAL TASKS FOR LESION STUDIES IN ANIMALS

One of the challenges in animal research has been to design behavioral tasks that are as close as possible to the episodic memory tests used in neuropsychological assessment with humans. Such tasks are critical to study the anatomical and functional organization

of episodic-like memory in animals. In non-human primates and rodents, episodic memory is often evaluated using trial-unique tasks in which animals have to remember a specific stimulus during a single trial. Each trial requires memory of a different object or image, in a similar way that we experience unique events in everyday life. There is a wide breadth of fascinating tasks, but to describe all of them here would exceed the aim of this review. We summarize one of the critical paradigms from which many different variants have emerged – namely a test of recognition memory. Remembering that you have seen/heard someone or something before is a critical component of episodic memory.

The recognition paradigm extensively used in the study of visual memory is the delayed non-matching to sample task (DNMS). Each trial in this type of task consists in a *sample phase* where the animal familiarizes with an item (visual, tactile, or more recently, auditory) and, after a variable delay, a *choice phase* in which the familiar item is presented again but this time paired with a novel one. Reward is delivered only if the animal chooses the novel item of the two, and so on. The delayed matching to sample task (DMS) is exactly the same, except that the animal is rewarded for choosing the familiar rather than the novel item (and in general is slightly harder). Whereas this type of tasks detect reliably the memory impairment due to perirhinal lesions in animals, variants of this task that involve object–context or object–object associations are more sensitive to hippocampal and entorhinal cortex (EC) lesions. In studies of auditory memory, equivalents of DNMS and DMS have been developed but because two sounds cannot be presented simultaneously in the choice phase without confusion, a sequential protocol originally developed by Konorski (1959) in Poland is adopted using a Go-No Go procedure (Fritz et al., 2005; Wright, 2007).

Back in the seventies, one of the pioneering memory studies in monkeys showed that only lesions that include the hippocampus, amygdala, and the adjacent entorhinal and posterior parahippocampal cortices impaired memory in a visual version of the DNMS task (Mishkin, 1978) in a similar way to humans (Scoville and Milner, 1957). A critical finding was that the lesions only caused memory impairment at long delays, while performance at short delays was normal, suggesting intact perception and working memory, but impaired long-term memory. This seminal study paved the way for detailed use of the DNMS task and its auditory variants to study recognition memory.

THE PERIRHINAL AND POSTERIOR PARAHIPPOCAMPAL CORTICES AND MEMORY

Research since then has shown that amongst the areas included in the original lesion (Mishkin, 1978), EC (area 28 of Brodmann, 1909) and perirhinal cortex (Brodmann's areas 35 and 36) are critical for visual recognition in DNMS tasks in non-human primates (Meunier et al., 1993). The memory deficit observed when these structures are lesioned is delayed-dependent and as severe as that observed in Mishkin's original study.

We now know from retrograde tract tracing studies that the perirhinal cortex receives the majority of its input from visual areas in the inferior temporal cortex (Suzuki and Amaral, 1994a) and sends this information to EC (Insausti et al., 1987a; Suzuki and Amaral, 1994b), from where the information is relayed on to the hippocampus (Witter and Amaral, 1991). A series of connections within the hippocampus characterized by being unidirectional are followed by hippocampal return projections to the cortex primarily via EC, but also directly to the perirhinal cortex (Insausti and Munoz, 2001; Lavenex et al., 2002; Witter and Wouterlood, 2002; Munoz and Insausti, 2005). These connections are thought to be critical for the encoding and long-term consolidation of visual recognition memory.

These neuroanatomical studies reveal the main flow of information underlying visual recognition, but one of the central features of episodic memory is that our memories of events are formed by information received via different sensory modalities (olfactory, somatosensory, auditory as well as visual) and, consequently, episodic memory is often said to be multimodal. Neuroanatomical tract-tracing studies show that, although some sensory-specific information reaches the medial temporal cortex directly (primarily olfactory and visual, as well as, although to a lesser extent, somatosensory and auditory), the great bulk of incoming connections originate in polymodal areas of the neocortex (see review in Mohedano-Moriano et al., 2007) providing our episodic memories with rich, complex contextual information.

WHAT IS DIFFERENT ABOUT AUDITORY MEMORY?

The possibility of multimodal inputs to the episodic-like memory system raises the question of how well matched is the picture emerging from anatomical and behavioral-lesion studies. To address this question, one study showed that lesions including areas 35 and 36 of the perirhinal cortex and the posterior parahippocampal cortex (areas TH and TF of Von Bonin and Bailey, 1947) impaired not only visual memory, but also tactile memory (Suzuki et al., 1993). This was established by conducting the sample and choice phases of the DNMS task in the dark.

At about the same time, an anatomical study showed that a higher order somatosensory area in the granular insular cortex sends projections directly to area 35 of the perirhinal cortex, and suggested that this pathway might be one direct link between the somatosensory and limbic systems (Schneider et al., 1993). This finding led naturally to the idea that this pathway could be critical for the long-term storage of tactile information. Area 35 of the perirhinal cortex also projects heavily to EC (Insausti et al., 1987a), and therefore information coming from area 35 forms part of the hippocampal–cortical loop (Witter and Amaral, 1991).

It appeared, then, that the perirhinal cortex mediates the storage of information in a multimodal way and hence satisfies one of the critical features of episodic memory. The perirhinal cortex became therefore one of the best candidate areas for episodic-like memory in non-human primates. There are important subtleties to this assertion such as whether the perirhinal cortex is involved in *familiarity* and the hippocampus is *recollection* (Brown and Aggleton, 2001; Yonelinas, 2002), but discussion about this subject would again exceed the scope of this review (but see **Table 1**).

Does auditory memory store in the same way as in the visual and somatosensory modalities? Are perirhinal and entorhinal cortices necessary for the formation of auditory memory as they are for visual and tactile memory? It is clear that auditory memory depends on medial temporal areas in humans (Prisko, 1963; Squire and Zola-Morgan, 1991), but work on non-human primates indicates that separate lesions of the hippocampus, of the perirhinal plus entorhinal cortex, or of the posterior parahippocampal cortex each fail to impair auditory recognition memory in a Konorski DMS

Table 1 | Some unresolved issues in the neuroanatomy of auditory memory.

Why is more difficult for monkeys to hold in mind auditory information than visual? Do humans have also more difficulties to store auditory information compared to visual?
Medial frontal cortex, especially area 25, is part of the limbic system that is associated with episodic memory. Is this area also important for auditory memory in primates and humans?
Is there an analogue of the perirhinal cortex important for auditory recognition memory?
Anterior cingulate area 24, prelimbic area 32, and area 25 of the infralimbic cortex may be involved in the production of monkey calls. What is their role in auditory processing?
Are motor patterns, such as those related with the articulation of sounds, important for auditory memory?
In monkeys, the dorsal part of the temporal pole receives its major input from the most rostral part of the superior temporal gyrus, but it also receives afferents from multimodal areas. What is the nature of its involvement in the processing of monkey calls?
What areas the similarities and differences of the auditory processing areas in humans and non-human primates?
What is the role of the amygdalar connections with hippocampal formation and the superior temporal gyrus? And how do they contribute to auditory memory?

task (Fritz et al., 2005). In fact, it is especially difficult for monkeys to hold auditory stimuli in memory for a long enough period of time to be considered outside the timeframe of working memory (Fritz et al., 2005). Furthermore, Fritz et al. (2005) reported that the performance of control monkeys in an auditory DMS task is as poor as monkeys with perirhinal cortex lesions in a visual version of a similar task, suggesting that there may be major differences between auditory and visual memory. The question then is that the delayed-dependent memory impairment seen for vision and touch is difficult to observe in audition – the control subjects showing too much forgetting over time to observe the impact of perirhinal cortex lesions. This immediately raised the possibility of a key difference between humans and non-human primates that, if valid, would be of interest in language research.

However, medial temporal lobe resections, that leave working memory intact in vision in human and non-human primates, critically impair this type of short-term memory in audition (Fritz et al., 2005). A possible explanation for this paradoxical finding comes from a combined lesion and tract tracing study showing that medial temporal removals inadvertently disconnect the rostral part of the superior temporal gyrus (STG) from frontal cortex and thalamus (Munoz et al., 2009). It seems, therefore, that humans and non-human primates may not be so different, but we are left with a puzzle about why auditory memory, as usually tested in the DMS, is so poor in macaques. However, the sounds used as stimuli in the tasks may be a critical variable in solving this puzzle, as suggested by a recent behavioral study (Ng et al., 2009). This study reported significant improvement in the performance of rhesus monkeys in a Go/No-Go DMS task when using species-specific vocalizations as stimuli, compared with non-vocalization sound types (Ng et al., 2009).

To better understand the anatomical organization of auditory memory we consider here a number of major tract tracing studies in the non-human primate brain. These studies reveal evidence for direct (monosynaptic) and indirect connections (two synapses) that finally link the STG with the medial temporal lobe memory system, comprising the hippocampal formation (dentate gyrus, hippocampal fields CA1–3, subiculum, presubiculum, parasubiculum, and EC), and the parahippocampal region (temporal pole, areas 35 and 36 of the perirhinal cortex, and the posterior parahippocampal cortex areas TH and TF of Von Bonin and Bailey, 1947).

ANATOMICAL PATHWAYS FOR AUDITORY MEMORY

Like in vision or touch, direct connections of the auditory cortex with the medial temporal cortex may be critical for the long-term storage of auditory information (Engelien et al., 2000). A better understanding of the auditory cortex anatomical organization may, therefore, contribute to clarify whether memory function is different in audition as compared with the visual and tactile modalities.

ARCHITECTONIC DIVISIONS OF THE STG AND MEDIAL TEMPORAL CORTEX

The amalgam of architectonic divisions comprising the STG and the medial temporal cortex; areas which interaction might be critical for the storage of auditory information are shown in **Figure 1**. The neuroanatomy of these areas has been primarily studied in two species of non-human primates, rhesus (*Macaca mulatta*) and cynomolgus monkeys (*Macaca fascicularis*). They are largely comparable, although there are subtle differences between them in the architectonic organization. The coronal sections shown in **Figure 1** illustrate some of the differences and similarities.

In rhesus monkeys, the STG was described in depth by Pandya et al. (Pandya and Sanides, 1973; Seltzer and Pandya, 1978, 1989) and we have adopted their nomenclature with some modifications. One modification is in relation with the temporal pole (TP), divided here (**Figure 1**) in four subareas: two in the medial surface (36p-dm and 36p-vm), with similar architecture to area 36 of the perirhinal cortex – and corresponding to area 36pm in the *M. fascicularis* (Insausti et al., 1987a) –; and two in the lateral surface (38DL, 38VL), which resemble the architectonics of the adjacent six-layered cortex of the superior and inferior temporal gyri, respectively. These latter divisions have not yet been recognized in the *M. fascicularis* – and corresponding to area 36pl in the *M. fascicularis* (Insausti et al., 1987a).

In the *M. fascicularis*, we have used the cytoarchitectonic divisions of the STG and TP described by Insausti et al. (1987a). As **Figure 1** illustrates two subareas have been described in the TP in this species and they are referred as 36pl and 36pm as they resemble the architectonic organization of area 36 of the perirhinal cortex (Insausti et al., 1987a).

The cytoarchitectonic areas RTL, RT, and RTM, as defined by Kaas and Hackett (2000) can be found in both species for the rostral portion of the supratemporal plane (Kaas and Hackett, 2000), which lies in the ventral bank of the lateral sulcus and differs

cytoarchitectonically from areas Ts1–3/STGo,l,f,p on the adjacent lateral convexity of the rostral part of STG. The remaining auditory core and belt areas (i.e. A1/R, AL, ML, MM, CL, and CM), located caudally in the superior temporal plane, were delineated according to Kaas and Hackett (2000). The cytoarchitectonic subdivisions of the entorhinal, perirhinal, and posterior parahippocampal cortices of Amaral et al. (1987) and Suzuki and Amaral (1994b) were also used for both species.

DIRECT INPUT FROM STG TO MEDIAL TEMPORAL CORTEX

Core (primary) and belt (secondary) areas of the auditory cortex in monkeys are characterized by a high density of reciprocal cortico–cortical connections (Hackett et al., 1998). Connections between belt and parabelt (tertiary) areas of the auditory cortex are also dense, but less well understood. Although rostral and caudal belt areas send projections to prefrontal cortex in rhesus (Romanski et al., 1999a,b) and marmoset monkeys (Roberts et al., 2007), a large proportion of long cortical connections with frontal, temporal, insular, and parietal areas appear to originate primarily in the parabelt areas. In contrast, to parabelt areas, medial temporal cortex connections with core and belt areas have not been reported in the literature so far. The most direct, but not necessarily densest afferent auditory projections to the medial temporal cortex, arise in the lateral parabelt areas of the auditory cortex (see Figure 3 in Amaral et al., 1983).

Apart from the better understood core and belt areas of the auditory cortex (Hackett, 2010), the functional properties of further auditory downstream areas of the STG are only beginning to be revealed by functional imaging studies in rhesus monkeys (Tian et al., 2001; Poremba et al., 2003; Gil-da-Costa et al., 2004, 2006; Poremba et al., 2004; Petkov et al., 2008). However, the neurophysiological features of neurons in the different architectonic areas of the parabelt and areas located just rostral to them, such as the anterior superior temporal plane and the TP, are less known. As a consequence, it is difficult to understand the type of information that is sent to the medial temporal cortex from the STG.

The study by Romanski et al. (1999a) revealed that whereas neurons in the anterior lateral belt show selective responses to particular features of auditory stimuli, neurons in caudal lateral belt have preferential responses to sound location and have different patterns of connections with the frontal cortex. The anterior lateral belt projects to the ventral frontal cortex, whereas the caudal lateral belt is connected with more dorsal aspects of the prefrontal cortex (Romanski et al., 1999b). This suggested that there might be, like in vision, "what" and "where" pathways in the auditory cortex; with the rostral part of the STG as the "what" pathway concerned with the identification of specific features of sounds. In line with this, a recent study showed that the anterior part of the superior temporal plane contains an area that responds specifically to monkey conspecific calls (Petkov et al., 2008). Neurons with species-specific calls have also been found in this area (Kikuchi et al., 2006). Another key area in the auditory ventral stream is the TP, but there is a section dedicated to this question later on in this review.

Entorhinal cortex

Evidence for the rostral STG projection to EC comes primarily from two retrograde tracer studies. The first one, having placed retrograde tracer injections in EC (Amaral et al., 1983), showed that the auditory input to the lateral EC (subfields E_R, E_{Lr}, rostral E_I) receives projections from the gyral surface of the STG. This projecting area in the STG extends from the tip of the TP to the rostral part of the lateral geniculate nucleus, a distance of approximately 10 mm in the *M. fascicularis*. This extent comprises an area that includes caudally the rostral part of the lateral parabelt of the auditory association cortex (area Ts3, see Figure 3 in Amaral et al., 1983). EC also receives projections from the opercular part of the STG (area TAa, Insausti and Amaral, 2008). However, in the study of Amaral et al. (1983), the authors stressed that not all the regions of the STG project equally heavily to EC; in fact, the multimodal area of the dorsal bank of the superior temporal sulcus (area TPO) consistently contained the largest number of retrogradely labeled cells. Amaral et al. (1983), in their report showed that the projection from the STG to EC was organized topographically; so lateral aspects of the STG (areas Ts1–Ts3 and TAa) project to lateral EC (subfields E_R, E_{LR}, and E_I), while more medial or proximal aspects of the STG (area TPO) project to intermediate and caudal levels of EC. This results were confirmed in a latter study concerned with the cortical afferents to EC (Insausti et al., 1987a), which showed additionally that EC receives information from diverse polysensory processing areas of the cerebral cortex, including agranular insula, orbitofrontal, and medial regions of the frontal cortex, retrosplenial cortex, inferior parietal cortex, TP, perirhinal, and posterior parahippocampal cortices (Insausti et al., 1987a; Insausti and Amaral, 2008).

Perirhinal and posterior parahippocampal cortex

Perirhinal and posterior parahippocampal cortices receive their densest input from higher order processing visual areas TE and TEO of the inferior temporal cortex, and the rest from multiple polymodal processing areas of the neocortex; i.e. the dorsal bank of the superior temporal sulcus (area TPO), the opercular area of the STG (TAa), to a lesser extent, from insular, anterior cingulate, medial and orbitofrontal cortex (Suzuki and Amaral, 1994a; Blatt et al., 2003).

In relation with auditory afferents, the rostral part of the STG (areas Ts1–3), including the TP, projects to areas 35 and 36 of the perirhinal cortex and to areas TH and TF of the posterior parahippocampal cortex. A restricted area of the caudal STG, which appears to include the caudal lateral parabelt area of the auditory cortex and area Tpt (see Figure 11 in Suzuki and Amaral, 1994a) projects specifically to area TH of the posterior parahippocampal cortex (Suzuki and Amaral, 1994a; Blatt et al., 2003). Area TH sends reciprocal projections to area Tpt of the caudal STG (Tranel et al., 1988). It is worth noting that, Tranel et al.'s report showed that posterior parahippocampal projections to area Tpt appear to arise exclusively in area TH, with no projections from area TF. Area Tpt has dense connections with the caudal medial belt, where auditory and somatosensory responses have been detected electrophysiologically, suggesting that this area may be a multimodal one (CM, Smiley et al., 2007). Although the specific function of area Tpt remains still unknown, this area in monkeys shows increased regional cerebral blood flow (rCBF) in the presence of species-specific vocalizations (Gil-da-Costa et al., 2006).

Furthermore, in humans, this area contributes substantially to the enlargement of the left planum temporale on the left hemisphere and it is considered part of Wernicke's area (Galaburda et al., 1978). Area Tpt might be, therefore, a higher order processing area related with comprehension or semantic recognition of auditory stimuli.

Temporal pole

The temporal pole has been considered part of the parahippocampal region both in humans and non-human primates (Insausti et al., 1987a; Blaizot et al., 2004; Blaizot et al., 2010). However, both architectonically, and in terms of its connections, TP is a transitional area between perirhinal cortex and the neocortical areas of the adjacent superior and inferior temporal gyri. Whereas the lateral dorsal and ventral divisions of TP (38DL, 38VL) are closely related to adjacent superior and inferior temporal gyri (Moran et al., 1987; Kondo et al., 2003; our own observations in rhesus monkeys), the medial ventral and dorsal subdivisions of TP (36p-vm, 36p-dm, in rhesus monkeys this study), have been considered as a dorsal extension of area 36 of the perirhinal cortex in different non-human primates (Insausti et al., 1987a; Suzuki and Amaral, 1994a; Blaizot et al., 2004).

Anatomical studies with wallerian degeneration techniques showed that early auditory and visual processing areas send projections to progressively more rostral portions of the STG and subsequently to TP (Jones and Powell, 1970). This stream of caudal-to-rostral connections has been later confirmed with more modern tract tracing studies (Galaburda and Pandya, 1983; Markowitsch et al., 1985; Moran et al., 1987; Cipolloni and Pandya, 1989). The work of Moran et al. (1987) showed that, the dorsal part of TP receives specifically input from auditory processing areas of the STG, and therefore, may participate in auditory processing, in contrast, to other TP regions, which receive olfactory and visual input. Further support to this anatomical and functional organization of TP has been recently reported in a 2-deoxyglocose activation study in monkeys that were exposed to auditory and visual stimuli (Poremba et al., 2003). The likely involvement of the dorsal TP in high order auditory processing has been also delineated by a recent FDG-PET study in monkeys stimulated with different types of sounds including simple, complex, and naturalistic sounds (Poremba et al., 2004). According to this study, the dorsal part of TP plays a special role in processing species-specific calls in rhesus monkeys; specifically, this area showed evidence of left hemisphere specialization for processing vocalizations like that shown in humans for processing speech. In fact, we have shown that the densest afferent connections to the dorsal part of TP originate in auditory-related areas of the rostral STG (areas RTL, Ts1–Ts3) and the polymodal areas TAa and TPO (Munoz et al., 2003).

On the other hand, the dorsal lateral TP receives input from medial, orbitofrontal, and insular cortex (Mesulam, 1982; Markowitsch et al., 1985; Moran et al., 1987; Munoz et al., 2002; Kondo et al., 2003), suggesting that it may be involved in auditory and multimodal processing. The TP has reciprocal connections with EC (Kosel et al., 1982; Insausti et al., 1987a; Munoz et al., 2003), the rostral part of areas 35 and 36 of the perirhinal cortex (Munoz et al., 2003; Lavenex et al., 2004) and areas TH and TF of the posterior parahippocampal cortex (Munoz et al., 2003).

The participation of TP in memory in humans has been shown in fMRI studies, and critically, by its involvement in semantic dementia (Olson et al., 2007; Patterson et al., 2007). However, in non-human primate models of amnesia TP has received considerably less attention than the hippocampus and parahippocampal region, and therefore, its participation in memory remains largely unknown. Nonetheless, the anatomical position of the dorsal part of TP within the auditory cortical system and its close relation with the medial temporal cortex, suggest that it might be one important entry point of highly processed auditory information to the medial temporal cortex, and therefore, participate in auditory memory processing, in parallel to the TE–perirhinal–entorhinal–hippocampus pathway in visual memory (Munoz et al., 2003).

In sum, the cortex of the rostral part of the STG, including the dorsal part of TP and, to a lesser extent, areas Ts1–3 of the auditory parabelt project directly to EC, the rostral part of areas 35 and 36 of the perirhinal cortex, and areas TH and TF of the posterior parahippocampal cortex. There is an additional projection from the caudal STG to area TH. The auditory projections to EC are, however, very meager in comparison with its polymodal input (Mohedano-Moriano et al., 2008). Similarly, auditory afferents to the perirhinal and posterior parahippocampal cortices are very meager compared to visual input. This is in line with the second hypothesis that the major route, by which the auditory information reaches the medial temporal cortex is via indirect connections, the dorsal TP possibly being one of the major indirect pathway (**Figure 2**).

INDIRECT AUDITORY INPUT TO MEDIAL TEMPORAL CORTEX

Dorsal bank of the superior temporal sulcus

Neurons in the operculum and the dorsal bank of the superior temporal sulcus in the non-human primate – the superior temporal polysensory area STP – show responses to stimuli from different sensory modalities such as auditory, visual, and somatosensory (Bruce et al., 1981; Baylis et al., 1987). It is reasonable then to assume that the auditory information that reaches the medial temporal cortex via the superior temporal sulcus may not be purely auditory, but has already been integrated with information from other modalities (**Figure 3**).

A possible pathway, and probably the densest route of indirect projections from the auditory areas of the STG to the medial temporal cortex, would start in the rostral divisions of the lateral parabelt through a series of synaptic relays:

a) Areas Ts1–Ts2 of the gyral surface of the STG (**Figure 1**) send a very meager direct projection to the memory-related areas of the medial temporal cortex (Amaral et al., 1983; Insausti et al., 1987a; Suzuki and Amaral, 1994a). In contrast, they send a dense one to the opercular area TAa and to the dorsal bank of the STG (Seltzer and Pandya, 1989).
b) Area TAa of the STG (**Figure 1**) send a weak projection to areas of the medial temporal cortex (Amaral et al., 1983; Insausti et al., 1987a; Suzuki and Amaral, 1994a), however area TAa has dense connections with the fundus and dorsal bank of the superior temporal sulcus (areas PGa and TPO of Seltzer and Pandya, 1989; **Figure 1**).

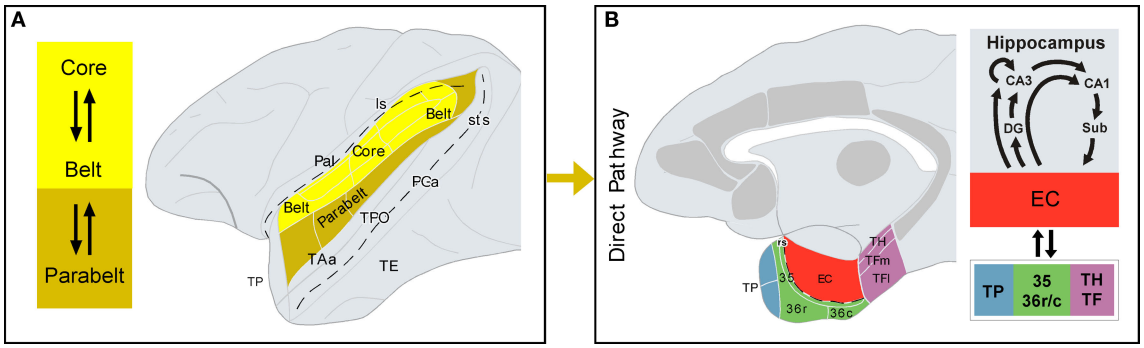

FIGURE 2 | Direct auditory pathway to the medial temporal cortex. **(A)** Core and belt areas of the auditory cortex, shown in the lateral view of the primate brain, have dense and reciprocal connections. Belt areas have dense connections with parabelt areas, where the projection to the parahippocampal region originates, i.e. *the direct pathway* **(B)** The architectonic areas that comprise the parahippocampal region are shown in a medial view of the primate brain. Additional cortical areas that receive auditory input and project to the parahippocampal region are shown in gray, but they form part of the indirect pathway (see **Figure 3** for further details). Connections between the parahippocampal region and the hippocampal formation are summarized on the right-hand side. See list of abbreviations.

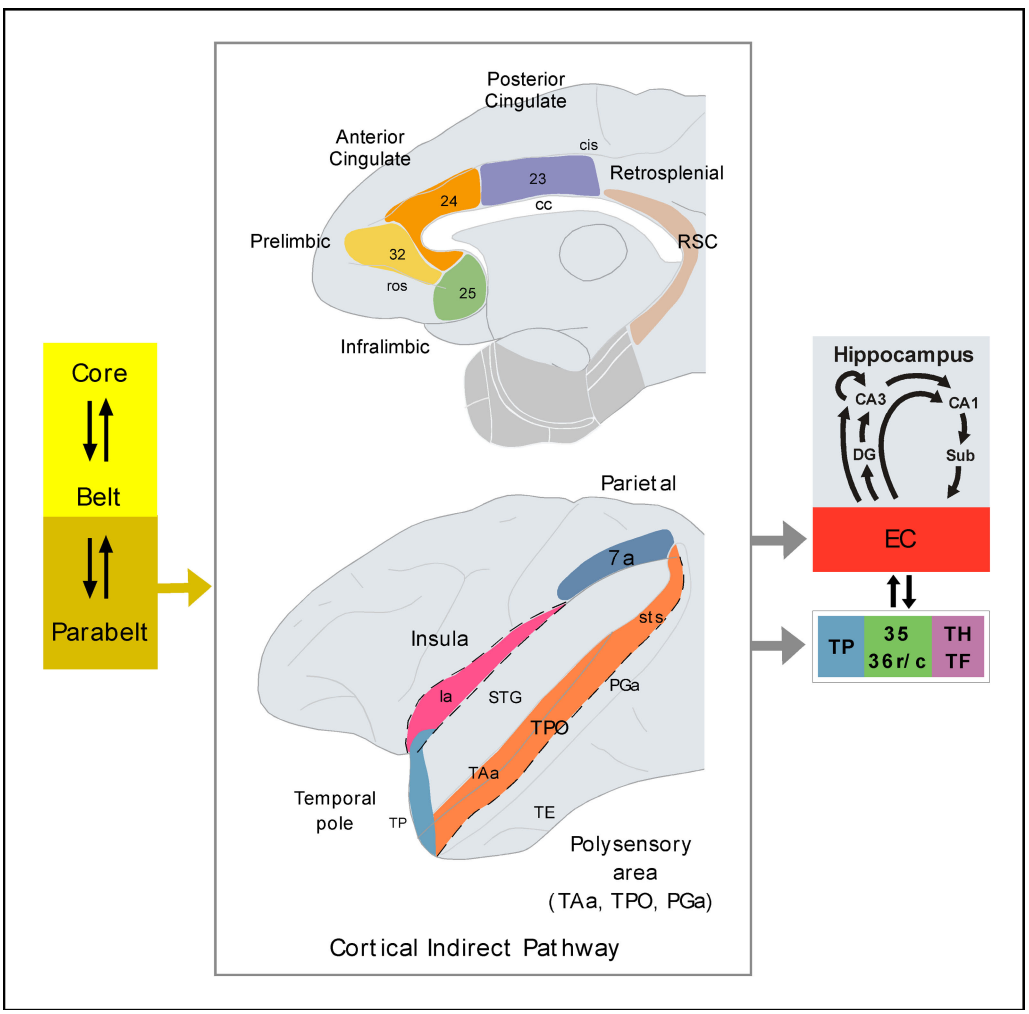

FIGURE 3 | Possible indirect pathways of auditory information to the medial temporal cortex. The schematic diagram of the primate brain illustrates the cortical areas reported to receive connections from parabelt areas of the auditory cortex and, critically, to send projections to the medial temporal cortex. The cortical areas shown in the figure represent synaptic relays of auditory information before it reaches the medial temporal memory system. The parahippocampal region is shown in light gray. See list of abbreviations.

c) Areas PGa and TPO (**Figure 1**) send projections to the entorhinal, perirhinal and posterior parahippocampal cortices, with the latter area originating the densest projection of all (Amaral et al., 1983; Insausti et al., 1987a; Suzuki and Amaral, 1994a).

In summary, one of the routes for auditory afferents to reach the hippocampal formation, perirhinal, and posterior parahippocampal cortices might be through polymodal areas of the dorsal bank of the superior temporal sulcus (**Figure 3**).

Insula

One of the sources of auditory information to the insula (**Figure 3**) originates within the superior temporal plane and especially in the more medial portions of the auditory belt area (Mufson and Mesulam, 1982). These projections form part of the complex pattern of afferent projections to the insular cortex, suggesting that the insula, among other functions, is involved in auditory processing.

Auditory–insular connections have received little attention, but a recent study reported that auditory-related areas located in the medial and lateral subdivisions of the caudal belt receive somatosensory information from retroinsular and granular insular cortex (Smiley et al., 2007). These areas also receive visual information from area prostriata localized in the anterior portion of the calcarine sulcus, visual cortex area V2, the polysensory area TPO of the dorsal bank of the superior temporal sulcus, and area Tpt (Falchier et al., 2010). Therefore, the medial and lateral caudal divisions of the auditory belt might themselves process polysensory information in higher degree than had previously been thought.

The agranular and disgranular divisions of the insula send dense projections to the rostromedial division of EC (Insausti et al., 1987a; Insausti and Amaral, 2008) to area 35, and to lesser extent to area 36 of the perirhinal cortex, and to the posterior parahippocampal areas TH and TF (Suzuki and Amaral, 1994a). This might be a second important source of indirect auditory input to the medial temporal cortex.

Anterior cingulate, prelimbic, and infralimbic cortex

Area 32 (Barbas, 1988), and areas 25 and 24 (**Figure 3**, Vogt and Pandya, 1987; Petrides and Pandya, 1988; Barbas et al., 1999; Munoz et al., 2009) receive strong projections from auditory association areas of the rostral STG, including parabelt and TP, primarily via the uncinate fasciculus. In contrast, the medial frontal cortex in marmosets receives projections from earlier (core) auditory processing areas (Roberts et al., 2007; Reser et al., 2009). These studies revealed another interesting difference between macaque and marmoset monkeys. Unlike rhesus monkeys, the medial frontal cortex of the marmoset monkey receive visual information via ventral temporal pole and inferior temporal gyrus. The temporal–medial frontal connections in marmosets appear, therefore, to arise earlier in the auditory sensory stream and might be less sensory-specific compared with macaque monkeys.

The STG-medial frontal projections in rhesus monkeys are organized topographically, in such a manner that the density of the projection decreases progressively from rostral to caudal in the STG. The lateral portion of TP and area Ts1 are the origin of the densest projection to areas 25, 32, and to a lesser extent to area 24, whereas the density of the projection decreases progressively from area Ts2 to Ts3 (Vogt and Pandya, 1987; Petrides and Pandya, 1988; Barbas et al., 1999). These auditory-processing projections are reciprocal, therefore axons from the anterior lateral, medial prefrontal, and orbitofrontal areas terminate in the anterior half of the STG (Barbas et al., 2005).

Areas 32, 24, and 25 have been associated with the production of calls in squirrel monkeys (Jürgens and Pratt, 1979; Kirzinger and Jurgens, 1982). Although the extensive work of Jürgens has elucidated the major pathways involved in the motor control of monkey vocalizations in the squirrel monkey, little is known in rhesus monkeys. In the late sixties, Robinson found that electrical stimulation of different territories of the medial frontal cortex elicited monkey calls in rhesus monkeys (primarily area 32, but it may be also area 24, Robinson, 1967; see review in Vogt and Barbas, 1987).

Ventral medial frontal areas 24, 32, and 25 have, on the other hand, lead the frontal projections with medial temporal cortex. In fact, among all the architectonic areas that form the frontal cortex, areas 25 and 32 have the densest connections with CA1/Subiculum and, and therefore, have a very direct access to the medial temporal memory system (Barbas and Blatt, 1995; Blatt and Rosene, 1998; Barbas et al., 1999; Insausti and Munoz, 2001). A similar pattern of frontal–hippocampal formation connections has been reported in marmosets (Roberts et al., 2007). Areas 24, 32, and 25 also send connections to TP, EC, and the posterior parahippocampal cortices and, to a lesser extent, with to 36 and 35 of the perirhinal cortex (Insausti et al., 1987a; Arikuni et al., 1994; Suzuki and Amaral, 1994a).

Although the role of these regions of the medial frontal cortex in working or long-term memory in audition is still puzzling, removals that include area 25 impair visual long-term recognition memory in monkeys (Bachevalier and Mishkin, 1986). In fact, Bachevalier and Mishkin (1986) suggested that, together with the medial thalamus and the medial temporal cortex, area 25 forms part of the limbic system important for episodic memory. Whether the role in recognition of area 25 is extensive to other sensory modalities, such as the auditory or somatosensory, calls for further research. Interestingly, the auditory input to areas 25, 32, and the pregenual portion of area 24 of the frontal cortex is disrupted by medial temporal removals (Munoz et al., 2009), the very same lesions that impair auditory (short-term) recognition memory (Fritz et al., 2005).

In sum, the complex anatomical and physiological organization of the medial frontal cortex suggests that areas 24, 25, and 32 are involved in some motor aspects of monkey call production, amongst other functions. In addition, they interact with auditory and medial temporal cortices and therefore, they may modulate auditory memory function. Emotional modulation of auditory memory might be mediated possibly by way of interactions via connections with the amygdala (Aggleton et al., 1980; Barbas, 1995) or autonomic responses through the hypothalamus (Ongur et al., 1998; Chiba et al., 2001).

Posterior cingulate and retrosplenial cortex

Superior temporal gyrus projections to area 23 of the caudal cingulate cortex and to areas 29 and 30 have been described by in retrograde tracer experiments, but they have been reported as very

modest and arising primarily from the dorsal bank of the superior temporal sulcus, rather than from auditory processing areas (Vogt and Pandya, 1987; Kobayashi and Amaral, 2003).

However, there might be a modest contribution of auditory projections to caudal cingulate (area 23) and retrosplenial cortex (area 29) as well as caudal presubiculum (Yukie, 1995), both of which project to EC (Insausti et al., 1987a).

Area 29 of the retrosplenial cortex and area 23 of the posterior cingulate cortex are important sources of cortical afferents to the caudal entorhinal cortex, the posterior parahippocampal areas TH and TF, and to a lesser extent, to perirhinal cortex areas 35 and 36.

Parietal cortex

The intraparietal sulcus is involved in spatial auditory processing (Cohen and Andersen, 2000; Cohen et al., 2004). Functional imaging and event-related potential studies in humans also indicate that the parietal cortex, particularly in the right hemisphere, is active during tasks requiring active localization of sounds (Maeder et al., 2001).

Some studies have failed to find direct connections between auditory areas of the STG and the intraparietal sulcus (Cavada and Goldman-Rakic, 1989; Neal et al., 1990), and it has therefore auditory information likely reaches the intraparietal sulcus primarily via area Tpt (Smiley et al., 2007) and the dorsal bank of the superior temporal sulcus (Neal et al., 1990).

Tract tracing studies indicate that the medial part of area Tpt in the caudal STG sends projections to the ventral intraparietal area, an area that has been involved in neuroanatomical networks functionally related to visual, vestibular, somatomotor, and auditory processing (Lewis and Van Essen, 2000).

In sum, this pathway arises in the caudal parabelt areas and projects via inferior pariental cortex (area 7a) to areas TH and TF of the posterior parahippocampal cortex (Suzuki and Amaral, 1994a) and to caudal entorhinal cortex (Insausti et al., 1987a).

Amygdala and thalamus

The amygdaloid complex, a group of nuclei with dense cortical and hypothalamic connections, is important in emotion, motivation, memory, and social behavior.

Connections between auditory-related areas of the rostral half of the STG and the amygdala in monkeys have been reported previously (Nauta, 1961; Aggleton et al., 1980; Van Hoesen, 1981; Amaral and Price, 1984; Stefanacci and Amaral, 2002). Within the amygdaloid complex, the lateral nucleus receives the densest projection from auditory-related areas. There is then an intrinsic projection from the lateral nucleus to the lateral basal nucleus (Pitkanen and Amaral, 1991, 1998), and the lateral basal nucleus sends reciprocal projections to auditory processing cortical areas. There is some indication that this amygdalofugal outflow of projections to cortical areas, including that to auditory-related areas, might be more widespread and more complex than the afferent projections (Amaral and Price, 1984).

The lateral nucleus of the amygdala provides the densest input to EC, with additional projections also originating in the basal and accessory basal nucleus (Insausti et al., 1987b; Saunders et al., 1988; Pitkanen et al., 2002; Stefanacci and Amaral, 2002). It is interesting to note that the projections from some cortical and subcortical areas converges with auditory input in to the lateral EC (Amaral et al., 1983; Insausti et al., 1987b; Mohedano-Moriano et al., 2007; Mohedano-Moriano et al., 2008).

The amygdala, therefore, may influence EC, and moreover has further access to the hippocampus. Many of the amygdalar nuclei, primarily basal, lateral basal, medial basal, cortical nucleus and cortical–amygdaloid area send direct projections to the molecular layer of the amygdalo–hippocampal area and stratum lacunosum moleculare of the uncal portions of CA3 and less densely to CA1, and the CA1/Subiculum area, also called prosubiculum. Additional projections terminate in the presubiculum, parasubiculum, and layers I–III of the rostral one-half of EC (Rosene and Van Hoesen, 1977; Aggleton, 1986; Saunders et al., 1988).

In non-human primates, there is a direct thalamo–amygdaloid pathway that seems to be relatively minor. Among the multiple thalamic nuclei, only the peripeduncular nucleus was found to project substantially to the lateral amygdaloid nucleus (Jones et al., 1976; Aggleton et al., 1980; Amaral and Insausti, 1992). This connection is prominent in rats and has been considered to be a rapid route for acoustic signals of emotional significance (LeDoux et al., 1990). In non-human primates, the direct thalamo–amygdaloid projections seem to be less dense compared with the connections between the amygdala and cortical auditory processing areas.

Classical degeneration and more modern neuronal tracer techniques have been employed to discover and describe the thalamic connections to auditory areas (De Vito and Simmons, 1976; Kosmal et al., 1997; Hackett et al., 1998; Gutierrez et al., 2000; Hackett et al., 2007). The thalamic nucleus that leads the projection to the core, belt, and parabelt areas of the auditory cortex is the medial geniculate nucleus (MGd or MGv), but this cortical area also receives inputs from other thalamic nuclei such as the suprageniculate nucleus, limitans, medial dorsal, and rostral and medial nuclei of the pulvinar (Pandya et al., 1994; Hackett et al., 1998).

In the thalamus, the medial nucleus of the pulvinar, an area of multimodal convergence (Cappe et al., 2009), has been involved in sensory integration and attention (Ivanov et al., 2010), although its function remains not well understood. On one hand, the medial pulvinar is connected with the rostral part of STG (Trojanowski and Jacobson, 1975). On the other hand, the rostral and lateral divisions of EC, the same ones that receive direct auditory input and indirect via amygdala, receive also dense projections from the medial nucleus of the pulvinar (Trojanowski and Jacobson, 1977; Insausti et al., 1987b). It seems, therefore, that this thalamic nucleus may form part of the indirect subcortical pathway for audition to reach the medial temporal memory system.

CONCLUDING REMARKS

The primary aim of this review has been to draw attention to the complexity of additional indirect connections by which auditory information can get to memory processing areas of the medial temporal lobes. Specifically, the anatomical studies reviewed here indicate that, unlike the strong, direct and reciprocal connections of visual association areas between the inferior temporal cortex and areas 35 and 36 of the perirhinal and areas TH and TF of the posterior parahippocampal cortex, direct connections from auditory processing areas of the STG with medial temporal cortex appear

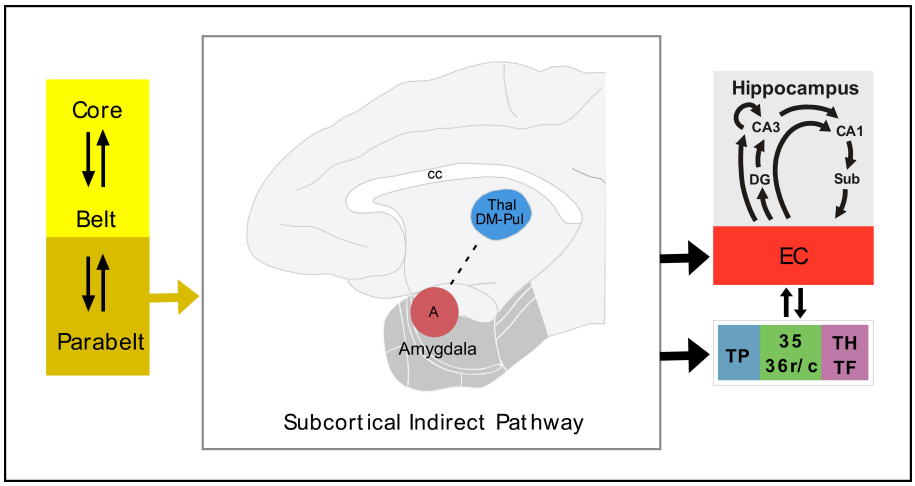

FIGURE 4 | Possible subcortical indirect pathway for auditory input to the medial temporal memory system. See list of abbreviations.

to be considerably more modest. Thus, whereas the visual "ventral stream" of processing in the Mishkin and Ungerleider (1982) framework is relatively direct, this principle does not appear to extend to the auditory domain. This may explain, at least in part, monkeys' poor ability for auditory memory (Fritz et al., 2005).

The entry of auditory information to the medial temporal cortex might be, therefore, more indirect in audition than in vision. In addition to the cortical direct and indirect pathways, auditory information may enter the medial temporal cortex via subcortical structures, like the lateral and basal nuclei of the amygdala and the thalamus, with possibly an especial role for the medial pulvinar. The direct connections of the amygdala with the hippocampus points to a possible role of emotion in auditory long-term memory.

It cannot be ruled out the contribution of other subcortical nuclei in the diencephalon or brainstem, although little or no neuroanatomical evidence exists. It is foreseeable that the auditory memory involves much more intricate and complex neural networks and that all this information may be translated to clinical practice.

The projections of neurons in auditory processing areas of the STG seem to reach memory-related areas of the medial temporal cortex and diencephalon via indirect connections with polysensory areas (**Figure 3**), such as the TP, the dorsal bank of the superior temporal sulcus, the insula, medial frontal cortex (areas 24, 32, and 25), and to a lesser extent posterior cingulate and retrosplenial cortex, and via amygdale and medial pulvinar (**Figure 4**). This is in line with the second of the two hypotheses we have considered, although there remain a number of unresolved issues (**Table 1**). Specifically, unlike in vision, the majority of auditory connections, before they reach the medial temporal cortex, make additional synaptic connections in intermediate, polymodal areas where they integrate with information from other sensory modalities, and only then do they enter in the medial temporal lobe memory system.

REFERENCES

Aggleton, J. P. (1986). A description of the amygdalo-hippocampal interconnections in the macaque monkey. *Exp. Brain Res.* 64, 515–526.

Aggleton, J. P., and Brown, M. W. (1999). Thanks for the memories, Extending the hippocampal-diencephalic memonic system. *Behav. Brain Sci.* 22, 471–489.

Aggleton, J. P., Burton, M. J., and Passingham, R. E. (1980). Cortical and subcortical afferents to the amygdala of the rhesus monkey (*Macaca mulatta*). *Brain Res.* 190, 347–368.

Amaral, D. G., and Insausti, R. (1992). Retrograde transport of D-[3H]-aspartate injected into the monkey amygdaloid complex. *Exp. Brain Res.* 88, 375–388.

Amaral, D. G., Insausti ,R., and Cowan, W. M. (1983). Evidence for a direct projection from the superior temporal gyrus to the entorhinal cortex in the monkey. *Brain Res.* 275, 263–277.

Amaral, D. G., Insausti, R., and Cowan, W. M. (1987). The entorhinal cortex of the monkey: I. Cytoarchitectonic organization. *J. Comp. Neurol.* 264, 326–355.

Amaral, D. G., and Price, J. L. (1984). Amygdalo-cortical projections in the monkey (*Macaca fascicularis*). *J. Comp. Neurol.* 230, 465–496.

Arikuni, T., Sako, H., and Murata, A. (1994). Ipsilateral connections of the anterior cingulate cortex with the frontal and medial temporal cortices in the macaque monkey. *Neurosci. Res.* 21, 19–39.

Bachevalier, J., and Mishkin, M. (1986). Visual recognition impairment follows ventromedial but not dorsolateral prefrontal lesions in monkeys. *Behav. Brain Res.* 20, 249–261.

Barbas, H. (1988). Anatomic organization of basoventral and mediodorsal visual recipient prefrontal regions in the rhesus monkey. *J. Comp. Neurol.* 276, 313–342.

Barbas, H. (1995). Anatomic basis of cognitive-emotional interactions in the primate prefrontal cortex. *Neurosci. Biobehav. Rev.* 19, 499–510.

Barbas, H., and Blatt, G. J. (1995). Topographically specific hippocampal projections target functionally distinct prefrontal areas in the rhesus monkey. *Hippocampus* 5, 511–533.

Barbas, H., Ghashghaei, H., Dombrowski, S. M., and Rempel-Clower, N. L. (1999). Medial prefrontal cortices are unified by common connections with superior temporal cortices and distinguished by input from memory-related areas in the rhesus monkey. *J. Comp. Neurol.* 410, 343–367.

Barbas, H., Medalla, M., Alade, O., Suski, J., Zikopoulos, B., and Lera, P. (2005). Relationship of prefrontal connections to inhibitory systems in superior temporal areas in the rhesus monkey. *Cereb. Cortex* 15, 1356–1370.

Baylis, G. C., Rolls, E. T., and Leonard, C. M. (1987). Functional subdivisions of the temporal lobe neocortex. *J. Neurosci.* 7, 330–342.

Blaizot, X., Mansilla, F., Insausti, A. M., Constans, J. M., Salinas-Alaman, A., Pro-Sistiaga, P., Mohedano-Moriano, A., and Insausti, R., (2010). The human parahippocampal region: I. Temporal pole cytoarchitectonic and MRI correlation. *Cereb. Cortex.* 20, 2198–2212.

Blaizot, X., Martinez-Marcos, A., Arroyo-Jimenez, M. M., Marcos, P., Artacho-Perula, E., Munoz, M., Chavoix, C., and Insausti, R. (2004). The parahippocampal gyrus in the baboon, anatomical, cytoarchitectonic and magnetic resonance imaging (MRI) studies. *Cereb. Cortex* 14, 231–246.

Blatt, G. J., Pandya, D. N., and Rosene, D. L. (2003). Parcellation of cortical afferents to three distinct sectors in the parahippocampal gyrus of the rhesus monkey, an anatomical and neurophysiological study. *J. Comp. Neurol.* 466, 161–179.

Blatt, G. J., and Rosene, D. L. (1998). Organization of direct hippocampal efferent projections to the cerebral cortex of the rhesus monkey, projections from CA1, prosubiculum, and subiculum to the temporal lobe. *J. Comp. Neurol.* 392, 92–114.

Brodmann, K. (1909). *Vergleichende Lokalisationslehere der Grosshimrinde in ihren Principien dargestellt auf des Grund des Zellenbayes*. Barth, Leipzig.

Brown, M. W., and Aggleton, J. P. (2001). Recognition memory, what are the roles of the perirhinal cortex and hippocampus? *Nat. Rev. Neurosci.* 2, 51–61.

Bruce, C., Desimone, R., and Gross, C. G. (1981). Visual properties of neurons in a polysensory area in superior temporal sulcus of the macaque. *J. Neurophysiol.* 46, 369–384.

Burwell, R. D., Witter, M. P., and Amaral, D. G. (1995). Perirhinal and postrhinal cortices of the rat, a review of the neuroanatomical literature and comparison with findings from the monkey brain. *Hippocampus* 5, 390–408.

Cappe, C., Morel, A., Barone, P., and Rouiller, E. M. (2009). The thalamocortical projection systems in primate, an anatomical support for multisensory and sensorimotor interplay. *Cereb. Cortex* 19, 2025–2037.

Cavada, C., and Goldman-Rakic, P. S. (1989). Posterior parietal cortex in rhesus monkey, I. Parcellation of areas based on distinctive limbic and sensory corticocortical connections. *J. Comp. Neurol.* 287, 393–421.

Chiba, T., Kayahara, T., and Nakano, K. (2001). Efferent projections of infralimbic and prelimbic areas of the medial prefrontal cortex in the Japanese monkey, *Macaca fuscata*. *Brain Res.* 888, 83–101.

Cipolloni, P. B., and Pandya, D. N. (1989). Connectional analysis of the ipsilateral and contralateral afferent neurons of the superior temporal region in the rhesus monkey. *J. Comp. Neurol.* 281, 567–585.

Cohen, Y. E., and Andersen, R. A. (2000). Reaches to sounds encoded in an eye-centered reference frame. *Neuron* 27, 647–652.

Cohen, Y. E., Cohen, I. S., and Gifford, G. W. (2004). Modulation of LIP activity by predictive auditory and visual cues. *Cereb. Cortex* 14, 1287–1301.

De Vito, J. L., and Simmons, D. M. (1976). Some connections of the posterior thalamus in monkey. *Exp. Neurol.* 51, 347–362.

Engelien, A., Stern, E., Isenberg, N., Engelien, W., Frith, C., and Silbersweig, D. (2000). The parahippocampal region and auditory-mnemonic processing. *Ann. N. Y. Acad. Sci.* 911, 477–485.

Falchier, A., Schroeder, C. E., Hackett, T. A., Lakatos, P., Nascimento-Silva, S., Ulbert, I., Karmos, G., and Smiley, J. F. (2010). Projection from visual areas V2 and prostriata to caudal auditory cortex in the monkey. *Cereb. Cortex* 20, 1529–1538.

Fritz, J., Mishkin, M., and Saunders, R. C. (2005). In search of an auditory engram. *Proc. Natl. Acad. Sci. U. S. A.* 102, 9359–9364.

Galaburda, A. M., and Pandya, D. N. (1983). The intrinsic architectonic and connectional organization of the superior temporal region of the rhesus monkey. *J. Comp. Neurol.* 221, 169–184.

Galaburda, A. M., Sanides, F., and Geschwind, N. (1978). Human brain. Cytoarchitectonic left-right asymmetries in the temporal speech region. *Arch. Neurol.* 35, 812–817.

Gil-da-Costa, R., Braun, A., Lopes, M., Hauser, M. D., Carson, R. E., Herscovitch, P., and Martin, A. (2004). Toward an evolutionary perspective on conceptual representation, species-specific calls activate visual and affective processing systems in the macaque. *Proc. Natl. Acad. Sci. U.S.A.* 101, 17516–17521.

Gil-da-Costa, R., Martin, A., Lopes, M. A., Munoz, M., Fritz, J. B., and Braun, A. R. (2006). Species-specific calls activate homologs of Broca's and Wernicke's areas in the macaque. *Nat. Neurosci.* 9, 1064–1070.

Gutierrez, C., Cola, M. G., Seltzer, B., and Cusick, C. (2000). Neurochemical and connectional organization of the dorsal pulvinar complex in monkeys. *J. Comp. Neurol.* 419, 61–86.

Hackett, T. A. (2010). Information flow in the auditory cortical network. *Hear. Res.* [Epub ahead of print].

Hackett, T. A., de la Mothe, L. A., Ulbert, I., Karmos, G., Smiley, J., and Schroeder, C. E. (2007). Multisensory convergence in auditory cortex, II. Thalamocortical connections of the caudal superior temporal plane. *J. Comp. Neurol.* 502, 924–952.

Hackett, T. A., Stepniewska, I., and Kaas, J. H. (1998). Subdivisions of auditory cortex and ipsilateral cortical connections of the parabelt auditory cortex in macaque monkeys. *J. Comp. Neurol.* 394, 475–495.

Insausti, R. (1993). Comparative anatomy of the entorhinal cortex and hippocampus in mammals. *Hippocampus* 3 Spec No, 19–26.

Insausti, R., and Amaral, D. G. (2008). Entorhinal cortex of the monkey, IV. Topographical and laminar organization of cortical afferents. *J. Comp. Neurol.* 509, 608–641.

Insausti, R., Amaral, D. G., and Cowan, W. M. (1987a). The entorhinal cortex of the monkey, II. Cortical afferents. *J. Comp. Neurol.* 264, 356–395.

Insausti, R., Amaral, D. G., and Cowan, W. M. (1987b). The entorhinal cortex of the monkey, III. Subcortical afferents. *J. Comp. Neurol.* 264, 396–408.

Insausti, R., and Munoz, M. (2001). Cortical projections of the non-entorhinal hippocampal formation in the cynomolgus monkey (*Macaca fascicularis*). *Eur. J. Neurosci.* 14, 435–451.

Ivanov, I., Bansal, R., Hao, X., Zhu, H., Kellendonk, C., Miller, L., Sanchez-Pena, J., Miller, A. M., Chakravarty, M. M., Klahr, K., Durkin, K., Greenhill, L. L., and Peterson, B. S. (2010). Morphological abnormalities of the thalamus in youths with attention deficit hyperactivity disorder. *Am. J. Psychiatry* 167, 397–408.

Jones, E. G., Burton, H., Saper, C. B., and Swanson, L. W. (1976). Midbrain, diencephalic and cortical relationships of the basal nucleus of Meynert and associated structures in primates. *J. Comp. Neurol.* 167, 385–419.

Jones, E. G., and Powell, T. P. (1970). An anatomical study of converging sensory pathways within the cerebral cortex of the monkey. *Brain* 93, 793–820.

Jürgens, U., and Pratt, R. (1979). The cingular vocalization pathway in the squirrel monkey. *Exp. Brain Res.* 34, 499–510.

Kaas, J. H., and Hackett, T. A. (2000). Subdivisions of auditory cortex and processing streams in primates. *Proc. Natl. Acad. Sci. U.S.A.* 97, 11793–11799.

Kikuchi, Y., Horwitz, B., and Mishkin, M. (2006). Neural representation of auditory stimulus-quality in monkey's rostral supratemporal plane. *Soc. Neurosci.* Abstract 344.6.Atlanta, GA, USA.

Kirzinger, A., and Jurgens, U. (1982). Cortical lesion effects and vocalization in the squirrel monkey. *Brain Res.* 233, 299–315.

Kobayashi, Y., and Amaral, D. G. (2003). Macaque monkey retrosplenial cortex, II. Cortical afferents. *J. Comp. Neurol.* 466, 48–79.

Kondo, H., Saleem, K. S., and Price, J. L. (2003). Differential connections of the temporal pole with the orbital and medial prefrontal networks in macaque monkeys. *J. Comp. Neurol.* 465, 499–523.

Konorski, J. (1959). A new method of physiological investigation of recent memory in animals. *Bull. Acad. Pol. Sci. CL II, Ser. Sci. Biol.* 7, 115–117.

Kosel, K. C., Van Hoesen, G. W., and Rosene, D. L. (1982). Non-hippocampal cortical projections from the entorhinal cortex in the rat and rhesus monkey. *Brain Res.* 244, 201–213.

Kosmal, A., Malinowska, M., and Kowalska, D. M. (1997). Thalamic and amygdaloid connections of the auditory association cortex of the superior temporal gyrus in rhesus monkey (*Macaca mulatta*). *Acta Neurobiol. Exp.* (Wars.) 57, 165–188.

Lavenex, P., Suzuki, W. A., and Amaral, D. G. (2002). Perirhinal and parahippocampal cortices of the macaque monkey, projections to the neocortex. *J. Comp. Neurol.* 447, 394–420.

Lavenex, P., Suzuki, W. A., and Amaral, D. G. (2004). Perirhinal and parahippocampal cortices of the macaque monkey, Intrinsic projections and interconnections. *J. Comp. Neurol.* 472, 371–394.

LeDoux, J. E., Farb, C., and Ruggiero, D. A. (1990). Topographic organization of neurons in the acoustic thalamus that project to the amygdala. *J. Neurosci.* 10, 1043–1054.

Lewis, J. W., and Van Essen, D. C. (2000). Corticocortical connections of visual, sensorimotor, and multimodal processing areas in the parietal lobe of the macaque monkey. *J. Comp. Neurol.* 428, 112–137.

Maeder, P. P., Meuli, R. A., Adriani, M., Bellmann, A., Fornari, E., Thiran, J. P., Pittet, A., and Clarke, S. (2001). Distinct pathways involved in sound recognition and localization, a human fMRI study. *Neuroimage* 14, 802–816.

Markowitsch, H. J., Emmans, D., Irle, E., Streicher, M., and Preilowski, B. (1985). Cortical and subcortical afferent connections of the primate's temporal pole, a study of rhesus monkeys, squirrel monkeys, and marmosets. *J. Comp. Neurol.* 242, 425–458.

Mesulam, M. M. (1982). Slowly progressive aphasia without generalized dementia. *Ann. Neurol.* 11, 592–598.

Meunier, M., Bachevalier, J., Mishkin, M., and Murray, E. A. (1993). Effects on

visual recognition of combined and separate ablations of the entorhinal and perirhinal cortex in rhesus monkeys. *J. Neurosci.* 13, 5418–5432.

Mishkin, M. (1978). Memory in monkeys severely impaired by combined but not by separate removal of amygdala and hippocampus. *Nature* 273, 297–298.

Mishkin, M., and Ungerleider, L. G. (1982). Contribution of striate inputs to the visuospatial functions of parieto-preoccipital cortex in monkeys. *Behav. Brain Res.* 6, 57–77.

Mohedano-Moriano, A., Martinez-Marcos, A., Pro-Sistiaga, P., Blaizot, X., Arroyo-Jimenez, M. M., Marcos, P., Artacho-Perula, E., and Insausti, R. (2008). Convergence of unimodal and polymodal sensory input to the entorhinal cortex in the fascicularis monkey. *Neuroscience* 151, 255–271.

Mohedano-Moriano, A., Pro-Sistiaga, P., Arroyo-Jimenez, M. M., Artacho-Perula, E., Insausti, A. M., Marcos, P., Cebada-Sanchez, S., Martinez-Ruiz, J., Munoz, M., Blaizot, X., Martinez-Marcos, A., Amaral, D. G., and Insausti, R. (2007). Topographical and laminar distribution of cortical input to the monkey entorhinal cortex. *J. Anat.* 211, 250–260.

Moran, M. A., Mufson, E. J., and Mesulam, M. M. (1987). Neural inputs into the temporopolar cortex of the rhesus monkey. *J. Comp. Neurol.* 256, 88–103.

Mufson, E. J., and Mesulam, M. M. (1982). Insula of the old world monkey. II, Afferent cortical input and comments on the claustrum. *J. Comp. Neurol.* 212, 23–37.

Munoz, M., and Insausti, R. (2005). Cortical efferents of the entorhinal cortex and the adjacent parahippocampal region in the monkey (*Macaca fascicularis*). *Eur. J. Neurosci.* 22, 1368–1388.

Munoz, M., Mishkin, M., and Saunders, R. C. (2002). Cortical connections of the lateral pole. *Soc. Neurosci.* Abstract 183.14.Orlando, FL, USA.

Munoz, M., Mishkin, M., and Saunders, R. C. (2003). Lateral temporal pole, input from the superior temporal gyrus and output to the medial temporal cortex in the rhesus monkey. *Soc. Neurosci.* Abstract 939.1. New Orleans, LA, USA.

Munoz, M., Mishkin, M., and Saunders, R. C. (2009). Resection of the medial temporal lobe disconnects the rostral superior temporal gyrus from some of its projection targets in the frontal lobe and thalamus. *Cereb. Cortex* 19, 2114–2130.

Munoz, M., and Morris, R. (2009). *Episodic Memory, Assessment in Animals. Encyclopedia of Neuroscience.* Oxford: Academic Press, pp. 1173–1182.

Nauta, W. J. (1961). Fibre degeneration following lesions of the amygdaloid complex in the monkey. *J. Anat.* 95, 515–531.

Neal, J. W., Pearson, R. C., and Powell, T. P. (1990). The connections of area PG, 7a, with cortex in the parietal, occipital and temporal lobes of the monkey. *Brain Res.* 532, 249–264.

Ng, C. W., Plakke, B., and Poremba, A. (2009). Primate auditory recognition memory performance varies with sound type. *Hear. Res.* 256, 64–74.

Olson, I. R., Plotzker, A., and Ezzyat, Y. (2007). The Enigmatic temporal pole, a review of findings on social and emotional processing. *Brain* 130, 1718–1731.

Ongur, D., An, X., and Price, J. L. (1998). Prefrontal cortical projections to the hypothalamus in macaque monkeys. *J. Comp. Neurol.* 401, 480–505.

Pandya, D. N., Rosene, D. L., and Doolittle, A. M. (1994). Corticothalamic connections of auditory-related areas of the temporal lobe in the rhesus monkey. *J. Comp. Neurol.* 345, 447–471.

Pandya, D. N., and Sanides, F. (1973). Architectonic parcellation of the temporal operculum in rhesus monkey and its projection pattern. *Z. Anat. Entwicklungsgesch.* 139, 127–161.

Patterson, K., Nestor, P. J., and Rogers, T. T. (2007). Where do you know what you know? The representation of semantic knowledge in the human brain. *Nat. Rev. Neurosci.* 8, 976–987.

Petkov, C. I., Kayser, C., Steudel, T., Whittingstall, K., Augath, M., and Logothetis, N. K. (2008). A voice region in the monkey brain. *Nat. Neurosci.* 11, 367–374.

Petrides, M., and Pandya, D. N. (1988). Association fiber pathways to the frontal cortex from the superior temporal region in the rhesus monkey. *J. Comp. Neurol.* 273, 52–66.

Pitkanen, A., and Amaral, D. G. (1991). Demonstration of projections from the lateral nucleus to the basal nucleus of the amygdala, a PHA-L study in the monkey. *Exp. Brain Res.* 83, 465–470.

Pitkanen, A., and Amaral, D. G. (1998). Organization of the intrinsic connections of the monkey amygdaloid complex, projections originating in the lateral nucleus. *J. Comp. Neurol.* 398, 431–458.

Pitkanen, A., Kelly, J. L., and Amaral, D. G. (2002). Projections from the lateral, basal, and accessory basal nuclei of the amygdala to the entorhinal cortex in the macaque monkey. *Hippocampus* 12, 186–205.

Poremba, A., Malloy, M., Saunders, R. C., Carson, R. E., Herscovitch, P., and Mishkin, M. (2004). Species-specific calls evoke asymmetric activity in the monkey's temporal poles. *Nature* 427, 448–451.

Poremba, A., Saunders, R. C., Crane, A. M., Cook, M., Sokoloff, L., and Mishkin, M. (2003). Functional mapping of the primate auditory system. *Science* 299, 568–572.

Prisko, L. (1963). PhD Thesis. Montreal: McGill University.

Reser, D. H., Burman, K. J., Richardson, K. E., Spitzer, M. W., and Rosa, M. G. (2009). Connections of the marmoset rostrotemporal auditory area, express pathways for analysis of affective content in hearing. *Eur. J. Neurosci.* 30, 578–592.

Roberts, A. C., Tomic, D. L., Parkinson, C. H., Roeling, T. A., Cutter, D. J., Robbins, T. W., and Everitt, B. J. (2007). Forebrain connectivity of the prefrontal cortex in the marmoset monkey (*Callithrix jacchus*), an anterograde and retrograde tract-tracing study. *J. Comp. Neurol.* 502, 86–112.

Robinson, B. (1967). Vocalization evoked from forebrain in *Macaca mulatta*. *Physiol. Behav.* 2, 345–354.

Romanski, L. M., Bates, J. F., and Goldman-Rakic, P. S. (1999a). Auditory belt and parabelt projections to the prefrontal cortex in the rhesus monkey. *J. Comp. Neurol.* 403, 141–157.

Romanski, L. M., Tian, B., Fritz, J., Mishkin, M., Goldman-Rakic, P. S., and Rauschecker, J. P. (1999b). Dual streams of auditory afferents target multiple domains in the primate prefrontal cortex. *Nat. Neurosci.* 2, 1131–1136.

Rosene, D. L., and Van Hoesen, G. W. (1977). Hippocampal efferents reach widespread areas of cerebral cortex and amygdala in the rhesus monkey. *Science* 198, 315–317.

Saunders, R. C., Rosene, D. L., and Van Hoesen, G. W. (1988). Comparison of the efferents of the amygdala and the hippocampal formation in the rhesus monkey, II. Reciprocal and non-reciprocal connections. *J. Comp. Neurol.* 271, 185–207.

Schneider, R. J., Friedman, D. P., and Mishkin, M. (1993). A modality-specific somatosensory area within the insula of the rhesus monkey. *Brain Res.* 621, 116–120.

Scoville, W. B., and Milner, B. (1957). Loss of recent memory after bilateral hippocampal lesions. *J. Neurol. Neurosurg. Psychiatry* 20, 11–21.

Seltzer, B., and Pandya, D. N. (1978). Afferent cortical connections and architectonics of the superior temporal sulcus and surrounding cortex in the rhesus monkey. *Brain Res.* 149, 1–24.

Seltzer, B., and Pandya, D. N. (1989). Intrinsic connections and architectonics of the superior temporal sulcus in the rhesus monkey. *J. Comp. Neurol.* 290, 451–471.

Smiley, J. F., Hackett, T. A., Ulbert, I., Karmas, G., Lakatos, P., Javitt, D. C., and Schroeder, C. E. (2007). Multisensory convergence in auditory cortex, I. Cortical connections of the caudal superior temporal plane in macaque monkeys. *J. Comp. Neurol.* 502, 894–923.

Squire, L. R., and Zola-Morgan, S. (1991). The medial temporal lobe memory system. *Science* 253, 1380–1386.

Stefanacci, L., and Amaral, D. G. (2002). Some observations on cortical inputs to the macaque monkey amygdala, an anterograde tracing study. *J. Comp. Neurol.* 451, 301–323.

Suddendorf, T., and Corballis, M. C. (1997). Mental time travel and the evolution of the human mind. *Genet. Soc. Gen. Psychol. Monogr.* 123, 133–167.

Suzuki, W. A., and Amaral, D. G. (1994a). Topographic organization of the reciprocal connections between the monkey entorhinal cortex and the perirhinal and parahippocampal cortices. *J. Neurosci.* 14, 1856–1877.

Suzuki, W. A., and Amaral, D. G. (1994b). Perirhinal and parahippocampal cortices of the macaque monkey, cortical afferents. *J. Comp. Neurol.* 350, 497–533.

Suzuki, W. A., Zola-Morgan, S., Squire, L. R., and Amaral, D. G. (1993). Lesions of the perirhinal and parahippocampal cortices in the monkey produce long-lasting memory impairment in the visual and tactual modalities. *J. Neurosci.* 13, 2430–2451.

Tian, B., Reser, D., Durham, A., Kustov, A., and Rauschecker, J. P. (2001). Functional specialization in rhesus monkey auditory cortex. *Science* 292, 290–293.

Tranel, D., Brady, D. R., Van Hoesen, G. W., and Damasio, A. R. (1988). Parahippocampal projections to posterior auditory association cortex (area Tpt) in old-world monkeys. *Exp. Brain Res.* 70, 406–416.

Trojanowski, J. Q., and Jacobson, S. (1975). A combined horseradish peroxidase-autoradiographic investigation of reciprocal connections between superior temporal gyrus and pulvinar in squirrel monkey. *Brain Res.* 85, 347–353.

Trojanowski, J. Q., and Jacobson, S. (1977). The morphology and laminar distribution of cortico-pulvinar neurons in the rhesus monkey. *Exp. Brain Res.* 28, 51–62.

Tulving, E. (2004). Episodic memory, from mind to brain. *Rev. Neurol. (Paris)* 160, S9–S23.

Van Hoesen, G. W. (1981) "The differential distribution, diversity and sprouting of cortical projections to the amygdala in the rhesus monkey," in *The Amygdaloid Complex* ed. Y. Ben-Ari (Amsterdam: Elsevier/North Holland Biomedical Press), 77–90.

Vogt, B. A., and Pandya, D. N. (1987). Cingulate cortex of the rhesus monkey, II. Cortical afferents. *J. Comp. Neurol.* 262, 271–289.

Vogt, B. A., and Barbas, H. (1988). "Structure and connections of the cingulate vocalization region in the rhesus monkey," in *The Physiological Control of Mammalian Vocalization,* ed. J. D. Newman (New York : Plenum), 203–225.

Von Bonin, G., and Bailey, P. (1947). *The Neocortex of Macaca Mulatta. Urbana,* Illinois: University of Illinois, Illinois Press.

Witter, M. P., and Amaral, D. G. (1991). Entorhinal cortex of the monkey, V. Projections to the dentate gyrus, hippocampus, and subicular complex. *J. Comp. Neurol.* 307, 437–459.

Witter, M., and Wouterlood, F. (2002). *The Parahippocampal Region, Organization and Role in Cognitive Function*. Oxford: Oxford University Press.

Wright, A. A. (2007). An experimental analysis of memory processing. *J. Exp. Anal. Behav.* 88, 405–433.

Yonelinas, A. (2002). The nature of recollection and familiarity. A review of 30 years of research. *J. Mem. Lang.* 46, 441–517.

Yukie, M. (1995). Neural connections of auditory association cortex with the posterior cingulate cortex in the monkey. *Neurosci. Res.* 22, 179–187.

Conflict of Interest Statement: The authors declare that the research was conducted in the absence of any commercial or financial relationships that could be construed as a potential conflict of interest.

Received: 01 April 2010; paper pending published: 17 May 2010; accepted: 28 July 2010; published online: 08 October 2010.
*Citation: Munoz-Lopez MM, Mohedano-Moriano A and Insausti R (2010) Anatomical pathways for auditory memory in primates. Front. Neuroanat. **4**:129. doi: 10.3389/fnana.2010.00129*